Technische Universität Braunschweig

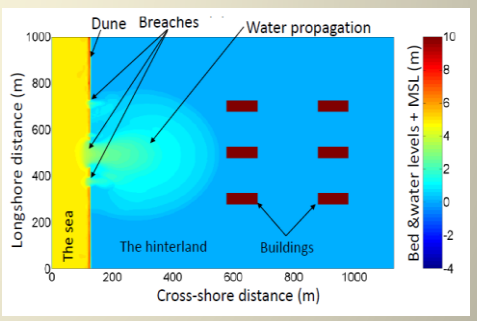

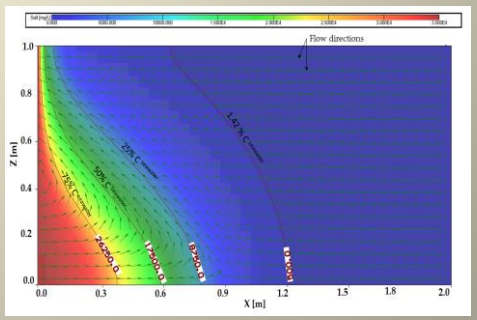

Breaching of Coastal Barriers under Extreme Storm Surges and Implications for Groundwater Contamination

Saber M. Elsayed

Braunschweig 2017

LWI
exceed
DAAD Deutscher Akademischer Austausch Dienst German Academic Exchange Service
Bundesministerium für wirtschaftliche Zusammenarbeit und Entwicklung

Breaching of Coastal Barriers under Extreme Storm Surges and Implications for Groundwater Contamination

Von der
Fakultät Architektur, Bauingenieurwesen und Umweltwissenschaften
der Technischen Universität Carolo-Wilhelmina
zu Braunschweig

zur Erlangung des Grades eines
Doktoringenieurs (Dr.-Ing.)
genehmigte

Dissertation

von
Saber Mohamed Elsayed Abdelaal, M.Sc.
geboren am 25. Dezember 1985
aus Fayoum, Ägypten

Eingereicht am: 16. Mai 2017
Disputation am: 31. August 2017

Berichterstatter Prof. Dr.-Ing. Hocine Oumeraci
Prof. Dr.-Ing. Holger Schüttrumpf

2017

Front cover pictures:
Photos of the cover are collected from diverse sources as respectively clarified:

- The cover of de Vet (2014), which is cited in the references.
- Photo taken by the author for the eroded beach of Lake Qarun in Fayoum, Egypt.
- Work crews push sand from a roadway in Fort Lauderdale, Florida, due to storm surge related to flooding induced by Hurricane Sandy on Monday, October 29, 2012. Downloaded from the website of The Economist and available at: https://www.economist.com/news/united-states/21579470-americans-are-building-beachfront-homes-even-oceans-rise-youre-going-get-wet (accessed on 21.08.2017)
- Photo developed by the author and presented in Chapter 5
- Photo developed by the author for the solution of the Henry saltwater intrusion problem (see Elsayed and Oumeraci, 2017 b).
- Photo for the installation of subsurface drainage system. Downloaded from the website of Vantage and available at: http://www.vantage-ssa.com/solutions# (accessed on 21.08.2017)

Back cover pictures:

- Photos for the covers of five technical reports that are authored by the author and his supervisor Prof. Dr. Ing Hocine Oumeraci. The summary of these reports constitutes the components of this dissertation. The reports are cited in the references of this dissertation.
- The first page of two journal papers that are published from this dissertation during the PhD programme.

For a proper citation of this dissertation, the preferred way is:

Elsayed, S. M. (2017): Breaching of Coastal Barriers under Extreme Storm Surges and Implications for Groundwater Contamination. PhD dissertation, Leichtweiß-Institute for Hydraulic Engineering and Water Resources, Technische Universität Braunschweig, Braunschweig, Germany, 208 p, Published by Universitätsbibliothek Braunschweig.

"When a man/woman dies, his/her deeds come to an end except for three things:

ceaseless charity,

a knowledge which is beneficial,

a virtuous descendant who prays for him."

Prophet Muhammad

Acknowledgements

First and foremost, I would like to express my deep thankfulness to my supervisor Prof. Dr.-Ing. Hocine Oumeraci. I appreciate all his contributions of time and ideas to make my PhD experience creative and professional. His wide knowledge and logical way of thinking have been of great value for me. Moreover, his understanding, encouraging and personal guidance have provided a good basis for the present dissertation. I also greatly appreciate the effort of Professor Holger Schüttrumpf and Professor Jochen Aberle in reviewing the manuscript and providing me with valuable comments.

I gratefully acknowledge the funding sources that made my PhD work possible. My PhD was funded by the German Academic Exchange Service (DAAD) and the German Federal Ministry for Economic Cooperation and Development (BMZ) in the frame of the Exceed-Swindon Project at Technische Universität Braunschweig. This support is gratefully acknowledged. I gratefully thank the Lower Saxony Water Management, Coastal Protection and Nature Conservation Agency (NLWKN) as contracting authority for making the GWK model tests data for Wangerooge for this research project available. With this in mind, I would especially like to acknowledge Mr Frank Thorenz the director of the Norden-Norderney division in NLWKN for his permission to use their own data for Wangerooge tests. I also appreciate the help of Dr. Robert McCall, who made the pre- and post-storm LIDER data for the Santa Rosa Island available for me. The data for the case study of near Bremerhaven is gratefully obtained from Prof. Dr. Thomas Graf and Dr. Jie Yang.

My wonderful colleagues at the Leichtweiß-Institute in Braunschweig, at the Coastal Research Centre (FZK) in Hannover and at University of Florence (Italy) have contributed immensely to my personal and professional time. The group has been a source of friendships as well as good advice and collaboration. I would especially like to acknowledge Prof. Dr. Andreas Haarstrick, Mrs Gabriele Fournier, Mrs Doris Hellmann, Mr Rainer Kvapil, Dr Stefan Schimmels, Dr Markus Brühl, Dr Agnieszka Strusińska-Correia, Dr Hisham Elsafti, Dr Lisham Bonakdar, Dr Michele Bendoni and Mr Moin Mojabi for their kind advice and collaboration.

The Egyptian scientific community in Braunschweig has also contributed to my personal and professional time, especially Dr. Nasser Hemdan and Dr. Mahmoud Saad, through the organised workshops and scientific meetings.

Lastly, I would like to thank my family for all their love and encouragement, especially my parents who raised me with unconditional love and supported me in all my pursuits, my elder brother Dr Adel M. Elsayed and my wife Doaa Abdelaziz who always gave me supportive and encouraging advice. I dedicate this work to the memory of my mother and to my daughter Arig.

Saber M. Elsayed
Braunschweig, 2017

Abstract

Coastal floods induced by a coastal barrier breaching under extreme storm surges represent a significant humanitarian, socioeconomic and ecological hazard. Moreover, it is a multiscale problem governed by complex interactions between a variety of hydrodynamic and sediment-related processes at different spatiotemporal scales. With global warming and expected climate change, many coastal systems may experience accelerated coastal erosion, coastal barrier breaching, coastal flooding and subsequent seawater intrusion into fresh groundwater. However, the current models of breaching-induced coastal floods and subsequent saltwater intrusion are mainly based on modelling each of these processes separately, which often leads to unreliable simulations because the mutual interactions among these naturally successive processes are ignored. Therefore, to consider such interactions, this study aims at exploring the possibility to simulate breaching, flooding and saltwater intrusion in a single model system in order to reliably draw the implications of coastal floods for groundwater contamination. For this purpose, this study aims first at selecting a suitable breaching model that can properly calculate inland discharges through breaching induced inlets. Second, the study attempts to couple the selected breaching model with suitable inundation and saltwater intrusion models in order to simulate successively the breaching-induced inundation and the subsequent saltwater intrusion.

For these specific purposes, this study starts with a comprehensive literature review of the causes and forms of coastal erosion and barrier breaching. The latter results in a summary of the reasons and components of extreme sea levels during extreme storm surges and how these extreme sea levels interact with coastal barriers until causing their damage and inducing full breaching. Therefore, hydrodynamic processes that might initiate a breach from the seaside and landside are highlighted. In addition, the geomorphological processes that might deepen and widen the initiated breach are addressed. Thereby, the state of the art breaching models are examined in order to select the most appropriate model for further analysis. As a result, the XBeach model is selected. The identified limitations of XBeach are then discussed, showing that XBeach overestimates coastal erosion and thus breaching dimensions for high overtopping rates and high flow velocities. Thus, two model limitations related to the sediment stirring in XBeach are selected as the model limitations that need to be urgently addressed in order to predict adequate breaching dimensions and reliable inland discharges through breach-induced inlet(s). Such a comprehensive literature review includes also a summary of the possible consequences of breaching-induced floods, especially for coastal aquifer contamination by salt water. Moreover, the review of the state of the art modelling tools for predicting coastal flood extent, water depths and associated kinematics showed that the current approach for breaching-induced flood is still based on modelling these two processes separately. Thus, combined modelling of these two processes using XBeach is suggested. The review, in addition, showed that the most recent studies on storm-driven salt water intrusion lack proper modules to simulate the processes leading to coastal floods (e.g. overtopping, breaching). Thus, XBeach is introduced, after the suggested improvements and extensions, as the most suitable model to perform the coupling among the involved processes.

In order to examine the performance of XBeach before any extension or development, it is preliminarily applied to reproduce 17 large-scale laboratory tests that were performed in 2013 in the large-scale flume (GWK) of the Coastal Research Centre (FZK) in Hannover to simulate the coastal dune erosion at the western coast of Wangerooge Island (northern Germany). The numerical results showed that XBeach overestimates dune erosion. Moreover, such overestimation increases dramatically with significant overtopping rates on coastal barriers. As a result, this step confirmed the urgent necessity of the pre-selected two model improvements related to the sediment stirring in XBeach. These improvements are related to (i) the wave nonlinearity effect on sediment transport, which is described in XBeach by a calibration factor for the time-averaged flow depending on the wave skewness and asymmetry and (ii) the considerable excess of the actual shear stress required to initiate the sediment particle motion as compared to that predicted by the common Shields criterion. As a first step toward improving the prediction capability of XBeach, a novel formula is developed that predicts the calibration factor for the time-averaged flow depending on the wave nonlinearity. On the other side, this study introduces a novel approach to account for the grain-stabilization effect in reducing

sediment transport and coastal erosion in compacted to highly compacted soils. These two improvements are implemented in XBeach and the improved model is then very successfully tested for dune erosion, for barrier breaching as well as for a barrier island overwash under an extreme storm surge event. Particularly, the second model improvement opens the way toward further improvements to account for spatially varying soil resistance, which is crucial for a reliable prediction of breach locations along the barrier.

In a further step, this study has shown that the scope of XBeach, initially developed for near shore hydrodynamic processes and associated morphodynamics, can be extended for coastal inundation, so that XBeach can be used to simulate both barrier breaching and subsequent hinterland inundation in a single model system. In addition, the study has examined the feasibility of using the groundwater module of XBeach to simulate the vertical salt water intrusion induced by coastal inundation. The latter step aimed at examining the feasibility of simulating the breaching, induced inundation and subsequent saltwater intrusion in a single model system that considers the mutual interaction among the involved processes so that the outcomes of one process is "automatically" transferred to the next model. Regarding the feasibility of using XBeach as a salt water intrusion model, it was shown that XBeach still needs to account for the advection-dispersion of density dependent transport. Thus, at this stage, a separate modelling of the flood-induced salt water intrusion using Visual Modflow/SEAWAT was found as the most feasible alternative.

As coastal flooding is one of the major threats to groundwater quality in coastal aquifers, the study has also addressed this issue, its implications for sustainable development in coastal zones and the current modelling approaches. Moreover, the common structural approaches to mitigate saltwater intrusion are also summarised. None of these measures is suitable for mitigating vertical salt water intrusion. Therefore, the study suggested using subsurface drainage network so that percolating salt water might be drained before contaminating the aquifer.

To highlight the value of the study outcomes, the modelling system applying the improved XBeach to simulate both inland discharges and induced hinterland inundation in addition to Visual Modflow/SEAWAT to simulate the subsequent saltwater intrusion is used to draw the implications of possible coastal flood near Bremerhaven, northern Germany. The outcome of this case study showed that a flood event for 2.8 hours might contaminate the aquifers near Bremerhaven so that they might remain contaminated for around 45 years, i.e. until they get remediated naturally. The application of the subsurface drainage system shortens the latter interval to three years and prevents the contamination of the deeper aquifers.

Finally, the new contributions of the study and the lessons learnt from the case study are summarised and further improvements are suggested.

Keywords: Combined modelling; Breaching of coastal barriers; Coastal inundation; Storm-driven salt water intrusion; Coastal aquifers; Contamination; Mitigation measures.

Kurzfassung

Überflutungen im Küstenraum, die durch den Bruch von Küstenbarrieren infolge extremer Sturmfluten verursacht werden, stellen aus humanitärer, sozioökonomischer und ökologischer Sicht eine bedeutende Gefährdung dar. Darüber hinaus stellen sie ein Multiskalenproblem dar, das durch komplexe Wechselwirkungen zwischen einer Vielzahl hydrodynamischer und sedimentbezogener Prozesse in verschiedenen räumlich-zeitlichen Skalen charakterisiert wird. Mit den Folgen des Klimawandels werden an vielen Küsten beschleunigte Küstenerosion, Brüche von Küstenbarrieren, Überflutungen und anschließende Salzwasserintrusion in frisches Grundwasser erwartet. Allerdings basiert die bisherige Modellierung von bruchbedingten Küstenfluten und anschließender Salzwasserintrusion hauptsächlich auf der separaten Modellierung jedes dieser Prozesse, was oft zu nicht belastbaren Simulationsergebnissen führt, da dabei die entsprechenden Wechselwirkungen unberücksichtigt bleiben. Um diese gegenseitigen Interaktionen zwischen diesen natürlich aufeinanderfolgenden Prozessen zu berücksichtigen, zielt diese Studie darauf ab, die Machbarkeit der Kopplung dieser drei Prozesse in einem einzigen Modellsystem zu analysieren. Dadurch können die Auswirkungen von Küstenfluten auf die Grundwasser-Kontamination durch Salzwasser verlässlich ermittelt werden. Zu diesen Zwecken zielt diese Studie zunächst darauf ab, ein geeignetes Bruchmodell auszuwählen, das den Durchfluss ins Hinterland (durch die Bruchstelle) zuverlässig berechnen kann. Zweitens wird in dieser Studie versucht, das ausgewählte Bruchmodell mit geeigneten Überflutungs- und Salzwasserintrusionsmodellen zu koppeln, um nacheinander die bruchbedingte Überflutung und die anschließende Salzwasserintrusion zu simulieren.

Um die letzteren Ziele zu erreichen, wird zunächst mit einer umfassenden Literaturrecherche über Ursachen und Formen der Küstenerosion und Barrieren-Brüche begonnen. Dies resultiert in eine Zusammenfassung der Ursachen und Komponenten extremer Wasserspiegel bei extremen Sturmfluten und darüber, wie diese Komponente mit Küstenbarrieren interagieren und schließlich zu Barrieren-Brüche führen. Deshalb werden die hydrodynamischen Prozesse besonders unterstrichen, die einen Bruch auf der Seeseite bzw. auf der Landseite der Küstenbarriere einleiten können. Darüber hinaus wird auch auf die geomorphologischen Prozesse eingegangen, die den eingeleiteten Bruch vertiefen und erweitern können. Dabei wird der aktuelle Stand der vorliegenden Bruchmodelle analysiert, um das am besten geeignete Modell für die weiteren Untersuchungen zu identifizieren. Als Ergebnis wird das XBeach-Modell ausgewählt. Die identifizierten Einschränkungen von XBeach werden diskutiert. Dabei wird gezeigt, dass XBeach die Küstenerosion, und folglich auch die Abmessungen der Bruchstelle, bei sehr hohen Überlaufraten und Strömungsgeschwindigkeiten überschätzt. Somit werden zwei Modelleinschränkungen, die sich auf die Sediment-Verwirbelung in XBeach beziehen, als die Modelleinschränkungen ausgewählt, auf die dringend eingegangen werden muss, um belastbare Ergebnisse hinsichtlich der Abmessungen der Bruchstelle und der Durchflüsse ins Hinterland zu erzielen. Eine solche umfassende Literaturrecherche beinhaltet auch eine Zusammenfassung der möglichen Konsequenzen von bruchbedingten Überflutungen, insbesondere bei der Grundwasser-Kontamination durch Salzwasser. Darüber hinaus zeigte die Überprüfung der derzeitigen Modelle zur Vorhersage des Umfangs, der Wassertiefen und der Kinematik von Überflutungen im Küstenraum, dass die bisherige Modellierung bruchbedingter Überflutungen immer noch auf der separaten Modellierung des Barrieren-Bruches und der daraus resultierenden Überflutung des Hinterlands basiert. Daher wird in dieser Studie eine kombinierte Modellierung dieser beiden Prozesse mit XBeach vorgeschlagen. Die Überprüfung zeigte darüber hinaus, dass die jüngsten Studien über Sturmflut-bedingte Salzwasserintrusion keine Module für die Simulation der Prozesse aufweisen, die zur Überflutung führen können. So wird XBeach nach den vorgeschlagenen Verbesserungen und Erweiterungen als das geeignetste Modell hinsichtlich der Kopplung zwischen den beteiligten Prozessen angesehen.

Um die Leistungsfähigkeit von XBeach vor jeglicher Erweiterung oder Entwicklung zu analysieren, werden vorläufig 17 großskalige Modellexperimente über Dünenerosion an der Westküste der Insel Wangerooge, die 2013 im Großen Wellenkanal (GWK) des Forschungszentrum Küste (FZK) in Hannover durchgeführt wurden, numerisch reproduziert. Die Simulationsergebnisse zeigten, dass XBeach die Küstenerosion überschätzt. Darüber hinaus steigt diese Überschätzung dramatisch mit höheren Überlaufraten der Küstenbarrieren. Dadurch wird die dringende Notwendigkeit der vorgewählten zwei Modellverbesserungen hinsichtlich der Sediment-Verwirbelung bestätigt. Diese Verbesserungen beziehen sich auf (i) den Effekt der Nichtlinearität der Wellen auf den Sedimenttransport, der in XBeach durch einen Kalibrierungsfaktor für die zeitlich gemittelte Strömung in Abhängigkeit von der Schiefe und der Asymmetrie der Wellen beschrieben wird und (ii) der beträchtlichen Überschätzung der tatsächlichen Schubspannung für den Beginn der Sedimentpartikelbewegung im Vergleich zum kritischen Wert nach dem Shields-Kriterium. Als erster Schritt zur Verbesserung der Vorhersagefähigkeit von XBeach wird eine neue Formel entwickelt, die den Kalibrierungsfaktor für die zeitlich gemittelte Strömung in Abhängigkeit von der Wellen-Nichtlinearität prognostiziert, basierend auf Datensätzen, die aus früheren Studien zusammengestellt wurden. Außerdem wird ein neues Verfahren zur Berücksichtigung der Kornstabilisierung für

die Reduzierung des Sedimenttransports und der Küstenerosion in verdichteten bis stark verdichteten Böden vorgeschlagen. Diese beiden Verbesserungen werden in XBeach implementiert; das verbesserte Modell wird dann für Dünenerosion, für den Bruch von Küstendünen und für den Überlauf von Barriereinseln unter extremen Sturmfluten erfolgreich getestet. Insbesondere die zweite Modellverbesserung eröffnet den Weg zu weiteren Modellverbesserungen hinsichtlich der Berücksichtigung einer räumlichen Veränderung der Widerstandseigenschafen des Bodens, was für eine zuverlässige Vorhersage der Lokation möglicher Bruchstellen entlang der Küstenbarriere entscheidend ist.

In einem weiteren Schritt wird gezeigt, dass der Anwendungsbereich von XBeach, das ursprünglich für küstennahe hydrodynamische Prozesse und der damit verbundenen Morphodynamik entwickelt wurde, auch für Küstenüberflutungen erweitert wird. Somit kann XBeach verwendet werden, um den Bruch von Küstenbarrieren und die anschließende Überflutung des Hinterlands in einem einzigen Modell zu simulieren. Darüber hinaus wird die Anwendbarkeit des Grundwasser-Moduls von XBeach zur Simulation der vertikalen Salzwasserintrusion bei Überflutung des Hinterlands betrachtet. Der letztgenannte Schritt zielte darauf ab, den Bruch, die induzierte Überflutung und die anschließende Salzwasserintrusion in einem einzigen Modellsystem zu simulieren. Dadurch wird die Wechselwirkung zwischen den beteiligten Prozessen berücksichtigt, so dass die Ergebnisse eines Modells „automatisch“ zum nächsten Modell übergeben werden. Dennoch zeigte sich, dass XBeach noch nicht zur Simulation der Salzwasserintrusion verwendet werden kann. Hierfür muss noch die Advektion-Dispersion des dichteabhängigen Transports in XBeach berücksichtigen werden. Daher wird derzeit eine separate Modellierung der überflutungsbedingten Salzwasserintrusion mit Visual Modflow/SEAWAT als bestgeeignete Alternative herausgestellt.

Da die Überflutung im Küstenraum eine der größten Gefährdungen für die Grundwasserqualität der Küstenaquifere darstellt, wird in dieser Studie auch auf diesen Aspekt sowie auf die Implikationen für eine nachhaltige Entwicklung in den Küstengebieten und auf die derzeitigen Modellierungsansätze eingegangen. Darüber hinaus werden auch die aktuellen strukturellen Maßnahmen zur Reduzierung der Salzwasserintrusion zusammenfassend diskutiert, um festzustellen, dass keine dieser Maßnahmen für die vertikale Salzwasserintrusion geeignet ist. Daher wird ein unterirdisches Entwässerungssystem vorgeschlagen, das das sickernde Salzwasser dräniert, bevor es den Grundwasserleiter verunreinigt.

Um die Bedeutung der Ergebnisse dieser Studie hervorzuheben, wird, zusätzlich zum verbesserten XBeach Modellsystem für die Simulation der Durchflüsse ins Hinterland und der induzierten Überflutung, das Modellsystem Visual Modflow/SEAWAT zur Simulation der nachfolgenden Salzwasserintrusion eingesetzt. Anschließend werden die Implikationen aus einer möglichen Küstenüberflutung in der Nähe von Bremerhaven gezogen. Das Ergebnis dieser Fallstudie zeigte, dass ein Hochwasserereignis von 2,8 Stunden die Grundwasserleiter in der Nähe von Bremerhaven verunreinigen könnte, so dass sie etwa 45 Jahre lang verunreinigt bleiben würden, d.h. bis zur natürlichen Wiederherstellung des ursprünglichen Zustands. Durch das unterirdische Entwässerungssystem wird letzteres Intervall auf drei Jahre verkürzt; zugleich wird die Verunreinigung der tieferen Grundwasserleiter verhindert.

Abschließend werden die erzielten neuen Beiträge, die Lehren aus der Fallstudie bei Bremerhaven sowie Empfehlungen für mögliche zukünftige Verbesserungen zusammenfassend dargestellt.

Schlüsselwörter: Kombinierte Modellierung; Bruch von Küstenbarrieren; Küstenüberflutung; Sturmflut-bedingte Salzwasserintrusion; Küstenaquifere; Salzwasserkontamination; Minderungsaßnahmen.

Abstract (Arabic)

"إختراق الحواجز الساحلية تحت تأثير العواصف البحرية الهوجاء و آثار ذلك علي تلوث المياه الجوفية"

تقدم هذه الأطروحة دراسة شاملة لمُسببات إختراق الحواجز البحرية تحت تأثير ارتفاع منسوب مياه البحر أثناء العواصف البحرية القوية. كذلك تقدم هذه الدراسة طرق النمذجة الرقمية لمثل هذه الإختراقات بالإضافة إلي نمذجة كلا من الفيضانات الناجمة عنها وما قد تسببه من تسرب للمياه المالحة خلف الحواجز المُخترقة إلي الخزان الجوفي. تهدف هذه الأطروحة إلي نمذجة كلا من إختراق الحواجز الساحلية والفيضان الساحلي الناتج عنه بالإضافة إلي تسرب مياه الفيضان المالحة إلي الخزان الجوفي في نموذج عددي (رقمي) واحد أو علي الأقل بشكل متكامل بحيث يمكن الأخذ في الإعتبار التفاعلات المتبادلة بين هذه العمليات المتتالية.

تعتبر نمذجة إختراق الحواجز الساحلية من أكثر التحديات ، وخصوصا بعد التغيرات المناخية المُلاحظة والمُسجلة ، لما لها من أبعاد متعددة وإشتمالها علي عدة تفريعات منها: تفاعل الحمل الهيدروليكي مع الحواجز حال إرتفاع منسوب مياه البحر أثناء العاصفة ، و إنتقال الرواسب الناتجة عن هذا التفاعل وما يصحبه من تغيرات مورفولوجية ، بالإضافة إلي إنزلاقات التربة من أمام و من علي جانبي الإختراقات. وفي هذا السياق قامت الدراسة بتقديم تطويرين جديدين لبرنامج حساب التغيرات المورفولوجية "XBeach" ، والذي أنتجته جامعة Delft الهولندية بدعم مالي من منظمة اليونيسكو وآخرين ، كي يتمكن البرنامج من حساب التغيرات المورفولوجية والإختراقات الناجمة عن العواصف بشكل صحيح. كما قامت الدراسة بتطوير إستخدام البرنامج ذاته في حساب حركة الفيضانات الناتجة عن العواصف البحرية دون الحاجة إلي نموذج عددي منفصل لنمذجة الفيضانات الساحلية. بالإضافة إلي ذلك تقدم الأطروحة ملخص وافي و مختصر عن تأثير الفيضانات الساحلية علي المياه الجوفية وأثر ذلك علي خطط التنمية المستدامة في المناطق المعرضة لفيضانات ساحلية. كما تقدم تطبيق علي حالة دراسة قريبة من مدينة Bremerhaven شمالي المانيا. يشمل هذا التطبيق نمذجة لشبكة صرف مغطي لإمتصاص المياة المالحة قبل وصولها إلي المياه العذبة في الخزان الجوفي و تلويثها ، والتي قد تظل ملوثة بتركيزات ملحية عالية لفتره تزيد علي العشرين عاما حال عدم إستخدام هذا الحل لدرئ مثل هذا التسرب وتخفيف أثره.

في الفصل الاول من الأطروحة تم إيجاز دوافع الدراسة وأهدافها بالإضافة الي سبل الوصول لهذه الأهداف. وبناءاً عليه يقدم الفصل الثاني عرض لمكونات وأسباب إرتفاع منسوب مياه البحر أثناء العواصف وأثر ذلك علي تآكل الشواطيء والحواجز البحرية. بالإضافة إلي ذلك تستعرض الدراسة المسببات المختلفة التي قد تؤدي إلي إختراقاً او أكثر في مثل هذه الحواجز. وكنتيجة لذلك إستعرضت الدراسة كافة أنواع النماذج العددية المتاحة لنمذجة تآكل الشواطئ وما قد يتبعه من إختراقات ، بناءاً علي ذلك تم اختيار برنامج "XBeach" كأفضل برنامج في هذا الصدد.كما شملت بداية الأطروحة أيضا علي إستعراض للتوابع التي قد تسببها الفيضانات الساحلية بما في ذلك من تلوث للمياه الجوفية. وبناء عليه تم إستعراض أحدث الطرق المستخدمة لنمذجة الفيضانات الساحلية وما قد يتبعه من تسرب للمياه المالحة إلي الخزان الجوفي.

في الفصل الثالث من الدراسة تم إستخدام البرنامج "XBeach" لإعادة إنتاج سبعة عشر تجربة معملية كان قد تم إجرائها في مركز أبحاث الشواطئ بجامعتي هنوفر وبرنشفايج من أجل التأكد من قدرة البرنامج علي نمذجة تآكل الشواطئ وما قد يتبعه من إختراقات للحواجز الساحلية. بمقارنة النتائج المعملية مع مخرجات البرنامج ثَبُت أن البرنامج يعطي قيم أكبر للتآكل، وتزداد هذه القيم بشكل مطرد مع زيادة إرتفاع منسوب المياه وما يتبعه من زيادة قيم إرتفاعات الأمواج أعلي الحواجز.

كي يتم معالجة هذا السلوك تم في الفصل الرابع من الأطروحة إكتشاف وصياغة معادلات رياضية لسببين فيزيائيين كانا هما السبب في عدم دقة حسابات البرنامج: السبب الأول يرجع إلي عدم قدرة البرنامج علي تمثيل دور عدم خطية الأمواج القريبة من الشاطئ علي إنتقال الرواسب بشكل صحيح ، أما السبب الثاني يرجع إلي عدم أخذ عوامل ترابط حبيبات التربة وتماسكها في الاعتبار. تم برمجة التعديلات المقترحة داخل البرنامج وإعادة الحساب بالبرنامج المعدل للتأكد من جدوي التعديلات المقترحة من خلال إعادة انتاج بعض التجارب المعملية السابق ذكرها بالإضافة إلي حالتي تآكل و اختراق حقليين. وقد ثبت بناء علي هذا أن التعديلات المضافة قد حسنت بشكل كبير من أداء البرنامج بحيث أصبح قادراً علي إجراء الحسابات بشكل أدق.

تم في الفصل الخامس إستخدام البرنامج المُطور لنمذجة كلا من الفيضانات الساحلية مع الإختراقات المسبب لها في نموذج واحد وهو ما يعتبر إسهاماً كبيراً لهذه الدراسة كونها أثبتت أن برنامج ك "XBeach" مُعد خصيصاً لحساب التآكلات والإختراقات الساحلية يمكنه أيضا حساب جريان مياه الفيضانات في المناطق الساحلية. تم إثبات ذلك بمقارنة الصيغ الرياضية لبرنامج "XBeach" مع الصيغ الرياضية لبرامج معدة خصيصاً لحساب جريان مياه الفيضانات كبرنامج "HEC-RAS" وبرنامج "River-2D". بالإضافة إلي المقارنة السابقة تم تطبيق البرامج الثلاثة علي حالتي دراسة إصطناعيتين بالإضافة إلي حالة دراسة واقعية. أثبتت الدراسة في هذه الخطوة أن إستخدام برنامج "XBeach" لنمذجة

الإختراقات و الفيضانات الناجمة عنها أكثر دقة من طرق النمذجة السابقة والتي عادة ما تستخدم نموذجين مختلفين لمثل هذا الغرض.

في الفصل السادس ولكون الفيضانات الساحلية أصبحت من أقوي المُهددات لجودة وعذوبة المياة الجوفية بالمناطق الساحلية وما قد يتبع ذلك من تأثيرات علي تنمية مثل هذه المناطق حال تلوث خزاناتها الجوفية بمياة الفيضانات الساحلية والتي قد تتسرب رأسياً لتلوث مثل هذه الخزانات وتزيد ملوحتها ،يقدم هذا الفصل دراسة وافية في هذا الشأن تشمل البرامج العددية المستخدمة و أوجه إستخدام كل منها بالإضافة إلي طرق مكافحة ودرئ تسرب المياه الجوفية. هذه المرحلة من الدراسة أوضحت أن برنامج "XBeach" لازال بحاجة إلي مزيد من التطوير حتي يمكنه أيضا نمذجة تسرب المياه المالحة بإستخدام قسمه المُخصص لنمذجة حركة المياه الجوفيه. لذلك تم إستخدام برنامج " Visual Modflow/SEAWAT" لحساب تسرب مياه الفيضان المالحة إلي المياه الجوفية العذبه. بالإضافة إلي ذلك تم اقتراح عمل شبكة صرف مغطي بالمناطق المُحتمل تعرضها لفيضانات ساحلية حتي يمكنها - بجانب تحسين ألحصيلة الزراعية في غير أوقات الفيضان - سحب المياه المالحة المتسربة قبل وصولها إلي المياه العذبة وتلويثها في أوقات الفيضان.

لإثبات واقعية الدراسة وأهميتها تم في الفصل السابع تطبيق مخرجات الأطروحة علي حالة دراسة شمالي ألمانيا بالقرب من مدينة Bremerhaven حيث تم إستخدام برنامج "XBeach" لحساب تصرفات المياه من فوق حاجز ساحلي مطل علي بحر الشمال نتيجة إرتفاع مُفترض في منسوب مياه البحر أثناء عاصفة بحرية وفي الوقت ذاته يقوم نفس البرنامج بحساب حركة الفيضان في المنطقة الساحلية خلف الحاجز. وبناء عليه تم استخدام "SEAWAT " لنمذجة تسرب مياه الفيضان إلي الخزان الجوفي . ثَبُت من خلال ذلك أن الفيضان الساحلي قد يُسبب تلوث للخزان الجوفي لمدة تصل الي خمسة وأربعون عاماً بعد الفيضان حتي يمكن إعادة ضخ مياه صالحة للإستخدام الآدمي طبقا لمواصفات منظمة الصحة العالمية من مثل هذه الخزانات الجوفية. ولتقليل هذه الفتره ثَبُتَ أن إستخدام شبكة صرف مغطي قد يقلل الفتره السابقة إلي ثلاث سنوات فقط مع عدم تسرب المياة المالحة إلي أعماق كبيره في الخزان الجوفي.

وفي النهاية قدمت الدراسة مُلخص لما تم إنجازه من تطويرات في مجال تآكل الشواطيء ونمذجتها وما يتبعه من إختراق للحواجز الساحلية و مجال نمذجة حركة الفيضانات الساحلية بالإضافة إلي مجال تسرب الملوثات إلي المياه الجوفية. كما قدمت الأطروحة إقتراحات للنقاط البحثية التي يجب الاهتمام بها مستقبلاً حتي يمكن تحسين نتائج الدراسة وطرق النمذجة.

Table of contents

Acknowledgements ii
Abstract iii
Kurzfassung v
Abstract (Arabic) vii
Table of contents ix
List of figures xiii
List of tables xxi
Nomenclature xxiii
Abbreviations xxvii
1 Introduction 1
1.1 Problem statement and motivations 1
1.2 Objectives 3
1.3 Methodology and organisation of the thesis 3
2 Review and analysis of current knowledge and modelling tools 5
2.1 Brief overview of storm surges 6
2.1.1 Components of a storm surge 6
2.1.2 Classification of extreme sea level components 7
2.2 Breaching of coastal barriers under extreme storm-tides 9
2.2.1 Breach initiation and relevant hydrodynamic processes 9
2.2.2 Breaching development and related geomorphological processes 14
2.3 Classification of available breaching models 16
2.4 The XBeach model 18
2.4.1 Identification, modes and components of the XBeach model 18
2.4.2 Brief overview of model formulation 20
2.5 XBeach limitations and recent model developments 22
2.5.1 Limitations related to barrier material 22
2.5.2 Limitations related to bed friction 23
2.5.3 Vegetation effect on coastal erosion and sediment entrainment 23
2.5.4 Limitations related to depth-averaged computations 24
2.5.5 Limitations related to phase-averaged computations 24
2.5.6 Overestimation of erosion rates for high flow velocity regimes 25
2.5.7 Limitations related to grain-stabilisation and soil compaction 26
2.5.8 Limitations related to longshore variability of soil strength 27
2.6 Coastal floods induced by barrier breaching 29
2.6.1 Consequences of coastal floods caused by barrier breaching 29
2.6.2 Current modelling approaches of a coastal flood 30
2.7 Breaching-induced salt water intrusion 32
2.8 Specification of objectives and methodology for the PhD study 35
2.8.1 Summary of knowledge gaps and research needs 35
2.8.2 Specification of objectives 37
2.8.3 Specification of methodology 39
3 Investigation of the XBeach model performance using GWK-tests 41
3.1 Description of the GWK-tests 41
3.2 Physical model setup in GWK 43
3.3 Numerical model setup 45
3.4 Assessment of XBeach performance based on simulations outcomes 46
3.5 Summary and discussion of the results 49
4 Improvement of sediment stirring modelling in XBeach 51
4.1 Theoretical background of sediment transport calculations in XBeach 52

4.1.1 Sediment transport formulation in the current XBeach model 52
4.1.2 Effect of wave nonlinearity on sediment transport in the current XBeach model 54
4.1.3 Effect of onset of sediment motion on over-predicted erosion in the current XBeach model 55
4.2 Proposed improvements for sediment stirring calculations in XBeach 56
4.2.1 Bed slope effect on wave nonlinearity and sediment transport 56
4.2.2 Grain-stabilization effect on the inception of sediment motion 58
4.3 Test cases for model validation 60
4.3.1 Large-Scale Dune Erosion Tests in GWK 60
4.3.2 Zwin Dam Breaching Test 62
4.3.3 Dune overwash and erosion at Santa Rosa Island 64
4.4 Summary, discussion and implications of the results 69
5 Combined modelling of coastal barrier breaching and inundation using the improved XBeach code 71
5.1 Equations/assumptions underlying flood propagation models 72
5.1.1 1D inundation models 72
5.1.2 2D inundation models 73
5.1.3 XBeach as an inundation model 73
5.2 Validation of XBeach as a 1D inundation model using a synthetic cross-shore profile 76
5.2.1 Test programme and validation procedure 76
5.2.2 Validation results 78
5.3 Validation of XBeach as a 2D inundation model using 2D synthetic coastal zone 84
5.3.1 Test programme and validation procedure 84
5.3.2 Validation results 86
5.4 Validation of XBeach using the real dam breaching case of Het Zwin 92
5.4.1 Test programme and validation procedure 92
5.4.2 Validation results 93
5.5 Summary, discussion and implications of the results 96
6 Implications of coastal floods for groundwater contamination: Modelling scenarios and mitigation measures 101
6.1 Modelling of water flow and contaminant transport in porous media 102
6.1.1 Flow in the unsaturated zone above the phreatic line 103
6.1.2 Flow in the aquifer zone beneath the phreatic line 104
6.1.3 Contaminant transport in porous media 105
6.2 Brief overview of groundwater models for contaminant transport 106
6.3 Brief review of storm-driven salt water intrusion modelling studies 108
6.4 Coupling scenarios for breaching, inundation and saltwater intrusion modelling 114
6.5 Management of storm-driven salt water intrusion 116
6.6 Summary and discussion of the results 119
7 Modelling and mitigating flood-induced saltwater intrusion near Bremerhaven using XBeach and SEAWAT 121
7.1 SEAWAT/Visual Modflow 121
7.2 Study area and available data 122
7.2.1 Aquifer parameters 123
7.2.2 Storm surge scenario 124
7.3 Combined modelling of water overtopping and induced flood propagation 125
7.3.1 Model set-up in XBeach 125
7.3.2 Role of bed friction and hinterland topography 128
7.3.3 Outcomes of the combined modelling of overtopping flow and inundation using XBeach 129
7.4 Modelling storm-driven saltwater intrusion near Bremerhaven using SEAWAT 130

7.4.1 Modelling hypotheses and conceptual SDSWI model for the selected site 130
7.4.2 Numerical model setup in Visual Modflow 132
7.4.3 Modelling pre-storm conditions 133
7.4.4 Modelling storm and post-storm conditions 137
7.5 Subsurface drainage effect on coastal aquifers resilience against coastal floods 143
7.5.1 Model set up and parametrization for the aquifer with subsurface drainage in Visual Modflow 145
7.5.2 Subsurface drainage effect on water flow in Bremerhaven aquifer 146
7.5.3 Subsurface drainage effect on saltwater intrusion to the aquifer near Bremerhaven 147
7.6 Summary and discussion of the results 151
8 Summary, concluding remarks and outlook 153
8.1 Novel contributions of the PhD study 154
8.2 Summary of main results and conclusions 154
8.3 Recommendations for practical applications 156
8.4 Limitations of the results and implications for future research 156
Bibliography 159

List of figures

Fig 1.1: Flow domains for seawater during an extreme storm surge event: (a) waves are driven by wind toward the shoreline and may overtop and/or breach the protective dune [voices.nationalgeographic.com], (b) subsequent wave action during storm surges might induce a barrier breach (De Vet 2014), (c) breaching of coastal barriers allows seawater to propagate in the hinterland [www.dutchwatersector.com], and (d) propagating seawater percolates vertically to fresh groundwater causing its contamination (Yang et al. 2013)..... 2
Fig 1.2: Tentative methodology of the research consisting of seven successive phases. 4
Fig 2.1: Processes involved in breaching of coastal barriers and subsequent groundwater contamination: storm surges represent the hydraulic load that might result in breach initiation and development. Through the breach induced inlet, inland sea water flow will thus propagate in the hinterland. During and after flood propagation, salt water infiltrates to fresh groundwater, causing its contamination. 5
Fig 2.2: Definition sketch of storm surge: sea water level (SWL) temporally rises during storms, mainly induced by extreme winds and a storm accompanying low pressure, to reach the surge level. Thus, shortwaves riding on the surge level start to hit the protective coastal barriers (e.g. dunes). 6
Fig 2.3: Main components interacting for the generation of extreme water levels during a storm surge event: astronomical tides represent a deterministic component while metrological components (e.g. wind, barometric and wave setups) represent stochastic components. Climate-change-induced sea level rise represents an example of long-term components (Tayel and Oumeraci 2015)..... 7
Fig 2.4: Vertical cross-section of a schematic sea/land boundary. Drawn in the figure are symbols representing low pressure out at sea, extreme winds over the sea, breaking surf waves, and indications for wave setup and wave run-up in the coastal area. Tide marks are drawn indicating the different tide heights under different scenarios: Mean sea level (MSL), expected high tide, storm surge, wave setup and wave runup (Mullan et al. 2005)..... 8
Fig 2.5: Possible scenarios for the total sea level during a storm surge: (a) during normal conditions (no setup), (b) under a setup of sea level during a storm surge, short waves hit the protective barrier (dune), (c) with a further setup, short waves may overtop the barrier, and (d) in the extreme situations, seawater overflows the barrier. 8
Fig 2.6: Hydrodynamic processes that may initiate a coastal barrier breach from seaward and landward/bay sides: during a storm-induced sea level rise, barriers become exposed to diverse hydrodynamic processes that may initiate a breach depending on the relationship between the storm-tide level and crest level of the barrier. 9
Fig 2. 7: Series of storm impact regimes as defined by Sallenger (2000): (a) definition of variables used in scaling the impact of storms on barriers, and (b) different storm regimes, after De Vet (2014). 10
Fig 2.8: Hydrodynamic processes that might initiate a breach from the seaward slope of a barrier: (a) breaking wave-induced turbulence due to spilling breakers over a mild slope, (b) breaking wave-induced impact due to plunging breakers over a moderately steep slope, and (c) breaking wave-induced turbulence due to surging and collapsing breakers over a steep slope. Flow velocities induced by wave run-up (upwards) and wave rundown (downwards) contribute with breaking wave effects in a breach initiation from the seaside. Breakers types are often determined depending on the surf similarity parameter, which is a function of the breach slope β, wave height H, and wavelength L0, after Oumeraci (2017). Numbers (1-9) indicate wave propagation direction and relevant waveform/shape during propagation from offshore indicated by 1 to onshore indicated by 7, 9 and 6 in (a), (b) and (c), respectively.... 11

Fig 2.9: Barrier erosion from the seaside during a storm surge event: During a storm surge, sea level rises temporally and hence barriers become subject to successive impacts by breaking waves in addition to successive wave run-up and run-down, after Van Thiel de Vries (2009).....11
Fig 2.10: Types of flow over coastal barriers: (a) wave overtopping/overwash which may also occur at local discontinuities or depressions, (b) overflow/inundation which occurs due to high surge level exceeding the barrier crest, (c) combined wave overtopping and surge overflow, after Hughes (2008).....12
Fig 2.11: Erosion of coastal barriers from the landward side owing to combined flow: non-cohesive barriers erode progressively where eroded sediments are relocated in the downstream, after Donnelly et al. (2004).....13
Fig 2.12: Landward barrier breaching induced by seepage and piping: (a) breach initiation, (b) breach development, after Wu et al. (2011).....13
Fig 2.13: Sediment transport modes: bedload, suspended load and sediment sheet flow (De Vet 2014).....14
Fig 2. 14: Soil avalanching: (a) and (b) slumping of barrier slope as water reaches the barrier toe in the collision regime, leaving a dry scarp surface (after Masselink and van Heteren 2014), (c) avalanching of breaching side slopes (after Bakker et al. 1996).....15
Fig 2.15: Hydrodynamic and geomorphological processes related to a breach initiation and development under (a) impact/collision regime, (b) overtopping/overwash regime, and (c) overflow/inundation regime, including the ebbing conditions, after Muller et al. (2016).....16
Fig 2. 16: Classification of breaching models.....16
Fig 2.17: Main modes and components of the XBeach model with objectives of each module. Both hydrostatic and non-hydrostatic modes share the same morphodynamic and groundwater modules, but use different hydrodynamic module.....19
Fig 2. 18: Vegetation role in improving the resilience of coastal barriers: Vegetation increases barrier strength against coastal erosion and breaching (option A). Moreover, aquatic plants reduce the hydraulic load through wave and current attenuation (option B), after Schiereck (2005).....23
Fig 2. 19: Artificial and physically-based sediment transport limiters to reduce the erosion rates over-predicted by XBeach.....25
Fig 2. 20: Schematic representation of the effect of longshore variability of soil strength on barrier breach initiation.....28
Fig 2. 21: Hydrodynamic and sediment-related processes that govern coastal flooding: the upper panel is a cross shore cross-section through a breached barrier showing the flood source (storm surge), the flood pathway (breach) and the flood receptor (hinterland), the lower panel is a plan view shows the spatial scale of the coastal flood (Oumeraci et al. 2015).....29
Fig 2. 22: Implications of breaching-induced coastal inundation for the analysis of subsequent saltwater intrusion: Due to flood propagation, the inundation extents over time. Saltwater infiltrates vertically causing aquifers contamination. Inundation extent (IE) and water depths are important information for the analysis of the SWI.....32
Fig 2. 23: Common reasons and involved processes in saltwater intrusion into fresh coastal aquifers 33
Fig 2. 24: Schematic diagram for the hydrostatic equilibrium between sea and fresh water in a coastal aquifer (U-tube manometer analogy). Seawater (red colour) and freshwater (sky blue colour) meet at the salt-freshwater interface. Water discharge due to overtopping/breaching propagates over the land surface behind the barrier (dyke) and intrudes vertically to the originally fresh groundwater, causing its contamination.....34
Fig 2. 25: Flowchart for processes and planned research tasks in the framework of this study.....38
Fig 2. 26: Specified methodology of the of the PhD study and organisation structure of the rest of the thesis.....39
Fig 3. 1: Wangerooge Island, northern Germany: the western part of Wangerooge is exposed to coastal erosion during extreme storms from the North Sea [https://www.google.de/maps].....41

Fig 3. 2: Revetments at western Wangerooge, in front of a sand dune prone to erosion under extreme storm events.....42
Fig 3. 3: Large Wave Flume (GWK) in Hannover: (a) GWK-test of coastal dune erosion in Wangerooge and (b) wave maker in GWK.....42
Fig 3. 4: Cross-shore profiles tested in GWK (all levels and dimensions are in meters and level 0.00 represents the flume bottom): left panel shows profiles 1 and 2 while right panel shows profiles 3, 4 and 5; differences among profiles in both panels, separately, lie in the offset of the dune front. 43
Fig 3. 5: Physical model setup in GWK: dune extension with a front slope of 1:1 is built behind the revetment crest with (a) no offset for profiles 1 and 3, (b) with offset of 3.33 m width for profiles 2 and 4, and (c) with double offset of 6.66 m width for profile 5. 44
Fig 3. 6: Forms of dune erosion observed in the GWK tests of Wangerooge (Oumeraci et al. 2014). 45
Fig 3. 7: Example of BSS ranges for an exemplary linear profile of one movable end; BSS values and ranges are calculated by considering N = 2. 47
Fig 3. 8: Measured (GWK test 04) and calculated (XBeach test XB3) cross-shore profiles after 6705 s of wave action with a lower overtopping rate qnom = 16.35 l/(s·m); BSS and RMSE are calculated for the cross-shore distance x (76 m ≤ x ≤ 83 m) showing that BSS = 0.915 and RMSE = 0.30 m. 47
Fig 3. 9: Measured (GWK tests 15-17) and calculated (XBeach test XB8) cross-shore profiles after 8908 s of wave action with a higher overtopping rate qnom = 423 l/(s·m); BSS and RMSE are calculated for the cross-shore distance x (70 m ≤ x ≤ 85 m) showing that BSS = 0.68 and RMSE = 0.38 m. 48
Fig 3. 10: Modelled vs observed crest recessions for the GWK tests 01-17 with different overtopping rates (qnom = 1.92 - 423 l/(s.m)) and different dune offsets widths (0 – 6.66 m). 48
Fig 4. 1: Sediment transport under saw-tooth forcing (solid curve) and single sinusoidal forcing (dashed curve) of wave periods T = 6.0 s. (a) free-stream velocity, (b) free-stream acceleration, and (c) non-dimensional bed shear stress (Hsu and Hanes 2004).....54
Fig 4. 2: Relation between the average seaward slope steepness and facua parameter.....57
Fig 4. 3: Shields threshold criterion plotted against grain Reynolds Number for Turkey Brook. Initial and final motions were higher than that predicted by Shields thus Shields curve is more applicable if D90 of the sampled bedload is taken as representative of particle size (Reid and Frostick 1984).....59
Fig 4. 4: Results of testing the modified XBeach code by considering dune erosion test XB8 (zoom in the dune extension zone).....61
Fig 4. 5: Results of testing the modified XBeach code, including a comparison between the profile of best fit and the dilatancy profile. 61
Fig 4. 6: Zwin dam breach initiation, after Bakker et al. (1996). 63
Fig 4. 7: Zwin Dam Breaching Test: Temporal evolution of breach width for the different runs. 63
Fig 4. 8: Aerial photo for the study site in Santa Rosa Island before (a) and after (b) Hurricane Ivan, after McCall (2008).....65
Fig 4. 9: LIDAR-measured bed elevation of the study site: (a) before Hurricane Ivan, (b) after Hurricane Ivan and (c) erosion–deposition plot based on the pre- and post-storm LIDAR data (McCall et al. 2010). 65
Fig 4. 10: Model boundary conditions: (a) significant wave height, (b) peak wave period on the offshore boundary, (c) surge level on the offshore and (d) surge level on the bay side (McCall et al. 2010).....66
Fig 4. 11: Plan view of Pre- and post-storm simulated topographies as well as the simulated erosion and depositions zones when a very high facpi of 7.1 is used to represent the grain-stabilization effect (run 09).....67

Fig 4. 12: Comparison between final profiles by non-modified and improved XBeach model as well as observed profiles at different cross-shore cross-sections: (a) at 500 m longshore, (b) at 1000 m longshore, (c) at 1500 m longshore and (d) at 1800 m longshore. 68
Fig 5. 1: Test case 1: 1D synthetic cross-shore profile (a) 1D synthetic profile used in XBeach to simulate a 1D overwash event and the induced flood propagation in the hinterland and (b) the inland discharge Q(t) is computed from XBeach at point P2, where Q(t) serves as inflow boundary condition for the HEC-RAS inundation model for the hinterland. The outcomes of the inundation from XBeach and HEC-RAS are compared at reference points P3, P4 and P5. ...76
Fig 5.2: Synthetic cases of the rise of the sea level (SWL) under the effects of both meteorological and astronomical tides during the simulation interval (1.0 hour). 78
Fig 5. 3: Evolution of the bed level (BL) and water level (WL) for the synthetic profile in Fig 5.1.a under load case LC1 as defined in Fig 5.2. 79
Fig 5. 4: Evolution of the bed level (BL) and water level (WL) for the synthetic profile in Fig 5.1.a under load case 2 (LC2) as defined in Fig 5.2. 80
Fig 5. 5: Calculated inflow discharge to the hinterland at P2 of both seawater Q (measured from LHS axis) and sediment Qs (measured from RHS axis); blue and red colours refer to Q and Qs, respectively; dark colours indicate outcomes under the rectangular load case (LC1) while light colours indicate outcomes under the triangular load case (LC2); Detail (A) shows Q and Qs under LC1, both drawn using one vertical scale. 81
Fig 5. 6: Comparison of water levels calculated by both HEC-RAS and XBeach (1D) at times 45, 50, 54 and 60 min under the rectangular load (LC1). 82
Fig 5. 7: Comparison of water levels calculated by both HEC-RAS and XBeach (1D) at times 35, 40, 45, 50 and 60 min under the triangular load (LC2). 83
Fig 5. 8: Comparison of local water depths (a) and local depth-averaged velocities (b), calculated by both HEC-RAS and XBeach (1D) at the measuring point P3, P4 and P5 under the rectangular load (LC1). 83
Fig 5. 9: Comparison of local water depths (a) and local depth-averaged velocities (b), calculated by both HEC-RAS and XBeach (1D) at the measuring point P3, P4 and P5 under the triangular load (LC2). 84
Fig 5. 10: Test case 2: Synthetic 2DH case study showing the sea, the dune, and the hinterland, including the building locations in the hinterland, sections A-A (cross-shore cross-section), B-B and C-C (alongshore sections) show the important details (all dimensions and levels are set in metre and not to scale). 85
Fig 5. 11: Application of XBeach for the 2D synthetic coastal zone in Fig 5.10, showing: (a) 3D view of the bed levels and the buildings, (b) plan view of the bed levels and building locations, (c) main breach location and inundation extent at t = 45 min, (d) locations of breaches and inundation extent at the storm end (t = 60 min), (e) distribution of the wave height over the model domain at the storm end and (f) morphological changes at the storm end. 87
Fig 5. 12: Approach for the calculation of the inland water discharge Q(t) through a breach using XBeach, n = number of longshore stretches, wi represents stretch width, di and uiE are the local water depth and Eulerian velocity at dune landward toe of each stretch (schematic). . 88
Fig 5. 13: Total inland discharge of water (Q) and sediment (Qs) calculated at the landward toe of the dune under the rectangular load case (LC1). 89
Fig 5. 14: Flood extent and water depths calculated by River-2D: (a) at t = 45 min and (b) at storm end (1.0 hour), both under the rectangular load case (LC1). 90
Fig 5. 15: Comparison of the temporal evolutions of water depths by XBeach and River-2D at t = 26, 30, 45, 50, 54 and 60 minutes at (a) Sec A-A, (b) Sec B-B and (c) Sec C-C, showing higher predictions of water depths and flood extent by River-2D at all sections. 91
Fig 5. 16: Comparison of flow velocities obtained from XBeach and from River-2D at the reference points N1, N2 and N3 for load case LC1. 92

Fig 5. 17: Test case 3: The 1994 dam at Het Zwin: (a) dimensions of the dam and the enforced pilot channel (sec X-X), (b) locations of the measuring stations, after Visser (1998)..... 93
Fig 5. 18: Reproduction of Het Zwin breach by XBeach: (a) breach development in cross-shore direction, (b) breach development in longshore direction and (c) simulated vs observed breach width evolution. 94
Fig 5. 19: Observed vs computed (XBeach) water depths and flow velocities at different measuring stations in Fig 5.17.b. 95
Fig 5. 20: Water discharge calculation through the Zwin dam breach (a) discharges qi over the 101 cross-shore stretches and (b) total inland discharge Q(t). 96
Fig 5. 21: Triggering factors associated with longshore variability for breach initiation along a dune. 98
Fig 6. 1: Cross-shore conceptual model illustrating a contaminant transport process occurring in a coastal groundwater system due to seaward directed flow, after Chang and Clement (2013). 103
Fig 6. 2: Designation of hydrologic soil profile horizons. Note that this figure is idealised and that one or more of these horizons may be absent in a given situation (Dingman 2015). 103
Fig 6. 3: Classifications of numerical models for contaminant transport in porous media. 107
Fig 6. 4: Calculated salinity distribution after 200 years of an SLR scenario for (a) a sandy aquifer, (b) clayey aquifer and (c) clayey layer overlying a sandy aquifer; Salt mass fraction increases with the darkness of shading, after Kooi et al. (2000). 108
Fig 6. 5: Physical model of salt water injection from top and infiltration into a shallow coastal sandy aquifer at (a) 2, (b) 5, (c) 11, and (d) 19 min; white colour indicates the fresh water, green colour indicates the intrusion owing to the hydraulic connectivity. Seaward-directed flow results in natural remediation of the freshwater (Illangasekare et al. 2006). 109
Fig 6.6: Distribution of salt concentration in the coastal aquifer at different times after the storm surge; Black lines are the iso-concentration lines of 500 mg/l (Yang et al. 2013). 111
Fig 6. 7: Effect of aquifer heterogeneity on SWI near Bremerhaven: (a) Six different zones of hydraulic conductivity to incorporate geological heterogeneity; Numbers are the hydraulic conductivities [m/s] for each zone, and (b) Distribution of salt concentration in the coastal aquifer of soil heterogeneity described in (a) at different times after the storm surge. Black lines are the 2% salt concentration (500 mg/l) of that in seawater (25000 mg//l) (Yang et al. 2015b)..... 112
Fig 6. 8: Coupling scenarios among breaching, induced inundation and subsequent saltwater intrusion. 114
Fig 6. 9: Abstraction, Desalination and Recharge (ADR) technique to control SWI owing to SLR (Abd-Elhamid 2010). 117
Fig 6.10: Example of 'flood-proofed' water well as a tool to prevent vertical salt water intrusion through wells (Villholth and Neupane 2011). 118
Fig 6. 11: Schematic illustration of the flow of water through soil with respect to salt leaching and root zone drainage (Grismer 1990). 118
Fig 7.1: Location of the study area: (a) selected cross section near Bremerhaven (red line), (b) state of Niedersachsen (Lower Saxony) and (c) Germany (Yang et al. 2013). 123
Fig 7.2: Bathymetry and ground elevations above SWL for the considered cross-shore profile near Bremerhaven, Germany (profile is obtained from Yang and Graf). The colours indicate different values for Manning coefficient. 123
Fig 7. 3: Applied time history of the sea level during a storm surge event for the study site near Bremerhaven: the dashed line represents the elevation of the dyke crest (Yang et al. 2013). 125
Fig 7. 4: Temporal development of inland discharges q calculated at the dyke crest (Point A in Fig 7.2) for both modelling scenarios Morpho-off and Morpho-on during the 2.8 h dyke overtopping as indicated by the storm surge event in Fig 7.3..... 127

Fig 7. 5: Evolution of the bed level (BL) and water levels (WL) for the cross-shore profile in Fig 7.2 under the effect of the storm surge event in Fig 7.3 with and without considering the morphological evolution. 127
Fig 7. 6: Pre- and post-storm sea, inundation and bed levels at Bremerhaven for both Morpho-on and Morpho-off scenarios. The flood extends 5 km behind the dyke until water is blocked at a cross-shore distance of 6400 m. Water depths at t = 10 h are spatially varying because of the spatial variation of the ground elevations. 128
Fig 7. 7: Evolution of bed and water levels during the overtopping event near Bremerhaven for the scenario of using uniform and low bed roughness coefficient over the entire shore profile (beach, dyke and hinterland). 129
Fig 7. 8: Temporal and spatial variations of the water depths in front and behind the dyke at near Bremerhaven owing to the sea level rise scenario in Fig 7.3. 130
Fig 7. 9: Substitution of the spatially variable water depth h(x) in the hinterland by a water depth (h = 0.44 m) averaged over the entire flood extent (5 km) for simplifying the input head to the saltwater intrusion model. 131
Fig 7. 10: Conceptual model for storm-driven saltwater intrusion (SDSWI) in the selected aquifer near Bremerhaven: Red colour indicates seawater inflow with saline concentration (C) equals saline concentration in seawater while green colours indicate freshwater inflow with C = 0. 132
Fig 7. 11: Setup of Bremerhaven aquifer model in Visual Modflow: Grid setup 132
Fig 7. 12: Net flow rates from/to the aquifer under the considered boundary conditions in Fig 3.14 without the vertical saltwater intrusion: a steady state is reached after 1095 days. 133
Fig 7. 13: Head distribution (equipotential heads above m.a.s.l) and flow field in Bremerhaven aquifer after (a) 3 months, (b) 1 year, (c) 3 years and (d) 10 years, all under the effect of 4.0 m and 0.0 m constant heads at the landward and seaward boundaries, respectively. Arrows represent the flow directions from the landward to seaward. Equipotential head contours (m) are stationary after 3 years (c and d) because the system reaches a steady state. 134
Fig 7. 14: Accumulative salt masses entering the aquifer as a source in (red curve), leaving the aquifer as a sink out (green curve) and accumulative salt mass remaining in the aquifer (brown curve). The latter mass curve represents the mismatch between the former two masses and it is stationary after 290 days because the system reaches an equilibrium state. 135
Fig 7. 15: Salt distribution in Bremerhaven aquifer due to the lateral intrusion after (a) 3 months, (b) 1 year, (c) 3 years and (d) 10 years. Salt-freshwater interface represented by 50% isoconcentration and the isoconcentration line of 500 mg/l (2%) are stationary in panels b, c and d (500 mg/l = max. salt concentration for drinkable water according to WHO). 136
Fig 7. 16: Net flow rates from/to the aquifer under the considered boundary conditions: the system reaches a steady state after 1095 days (3 yr) and remains steady until the inundation event at t = 1825 days. Inundation disturbs the system, inducing transient flow for 975 days till flow returns to pre-flood conditions. 138
Fig 7. 17: Head distribution (equipotential heads above m.a.s.l) in Bremerhaven aquifer at (a) t = 1825 days (directly before the inundation), (b) t = 1827 days (during the inundation), where flow is directed downward beneath the inundated zone, (c) t = 2152 days (after the inundation interval by ~ 1 yr) and (d) t = 3000 days (after 3.2 yrs.). Inundation event starts at t = 1825 and ends at t = 1829. Constant heads of 4.0 m and 0.0 m at the landward and seaward boundaries, respectively, results in seaward directed flow. Arrows represent the flow directions. Equipotential head contours are stationary in panels a and d, meaning that flow reached again a steady state. 139
Fig 7. 18: Accumulative salt masses along the fifty years of simulation: red curve represents salt entering the aquifer as a source in, green curve represents salt leaving the aquifer as sink out and blue curve represents accumulative salt mass remaining in the aquifer. Detail (b) shows the increase of the source in starting from t = 1825 to t = 1829 days because of saltwater inundation,

which results in an increase of the total mass in the aquifer by 54.9 tons during the inundation interval (4 days). The aquifer is remediated naturally after 44.3 years. 141
Fig 7.19: Evolution of salt distribution in Bremerhaven aquifer: (a) directly before inundation where the lateral intrusion only exists and (b - h) after the flood event where both lateral and vertical intrusions exist. Contamination extent is shown after 1 day (b), after 3 months (c), after 1 year (d), after 10 years (e), after 20 years (f), after 25 years (g) and after 45 years (h). Arrows represent the flow directions. Intruding salt water from the land surface moves almost vertically until it contaminates the whole aquifer depth (b-d) then it moves horizontally seaward (e - h) until reaching again the pre-flooding situation. Salt-freshwater interface, represented by the 50% iso-concentration contour, and the iso-concentration contour of 500 mg/l (2%) reach again the pre-flood situation (a) after 44.3 years (500 mg/l = max. salt concentration for drinkable water according to WHO)..... 142
Fig 7. 20: Subsurface drainage: upper panels show the installation process and lower panels show the role of subsurface drains in lowering the GWT based on the spacing and depths of inceptor drains, after Blann et al. (2009)..... 144
Fig 7. 21: Conceptual model for the aquifer near Bremerhaven with subsurface drainage of salt water infiltrating under storm-driven inundation: Red colours indicates seawater inflow with saline concentration (C) with the same value as in sea water while green colours indicate freshwater inflow. Purple colour indicates the subsurface drains, which are simulated in Visual Modflow as rectangle cells as shown in Detail C. 145
Fig 7. 22: Assumed values for subsurface drain conductance in Bremerhaven aquifer along the 50 years of simulation..... 146
Fig 7. 23: Total inflow rate through the ground surface [left axis] vs drainage rate through the subsurface drains [right axis], Cd represents the conductance value for each individual drain [m3/day/m]. 147
Fig 7. 24: Accumulative salt masses over the fifty years of simulation with subsurface drains: red curve represents salt entering the aquifer as a source in, green curve represents salt leaving the aquifer as a sink out and blue curve represents the accumulative salt mass remaining in the aquifer (blue = red – green). Detail (E) shows that the mismatch between the source in and sink out masses increases with higher drain conductance values, leading to more salt remaining in the aquifer. 148
Fig 7. 25: Comparison between salt masses remaining in the aquifer after and before the inundation with and without subsurface drains. In the case of drainage, more salt intrudes to the aquifer, especially during higher conductance intervals..... 148
Fig 7. 26: Evolution of salt distribution in the aquifer with subsurface drains near Bremerhaven: (a) 2 years before inundation when lateral intrusion only exists without drainage, (b) directly before inundation with unnoticed shift of the 50% contour landward than in (a) because of drainage, and (c - i) after the flood event where both lateral and vertical intrusions exist. Contamination extent is shown after 1 day (c), after 4 days (d), after 3 months (e), after 1 year (f), after 2 years (g), after 3 years (h) and after 45 years (i). Arrows represent the flow directions. Salt-freshwater interface, represented by the 50% iso-concentration contour, and the iso-concentration contour of 500 mg/l (2%) are shown on each panel. The 2% contour forms a zigzag-like during the conduction interval from the land surface (c - d) because part of the infiltrating water escapes downward in between drains. The interface shifts landward with higher conductance values. Nevertheless, salt dispersion to the deep aquifer is controlled by drainage and acceptable concentrations are achieved after 3 years (panel h). By reducing drain conductance, the interface shifts back seaward as in panel (i)..... 150
Fig 8. 1: Sea/land boundary (a) during moderate sea conditions, wave attack and induced coastal erosion are limited to nearshore and beach erosion. Moreover, freshwater and saltwater are in equilibrium determined by the interface; (b) during extreme storm surges, the coastal

barrier is directly attacked by shortwaves riding on the surge thus possibly causing barrier breaching, coastal inundation and subsequent vertical salt water intrusion. 153
Fig 8. 2: Recommended improvements/extensions for both XBeach and HydroGeoSphere to successively simulate breaching/overtopping of coastal barrier, induced inundation and subsequent saltwater intrusion. 157

List of tables

Table 2. 1: Current Knowledge gaps/limitations and planned improvements/extensions 36
Table 3. 1: Test conditions for dune erosion in GWK and in XBeach 44
Table 3. 2: Main parameter settings and boundary conditions for the reproduction of GWK tests in XBeach 46
Table 4.1: Summary of data from previous studies for the relation between the average slope steepness and facua parameter, including statistical indicators for best fit. 57
Table 4. 2: Statistical indicators for the simulation of Zwin breach width evolution using different facpi values. 64
Table 4. 3: BSS and RMSE for the different attempts to overcome the erosion overestimation at Santa Rosa Island 67
Table 4. 4: Values of the new parameters asabeta and facpi used in this chapter to overcome the overestimation of erosion and overwash volumes. 69
Table 5. 1: Main parameters and boundary conditions used in XBeach for the analysis of the 1D synthetic profile (Fig 5.1.a). 77
Table 5. 2: Main parameters and boundary conditions used in XBeach for the analysis of the 2D synthetic coastal area (Fig 5.10) 86
Table 5. 3: Main parameters used XBeach for the analysis of the breaching of the Het Zwin dam and the induced flooding 93
Table 7. 1: Parameters of the coastal aquifer near Bremerhaven, northern Germany (same values of Yang et al. (2013)). 124
Table 7. 2: Main parameters and boundary conditions used in analysing the free surface flow over the cross-shore profile in Fig 7.2 using XBeach. 125
Table 7. 3: Comparison of the main outcomes of analysing water overtopping and flood propagation using XBeach with the outcomes of Yang et al. (2013). 129
Table 7. 4: Reasoning behind assumed values for subsurface drain conductance in Bremerhaven aquifer along the 50 years of simulation. 146

Nomenclature

<>	[-]	Average of N readings of the bed levels along the cross-shore profile
∂t	[s]	time interval
$\partial\theta$	[-]	change in volumetric moisture content
Δx	[m]	Spatial step in cross-shore direction
Δy	[m]	Spatial step in longshore direction
Δz	[m]	Spatial step in gravitational direction
$\sum\Gamma$	[s^{-1}]	the volumetric fluid recharges rate
a	[m]	Wave amplitude (H/2)
A_p	[m^2]	Polder area
A_s	[-]	Wave asymmetry
A_{sb}	[-]	Bed load coefficient
A_{ss}	[-]	Suspended load coefficient
B	[-]	Total (non-dimensional) non-linearity
C	[$m^3.m^{-3}$]	Depth averaged sediment concentration
C	[kg/m^3]	dissolved concentration of a solute
C_{ch}	[$m^{0.5}s^{-1}$]	Chezy parameter
C_d	[$m^3/d/m$]	Conductance of aquifers to a subsurface drain
C_{eq}	[$m^3.m^{-3}$]	Depth averaged equilibrium sediment concentration
c_f	[-]	Coefficient of bed roughness
c_{max}	[m^3/m^3]	Maximum sediment concentration
C_r	[m^2/d]	Conductance of surface water body (e.g. river) to groundwater
D	[m]	Grain diameter
d	[m]	Local water depth
$D(\theta)$	[m^2/s]	soil water diffusivity function
D_*	[-]	Dimensionless particle size
D_{50}	[m]	Median sediment particle size
$d_{A,max}$	[m]	Maximum accumulation height at the foreshore model
$d_{E,max}$	[m]	Maximum depth of erosion at revetments foot
D_h	[$m^2.\ s^{-1}$]	Horizontal sediment diffusion coefficient
$d_{K,max}$	[m]	Max. scour depth
f	[s^{-1}]	Coriolis coefficient
F	[$kg.m^{-1}.s^{-2}$]	Wave induced stresses
f_{mor}	[-]	Morphological acceleration factor
f_{Ts}	[-]	Correction factor in the expression of the adaptation time scale
F_x	[Pa]	Wave-induced stresses in x direction
F_y	[Pa]	Wave-induced stresses in y direction
g	[$m.s^{-2}$]	Gravitational acceleration
h	[m]	Water depth at the flume
H	[m]	Wave height
$h(\vartheta)$	[m]	Matric potential as a function of water content
H_{rms}	[m]	Root mean square wave height
H_S	[m]	Significant wave height
K_r	[$m.\ s^{-1}$]	a representative value for hydraulic conductivity of the soil beneath the river bed in the Modflow river package
k	[-]	Wave number
$K(\vartheta)$	[m/s]	Unsaturated hydraulic conductivity as a function of water content
K_s	[m/s]	saturated hydraulic conductivity

L	[-]	Short wavelength
M	[m]	the vertical distance between riverbed and the GWT in the Modflow river package
n	[$m^{-1/3}.s$]	Manning roughness coefficient
n	[-]	Porosity
n_0	[-]	Bed porosity before erosion occurs
N_{ursell}	[-]	Ursell number
P	[-]	Geometric parameter in the formulation of Van Rhee
p	[m^2]	permeability
Q	[s^{-1}]	fluid flux per unit volume from a source or a sink (negative)
q	[$m^3\ m^{-1}.s^{-1}$]	inland discharge induced by wave overtopping per meter run
$Q(t)$	[$m^3.s^{-1}$]	Inland discharge induced by wave overtopping or a barrier breach
q(t)	[$m^2.s^{-1}$]	Inland flow discharge per meter run
q_{nom}	[l/(s·m)]	Nominal overtopping rate
q_s	[$m^2.s^{-1}$]	Sediment transport rate per unit width
q_{ss}	[$m^3/s/m$]	Suspended volumetric sediment transport discharge per unit width
q_{sT}	[$m^3/s/m$]	Total volumetric sediment transport discharge per unit width
q_{sx}	[$m^2.\ s^{-1}$]	Cross shore sediment transport discharge
q_{sy}	[$m^2.\ s^{-1}$]	Longshore sediment transport discharge
R	[-]	Correlation coefficient
r	[-]	non-linearity measure
R_c	[$kg/m^3/s$]	Source or sink term
Re*	[-]	Particle Reynolds number
s	[-]	Relative density of sediment (ρs/ρ)
S_f	[-]	Friction slope
S_k	[-]	Wave skewness
S_o	[-]	Bottom slope
S_s	[-]	Average seaward slope steepness
S_s	[m^{-1}]	specific storage
t	[s]	Time
T	[s]	Wave period
T_0	[s]	Dimensionless wave period
$T_{nom,m-1,0}$	[s]	Nominal wave period
T_p	[s]	Peak period
T_s	[s]	Adaptation time scale in advection-diffusion equation for sediment
U	[$m.s^{-1}$]	Depth averaged flow velocity
u	[m/s]	Velocity field in x direction
u_*	[$m.s^{-1}$]	Bed shear stress velocity
u_a	[$m.s^{-1}$]	Mean flow component due to nonlinear waves
u_{cr}	[$m.s^{-1}$]	Critical flow velocity for sediment entrainment
$u_{cr,c}$	[$m.s^{-1}$]	Critical flow velocity for sediment entrainment due to currents only
$u_{cr,w}$	[$m.s^{-1}$]	Critical flow velocity for sediment entrainment due to waves only
u^E	[$m.s^{-1}$]	Eulerian flow velocity in cross shore direction
u^L	[$m.s^{-1}$]	Lagrangian flow velocity in cross shore direction
u_{rms}	[$m.s^{-1}$]	Root-mean-square velocity
u^S	[$m.s^{-1}$]	Stokes drift in cross shore direction
U_{sf}	[$m.s^{-1}$]	The value of the depth-averaged velocity when sheet flow occurs
$U_{stirring}$	[$m.s^{-1}$]	Depth average stirring velocity
$U_{cr_{pi}}$	[$m.s^{-1}$]	Depth averaged critical velocity considering the particles interaction

v	[m.s^{-1}]	Flow velocity in y-direction
v^E	[m.s^{-1}]	Eulerian flow velocity in longshore direction
V^L	[m.s^{-1}]	Lagrangian flow velocity in longshore direction
v_{mg}	[m.s^{-1}]	Velocity magnitude
v^S	[m.s^{-1}]	Stokes drift in longshore direction
w	[m/s]	Velocity field in z direction
w_0	[m.s^{-1}]	Fall velocity of a single grain
w_s	[m.s^{-1}]	Fall velocity
x	[-]	Cross-shore axis coordinate
y	[-]	Longshore axis coordinate
z	[-]	Vertical axis coordinate
z_b	[m]	Bed level elevation
z_b	[m]	Initial (pre-storm) bed level
z_m	[m]	The measured post-storm bed level
z_p	[m]	Predicted profile from X-Beach
z_s	[m]	Water surface elevation
α	[deg]	Orientation of computational coordinates system in relation to the real world
α	[-]	Weighting factor
β	[deg]	Average seaward slope angle
γ_a	[-]	Coefficient for time-averaged flow due to wave asymmetry
γ_s	[-]	Coefficient for time-averaged flow due to wave skewness
γ_{ua}	[-]	Coefficient for time-averaged flow due to nonlinear waves
γ_{pi}	[-]	Calibration factor for the particle interaction effect
Δ	[-]	Difference operator
Δt	[s]	Time step
Δx	[m]	Grid spacing
θ	[-]	Effective Shields parameter
θ	[deg]	Wave direction
ϑ	[m^3/m^3]	volumetric water content
θ_c	[-]	Critical Shields parameter for the initiation of motion
θ_m	[deg]	Mean wave angle
θ_{sf}	[-]	Value of Shields parameter when sheet flow occurs
ν	[m^2/s]	Kinematic viscosity of water
ρ	[kg/m^{-3}]	Mass density of water
ρ_s	[kg/m^{-3}]	Mass density of sand
τ_b	[kg.m^{-1}.s^{-2}]	Bed shear stress

Abbreviations

1D	One Dimensional
2D	Two Dimensional
2DH	Two-dimensional horizontal
2DV	Two-dimensional vertical
3D	Three-dimensional
3DVDF	Three-dimensional variable-density flow
ASCE	American Society of Civil Engineers
BRES	Model for BReach Erosion in Sand dykes by Visser (1999) (BRES is the Dutch word for breach)
BSS	Brier Skill Score
CFD	Computional fluid dynamics
CFL	Courant–Friedrichs–Lewy condition
CHB	Constant head boundary
DEM	Digital Elevation Model
DRN	Modflow Drain Package
DWD	Drinking Water Directive
EU	European Union
FDM	Finite difference method
FEFLOW	Finite Element subsurface FLOW system
FEM	Finite element method
FVM	Finite volume method
GLM	Generalised Lagrangian Mean
GWK	The large-scale flume at the Coastal Research Centre (FZK) in Leibniz Universität Hannover, Germany
GWK-tests	Large scale flume data, funded by the NLWKN, which was performed in the Wangerooge project by LWI
GWT	Groundwater table = phreatic line
HGS	HydroGeoSphere modelling system
HYDRUS	Software package for simulating water, heat and solute movement
IE	Inundation extent
LHS	Left Hand Side
LIDAR	Light Detection and Ranging
LNHE	The National Hydraulics and Environment Laboratory (Laboratoire National d'Hydraulique et Environnement)
LWI	Leichtweiß-Institute, TU-Braunschweig
MSL	Mean Sea Level
MT3DMS	A Modular Three-Dimensional Multispecies Transport Model
NAP	Dutch datum (benchmark) , approx. MSL
NCBs	Natural Coastal Barriers
NLSWEs	Nonlinear shallow water equations
NLWKN	Lower Saxony State Office for Water Management, Coastal and Conservation = Niedersächsischer Landesbetrieb für Wasserwirtschaft, Küsten- und Naturschutz
NOAA	The National Oceanic and Atmospheric Administration (an American scientific agency within the United States Department of Commerce)
NRP	Natural remediation process
PDEs	Partial differential equations
PHT3D	Reactive Multicomponent Transport Model for Saturated Porous Media
PR	Progress Report

RCH	Recharge boundary
REB	Roller Energy Balance
RHS	Right Hand Side
RIV	Modflow River Package
RMSE	Root Mean Square Error
RT3D	Reactive Transport in 3-Dimensions
SDSWI	Storm-driven saltwater intrusion
SEAWAT	Model for Simulation of Three-Dimensional Variable-Density Ground-Water Flow (e.g. SEAWATer intrusion)
SFGD	Submarine Fresh Groundwater Discharge
SLR	Sea level rise
SVEs	Saint-Venant equations
SWAN	A numerical model for Simulating WAves Nearshore by Booij et al. (1997)
SWI	Saltwater intrusion
SWL	Sea water level
SWL	Still-Water Level
TIN	Triangulated Irregular Network
TUD	Delft University of Technology
UNESCO-IHE	Institute for Water Education is the largest international postgraduate water education facility in the world and is based in Delft, the Netherlands.
USA	The United States of America
USACE	U.S. Army Corps of Engineers
USGS	United States Geological Survey
UTC	Coordinated Universal Time
UTM	The Universal Transverse Mercator coordinate system
VDF	Variable density flow
W.r.t	With respect to
WAB	Wave Action Balance equation
Wangerooge	One of the 32 Frisian Islands in the North Sea
WFD	Water Framework Directive
WHO	World health organisation

1 Introduction

1.1 Problem statement and motivations

Coastal areas and coastal aquifers are highly vulnerable environments and may experience severe impacts from coastal storms (Yang et al. 2013, 2015a; b). With global warming and sea level rise, many coastal systems may experience accelerated coastal erosion, coastal barrier breaching, coastal flooding and subsequent seawater intrusion into fresh groundwater (Elsayed and Oumeraci 2016b, 2017a; Giambastiani et al. 2017; Ranasinghe 2016). Changing climate might lead to changes in the frequency, intensity, spatial extent, duration and timing of weather events, possibly resulting in unprecedented extreme events (Parry et al. 2007; Stocker et al. 2014; Vousdoukas et al. 2017; de Winter and Ruessink 2017). Extreme storm surges and subsequent coastal erosion/breaching and flooding have the potential to result in severe direct and indirect consequences (Izaguirre et al. 2017; Oumeraci et al. 2015). The direct consequences might, for instance, be associated with damages to lifelines and infrastructures as well as with fatalities and injured people while interruption of production processes represents an example of indirect economic damages that can be accounted for in flood risk assessments (e.g. Ujeyl and Rose, 2015). Nevertheless, groundwater contamination owing to infiltrating seawater behind breached coastal defences during and after coastal floods represents one of the main indirect damages that are often not included in flood risk assessments. Therefore, systematic research to assess the safety of coastal defences under extreme storm surge conditions and the consequences of possible barrier breaching and overwash on subsequent flooding and saltwater intrusion into groundwater is urgently needed. In fact, many countries (e.g. the Netherlands) have started extensive research programmes on climate-proof coastal defences (e.g. Özer et al., 2016). These programmes generally focus (i) on making the existing sea dykes, levees and other man-made structures overtopping resistant, and (ii) on developing new structures that can cope with extreme overtopping without breaching. However, for dunes and natural barriers, no systematic research has yet addressed the safety under extreme storm conditions together with the consequences of possible barrier breaching and overwash on subsequent flooding and saltwater intrusion into fresh groundwater.

The lack of research on the possible consequences of extreme storm surges on coastal flooding induced by barrier breaching and subsequent saltwater intrusion into coastal aquifers is certainly due to the high complexity and diversity of the processes/interactions to be considered. Different flow domains are involved starting from the sea where waves propagate toward the coastal barriers (Fig 1.1.a), which might result in their overtopping and/or breaching (Fig 1.1.b), thus leading to coastal floods behind the barriers (Fig 1.1.c) and subsequently to saltwater intrusion due to infiltrating seawater in the hinterland (Fig 1.1.d). On the other hand, diverse processes are involved (e.g. coastal hydrodynamics, sediment transport, soil avalanching on barriers' slopes and/or from breaching wedges, surface runoff of seawater over the hinterland and subsurface flow of the infiltrating seawater). In addition, several interactions among the latter processes exist. For instance, the breaching process represents the outcome of complex interactions between hydrodynamics, sediment transport and soil avalanching processes (Elsayed and Oumeraci 2016b). Moreover, propagation of salt water over the hinterland and subsequent infiltration to aquifers represent a surface-subsurface interacting transport of a conservative solute (Holding and Allen 2015; Yang et al. 2013; Yu et al. 2016b).

Though breaching, subsequent flooding and saltwater intrusion are naturally successive and hydraulically interconnected processes, the complexity of these three main processes has led to split the modelling by considering each individual process separately. This modelling approach does not account for the interactions among these processes, thus requiring a "manual" transfer of the results of the one model as input boundary conditions to another model (Christensen et al. 2013). Therefore, the importance of considering these three main processes in a single system of fully coupled models has become an increasing necessity in order to achieve reliable simulation results. Therefore, the feasibility of modelling the aforementioned three processes in a single model system need to be addressed. For this purpose, the state of the art prediction models for coastal barrier breaching, coastal flood

propagation and salt water intrusion need to be evaluated and possibly improved. Moreover, possible scenarios for model coupling need to be introduced.

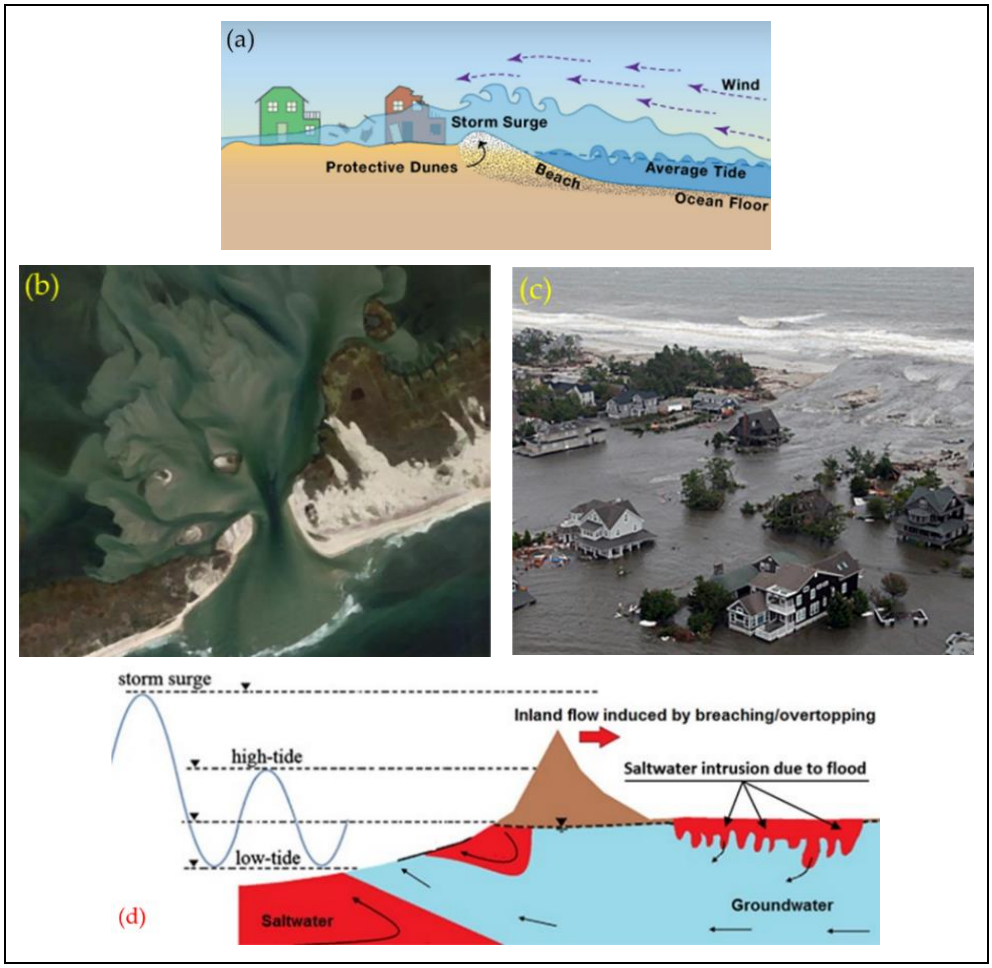

Fig 1.1: Flow domains for seawater during an extreme storm surge event: (a) waves are driven by wind toward the shoreline and may overtop and/or breach the protective dune [voices.nationalgeographic.com], (b) subsequent wave action during storm surges might induce a barrier breach (De Vet 2014), (c) breaching of coastal barriers allows seawater to propagate in the hinterland [www.dutchwatersector.com], and (d) propagating seawater percolates vertically to fresh groundwater causing its contamination (Yang et al. 2013).

Breaching of coastal barriers represents the most important source of coastal flooding, where breach induced inlets work as pathways to inland inundation and subsequent saltwater intrusion. Therefore, reliable breach prediction is crucial to achieve reliable estimations of flood depths and intrusion extents. However, the state of the art prediction models for erosion and breaching of dunes and coastal barriers (e.g. XBeach of Roelvink et al. 2009) overestimate the erosion rate induced by high flow velocities (Bisschop et al. 2010, 2016), which are common during extreme storm surge events, particularly for the flow through breach induced inlets (Elsayed and Oumeraci 2017a; McCall et al. 2010; De Vet 2014). Moreover, these models do not yet account for the large uncertainties involved in storm surge characteristics (water level and waves), alongshore variability and grain-stabilization effect (Elsayed and Oumeraci 2016b, 2017a). These uncertainties and the limitations of the existing models prevent indeed a reliable assessment of the safety of dunes and coastal sand barriers under future extreme storm conditions. Therefore, the current prediction models for coastal erosion and breaching (e.g. XBeach) need to be improved, extended and coupled with a selected inundation model and an appropriate infiltration model to obtain an overall model system for the combined assessment of the safety of coastal dunes and sand barriers, the subsequent flood wave propagation as well as the

implications of the subsequent flooding for groundwater contamination. Once the erosion and breaching model is improved, it can also be used to reliably calculate inland discharges during extreme storm surges rather than using common empirical models (e.g. EurOtop of Pullen et al. (2007) and Van der Meer et al. (2016)), which provide incorrect estimates of inland discharges as proved by Gallien (2016). Moreover, such empirical models cannot be used to calculate the inland discharge through a breach induced inlet because of the dynamic nature of the breaching process, which cannot be analysed based on static and empirically-based overtopping models (e.g. EurOtop) by simply comparing water levels and land elevations.

1.2 Objectives

Based on the aforementioned considerations and motivations, the primary objectives of this study, which will be specified more precisely in Section 2.8.2, may be outlined as follows:

(i) Developing an overall generic methodology and models to assess the safety of coastal dunes and sand barriers, the subsequent flood wave propagation as well as the implications of coastal floods for groundwater contamination.

(ii) Improving, extending and validating one of the state of the art prediction models for erosion and breaching of dunes and coastal barriers (e.g. XBeach) and coupling it with an appropriate inundation model and an appropriate infiltration model to simulate the salt water intrusion to coastal aquifers.

(iii) Identifying appropriate techniques and measures to mitigate the risk during extreme storm surges along the entire risk pathways, i.e. from the risk source (e.g. extreme storm surge) to the risk receptor (e.g. coastal aquifers), and considering the whole chain of pathways and hazards (e.g. barrier breaching, flooding, saltwater infiltration and groundwater contamination) as well as determining and numerically testing an appropriate approach to mitigate saltwater intrusion due to coastal flooding.

(iv) Implementing and applying the well-validated modelling tools and one of the most promising risk mitigation measures exemplarily for a pilot site in order to evaluate, among others, the implications of coastal floods for groundwater contamination.

1.3 Methodology and organisation of the thesis

As shown in Fig 1.2, the methodology proposed to achieve the aforementioned objectives includes seven work phases, which are addressed in the following seven chapters.

In chapter 2, Phase 1 is addressed through a comprehensive review and analysis of the current knowledge and modelling tools for the physical processes related to the following three main issues: (i) coastal barrier breaching, (ii) induced coastal flood propagation and (iii) subsequent saltwater intrusion. Thus, appropriate modelling tools are selected, the associated knowledge gaps are identified and implications for this PhD study are drawn. Based on these implications, the objectives and methodology for this study are specified more precisely (Section 2.8).

In chapter 3, Phase 2 is addressed through assessing the performance of the selected breaching model by means of existing large-scale experiments for dune erosion. In the light of these experiments, the model capabilities are investigated and possible model improvements are introduced.

In chapter 4, Phase 3 is addressed through introducing improvements of the selected breaching model in order to achieve a more reliable prediction of coastal erosion and induced coastal barrier breaching. As a result, a tentative validation of the improved breaching model is performed based on breaching and overwash cases collated from previous studies.

In chapter 5, Phase 4 is addressed through elaborating possible coupling approaches of the breaching model improved in Phase 3 and the inundation model selected in Phase 1. The outcome of Phase 4 is a model that can simulate breaching and coastal flooding simultaneously by considering the mutual interactions among the involved processes. Thus, another tentative validation is performed for the coupled model by means of synthetic and real breaching/inundation cases.

Phase 1	**Review and analysis of current knowledge and modelling tools**
Contents	1. Knowledge gaps and modelling weaknesses for barrier breaching.
	2. Knowledge gaps and modelling weaknesses for coastal flooding and saltwater infiltration.
	3. Selection of models for further improvement /extension.
Phase 2	**Assessment the performance of the selected breaching model**
Phase 3	**Improvement of the selected breaching model**
Phase 4	**Coupling approaches of a barrier breaching and subsequent flooding**
Phase 5	**Implications and modelling scenarios of storm-driven saltwater intrusion**
Phase 6	**Application of the overall methodology to a selected pilot site**
Phase 7	**Summary, discussion and outlook**

Fig 1.2: Tentative methodology of the research consisting of seven successive phases.

In chapter 6, Phase 5 is addressed through elaborating possible modelling scenarios of the three processes (breaching, inundation and induced saltwater intrusion). As a result, an appropriate modelling scenario is selected to draw the implications of storm-surge-driven coastal floods for groundwater contamination. Based on the latter implications, appropriate mitigation measures are suggested along the entire risk pathways. Finally, the most suitable measure is selected and applied to mitigate storm-driven salt water intrusion event in a selected pilot site

In chapter 7, Phase 6 is addressed through applying the overall modelling methodology to a selected pilot site. The pre-selected mitigation tool (from Phase 5) is applied to mitigate possible salt water intrusion owing to coastal floods.

Chapter 8 summarises the key results and concluding remarks (Phase 7). In addition, suggestions for a further development of the overall modelling methodology or any part of its individual components are provided.

2 Review and analysis of current knowledge and modelling tools

In this chapter[††], the current knowledge and modelling tools for the following three main processes (i) coastal barrier breaching, (ii) induced flood wave propagation and (iii) subsequent saltwater intrusion are reviewed and analysed, the knowledge gaps and modelling weaknesses are identified, and implications are drawn for this PhD study. The structure of the chapter is summarised in Fig 2.1, where the relation between the aforementioned three successive processes is schematized.

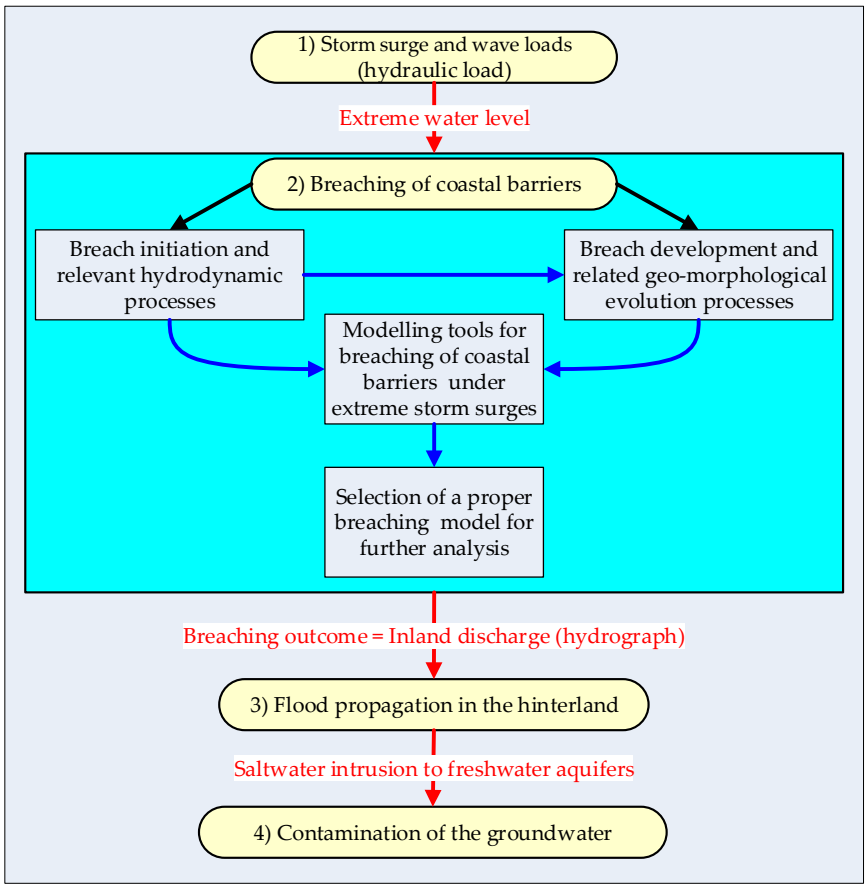

Fig 2.1: Processes involved in breaching of coastal barriers and subsequent groundwater contamination: storm surges represent the hydraulic load that might result in breach initiation and development. Through the breach induced inlet, inland sea water flow will thus propagate in the hinterland. During and after flood propagation, salt water infiltrates to fresh groundwater, causing its contamination.

First, a brief overview of storm surges, as the hydraulic load causing the breaching, will be introduced. Second, interactions between storm surges and coastal barriers and associated processes will be addressed, including breach initiation and development. In addition, the state of the art breaching models will be examined in order to select a proper model for further analysis. The selected model will be used to calculate the breach-induced inland discharge (inland hydrograph). Third, state of the art approaches and modelling tools for coastal flooding will be examined. Fourth, the implications of coastal floods for groundwater contaminations as well as the state of the art modelling tools will be addressed. Finally, in the concluding section, the specific objectives and methodology of this study are derived from the results of previous sections.

[††] This chapter represents the summary (with updates) of the comprehensive state of the art report:
Elsayed, S. M.; Oumeraci, H. (2014): Breaching of coastal barriers under extreme storm surges and implications for groundwater contamination: State of the art report. Internal report no 1071, Leichtweiß-Institut for Hydraulic Engineering and Water Resources, TU Braunschweig, Braunschweig, Germany, p. 134.
Freely available at:
https://www.researchgate.net/publication/304539691_State_of_the_Art_on_Breaching_of_Coastal_Barriers_under_Extreme_Storm_Surges_and_Implications_for_Groundwater_Contamination

2.1 Brief overview of storm surges

A storm surge (Fig 2.2) is a rapid short-term rise of the sea water level that takes the form of a very long wave which may last several hours or even days. It is mostly caused by strong winds during a hurricane or a tropical storm. In fact, hurricanes, typhoons, monsoons and other tropical storms consist of large wind fields driven by pressure gradients from a central low pressure and temperature gradients in the atmosphere. Both high wind speed and pressure gradients constitute part to the temporal sea level rise. The other components are discussed in the following two subsections.

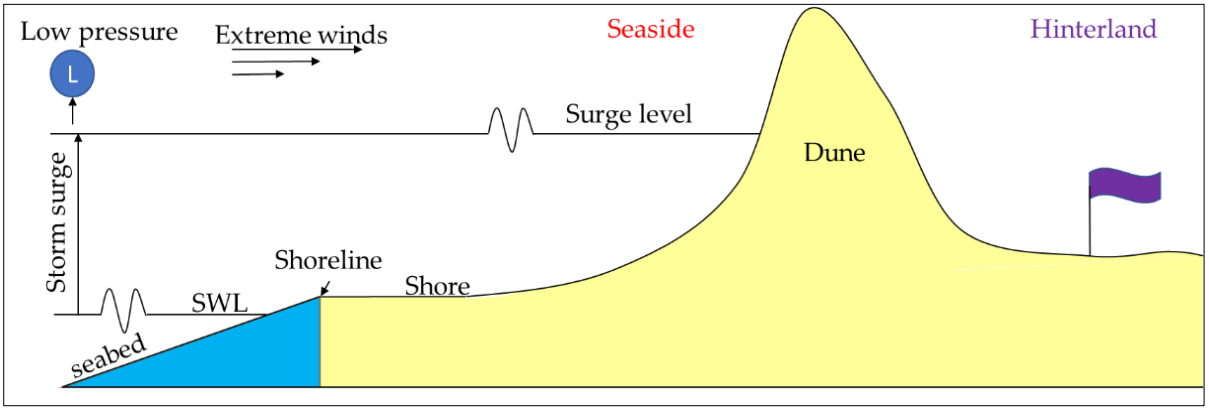

Fig 2.2: Definition sketch of storm surge: sea water level (SWL) temporally rises during storms, mainly induced by extreme winds and a storm accompanying low pressure, to reach the surge level. Thus, shortwaves riding on the surge level start to hit the protective coastal barriers (e.g. dunes).

2.1.1 Components of a storm surge

As hurricanes or storms reach the coast, they drive a huge amount of water towards the shoreline, causing extreme sea level as shown in Fig 2.2. Such a storm-driven sea level rise is known as storm surge or meteorological tide. In fact, a storm surge consists of several components induced by different forces, arising from the reduction of barometric pressure, increasing wind stresses, wave setup and Coriolis force (Sorensen 2006; Tayel 2015; Tayel and Oumeraci 2015). The sum of these four components constitute the total storm surge as described below:

(i) Barometric surge is the response of coastal waters to the low pressure at the centre of a storm. At the site of the storm, the water is drawn up into the low-pressure region by the surrounding high-pressure air. However, this is not the main contributor of a storm surge.

(ii) Wind-induced surge (wind setup) is created by the frictional drag of the wind blowing over the water.

(iii) Wave setup which occurs primarily within the wave-breaking zone and results in elevating the water level. Wave setup can cause an increase in sea water level elevation on the order of 20% of the offshore breaking wave height and can thus be a significant portion of the overall sea water level during storms inside the surf zone (Tayel 2015; Vousdoukas et al. 2017; Weaver and Slinn 2005).

(iv) The Coriolis surge is a surge component induced by the rotation of the earth (Sorensen 2006). Such surge occurs when a storm forces strong currents to flow along the shoreline. Thus, the Coriolis force due to the rotation of the earth induces a hydrostatic variation in the water surface due to the inertial effect of the alongshore current.

In general, the major contributor to a storm surge is the wind setup component as storms can produce wind speeds exceeding 200 km/hr according to the National Oceanic and Atmospheric Administration agency (NOAA 2008). Nevertheless, storm surges combined with astronomical tides and other components can results in extreme sea levels during a storm event (Tayel and Oumeraci 2015). These components are briefly addressed in the following section.

2.1.2 Classification of extreme sea level components

Storm surge, including the previous four components, represent only a part of what causes water levels to rise along the coast during a storm. Other factors, e.g. astronomical tides, contribute the rest of the total (extreme) water level. In general, sea level may rise owing to (i) short-term factors that occur in minutes, hours or even days (e.g. storm surges) in addition to (ii) long-term factors that occur in years and decades like the sea water variation because of the climate change (Church 2013; Parry et al. 2007). These factors can be classified into three categories as depicted in Fig 2.3.

(i) Deterministic factors: like astronomical tides.

(ii) Meteorological factors, with non-stationary and stochastic characteristics, such as wind speed and direction, storm characteristics and its track, sea level pressure and rivers discharge.

(iii) Local factors in shallow water regions such as local bathymetry changes, roughness of the continental shelf and shoreline geometry.

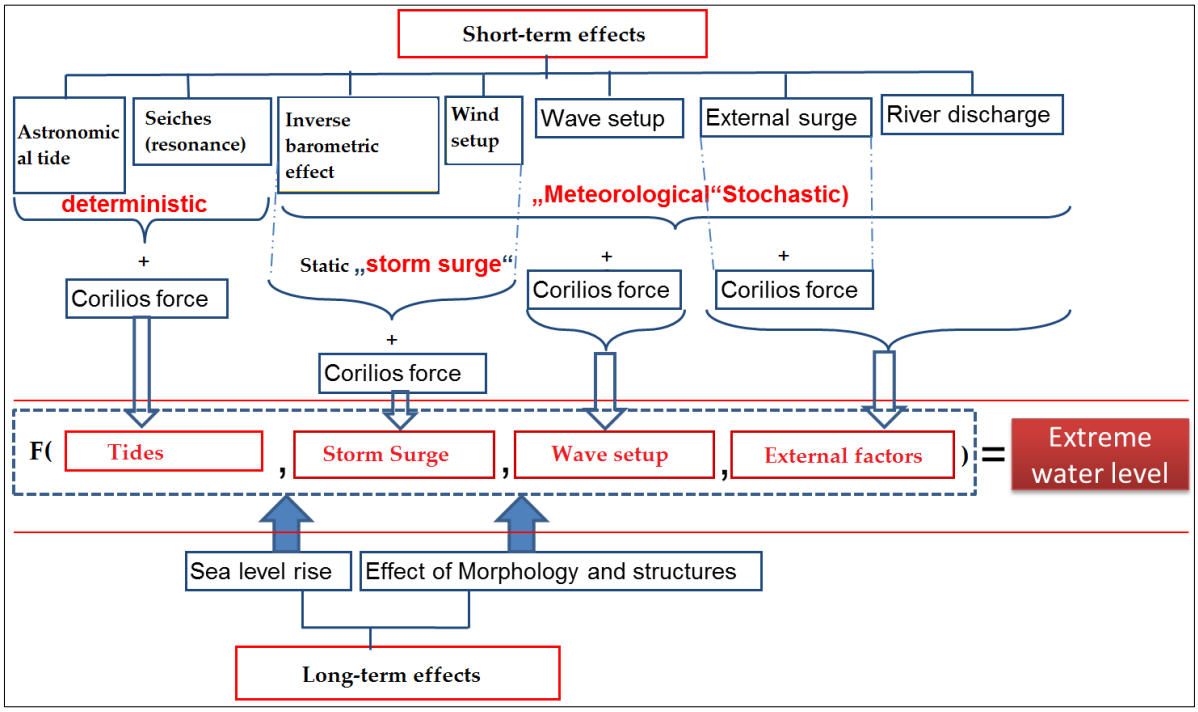

Fig 2.3: Main components interacting for the generation of extreme water levels during a storm surge event: astronomical tides represent a deterministic component while metrological components (e.g. wind, barometric and wave setups) represent stochastic components. Climate-change-induced sea level rise represents an example of long-term components (Tayel and Oumeraci 2015).

The astronomical tide represents a water level rise that falls along the coast every day due to the gravitational pull of the moon and the sun. When tide is combined with a storm surge, the induced sea level rise is called "storm-tide" (Fig 2.4). Freshwater inputs in the form of heavy rainfall or river discharges contribute to the latter storm-tide resulting in further increase in sea levels. Therefore, extreme water levels at an open coast may consist mainly of the five components: wind setup (wind surge), pressure setup (barometric surge), wave setup, Coriolis surge and astronomical tide.

Coastal barriers such as dunes (Fig 2.2) represent an important component of the defence system against storm surges and subsequent coastal floods. However, with extreme water levels during an extreme storm event, the protective barriers may breach, possibly resulting in an inundation of near shore areas. Effects of such extreme sea levels on the breach initiation and development of a coastal barrier are discussed in the following sections.

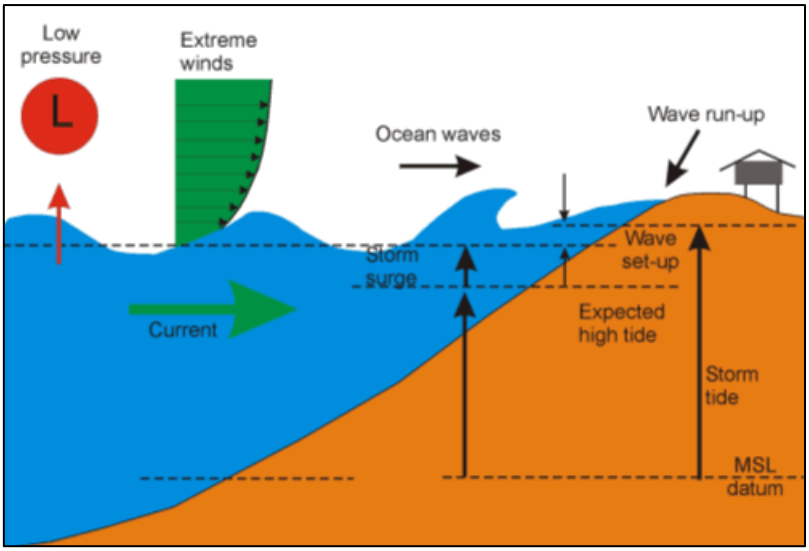

Fig 2.4: Vertical cross-section of a schematic sea/land boundary. Drawn in the figure are symbols representing low pressure out at sea, extreme winds over the sea, breaking surf waves, and indications for wave setup and wave run-up in the coastal area. Tide marks are drawn indicating the different tide heights under different scenarios: Mean sea level (MSL), expected high tide, storm surge, wave setup and wave runup (Mullan et al. 2005).

Implication 1: Risk related to storm surges

1. Storm-tide might result in an extreme sea level, so that protective barriers become directly exposed to higher attack by short waves riding on the extreme sea level as shown in Fig 2.2.
2. The hydraulic loading to coastal barriers from the sea may be subdivided in two main categories: (i) sea level changes due to storm-tide and further long waves of different origins, and (ii) storm-induced short waves. The former load category represents, in essence, very long waves that generally induce a set-up of a lower mean sea level (MSL) as indicated in Fig 2.5.a to a higher seawater level (SWL), so that the shorter storm waves riding on the higher SWL will hit (Fig 2.5.b), overtop (Fig 2.5.c) and/or overflow (Fig 2.5.d) the barriers of the sea defense system, possibly causing coastal erosion and barrier breaching.

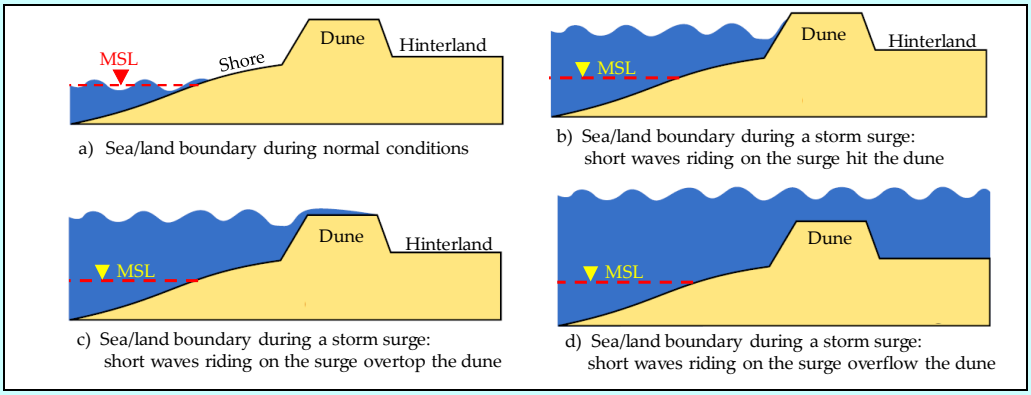

Fig 2.5: Possible scenarios for the total sea level during a storm surge: (a) during normal conditions (no setup), (b) under a setup of sea level during a storm surge, short waves hit the protective barrier (dune), (c) with a further setup, short waves may overtop the barrier, and (d) in the extreme situations, seawater overflows the barrier.

3. A storm-tide-induced coastal erosion and barrier breaching may result in further coastal flooding, significant loss of life and injuries, direct and indirect economic damages as well as in long-term damages to coastal ecosystems and landscapes.

2.2 Breaching of coastal barriers under extreme storm-tides

Many coastal flood defence structures, including levees, dykes, dunes, barrier islands, barrier spits and tombolos, have been formed naturally or man-made along the world's coastal lines. Most of these structures play an important role as coastal defence against floods and wave attack. However, they may breach under extreme storm-tides, causing dramatic inundation in the hinterland. According to D'Eliso (2007), Stanczak (2008) and Tuan and Verhagen (2008), two hydro-morphological processes are involved in barriers breaching: (i) barrier response to storm-tide and wave attack (erosion and breach initiation), and (ii) barrier breach growth and development. The relevant hydrodynamic processes that can initiate a breach are addressed in the following subsection.

2.2.1 Breach initiation and relevant hydrodynamic processes

Breaching is a complex hydro-geo-morphodynamic process, which is initiated, in the most common situation, when water overflows a depressed portion in a narrow landmass such as a barrier spit, a barrier island or a protective dune. Given sufficient time, the flow will induce a breach (channel/inlet) that causes water to flow across the breached barrier. Nevertheless, the initiation of a coastal barrier breach is more complex than this common case as it depends on the relationship between the storm-tide level and the crest level of the barrier, which is not necessarily beneath the extreme water level (Muller et al. 2016). Based on the latter relationship, the associated hydrodynamic processes of short waves riding on the storm-tide level (e.g. breaking impact, run-up, rundown, overtopping and overflow) might trigger breaching initiation (D'Eliso 2007; Sallenger 2000; Stanczak 2008; Tuan and Verhagen 2008). Therefore, a barrier breach may initiate from the seaside as long as the dune crest level is not exceeded by the storm-tide level as shown in Fig 2.5.b (see also e.g. Stanczak (2008) or Van Thiel de Vries, 2009). However, in the case of wave overtopping (Fig 2.5.c) and overflow (Fig 2.5.d), breaches may initiate from the landward/bay side (see e.g. D'Eliso, 2007). Fig 2.6 gathers all hydrodynamic processes relevant to a breach initiation. Based on these processes, four flow regimes may be distinguished as in the following subsection.

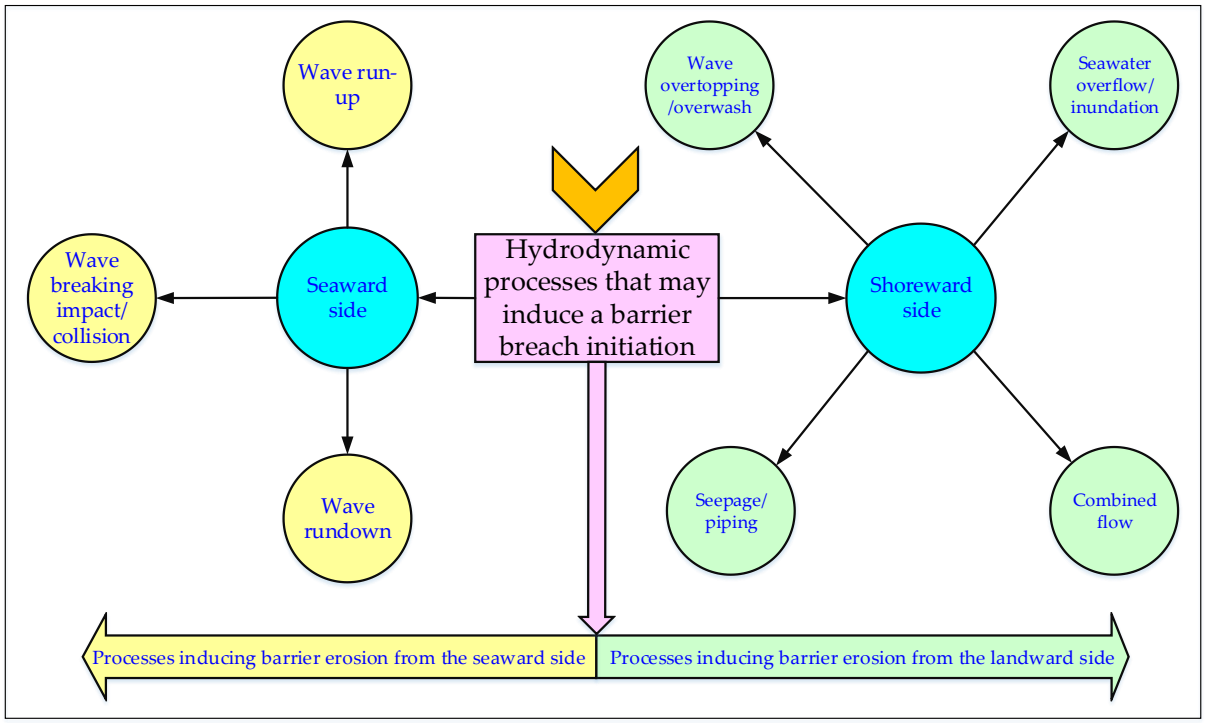

Fig 2.6: Hydrodynamic processes that may initiate a coastal barrier breach from seaward and landward/bay sides: during a storm-induced sea level rise, barriers become exposed to diverse hydrodynamic processes that may initiate a breach depending on the relationship between the storm-tide level and crest level of the barrier.

2.2.1.1 *Sallenger's flow regimes during storm surges*

Sallenger (2000) distinguishes four flow regimes during storm surges based on barrier height and storm-tide level (Fig 2.7) as follows:

(i) *Swash regime*: the condition, during a storm, where swash is confined to the foreshore of the beach. This regime results in erosion of the shore without barrier erosion, where eroded sediment is transported offshore.

(ii) *Collision/impact regime*: the condition when breaking waves collide with a barrier's seaward slope, forcing barrier erosion from the seaside. This regime results in the erosion of the barrier, where sediment is also transported offshore.

(iii) *Overwash regime*: the condition when overwash/overtopping of the barrier takes place. During this regime, erosion of barriers is common from the landward side where eroded sediment deposit landward, often in the form of washover fans (Donnelly 2007).

(iv) *Inundation regime*: the condition when the storm-tide is sufficient to completely submerge a barrier. Thus, the flows over the barrier are no longer simple overwash. Rather, the once subaerial part of the barrier becomes impacted directly by surf-zone processes (Sallenger 2000). Therefore, flow and morphology characteristics determine the direction and quantity of sediment transport during this regime (Masselink and van Heteren 2014).

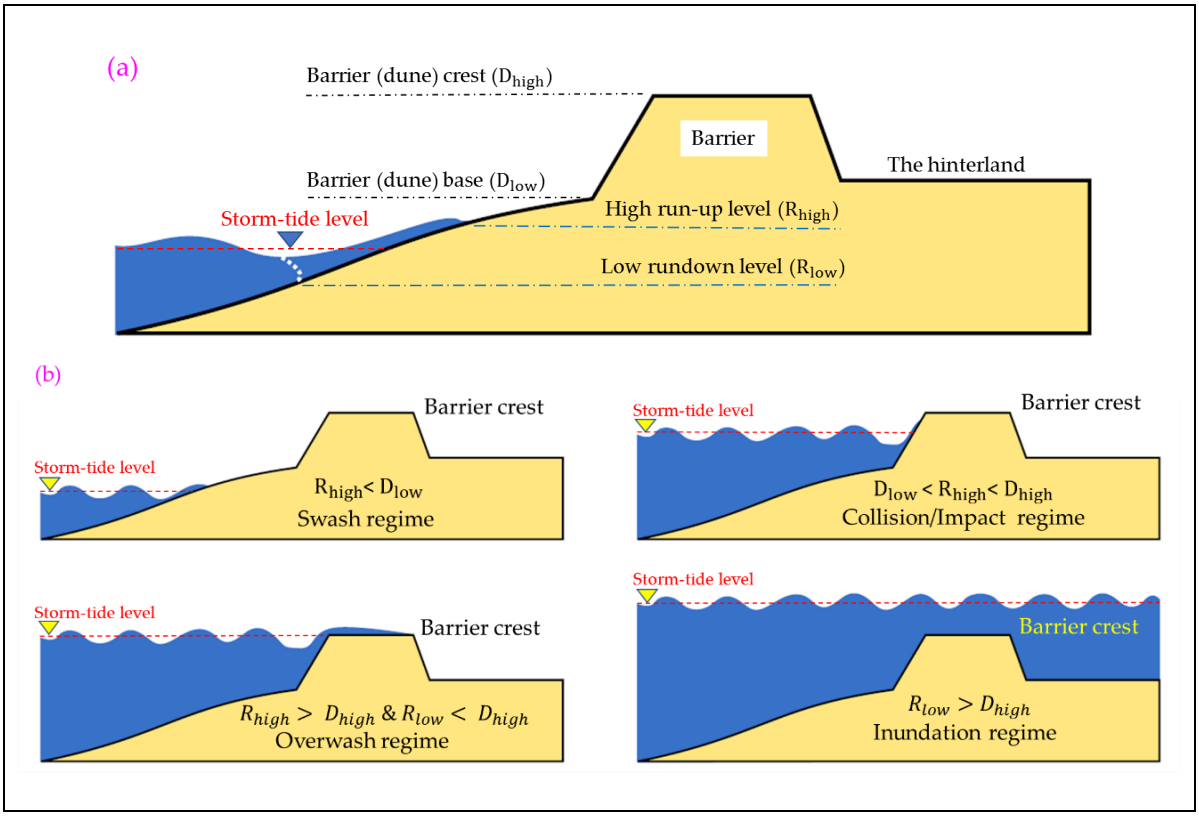

Fig 2. 7: Series of storm impact regimes as defined by Sallenger (2000): (a) definition of variables used in scaling the impact of storms on barriers, and (b) different storm regimes, after De Vet (2014).

These four regimes may occur successively during a storm surge depending on the storm-tide level (Elsayed and Oumeraci 2016b, 2017a; Masselink and van Heteren 2014; McCall et al. 2010). In fact, the combination or succession of these four regimes during a storm event may result in severe erosion and in barrier breaching (Muller et al. 2016). For instance, a rising storm surge can initiate a swash regime followed by a collision regime and finally by an overwash regime (de Santiago et al. 2017). Besides variations in time, spatially varying regimes in longshore direction can also be observed based on the longshore variability of both hydraulic load and barrier topography (Elsayed and Oumeraci 2016b). The hydrodynamic processes that might be observed during such regimes are described in the following sections.

2.2.1.2 *Hydrodynamic processes relevant to breach initiation from the seaside*

(i) Impact/collision of breaking waves

Short waves break when they reach a limiting steepness as shown in Fig 2.8. Breaking waves on a mild slope result in a very turbulent motion of breaking waves and possibly stir sediment from the barrier's seaward slope at the turbulence location (Stanczak 2008). Wave impact as shown in Fig 2.8.b enhances sediment stirring as it causes steep pressure gradients and possibly collision due to impacts between breaking waves and the barrier's seaward slope (Schiereck 2005; Stanczak 2008). A detailed overview of breaking waves effect on breach initiation is presented in Elsayed and Oumeraci (2014).

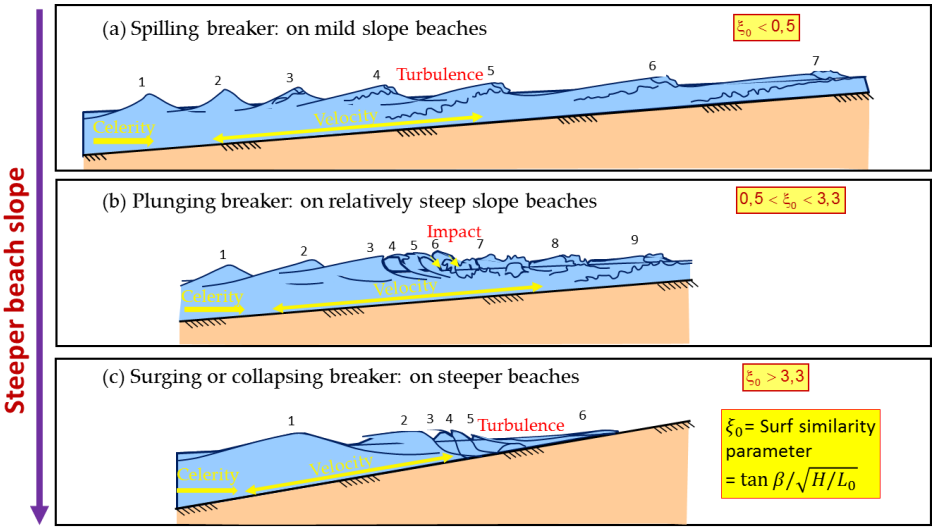

Fig 2.8: Hydrodynamic processes that might initiate a breach from the seaward slope of a barrier: (a) breaking wave-induced turbulence due to spilling breakers over a mild slope, (b) breaking wave-induced impact due to plunging breakers over a moderately steep slope, and (c) breaking wave-induced turbulence due to surging and collapsing breakers over a steep slope. Flow velocities induced by wave run-up (upwards) and wave rundown (downwards) contribute with breaking wave effects in a breach initiation from the seaside. Breakers types are often determined depending on the surf similarity parameter, which is a function of the breach slope β, wave height H, and wavelength L_0, after Oumeraci (2017). Numbers (1-9) indicate wave propagation direction and relevant waveform/shape during propagation from offshore indicated by 1 to onshore indicated by 7, 9 and 6 in (a), (b) and (c), respectively.

(ii) Wave run-up and run-down

Fluctuations of sea water in the swash zone in the form of swash (run-up) and backwash (run down) represent the second most important reason for a breach initiation from the seaside. In fact, upwards directed (positive) flow velocity (see Fig 2.8) causes sediment to be transported onshore while downwards directed (negative) flow velocity causes sediment to be moved offshore.

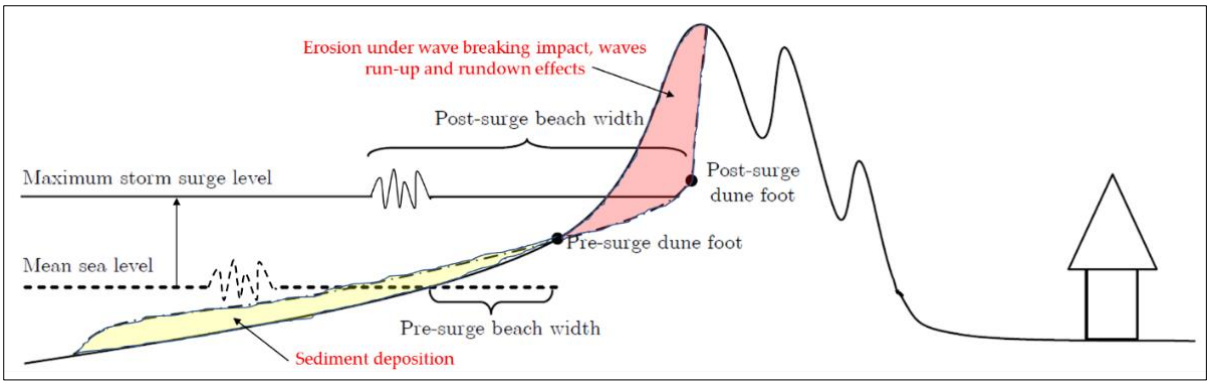

Fig 2.9: Barrier erosion from the seaside during a storm surge event: During a storm surge, sea level rises temporally and hence barriers become subject to successive impacts by breaking waves in addition to successive wave run-up and run-down, after Van Thiel de Vries (2009).

The sediments stirred by the aforementioned hydrodynamic processes (i.e. impact, run-up and run-down) may lead to barrier erosion from the seaside as shown in Fig 2.9, where the eroded sediments are carried in seaward direction by wave-induced near-bed return currents (undertow) to deposit offshore in the near shore breaker bar systems (Van Thiel de Vries 2009). As a result, successive impacts, run-ups and rundowns transport sediment from the barriers seaward slope to offshore, thus narrowing the dune cross-section as shown in Fig 2.9 and possibly leading to barrier breaching.

2.2.1.3 Hydrodynamic processes relevant to breach initiation from the land side

(i) Overtopping/overwash

A storm surge may increase the water level so that wave run-up becomes higher than the barrier crest as shown in Fig 2.10.a. As a result, volumes of water pass the barrier intermittently in the form of pulses. The flow over the landward slope has often a high flow velocity because of the inclination, thus resulting in higher shear stresses and possibly in landward erosion and breach initiation from the landside. In the latter case, high overtopping flow velocities may gradually scour a channel across the barrier, leading to a barrier breaching. The terms "wave overtopping" (Fig 2.10.a) and "overflow" (Fig 2.10.b) describe respectively intermittent flow and continuous flow over a barrier, while "overwash" (Fig 2.10.a) is commonly used to describe the flow of water and sediment over dune and beach crests during storms.

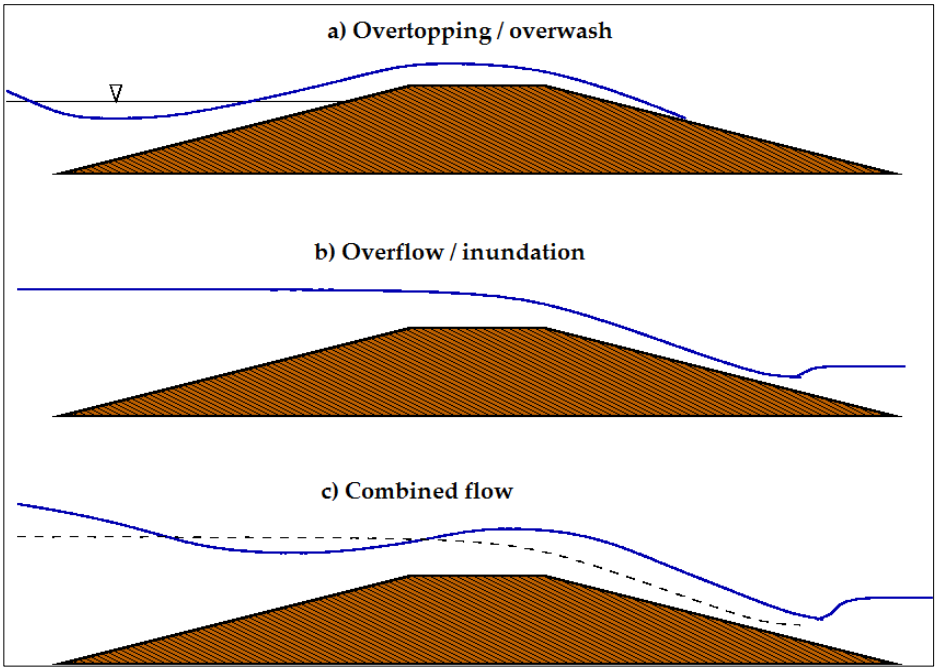

Fig 2.10: Types of flow over coastal barriers: (a) wave overtopping/overwash which may also occur at local discontinuities or depressions, (b) overflow/inundation which occurs due to high surge level exceeding the barrier crest, (c) combined wave overtopping and surge overflow, after Hughes (2008).

(ii) Overflow/combined flow/inundation

Overflow occurs when the storm-tide level exceeds the barrier crest. In reality, this type of flow does not exist since water (surge) overflow is often combined with wave overtopping as shown in Fig 2.10.c, resulting in a combined flow (Hughes 2008). During overflow and combined flow regimes, barriers are totally inundated. The flow over the barrier's landward side corresponds to a water sheet flow regime associated with very high flow velocities. The latter may result in barrier erosion from the landside as shown in Fig 2.11 and possibly also in barrier breaching. The critical erosion mode, in this case, is usually progressive surface erosion for non-cohesive barriers and headcut erosion (formation and migration of vertical or nearly vertical lumps of the bed) for cohesive barriers (Zhong et al. 2017). However, non-cohesive heavily compacted barriers may also erode in the form of a headcut (Wu et al. 2011).

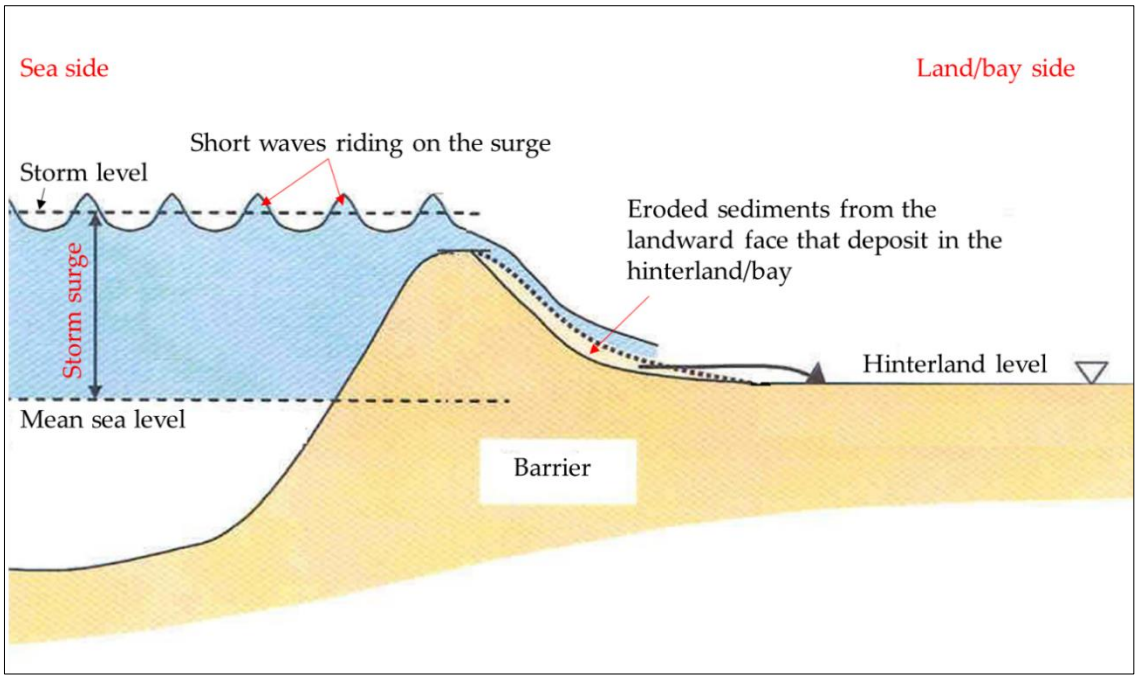

Fig 2.11: Erosion of coastal barriers from the landward side owing to combined flow: non-cohesive barriers erode progressively where eroded sediments are relocated in the downstream, after Donnelly et al. (2004).

Barrier overwash and inundation may initiate a breach from the landside as the flow velocities over the landward slope are often very high (Donnelly 2007; Donnelly et al. 2004, 2006, 2007). Indeed, these two flow regimes are often successive (Elsayed and Oumeraci 2016b). They start with overtopping through local discontinuities or depressions. Overwash volumes are then transported to the hinterland, leading to enlargement and deepening of the depressions. With the latter enlargement, the barrier crest at the depressions is lowered allowing water overflow on the barrier, which accelerates the landward erosion and breach development.

(iii) Seepage and piping

Seepage through porous barriers caused by the difference in water heads on barrier sides might liquefy the sediment-water mixture as shown in Fig 2.12, allowing large volumes of material to be transported quickly as a slurry. Thus, piping is a phenomenon by which the soil on the downstream side of a barrier gets lifted up due to excess pore water pressure. The breaching potential, in this case, is minimised if the barrier is wide and impermeable enough. Moreover, Elsayed (2013) reported that a breaching initiation by piping is not a likely breaching mechanism in the case of short-term events (e.g. storm surges) as the seepage and induced piping takes long-term intervals to initiate a breach. However, seepage and piping might reduce the strength of the barrier, which facilitates the initiation of a breach under other mechanisms for breach initiation (e.g. wave impact, wave overtopping, wave runup and run down). Furthermore, they might accelerate the breach development (D'Eliso 2007; Morris et al. 2009).

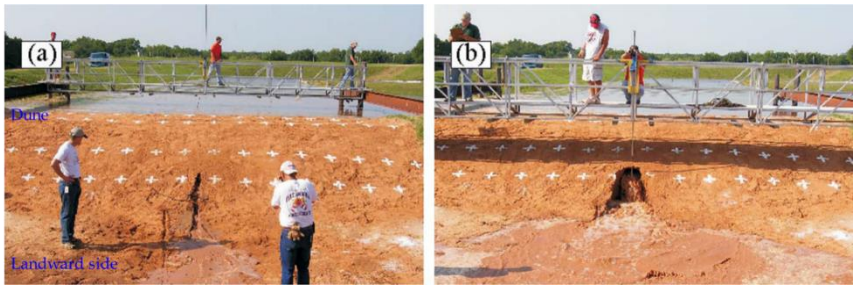

Fig 2.12: Landward barrier breaching induced by seepage and piping: (a) breach initiation, (b) breach development, after Wu et al. (2011).

2.2.2 Breaching development and related geomorphological processes

Breach development means progressive growth and widening of an initiated scour in a coastal barrier, including the related geomorphological evolution processes and side slopes instabilities of the breach. In fact, there are two main processes that control a breach development of barely vegetated barriers: (i) sediment transport and induced morphological changes and (ii) soil avalanches and slopes instabilities.

(i) Sediment transport and induced morphological evolution

Barriers response to storms involves both internal sediment redistribution and sediment exchange with adjacent environments in the coastal tract (Masselink and van Heteren 2014). Widening and deepening of an initiated scour in a barrier's body under the effect of the aforementioned hydrodynamic processes (e.g. wave impact, run up, etc.) during a storm surge event is possible through the sediment transport from the initiation zone to elsewhere based on the storm surge regime. In fact, flowing water picks up sediments as load and transport them to locations of low-velocity fields to deposit there (Van Rijn 2007a; b; c; d). Thus, successive scouring and transport may lead to a full barrier breach.

Sediment transport consists of three stages (i) sediment entrainment, (ii) transport with the flow and (iii) sediment deposition and accretion. Regarding the transport itself, a distinction is made between three transport modes as shown in Fig 2.13 (Bagnold 1956):

(i) *Bed load*: the particles are rolling and making small jumps on the bed (Van Rijn 2007a).
(ii) *Suspended load*: the particles are suspended in the water column and are not in contact with the bed (Van Rijn 2007b).
(iii) *Sediment sheet flow*: the particles move in multiple layers under high shear stresses when the effective Shields parameter (Shields 1936) exceeds 1.0 [-] (Bosboom and Stive 2015; Camenen and Larson 2007; Shibayama and Horikawa 1982).

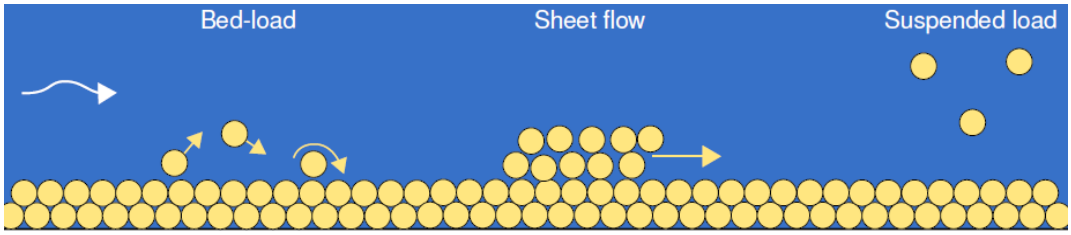

Fig 2.13: Sediment transport modes: bedload, suspended load and sediment sheet flow (De Vet 2014).

Morphological changes induced by sediment transport determine the bed evolution and the breach development. Thus, the better the prediction of the sediment stirring and transport is, the more accurate the prediction of the breach evolution (Elsayed and Oumeraci 2017a).

(ii) Soil avalanching and slopes instabilities

Slope adjustment and collapse dynamics during a storm surge represent one of the major processes that govern a breach development (Wainwright and Baldock 2015). With the sediment transport induced by wave-induced processes at a barrier's toe or at the bed of an initiated breach, portion of the barrier front or the breach wedges may avalanche when the local slope angle is larger than the equilibrium slope. Thus, lumps of sediment slide downwards where it can be eroded again by wave-induced processes (Fig 2.14). Nevertheless, such discontinuities in the mass failure makes indeed the modelling of the interaction between slumping soil and flowing water through the breach more complicated and challengeable.

In fact, the stability of a side slope depends on the relative strength of the resisting forces (e.g. internal friction, soil cohesion and suction) against the driving forces (e.g. gravity) (Al-Riffai 2014; Wu et al. 2011). Soil cohesion and suction tend to allow for vertical breach sides in lower barriers, whereas gravity tends to cause the collapse of side walls in high barriers. In addition, chemical substances (e.g. salinity) and organic materials in water and soil may also affect the breach shape because they modify the geotechnical properties (Elsayed and Oumeraci 2017a).

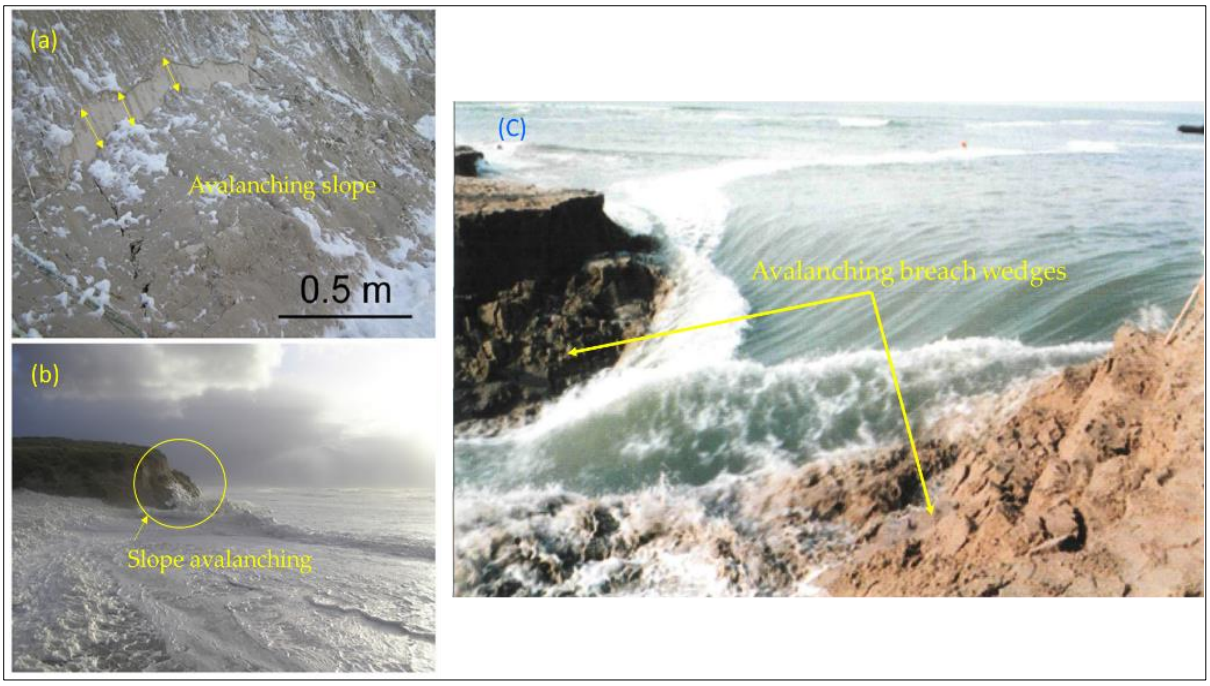

Fig 2. 14: Soil avalanching: (a) and (b) slumping of barrier slope as water reaches the barrier toe in the collision regime, leaving a dry scarp surface (after Masselink and van Heteren 2014), (c) avalanching of breaching side slopes (after Bakker et al. 1996).

Based on the previous initiation and development processes, three breaching mechanisms may be distinguished for barrier systems exposed to storm conditions (Chaumillon et al. 2017; Elsayed and Oumeraci 2017a; Muller et al. 2016). The first breaching mechanism is caused by the impact/collision of breaking waves on the barrier seaward slope in addition to the wave run-up and run-down during the collision regime (Fig 2.15.a), when the water level is lower than the barrier crest, inducing external erosion on the seaside. This process may result in barrier instability and seaward avalanching, which can lead to lowering of the crest and allow for overtopping followed by overflow. In this case, the breach development starts from the seaward side. The second mechanism is caused by overtopping of waves and may result in external erosion on the landward side during the overwash regime (Fig 2.15.b). In extreme cases, this erosion combined with instabilities can also lower the crest. As a third mechanism, overflow may occur during a storm when the mean water level exceeds the crest during the inundation regime (Fig 2.15.c). In this case, the continuous erosion on the landward side is relatively intense and may lead to a breach. For both overtopping and overflow, the breach initiation is on the landward slope of the barrier. During conditions of water ebbing/recession, a similar phenomenon can occur in the opposite direction due to overflow as shown in Fig 2.15.c.

Implication 2: Selection criteria of a breaching model

The description of the initiation and development processes in Section 2.2 allowing us to identify the following three selection criteria of a breaching model for further analysis.

a. Capability of describing and applying the hydraulic load (combined storm-tide with short waves) to coastal barriers.
b. Capability of describing the local discontinuities or depressions in the barrier crest by imposing the longshore and cross-shore variations of topography/bathymetry.
c. Capability of describing the initiation and development of a coastal barrier breach by considering the processes associated with the four flow regimes proposed by Sallenger (2000).

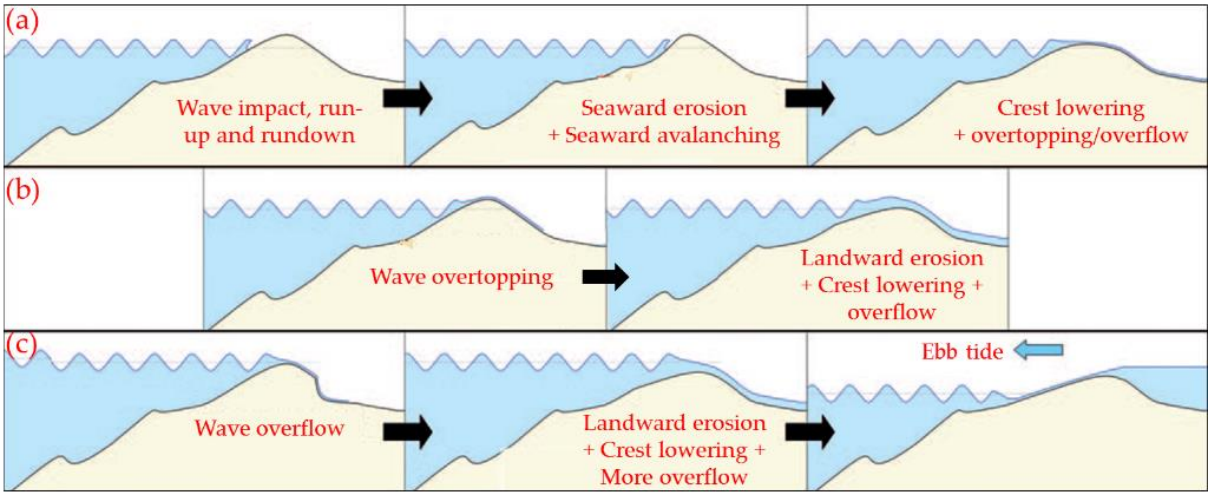

Fig 2.15: Hydrodynamic and geomorphological processes related to a breach initiation and development under (a) impact/collision regime, (b) overtopping/overwash regime, and (c) overflow/inundation regime, including the ebbing conditions, after Muller et al. (2016).

2.3 Classification of available breaching models

Assessing the safety of complex barrier systems and possible barrier breaching requires suitable modelling tools. In fact, many breaching models have been developed to assess coastal safety. Frank (2016), Morris et al. (2009) and Wu et al. (2011) summarised the most important breaching models (see also Elsayed and Oumeraci, 2014). Such models may be categorised based on the barrier type, material or soil type, mathematical representation, breach hydrodynamics and physical background (Wu et al. 2011) as the following (Fig 2.16).

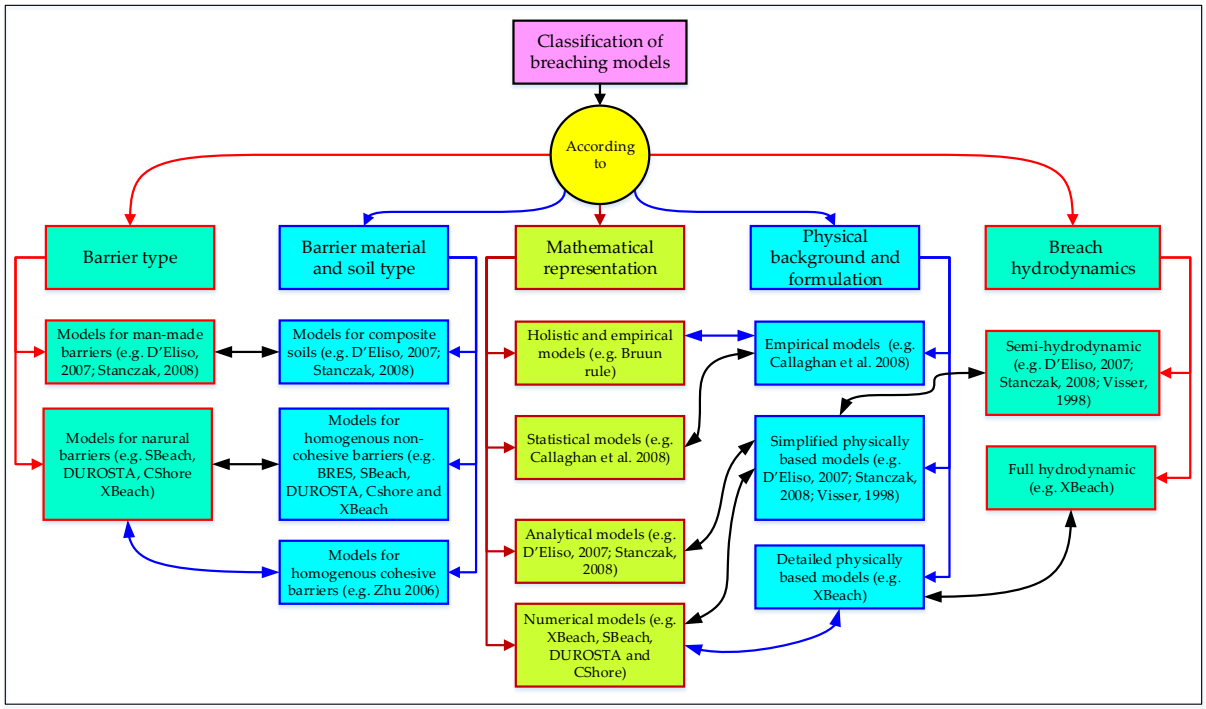

Fig 2. 16: Classification of breaching models

Regarding barrier types, distinction may be made between models for man-made coastal barrier (e.g. D'Eliso, 2007; Stanczak, 2008) and models for natural barriers (e.g. dunes and barrier islands) such as SBeach (Larson et al. 1989), DUROSTA (Steetzel 1993), CShore (Johnson et al. 2012; Kobayashi et al. 2007) and XBeach (Roelvink et al. 2009). The reason for the latter classification is the restriction in

applicability due to the barrier material. Man-made coastal barriers often consist of composite soils e.g. clayey cover and sandy core or vice verse and often with seagrasses (e.g. typical Dutch and German dykes). Thus, models developed for homogeneous non-cohesive barriers (e.g. the model of Tuan (2007), the BRES model of Visser (1998) and XBeach) and those developed for homogeneous cohesive barriers (e.g. Zhong et al. 2017; Zhu 2006) cannot be applied for both cases together. They are also not applicable for composite barriers made of cohesive and non-cohesive material.

From the perspective of the modelling approach, one may further classify erosion/breach models into holistic and empirical models (e.g. Bruun rule (Bruun 1962) and DUROS model (van Gent et al. 2008; Vellinga 1982)), statistical (e.g. Callaghan et al. 2008), analytical models (e.g. D'Eliso, 2007; Stanczak, 2008) and numerical models (e.g. XBeach, SBeach, DUROSTA and CShore). From the hydrodynamics viewpoint, one may classify breach models into "semi-hydrodynamic" (e.g. D'Eliso, 2007; Stanczak, 2008; Visser, 1998) and "full hydrodynamic" (e.g. XBeach). In the first category, to which several models belong, empirical flow formulations such as the broad-crested weir formula are used for describing the breach flow in several flow regimes. In the full hydrodynamic group, the breach flow is resolved usually using 1D or 2D St. Venant equations (Saint-Venant 1871).

Depending on the physical background and based on the model formulation and approximation of physical processes, breaching models may be classified into (i) empirical (e.g., Callaghan et al. 2008), (ii) simplified physically-based (e.g. D'Eliso 2007; Stanczak 2008; Visser 1998; Zhong et al. 2017) and (iii) detailed physically-based (e.g. XBeach). These can be further divided into statistical, analytical and numerical models based on the solution approach used. Statistical models use statistically derived regression equations for estimating the breach dimensions and thus they are usually empirical models. Simplified physically based models may be solved analytically or numerically whilst detailed physically based models (e.g. XBeach) need to be solved numerically. Simplified physically based breaching models often simplify the breach cross-section as a trapezoid, rectangle, or triangle. Moreover, they often approximate the flow through the breach by using the broad-crested weir relation; i.e. semi-hydrodynamic.

Detailed physically based one-dimensional (1D) cross-shore numerical models (e.g. SBeach, DUROSTA and CShore) have been developed to simulate the time-dependent cross-shore evolution of a storm profile and associated dune erosion. However, none of these models can (or only partly) consider longshore variability and related interactions (Van Dongeren et al. 2017; Van Thiel de Vries et al. 2011). Therefore, they are only suitable for analysing dune erosion but not suitable for analysing barrier breaching, which is a three-dimensional (3D) process and which thus needs at least a two-dimensional (2D) model. For this purpose, the 2D depth-averaged model XBeach was developed by Roelvink et al. (2009). The XBeach model is a model for dune erosion, overwash and breaching as it fully includes the longshore direction and therefore seems a useful tool to assess complex beach/dune systems in which longshore effects might be important (Van Thiel de Vries et al. 2011).

The suitability of XBeach for modelling barrier breaching, rather than other fully hydro-morphodynamic models (e.g. coupled Delft3D-WAVE (SWAN) with Delft3D-Flow (Booij et al. 1997) or coupled TELMAC ® with one of its wave modules TOMAWAC or ARTEMIS and with its morphological module SISYPHE (see, e.g. Larroudé et al., 2015)) arises from the exclusive inclusion in XBeach of an algorithm that can determine the soil avalanching and slopes/banks instabilities. In fact, the model system XBeach includes a solver for the nonlinear shallow water equations (NLSWEs) with an embedded wave module as well as a morphodynamic solver together with a soil avalanching module, which revolves around a user-defined critical slope. The latter makes XBeach the most eligible model for modelling coastal barrier breaching under wave action.

Implication 3: Model selection and preliminary limitations

Among the aforementioned types of breaching models, the XBeach model seems to be the most suitable model to be considered for further analysis due to the following reasons:

1. It is a full hydro-geo-morphological model, which means that flow through the breach is described using fully hydrodynamic equations by considering the induced morphological changes and the subsequent soil instabilities and avalanches. The other hydro-morphological models (e.g. coupled Delft3D-SWAN or coupled TELMAC-TOMAWAC-SISYPHE) do not either include an avalanching module or do not include a proper wave action module (e.g. Basement by ETH Zürich (Vetsch et al. 2015; Worni et al. 2014)).

2. It is a physically-based and processes-based model and can therefore simulate the processes in the four flow regimes of Sallenger (2000) for breach initiation and development as described in Section 2.2.

3. It accounts for the longshore variability of the beach/barrier topography/bathymetry and can therefore account for the local discontinuities or depressions in the barrier crest and related interactions.

In addition to these advantages, XBeach is an open-source and freely available code, which means that users can make changes in the code to suit the requirements of individual projects. Moreover, the model is being continuously improved by an increasing community of users through diverse applications in different coastal environments worldwide. Furthermore, many studies worldwide (e.g. Bendoni 2015; Elsayed and Oumeraci 2016, 2017; Van Geer et al. 2014; Van Rooijen et al. 2015; De Vet 2014) have been attempting and still attempt to further develop and extend XBeach in order to include further nearshore processes in addition to those initially considered in the model (see Section 2.5).

The preliminary model limitations lie mostly in the restriction in applicability due to the barrier material (Fig 2.16) as follows:

1. XBeach is initially developed as a model system to simulate erosion of non-cohesive barriers (e.g. sand dunes, barrier islands and barrier spits) and subsequent breaches. Nevertheless, the PhD study of Bendoni (2015) represents a step in the right direction toward extending the model to simulate erosion of cohesive barriers.

2. The model can therefore not yet be applied to barriers with cohesive or composite materials.

3. Hindered erosion by seagrasses (e.g. D'Eliso, 2007; Stanczak, 2008) is not implemented yet in XBeach. Therefore, erosion of non-vegetated or barely vegetated non-cohesive barriers can only be simulated.

Further limitations of XBeach are identified in Section 2.5.

2.4 The XBeach model

In order to identify the capabilities and limitations of the XBeach model, the model components are briefly examined. As a result, breaching-related physics that are not modelled or modelled insufficiently by XBeach, as well as the physics dropped because of the schematization or any other effect are identified in section 2.5. Thus, new physics to be implemented in the model in order to improve its modelling capability may be purposed.

2.4.1 Identification, modes and components of the XBeach model

XBeach is a numerical processes-based hydro-geo-morphological model that has the ability to assess the coastal response of alongshore varying beaches/barriers during time-varying storm and hurricane conditions, including barrier erosion, overwash and breaching. The model includes processes of wave breaking, surf and swash zone processes, dune erosion, overwash and breaching. It also

includes an avalanching algorithm providing a smooth and robust solution for soil slumping during dune erosion and breaching. In fact, the need to XBeach model was urgent after the 2004 and 2005 Atlantic hurricane seasons and their catastrophic consequences because the existing tools at that time to assess barrier erosion under extreme storm conditions (e.g. SBeach, DUROSTA and CShore) were inadequate for coasts with significant alongshore variability (Van Dongeren et al. 2017; Harter and Figlus 2017; Van Thiel de Vries et al. 2011). Thus, the model presents a generic description for the breaching process where the evolution of the breaching-induced inlet(s) is calculated from the sediment transport induced by the dynamic flow in combination with avalanching-triggered slope/bank erosion.

XBeach can be operated in two main hydrodynamic modes (Fig 2.17): (i) a hydrostatic mode (also called Surf-beat mode) and (ii) a non-hydrostatic mode (Roelvink et al. 2017a).

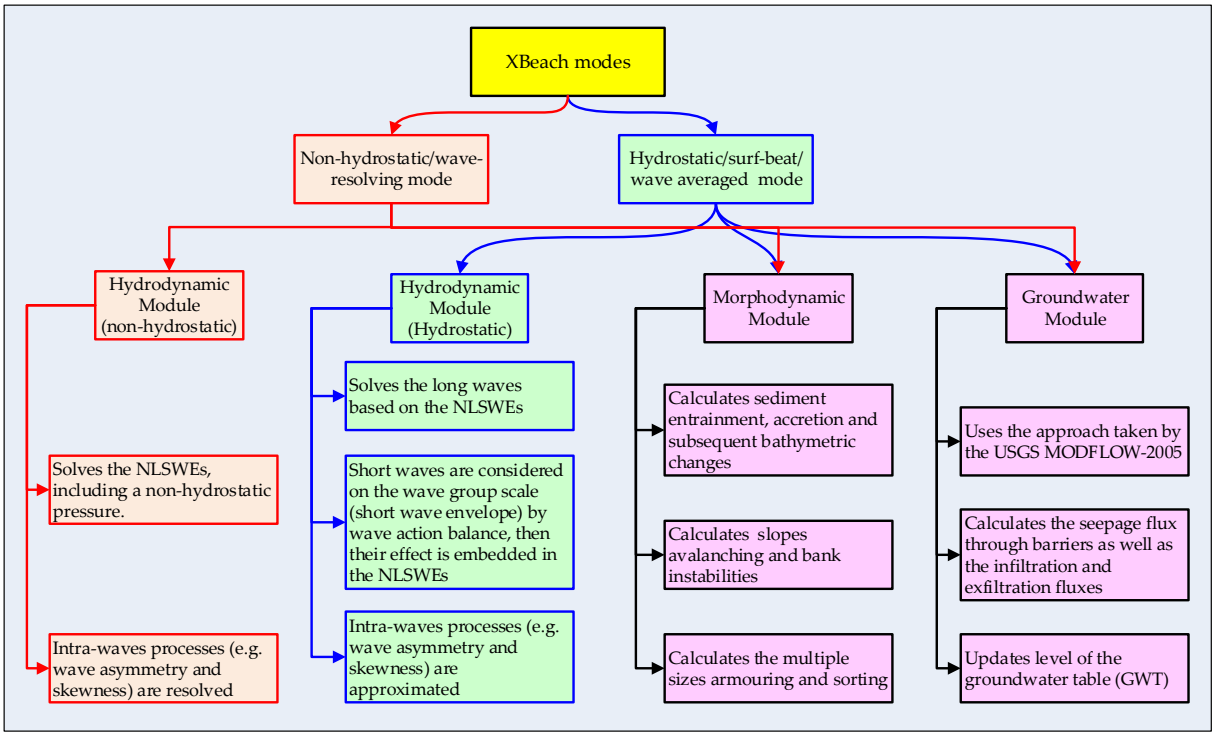

Fig 2.17: Main modes and components of the XBeach model with objectives of each module. Both hydrostatic and non-hydrostatic modes share the same morphodynamic and groundwater modules, but use different hydrodynamic module.

- *In the hydrostatic mode*, long waves (e.g. storm surges, tides and other infragravity waves) and as currents are solved separately from the short waves using NLSWEs form that is derived based on a hydrostatic pressure assumption. The short waves amplitude variations (i.e. envelopes of wave groups) are solved separately using a time-dependent wave action balance (Deltares 2015a; Holthuijsen et al. 1989; Roelvink et al. 2010, 2015). Thus, the NLSWEs equations are forced by the time-dependent wave action balance through radiation stress gradients (Longuet-Higgins and Stewart, 1962, 1964), i.e. effect of the short waves is embedded as a source term in the NLSWEs (see section 2.4.2). The separation in solving long waves (with currents) and short waves in the hydrostatic mode of XBeach allows the users to save indeed considerable computational time, but at the expense that the phase of the short waves is not simulated, thus causing the omission of intra-wave processes such as waves skewness and asymmetry (Elsayed and Oumeraci 2017a).
- *In the non-hydrostatic mode*, a more complete hydrodynamic mode of Smit et al. (2010), which solves all hydrodynamic processes without separation, including short wave motions, using a NLSWEs form that includes a depth-averaged normalized dynamic (non-hydrostatic) pressure (as a prototype version of the SWASH model of Zijlema et al., 2011). In fact, the non-hydrostatic mode represents an extension of the hydrostatic mode to provide XBeach with the

capability to model nonlinear waves, wave-current interaction and wave breaking in the surf zone, but with more computational demand as it requires much higher spatial resolution and associated smaller time steps to capture such intra-wave processes. The application of momentum conservative numerical schemes allows accurate modelling of wave breaking without the need of a separate breaking model as in the hydrostatic mode. Therefore, the non-hydrostatic mode represents an alternative and potentially more accurate approach for modelling wave-current interactions and the nonlinear evolution of a wave field. For the latter reasons, the non-hydrostatic mode has been recently extended to simulate the morphodynamic processes on gravel beaches (McCall 2015). Moreover, ship-induced waves can also be simulated using the non-hydrostatic mode (e.g. Zhou et al., 2014).

As breaching models use a suitable sediment transport module that is compatible with their assumptions, sediment transport and subsequent morphological changes are accounted for in both hydrostatic and non-hydrostatic modes of XBeach by means of the sediment transport equations of Van Rijn (2007a; b)-Van Thiel de Vries (2009) or Soulsby (1997)-Van Rijn (1984), the advection-diffusion equation of Galappatti and Vreugdenhil (1985) and the Exner equation for bed update in addition to an avalanching algorithm to account for slope slumping and bank instabilities. Moreover, XBeach includes a groundwater module, solving a generalised form of Darcy equation (Darcy 1856; Tek 1957). This module has been implemented in XBeach in order to simulate seepage and infiltration processes through coastal barriers during storms using a quasi-3D approach (McCall 2015; McCall et al. 2012). The latter means indeed that XBeach can work as a surface-subsurface model, utilising the NLSWEs for the surface propagation and couples them with 3D form of Darcy equation to simulate the subsurface processes (i.e. infiltration, exfiltration and seepage).

Implication 4: Hydrodynamic mode

XBeach was originally developed as a surf-beat mode model solving the propagation of long waves and currents using a deterministic approach to solve the hydrostatic form of the NLSWEs while short waves are solved stochastically using a phase-averaged approach based on the time-dependent wave action balance (Buckley et al. 2014). Thus, short-waves processes (e.g. wave breaking, wave skewness and asymmetry) are integrated into the main modelling system using approximation models (e.g. Elsayed and Oumeraci, 2017). Though these processes are simulated (i.e. not approximated) in the non-hydrostatic mode, the hydrostatic mode is the commonly used mode since the model development in 2009 as considerable computational time can be saved, which is important for a fast evaluation during extreme storm conditions. In fact, the use of the non-hydrostatic mode of Smit et al. (2010) is particularly important for applications on gravel beaches, where due to steep slopes swash motions (runup and rundown) because of individual short waves are dominant (McCall 2015; McCall et al. 2014; Roelvink et al. 2017b). On the other side, infragravity wave motion, which dominates the inner surf and swash zone on sandy beaches during storms, is of secondary importance. Because gravel beaches are not addressed in this PhD study, the surf-beat mode of Roelvink et al. (2009) is selected as the hydrodynamic module of XBeach. Another reason for this selection is addressed in *Implication 5*

2.4.2 Brief overview of model formulation

A full description of the XBeach model formulation can be found in Deltares (2015) and Roelvink et al. (2015, 2010, 2009). However, for the implications of this chapter (see *Implication 5*), the hydrodynamic formulation is briefly addressed in this section while the morphodynamic module is addressed in chapter 4. In fact, XBeach is a depth-averaged numerical model describes short-wave processes in a stochastic manner, solving the phase-averaged wave action equation of Holthuijsen et al. (1989) often based on empirical formulations calibrated to field or laboratory data (Buckley et al. 2014). However, the infragravity wave motions and mean flows induced mass-flux are modelled in a

deterministic manner based on mass and momentum conservation laws, solving a Generalised Lagrangian Mean (GLM) form of the NLSWEs (Andrews and McIntyre 1978; Walstra et al. 2000) using a finite difference scheme. The GLM approach unambiguously splits a motion into a mean part and an oscillatory part, thus giving a mixed Eulerian–Lagrangian description for the flow field for wavy water surfaces, but appointed to fixed Eulerian coordinates. Therefore, the GLM approach does not suffer from the strong drawback of the Lagrangian specification of the flow field – following individual fluid parcels – that Lagrangian positions which are initially close gradually drift far apart (Andrews and McIntyre 1978). In the Lagrangian frame of reference, it, therefore, becomes often difficult to attribute Lagrangian-mean values to some location in space while a pure Eulerian frame of reference (as in the common flood propagation models) omits the oscillation induced by wavy water surfaces. Thereby, the short waves induced radiation forces (F_x and F_y $[N/m^2]$) are input as external source term in the NLSWEs as follows

$$\frac{\partial z_s}{\partial t} + \frac{\partial (d\,.\,u^L)}{\partial x} + \frac{\partial\,(d\,.\,v^L)}{\partial y} = 0 \tag{2. 1}$$

$$\frac{\partial u^L}{\partial t} + u^L.\frac{\partial u^L}{\partial x} + v^L.\frac{\partial u^L}{\partial y} - \nu_h\left(\frac{\partial^2 u^L}{\partial x^2} + \frac{\partial^2 u^L}{\partial y^2}\right) = \frac{\tau_{sx} - \tau_{bx}^E}{\rho d} - g.\frac{\partial z_s}{\partial x} + \frac{F_x}{\rho d} \tag{2. 2}$$

$$\frac{\partial v^L}{\partial t} + u^L.\frac{\partial v^L}{\partial x} + v^L.\frac{\partial v^L}{\partial y} - \nu_h\left(\frac{\partial^2 v^L}{\partial x^2} + \frac{\partial^2 v^L}{\partial y^2}\right) = \frac{\tau_{sy} - \tau_{by}^E}{\rho d} - g\,.\frac{\partial z_s}{\partial y} + \frac{F_y}{\rho d} \tag{2. 3}$$

Where z_s is the water surface level [m], z_b is the bed level [m] so that the water depth $d = z_s - z_b$, u and v are the depth-averaged flow velocities per meter width [m/s] in x- and y- directions, ν_h is the horizontal eddy viscosity coefficient $[m^2/s]$, ρ is the water density $[kg/m^3]$. τ_{sx} and τ_{sy} are the components of the surface shear stresses $[N/m^2]$ while τ_{bx} and τ_{by} are the components of the bed shear stresses $[N/m^2]$. Most of the terms in Eqs 2.1-2.3 are formulated in terms of the Lagrangian velocities (superscript L), which are defined as the distance a water particle travels in one wave period divided by this period. Only the bed shear stresses (Eq. 2.4) are formulated in terms of the Eulerian velocities (superscript E) and defined as the short-wave-averaged velocity observed at a fixed point. The difference between the Lagrangian velocities and the Eulerian velocities represents the Stokes drift.

$$\tau_{bx}^E = c_f \rho u^E \sqrt{(1.16u_{rms})^2 + u^{E^2} + v^{E^2}} \quad \text{with} \quad \tau_{by}^E = c_f \rho v^E \sqrt{(1.16u_{rms})^2 + u^{E^2} + v^{E^2}} \tag{2. 4}$$

c_f is a dimensionless bed friction coefficient $\{c_f = \sqrt{(g/(C_{ch}^2))} = \sqrt{((gn^2)/d^{1/12})}\}$, n is the Manning coefficient $[s/m^{\frac{1}{3}}]$. The root-mean-squared orbital velocity u_{rms} [m/s] is the short wave orbital velocity that is at bed obtained from the wave group varying wave energy using linear wave theory (Sultan 1992) as:

$$u_{rms} = \frac{\pi \mathrm{H}_{rms}}{T_{rep}.\sqrt{2}.sinh(k(d+\delta.H_{rms}))} \tag{2. 5}$$

T_{rep} is the representative wave period [s], H_{rms} is the root-mean-square wave height [m], k represents the wave number $[m^{-1}]$ and δ states what fraction of the wave height should be added to the water depth in order to account for the wave nonlinearity effect on u_{rms} (Roelvink et al. 2015).

Implication 5: XBeach as a flood propagation and saltwater intrusion (SWI) model

1. *XBeach as a flood propagation model*: The hydrostatic mode of XBeach describes the propagation of long waves and currents deterministically using the GLM form of the NLSWEs (Eqs 2.1-2.3). In fact, common state of the art flood propagation models (e.g. River-2D, BASEMENT-2D, MIKE FLOOD, BreZo, DIVAST, TELEMAC-2D, TUFLOW and SOBEK) also utilize a hydrostatic form of the NLSWEs similar to that in Eqs 2.1-2.3 but without using the GLM approach and without the short waves induced forces (Fx, Fy) (i.e. they utilise only the Eulerian frame of reference).
   The previous conclusion leads indeed to the following important research question, which will be addressed in this PhD study (Chapter 5):

- *Is the XBeach model capable to simulate the inundation induced by a barrier breaching instead of applying another inundation model?*

To facilitate the answer to this question, the surf-beat mode of XBeach is selected as the hydrodynamic module of XBeach in this PhD study because this mode is similar to the common state of the art flood propagation models, both utilizing hydrostatic forms of the NLSWEs to compute of the flow field, which facilitate the comparison.

2. *XBeach as a saltwater intrusion (SWI) model*: propagating seawater through and behind a breach infiltrates vertically to the freshwater aquifers. Given that XBeach includes a groundwater module, another research question arises:

- *Is the XBeach model capable to simulate the subsurface processes related to SWI by utilising its groundwater module?*

In the case of positive outcomes of the previous two research question, the breaching, induced flood propagation and the subsequent SWI might be simulated together in a fully coupled modelling system using XBeach.

2.5 XBeach limitations and recent model developments

XBeach has proven its modelling capability for simulating coastal barriers response to extreme storm-tide conditions through diverse studies (e.g. Van Dongeren et al. 2009; Muller et al. 2016; Roelvink et al. 2009). In fact, XBeach is capable of simulating coastal barrier response under the four flow regimes of Sallenger (2000) while accounting for the breaching initiation and development processes (Section 2.2). Nevertheless, the model suffers some limitations, which need to be identified for further model improvement. The model's limitations related to breaching of coastal barriers can be grouped as the following.

2.5.1 Limitations related to barrier material

The world's coastlines can be divided into two main sub-systems (Ranasinghe 2016): Open (non-cohesive) coasts and deltaic (cohesive) coasts. Open coasts are generally sandy coasts, which represent up to 40% of the world's coastline, in addition to cliffed coasts and gravel beaches while deltaic coasts include estuaries and mostly consist of muddy or silt-sand material. As aforementioned in Section 2.3, XBeach can simulate morphodynamics of non-cohesive beaches and barriers, e.g. protective dunes, barrier islands and gravel beaches. Nevertheless, the model is inappropriate for cohesive coastal environments (e.g. salt marshes), clayey dykes and composite (cohesive/non-cohesive) barriers for the following reasons:

(i) XBeach calculates sediment transport based mainly on the common Shields relationship for incipient motion (Shields 1936), which is often inappropriate for cohesive soils as transport of cohesive sediments significantly depend on their composition (Winterwerp and Kesteren 2004).

(ii) Slope avalanches and bank instabilities are much more complex in cohesive than in non-cohesive soils as they often take the form of head-cuts in the former soil type while debris flow and slipping are more common in non-cohesive soils (Bendoni 2015; Zhong et al. 2017).

For these reasons, the applicability of XBeach is still limited to non-cohesive soil environments. Since this PhD study concerns the breaching of coastal dunes and other natural barriers (e.g. barrier islands and barrier spits), which generally consist of sand material, the treatment of cohesive barriers is outside the scope of this study. Nevertheless, the PhD study of Bendoni (2015) represents an important step in the right direction toward extending the model to simulate erosion and breaching of cohesive barriers.

2.5.2 Limitations related to bed friction

In older versions of XBeach, a constant value for the bed friction coefficient is implemented over the whole model domain using Chezy coefficient. Recently, Roelvink et al. (2015) improved XBeach to account for other user defined friction coefficients (e.g. Manning and Nikuradse coefficients). Moreover, they allowed XBeach to accept spatially varying friction values by assigning a different friction coefficient for each cell of the computational grid. Nevertheless, implementing spatially varying friction values is at present only possible through Chezy coefficient. In this context, two more improvements could still be possible:

(i) Improving XBeach to accept spatially varying values for other friction coefficients such as Manning's and Nikuradse's coefficients.

(ii) Implementing an automatic procedure to account for bed friction based on the roughness of bed grains in addition to other friction sources such as bed forms and vegetation (e.g. Vetsch et al., 2015) so that the model can automatically account for spatiotemporal variation of the bed friction.

2.5.3 Vegetation effect on coastal erosion and sediment entrainment

Coastal vegetation represents an environmentally friendly coastal protection against coastal erosion and barriers breaching. In general, vegetation can improve barrier strength and attenuate wave load as shown in Fig 2.18.

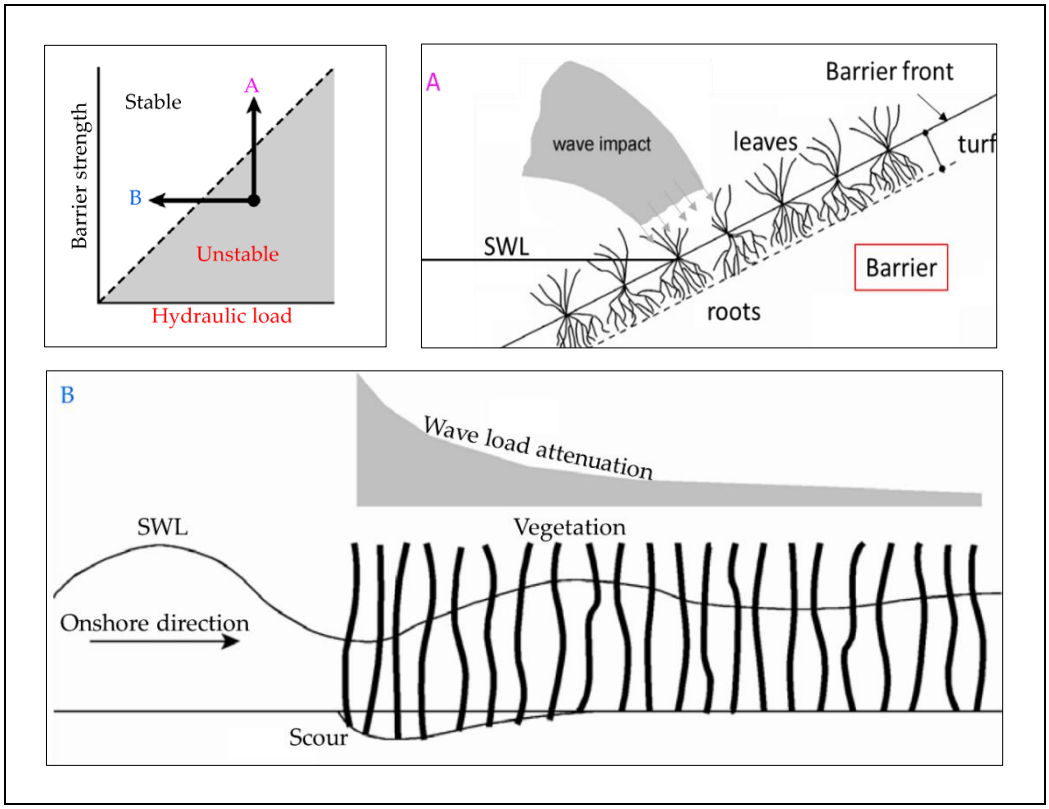

Fig 2. 18: Vegetation role in improving the resilience of coastal barriers: Vegetation increases barrier strength against coastal erosion and breaching (option A). Moreover, aquatic plants reduce the hydraulic load through wave and current attenuation (option B), after Schiereck (2005).

In fact, vegetation roots (option A) can hinder so much sediment entrainment and transport under successive sea loads (e.g. D'Eliso 2007, Schiereck 2005, Stanczak 2008). The roots may improve the resiliency of coastal defences against erosion as it increases the barrier resistance against erosion. The bio-stabilization effect induced by vegetation represents an important factor in hindering sediment transport and subsequent breaching. Moreover, such effect has been shown to be higher for sandy

barrier than for their cohesive counterparts (Bendoni 2015). Moreover, aquatic plants (e.g. reed, rush and willow trees; option B in Fig 2.18) may attenuate both waves and current velocities, which means the decrease of the hydraulic loads (e.g. Möller et al. 2014). With the recent development of XBeach by Van Rooijen et al. (2015, 2016a; b), XBeach becomes able to simulate wave attenuation by vegetation. Nevertheless, the effect of vegetation on barrier strength and resistance against erosion is still missing module in the present XBeach version.

2.5.4 Limitations related to depth-averaged computations

XBeach is a depth-averaged model, describing depth-averaged flow and induced sediment transport. Being a 2D horizontal (2DH) model, it applies its computations into a 2DH computational grid that represents the spatial domain. This means that the vertical dimension is modelled as one layer in the form of water column for each computational cell. Consequently, information of the vertical variation of the flow field and sediment concentration is missing as they are lumped and represented by one single number for each grid cell. The latter indeed has two important implications:

(i) Return flows (e.g. undertow) are implicitly included in the depth-averaged equations (the NLSWEs). Therefore, undertow and the associated sediment transport cannot be visualised independently in XBeach.

(ii) Model applicability is limited to shallow water at the nearshore, where water depths are small as compared to model domain (Vreugdenhil 2013; Weiyan 1992)

This limitation is part of the XBeach assumptions which is acceptable as long as vertical variations of flow fields and sediment concentrations are not of high interest. Nevertheless, the utilisation of depth-averaged computations is of particular importance for this PhD study as it facilitates comparing XBeach with common flood propagation models, which are often also based on depth-averaged calculations.

2.5.5 Limitations related to phase-averaged computations

The hydrostatic mode of XBeach (i.e. Surf-beat mode) resolves propagation of short waves in the scale of wave groups using the wave action balance. As a result, short waves effect is considered in the NLSWEs as a source term through radiation stress gradients (see Section 2.4). This means that surface elevations, shapes and phases of short waves are not resolved. Accounting for short waves shapes and phases, as in the non-hydrostatic mode, requires indeed very fine computational grid, often with cell sizes in the order of centimetres which lead to computationally expensive simulations. Therefore, most of the XBeach models that are applied in practical storm cases consist of grid sizes that are at least two orders of magnitude larger (De Vet 2014). Thus, the use of the surf-beat mode is more common in practical simulations, but at the expense that the phases and shapes of the short waves are not simulated.

Omitted short wave shapes have important implications on coastal sediment transport (Elsayed and Oumeraci 2017a; Van Thiel de Vries 2009). To indirectly account for their effects (e.g. wave skewness and asymmetry), Roelvink et al. (2010) and Van Thiel de Vries (2009) utilised empirical model that takes the following form

$$u_a = \gamma_{ua} u_{rms} (S_k - A_s) \tag{2.6}$$

Where u_a is a net flow velocity that stirs sediment to transport onshore under effect of short wave skewness and asymmetry (short wave nonlinearity), S_k and A_s are the wave skewness and wave asymmetry that are calculated in XBeach using either the formulation of Van Thiel de Vries (2009) or the formulation of Ruessink et al. (2012) while γ_{ua} is a calibration factor defined in XBeach by the keyword "*facua*" (*fac*tor for u_a) and has a default value of 0.1. In case of or on the locations where waves are linear (symmetric), u_a vanishes because both S_k and A_s equal zero. However, with highly nonlinear waves, higher values for u_a are expected since the difference between S_k and A_s is considerable. Consequently, higher values for u_a result in higher onshore sediment transport (Deltares 2015a; Nederhoff et al. 2015).

The limitation of XBeach regarding this point lies in the high model sensitivity to the calibration parameter γ_{ua}. It represents in fact one of the most important parameters in XBeach as it is the parameter mostly affecting the net cross-shore sediment transport (Bugajny et al. 2013; Vousdoukas et al. 2012). Therefore, many studies (e.g. Nederhoff 2014; Splinter and Palmsten 2012; De Vet et al. 2015; Vousdoukas et al. 2012) reported that *facua* usually need to be increased (than the default value 0.1) in order to achieve better prediction of the erosion rates. This means that the model of Van Thiel de Vries (2009) in Eq 2.6 needs to be improved in order to proparely calclate the sediment tranport induced by non-linear short waves.

2.5.6 Overestimation of erosion rates for high flow velocity regimes

The hydrodynamics and morphodynamics of XBeach were extensively calibrated and validated against (1D) flume experiments (e.g. Van Dongeren et al. 2009; Roelvink et al. 2009; Van Thiel de Vries 2009) and some (2DH) field cases (e.g. Roelvink et al. 2009): the model showed qualitatively a good agreement with measured cross-shore measurements of dune erosion and overwash. However, the overwash morphology is validated for the first time using the 2DH field case Santa Rosa Island (see Section 4.3.3) under Hurricane Ivan (McCall 2008; McCall et al. 2010). Such hurricane events often result in significant overtopping rates and high flow velocities, especially through breach induced inlets (Bisschop et al. 2010, 2016). The results of the Santa Rosa simulations have shown that XBeach substantially overestimates the erosion volumes and consequently the washover volumes (McCall 2008; McCall et al. 2010; De Vet 2014). As reported by McCall et al. (2010) and De Vet (2014), the overestimation of the erosion rates for the specific Santa Rosa case is certainly due to the limitations of the morphodynamic module of XBeach to reproduce sediment transport with sufficient accuracy rather than to the limitations of the hydrodynamic module. In fact, numerous studies (e.g. Daly et al. 2012; Deltares 2015a; b; Roelvink et al. 2009; De Vet 2014) reported that XBeach is generally capable of predicting hydrodynamics properly. In some cases, however, the sediment transport rates are overestimated, especially during extreme storm surge conditions where significant overtopping rates and high flow velocities are expected.

In order to overcome the overestimation of the erosion rates by XBeach under such conditions, previous studies such as those by De Vet (2014), McCall et al. (2010) and Terlouw (2013) suggested two artificial limiters as well as three physically-based limiters for the sediment transport (Fig. 2.19).

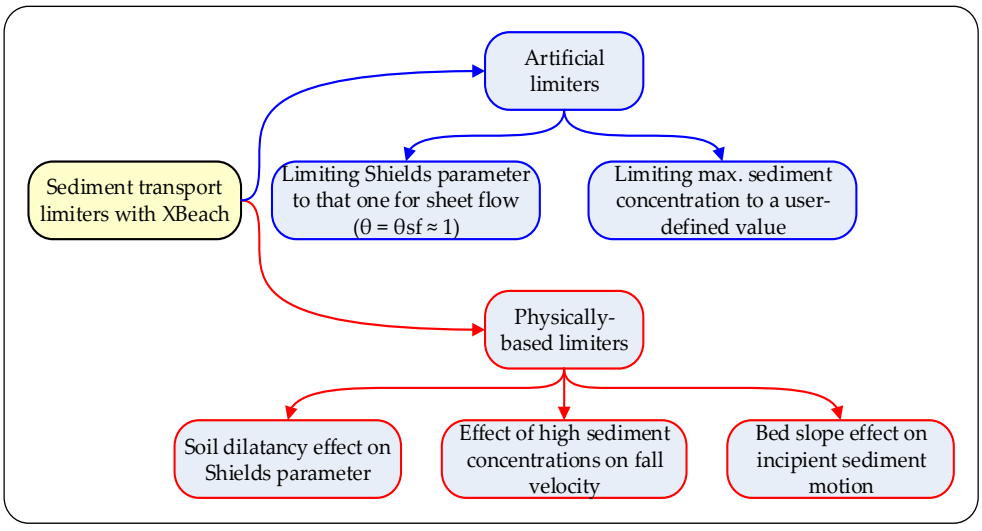

Fig 2. 19: Artificial and physically-based sediment transport limiters to reduce the erosion rates over-predicted by XBeach.

Artificial sediment transport limiters

1. *Effective Shields parameter* θ: it is restricted by a threshold value θ_{sf} at which sediment sheet flow occurs. In this case, the sediment stirring velocity is restricted to the velocity U_{sf} that corresponds to a Shields parameter value at which sheet flow of sediments occurs (usually at $\theta_{sf} \geq 1$). This

limiter sets an upper boundary for the difference between the effective and critical stirring velocities (Elsayed and Oumeraci 2017a) and thereby reduces sediment transport (McCall et al. 2010; De Vet 2014).

2. *Sediment concentration*: This limiter, suggested by Terlouw (2013) and De Vet (2014), restricts the maximum sediment concentration $C_{\max}$ in XBeach to a user-defined value instead of the current value $C_{max} = 0.1\ m^3/m^3$. As a result, this limiter also sets an upper boundary for sediment concentration and for the subsequent sediment transport.

Both artificial limiters showed unexpected side effects and in some cases led to significantly worse predictions than without any limiters (Terlouw 2013; De Vet 2014). Moreover, both limiters are rather artificial without any sound physical basis. Therefore, the overestimation of the erosion rates by XBeach means that it is due to either unknown or excluded physical processes that need to be explored and added to the model. Consequently, other studies attempted to improve the XBeach prediction capability by including new physical processes such as: (i) the hindered erosion due to soil dilatancy (Bisschop et al. 2010, 2016, Van Rhee 2007, 2010; De Vet 2014), (ii) the effect of high sediment concentrations on fall velocity (Richardson and Zaki 1997; De Vet 2014) and (iii) the bed slope effect on incipient sediment motion (De Vet 2014; Walstra et al. 2007).

Physically-based sediment transport limiters

1. *Hindered erosion by soil dilatancy*: Van Rhee (2007, 2010) reported that the erosion induced by high flow velocities might be affected by the bed soil dilatancy, which hinders the sediment pick up and reduces the sediment transport. As a result, Van Rhee derived a formula that amplifies the value of the critical Shields parameter θ_{cr} based on the soil properties. The latter increased critical Shields parameter, therefore, increases the critical velocity required to initiate the sediment particle motion. As a result, the difference between the stirring and the critical velocities reduces which reduces erosion rates accordingly. By other words, dilatancy causes an extra inward hydraulic gradient on the soil particles that increases the resistance of the soil mass to erosion. Although dilatancy is proven to be one of the most important erosions hindering processes (Bisschop et al. 2016), implementing the dilatancy effect to XBeach does not sufficiently reduce the erosion to achieve proper results (De Vet 2014; De Vet et al. 2015).
2. *Effect of high sediment concentrations on fall velocity*: High sediment concentrations reduce the settling velocity (Richardson and Zaki 1997) and hence decrease sediment response to deposition/entrainment which finally reduces sediment transport. De Vet (2014) implemented to XBeach the effect of high sediment concentrations on fall velocity and reported that this effect might slightly reduce the erosion rates over-predicted under extreme flow conditions.
3. *Bed slope effect on incipient sediment motion*: the critical Shields stress for initial sediment motion increases with bed slope, which indicates that particles of the same size are more stable on steeper slopes (Lamb et al. 2008; Prancevic and Lamb 2015; Walstra et al. 2007). As an attempt to reduce the erosion rates in XBeach, the latter fact is recently implemented through reducing the sediment discharges calculated based on the common Shields criterion (Roelvink et al. 2015; De Vet 2014). However, considering the bed slope effect does not sufficiently reduce the erosion to achieve proper results (De Vet 2014; De Vet et al. 2015).

These three physically-based sediment transport limiters do not sufficiently reduce the overestimated erosion rates during regimes of high flow velocities. Therefore, most recent studies (e.g. Harley et al. 2016; Muller et al. 2016) still use the artificial limiter of the sediment sheet flow. This means that the overestimation problem needs to be urgently addressed using other new physically-based means so that reliable erosion rates can be achieved.

2.5.7 Limitations related to grain-stabilisation and soil compaction

The experiments of Shields (1936), which build the basis of the Shields approach for the calculations of critical stirring velocity in XBeach, were carried out with steady uniform flow over a plane bed of uniform sediment with small grain-interlocking. Therefore, it is believed that the classical Shields concept for the inception of motion does not account for the grain-interlocking effect and the

soil texture effect, which are more pronounced for natural mixed-grain-size sediment beds than for uniform sediment beds. Therefore, a large part of the erosion overestimation by XBeach might be attributed to the underestimation of the critical Shields parameter for incipient sediment motion. By other words, there are unaccounted forces in the formulation of the critical Shields parameter such as the uprooting force (to overcome the sediment interlocking). In fact, this assumption is in line with:

(i) the studies of Morris (2011) and Özer et al. (2016), which reported that the soil erodibility depends on the soil texture as well as on the compaction energy and

(ii) the study of Reid and Frostick (1984) who reported, based on field measurements, that the shear stress required to initiate particle motion in natural sediment beds is considerably in excess of that predicted by the Shields curve.

For instance, the values of the effective shear stress measured by Reid and Frostick (1984) for incipient bedload were consistently higher, ranging from 1.2 to 6.2 times the common critical shear stress values predicted by the Shields curve. Reid and Frostick (1984) attributed this excess to the mutual interference of bed sediment particles (see also Section 4.2.2). The latter indeed ensure that the critical shear stress calculated based on Shields curve is underestimated as long as sediments are mutually interlocked and stabilised under compaction/consolidation effect. This might result in the over-predicted erosion rates by XBeach.

2.5.8 Limitations related to longshore variability of soil strength

The main motivation behind initiating the XBeach model was to account for the alongshore variability, which cannot be considered using only 1D coastal erosion models, e.g. SBeach, DUROSTA and CShore (Roelvink et al. 2009; Van Thiel de Vries et al. 2011). In this context, Elsayed and Oumeraci (2016) distinguish three types of the alongshore variability for which the location of incipient breaching is a function of the interaction among them:

1. *Topographical/bathymetrical variability:* It arises from local discontinuities or depressions in the barrier crest in addition to the longshore variability of the barrier width and foreshore bathymetry. XBeach can account for this variability type through the digital elevation model (DEM) imposed to XBeach through the computational grid. Thus, the more accurate the DEM and the finer the computational grid is the more accurate the accounting for this variability type.
2. *Hydraulic variability:* Real sea state consists of short-crested waves, which means that wave heights are varying alongshore. In the case of short-crested waves (or generally alongshore varying hydraulic loads), the hydraulic load is non-uniformly distributed alongshore, resulting in wave focusing at local zones in front of the barrier. Thus, alongshore varying wave impact, alongshore varying wave runup and run down are expected. As a result, the erosion, avalanching and the induced lowering of the barrier crest may also vary alongshore. XBeach can account for this variability type through using the standard JOint North Sea WAve Project (JONSWAP) spectrum for wave generation, which stochastically generates alongshore varying time series of the wave energy.
3. *Variability of soil strength*: soil response to coastal erosion may also vary alongshore as shown in Fig 2.20 because of the spatial variability of the soil characteristics. Thus, initiation of breaches is more expected in zones of lowly consolidated soil while highly compacted zones may sustain higher hydraulic loads with less erosion. XBeach does not yet account for this variability type because of its incapability to account for grain-stabilization and soil compaction (see Section 2.5.7). Thus, accounting for this variability represent a candidate topic for further development of XBeach.

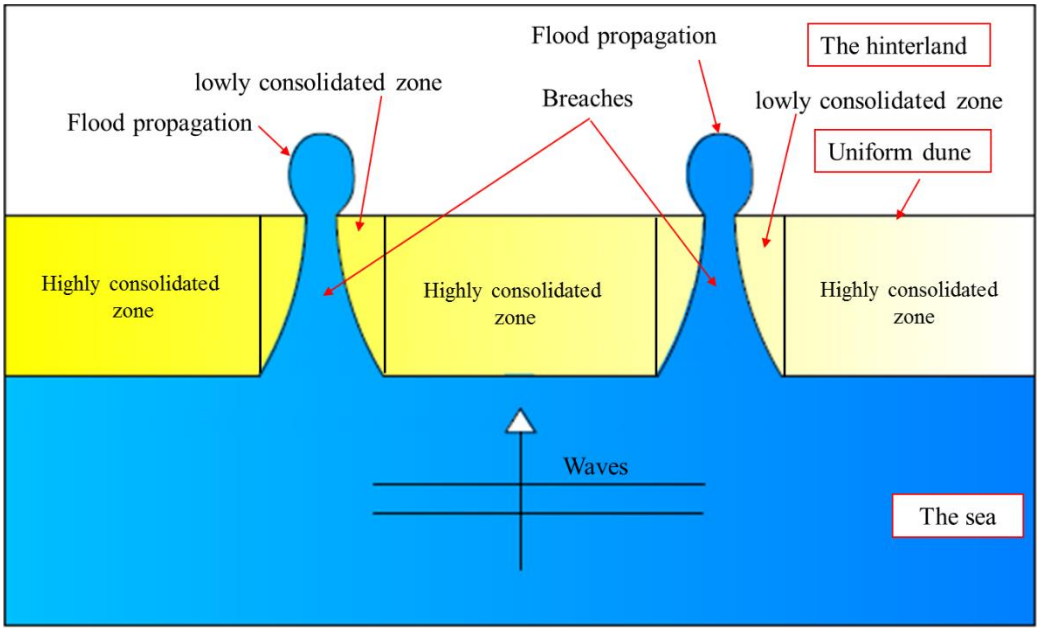

Fig 2. 20: Schematic representation of the effect of longshore variability of soil strength on barrier breach initiation.

Implication 6: Further improvements of XBeach

Predicting reliable breach dimensions is a crucial issue to obtain reliable inland discharges through breaching-induced inlet(s). As a result, realistic analysis of the induced coastal flood propagation in the hinterland and the subsequent groundwater contamination can be achieved. In fact, the addressed limitations of XBeach may obstruct achieving such reliable breach dimensions. For the latter purpose, improving XBeach is necessary. For non-cohesive and non-vegetated coastal environments, the priority in improving the model should first be given to the limitations related to the sediment stirring processes:

1. Effect of wave shape and nonlinearity on sediment transport (Section 2.5.5) and
2. Effect of grain-stabilization and soil compaction on coastal erosion (Section 2.5.7).

In addition to the recent developments of XBeach by De Vet (2014) to overcome the erosion overestimation for high flow velocities using the dilatancy effect (see Section 2.5.6), overcoming these two limitations would help in improving the XBeach prediction capability. For instance, the first improvement would result in a better prediction of sediment transport when using the surf-beat mode of XBeach, while the second improvement would open the way toward accounting for the longshore variability of soil strength, which might result in a better prediction of possible breaching locations along the barrier. The priority of overcoming these two model limitations arises from the need to solve the overestimation of the erosion rates, especially during high flow velocity regimes, which hinder obtaining reliable breach dimensions and inland discharges through breaching induced inlets. Due to the aforementioned bio-stabilization effect in vegetated zones of barriers, the non-vegetated zones became more probable for breaching, thus providing the priority to these selected model limitations as for instance compared to the limitation related to bio-stabilization effect of coastal vegetation. Therefore, these two limitations will be addressed through this PhD study (see Chapter 4) as a contribution to improve the XBeach model.

2.6 Coastal floods induced by barrier breaching

2.6.1 Consequences of coastal floods caused by barrier breaching

Coastal floods induced by extreme storm surges are among the most destructive natural disasters (Chaumillon et al. 2017; Smith 2013). They may become even more destructive, especially when these floods result from coastal barrier breaching (Fig 2.21), where significant inland flow with very high velocities can extend widely in the hinterland in relatively short time (Bisschop et al. 2010; Kraus and Wamsley 2003; Lilai et al. 2016; Roger et al. 2010; Wu et al. 2011).

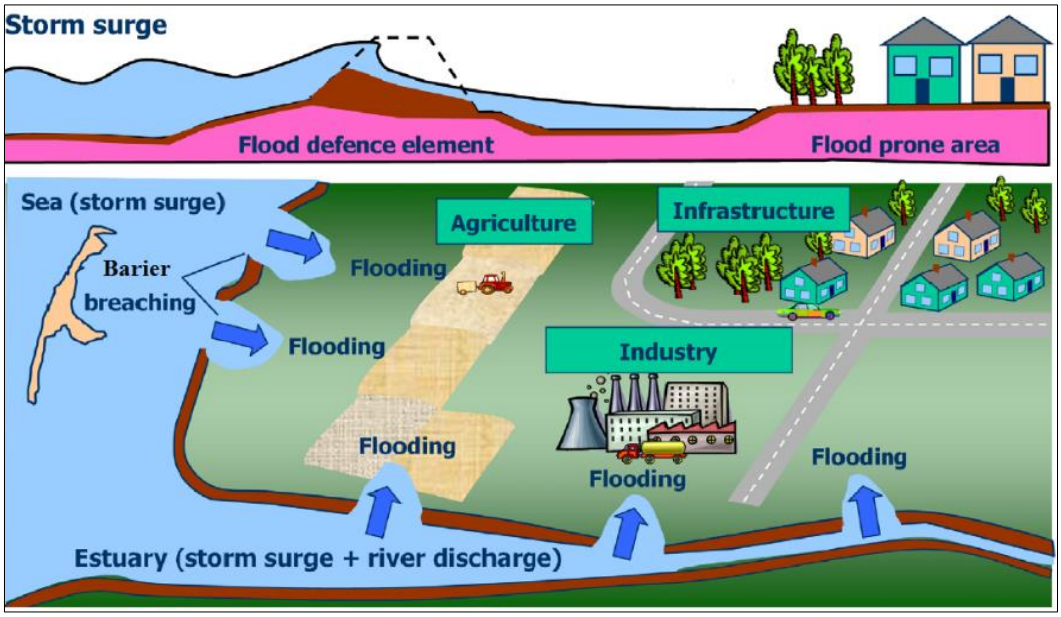

Fig 2. 21: Hydrodynamic and sediment-related processes that govern coastal flooding: the upper panel is a cross shore cross-section through a breached barrier showing the flood source (storm surge), the flood pathway (breach) and the flood receptor (hinterland), the lower panel is a plan view shows the spatial scale of the coastal flood (Oumeraci et al. 2015).

Catastrophic coastal floods are generally associated with loss of lives and injuries, as well as significant direct and indirect economic losses (e.g. Sills et al. 2008). In addition to these losses, coastal floods may have severe environmental and ecological consequences, e.g. ground water contamination due to saltwater intrusion into aquifers (e.g., Yang et al. 2013, 2015a; b).

The prediction of a storm-induced flood through a breach-induced inlet represents a real challenge because storm-induced breaches represent a multi-scale problem governed by complex interactions between a large variety of relatively uncertain hydrodynamic and sediment-related processes at different time and spatial scales (Chaumillon et al. 2017; Christensen et al. 2013; Elsayed and Oumeraci 2016b; He et al. 2015; Phillips et al. 2017; Wu et al. 2011). These processes and interactions are for instance

(i) combined water level rise and increased wave exposure during a storm surge (Section 2.1),
(ii) coastal barrier erosion and breach development (Section 2.2) and
(iii) subsequent flow into the hinterland and inundation during/after completion of the breach growth.

The entirety of all these processes constitutes coastal flooding as a physical system with its own characteristic dynamics. Because the outcomes of this system may lead to catastrophic consequences (e.g. Hinkel et al. 2014), it is important to analyse these system dynamics as well as the expected consequences and the human intervention with such a system. For this purpose, the knowledge of the distribution of the maximum water levels in the flooded area as well as the description of the path and the temporal propagation of the inundation by considering the size and shape of the flood prone area, its topography and any obstacles that can block or hinder the development of the flood are crucial. In

fact, they represent important and useful information to the decision makers, if implemented in rescue and emergency plans for the flood prone area (Cheung et al. 2003; Olbert et al. 2017). Moreover, they can be used to estimate the economic and the environmental consequences of a flood (see Section 2.7).

2.6.2 Current modelling approaches of a coastal flood

The main issue when modelling coastal inundation is the assessment of the volume flux of water that passes the sea defences (i.e. the inland flow hydrograph Q(t)) during an overtopping/overflow event and/or through a breach induced inlet. In earlier studies of coastal flooding (e.g. Bates et al. 2005; Chini et al. 2012; Smith et al. 2011), this information has been often missing. Only rough estimates could be proposed based on volume reconstruction using, for instance, aerial photographs to estimate the flood extent and then working out the water volume and hence the mean flow rate during the coastal inundation event. As a result, the mean flow rate is used as input for a common flood model to numerically reproduce the flood event. For the same purpose, other studies (e.g. Chini et al. 2012; Gallien et al. 2014; McCabe et al. 2013; Tsoukala et al. 2016) attempted to estimate temporally variable overflow rates along representative discrete transects using the empirical equations and/or neural network tool recommended by static models (e.g. EurOtop of Van der Meer et al. 2016). However, the inundation extent calculated based on such static models is often substantially overestimated when compared to real flood extent observations (Gallien 2016; Vousdoukas et al. 2016). Moreover, such empirical models cannot be used to calculate the inland discharge through a breach-induced inlet because of the dynamic nature of the breaching process, which cannot be analysed based on static and empirically-based overtopping/overflow models (e.g. EurOtop) by simply comparing water levels and land elevations. Recently, the XBeach model (Section 2.4) has been used in few studies (e.g. Barnard et al. 2014; Gallien 2016; Gallien and Guza 2015; Giardino et al. 2011) to numerically estimate temporally variable overtopping volumes (in the form of intermittent overtopping rates) along with representative discrete transects. The latter are also applied as input conditions for a common inundation model. The comparison between the overtopping rates calculated by static models (e.g. EurOtop) and dynamic models (e.g. XBeach) showed that the outcomes of the latter are more accurate (Gallien 2016). In fact, XBeach can predict overtopping rates with a relatively high determination coefficient ($R^2 = 0.87$) (Palmsten and Splinter 2016; de Santiago et al. 2017). However, the application of XBeach in coastal inundation studies is generally related to the estimation of wave overtopping rates.

To date, the modelling of coastal flood induced by wave overtopping is based on two subsequent and uncoupled modelling approaches: (i) empirical models (e.g. EurOtop) or numerical models (e.g. XBeach) to predict overtopping rates along representative discrete transects for overland flow model input, and (ii) computational fluid dynamic (CFD) solvers used as inundation models to simulate the overland and surface runoff using the results from the overtopping models as input conditions (Gallien 2016; Wadey et al. 2012; Worni et al. 2014). Such CFD models (e.g. River-2D, BASEMENT-2D, MIKE FLOOD, BreZo, DIVAST, TELEMAC-2D, TUFLOW or SOBEK) are generally based on the solution of the nonlinear shallow water equations (NLSWEs).

Similarly, the current modelling of a breach-induced flood is based on two subsequent and uncoupled modelling approaches: (i) breaching model (e.g. XBeach) to calculate the flow rates through a breach-induced inlet and (ii) CFD model as described above to simulate the inundation resulting from the breach. Indeed, such modelling approaches are more common in fluvial environments than in coastal environments, especially when analysing breaching-induced floods at conditions when a landslide dam retards the flow in a river stream (e.g. Elsayed 2013; Fan et al. 2012; Popescu et al. 2010; Radice and Elsayed 2014). The weaknesses of such uncoupled modelling approaches arise from the need to "manually" transfer the outcomes of the overtopping/breaching model to the inundation model. Moreover, by dividing the whole system into two subsystems (one for modelling breaching and another one for modelling the subsequent inundation), such separate modelling approaches partially omit the continuity of the processes and their interactions in both subsystems. Among these subsystems, the mass (flow) can be transferred in the form of inland hydrograph, but not the flow velocity and thus the momentum (Elsayed and Oumeraci 2016b). Though the momentum is mostly of

importance close to the breach because of the high flow velocities through and behind the breached/overtopped barrier, the omission of the momentum transfer between the decoupled breaching and inundation models would, even at less extent, affect the far field (see also chapter 5 for a comparison between combined and decoupled approaches of modelling breaching and induced inundation).

In order to overcome the weaknesses of such separate modelling approaches, combined modelling of overtopping/breaching of coastal barriers under extreme storm surges and subsequent coastal flooding is crucial. As a result, a single model system can carry out the computations over a single calculation mesh containing both the bathymetry of the nearshore area and the topography of the shore/hinterland. Indeed, many studies (e.g. Bertin et al. 2014; Christensen et al. 2013; He et al. 2015; Roland et al. 2012; Tadesse and Fröhle 2014; Vousdoukas et al. 2016) attempted to simulate storm surges and the induced coastal flooding in a single model. However, in these studies either the morphodynamics and thus the storm-induced breaches are omitted (e.g. Bertin et al. 2014; Roland et al. 2012; Vousdoukas et al. 2016) or a proper breaching/morphological module is lacking (e.g. Christensen et al. 2013; He et al. 2015; Tadesse and Fröhle 2014). However, all these studies were based on solving the NLSWEs over a single calculation mesh that contains the bathymetry of the nearshore area and the topography of the shore/hinterland.

Implication 7: Combined modelling of breaching and inundation processes

1. Current approaches for modelling breaching-induced coastal floods are based on separate modelling of barrier breaching and the induced flood in the hinterland, which may lead to significant modelling weaknesses (see Elsayed and Oumeraci 2016). Therefore, combined modelling of both breaching and flooding is crucial.

2. As XBeach includes a solver for the NLSWEs (CFD module) as well as a morphodynamic solver together with a soil avalanching module, its application can be extended to simulate overtopping/breaching in a single model system and subsequent coastal inundation together, using a unique calculation mesh for both CFD and morphodynamic modules (see Implication 5 in Section 2.4.2). While the morphodynamic solver is applied to simulate sediment transport and morphological changes including breach development, the CFD solver is used for the combined modelling of wave overtopping and overflow, for the flow through the developing breach and the subsequent coastal inundation processes. As a result, such a combined modelling may provide the advantages of (i) avoiding the "manual" transfer of the boundary conditions from the breaching model to the inundation model, which often leads to omitting the momentum transfer between the two processes, (ii) simulating the mutual interaction between hydrodynamics and morphodynamics, including soil avalanching, and (iii) considering the longshore variability of the hydraulic load and/or the coastal barrier topography (see Section 2.5.8). Thus, the application of XBeach can be extended to model coastal barrier breaching and inundation in combination, instead of the current approach, which addresses the modelling of each of these two processes separately. Nevertheless, the applicability of XBeach for the latter purpose still need to be tested. The testing procedure will be addressed in Section 2.8.

3. The outcomes of the inundation modelling (i.e. water depth and flood extent) are important information for further analysis and modelling of the vertical saltwater intrusion induced by the inundation (Fig 2.22). In fact, storm surge-induced breaching/overtopping event includes the following processes: (i) sea level rise, (ii) overtopping/breaching and ponding, (iii) sea level dropping and pond reduction and (iv) recovery of aquifer salinity to the initial state (remediation).

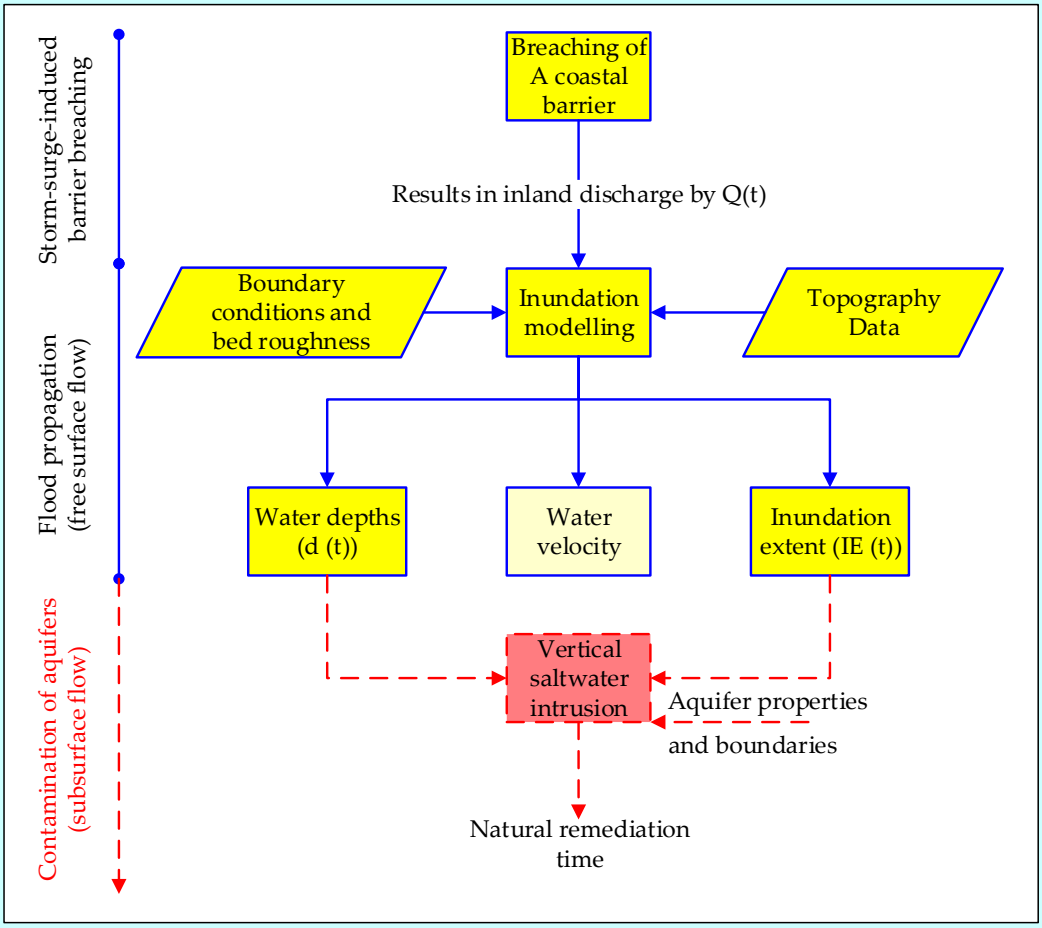

Fig 2. 22: Implications of breaching-induced coastal inundation for the analysis of subsequent saltwater intrusion: Due to flood propagation, the inundation extents over time. Saltwater infiltrates vertically causing aquifers contamination. Inundation extent (IE) and water depths are important information for the analysis of the SWI.

2.7 Breaching-induced salt water intrusion

During extreme storm surges, floods resulting from the overtopping/breaching of coastal barriers may represent a threat to people, assets and further resources onshore (Chaumillon et al. 2017). Moreover, coastal floods may result in saltwater intrusion (SWI) into coastal aquifers induced by the vertical infiltration of salt water behind the overtopped/breached coastal barriers (Yang et al. 2013, 2015a; b). Vertical SWI contaminates the originally fresh groundwater by increasing its salinity. This may thus significantly reduce the water quality and the environmental values of groundwater and may possibly hinder any possible sustainable development in coastal zones exposed to coastal flooding.

Mainly, the four reasons R1 - R4 illustrated in Fig 2.23 may lead to SWI in coastal aquifers. The first three reasons (R1 – R3) are mainly related to the hydraulic interconnection between seawater and groundwater. In fact, the mean sea level (MSL) and the groundwater table (GWT) in aquifers are interconnected like in a U-tube manometer as shown in Fig 2.24. The location of the salt-freshwater interface (sea water in red colour and fresh water in sky blue colour) depends indeed on the head difference Δh between the MSL and the GWT. The value of Δh increases spatially landward and thus results in lowering the interface in the same direction ($h = 40.\Delta h$ according to Herzberg (1901)). In the case of a long-term sea level rise (R1), the head difference Δh decreases. As a result, the interface moves landward to reach again the hydrostatic equilibrium. Such lateral shift of the interface represents a lateral seawater intrusion (see e.g. Ketabchi et al. 2016). The same type of intrusion may take place if

the GWT decreases (R2) under either a decrease of the rainfall rates or by human activities like excessive pumping (e.g. Mishra and Dwibedy 2015). Reason R3 related to local lateral intrusion (upconing) represents a special case of R2 that can take place in the case of a local lowering of the GWT under excessive pumping effect, leading to a local shift of the interface that often takes the form of an inverted cone (see e.g. Werner et al. 2009).

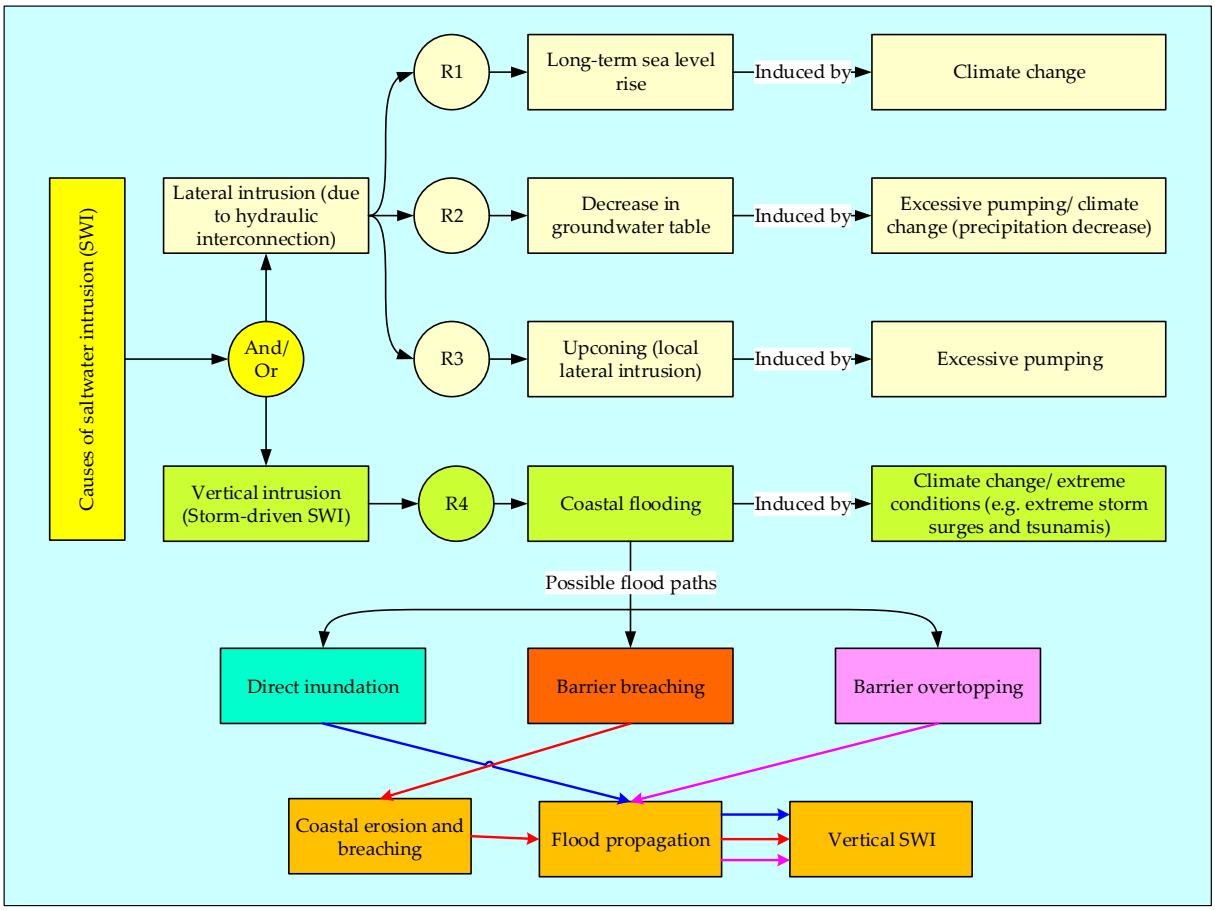

Fig 2. 23: Common reasons and involved processes in saltwater intrusion into fresh coastal aquifers

The fourth reason (R4) related to coastal flooding represents the most complex type of intrusion. The complexity arises indeed from the high diversity of the involved processes. Storm-driven saltwater intrusion (SDSWI) is often a cascading effect due to coastal barrier overtopping/breaching with subsequent vertical infiltration of the salt water propagating or/and standing behind the overtopped/breached barrier (Yu et al. 2016b). In fact, saltwater inundation due to coastal flooding has a substantial impact on the dynamics of coastal aquifers as well as on the salinity distribution in such aquifers (Violette et al. 2009; Werner et al. 2013; Yang et al. 2013, 2015a; b). Even a moderate storm surge event may significantly affect the usability of coastal aquifers for decades (Holding and Allen 2015; Wilson et al. 2011).

The breaching/overtopping of a coastal barrier, the induced inundation and the subsequent saltwater intrusion are naturally successive processes. Therefore, fluxes of water are continuous between the breach-induced inlet, the surface flow propagation and the subsurface intrusion, so that the flow through breaches represents the source for both surface runoff and the induced salt water infiltration. To predict the migration pathway and concentrations of contaminants in groundwater and to evaluate possible remediation scenarios of contaminated groundwater after a coastal flood, a proper processes-based numerical model is firstly needed.

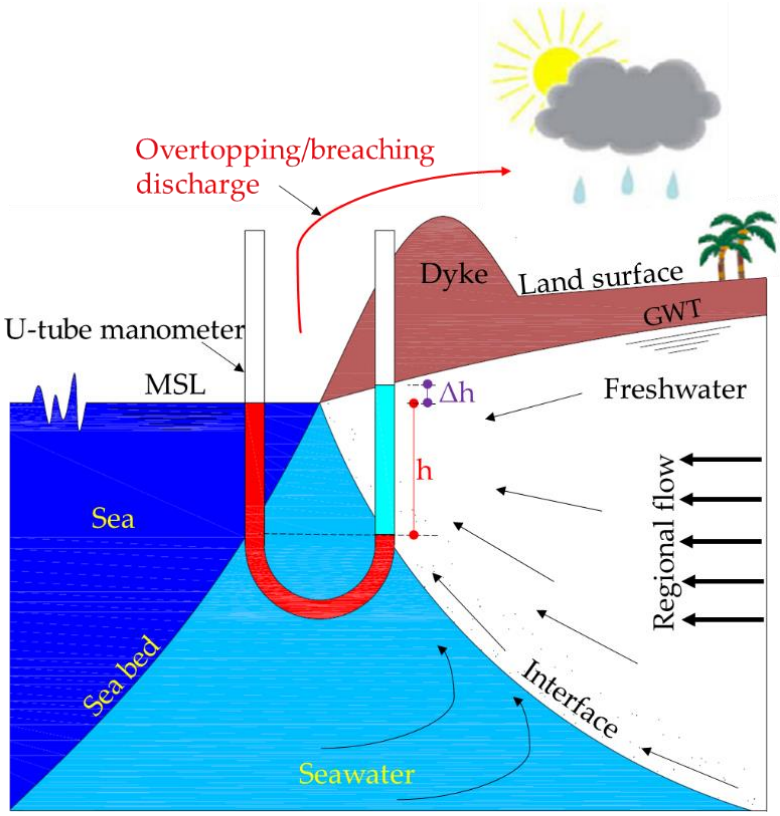

Fig 2. 24: Schematic diagram for the hydrostatic equilibrium between sea and fresh water in a coastal aquifer (U-tube manometer analogy). Seawater (red colour) and freshwater (sky blue colour) meet at the salt-freshwater interface. Water discharge due to overtopping/breaching propagates over the land surface behind the barrier (dyke) and intrudes vertically to the originally fresh groundwater, causing its contamination.

Many of the previous modelling studies for an SDSWI event (e.g. Yang et al. 2013, 2015a; b; Yu et al. 2016b) used the HydroGeoSphere (HGS) model of Therrien et al. (2010) for such purpose. The model has the advantage to account for the hydraulic coupling between the surface flow domain (simulated by diffusive wave approximation of the shallow water equations (Collier et al. 2011)) and the subsurface flow domain (simulated by Richards equation (Richards 1931) and the advection-dispersion equation for solute transport). As a result, HGS simplifies the flow and automatically transfer the boundary conditions from the surface to the subsurface domain. Nevertheless, the model does not simulate the breaching process. Using HGS, the studies of Yang et al. (2013, 2015a; b) reported that the natural remediation process after a coastal flood event takes 10 to 20 years. However, these studies have two main weaknesses:

(i) They roughly estimate the inland discharge based on a maximum admissible overtopping rate obtained from EurOtop of Pullen et al. (2007) as the case in Yang et al. (2013) or by assuming the overwash and breaching dimensions as the case in Yang et al. (2015a; b). EurOtop has shown an incorrect estimation of inland discharges and thus incorrect estimation of the coastal flood extent as shown by Gallien (2016) and Gallien et al. (2014), while assuming breaching dimensions in Yang et al. (2015a) results in incorrect estimates of the inland flow. Thus, the studies of Yang et al. (2013, 2015a; b) lack a proper estimation of the breaching dimensions and the induced inland discharge.

(ii) HGS predicts the surface propagation kinematics and inundation extent based on the diffusive wave approximation of the shallow water equations, which is unacceptable when calculating the overtopping rates or the flow through breaches because of the high flow velocity during such situations. In fact, the diffusive wave approximation is valid when the inertial acceleration is much smaller than all other forms of acceleration in the

shallow water equations, or in other words when there is primarily subcritical flow, which is often not the case through breaches or over barriers during overtopping.

Such incorrect estimates of the inland discharge and subsequent incorrect predictions of flood depths/extents would affect the natural remediation interval of coastal aquifers after an SWI event. Given that the XBeach model includes a groundwater module (See Fig 2.17), the feasibility of using XBeach as a model system to possibly simulate also the SWI, in addition to the simulation of coastal barrier breaching and the subsequent flood propagation as proposed in *Implication 7* (Section 2.6), need to be examined. Moreover, a suitable mitigation measure needs to be implemented in order to shorten the long natural remediation intervals after an SDSWI event.

Implication 8: Feasibility of XBeach as a saltwater intrusion (SWI) model

The XBeach model includes, besides the hydrodynamic and morphodynamic modules, also a ground water module. Thus, it might theoretically be used as a general modelling system to simulate the breaching processes, the induced flood propagation and the subsequent SWI. While the morphodynamic solver is applied to simulate sediment transport and morphological changes including breach development, the hydrodynamic (CFD) solver together with the groundwater module might simulate the surface-subsurface flows and interactions in addition to the contamination of the originally fresh groundwater. The capability of XBeach as a surface-subsurface model has tentatively been examined in the studies of McCall (2015) and McCall et al. (2012), showing model capability to simulate the infiltration, exfiltration and groundwater update. However, the feasibility of XBeach as SWI model still need to be addressed. This might help to simulate the breaching, induced coastal flooding and subsequent SWI in a single model system by considering the mutual interactions among the involved processes and to avoid splitting the naturally continuous processes in the modelling associated with a "manual" transfer of the results from one model to another. As a result, the aforementioned two weaknesses of Yang's studies using HGS as surface-subsurface model to simulate the coastal flood propagation and the subsequent SWI with rough estimation of the overtopping/breaching discharge might be overcome.

2.8 Specification of objectives and methodology for the PhD study

2.8.1 Summary of knowledge gaps and research needs

In the course of this systematic review and analysis of the current knowledge and modelling tools, the most relevant physics and models related to breach initiation and breach growth have been discussed. Besides the systematic identification of the knowledge gaps and of the weaknesses of the current models, the results also helped to select the most appropriate among the current breaching models for dunes and similar coastal barriers, namely the XBeach model. The recent research studies on XBeach (e.g. De Vet 2014) reported that XBeach is able to simulate the hydrodynamics properly, but it substantially overestimates the erosion rates during breaching and overwash events at dunes and barrier islands, especially under extreme storm surges that are often accompanied by high flow velocities and significant sediment transport rates. Given that XBeach is now widely also applied in operational modelling systems for coastal flood forecasting and warning in many European states (see e.g. Barnard et al. 2014; Bogaard et al. 2016; Giardino et al. 2011; Harley et al. 2016; de Santiago et al. 2017; Suh et al. 2017), besides its recent use to estimate inland flow during events of storm surges (e.g. Elsayed and Oumeraci 2016; Gallien 2016; Gallien et al. 2014; Gallien and Guza 2015), there is an urgent necessity to address the aforementioned overestimation problem using new physically-based approaches, so that reliable predictions of inland discharges can be achieved. The overestimation of the sediment transport rates might be due to the lack of some physical effects in the model such as the effects of grain-stabilization and vegetation on sediment transport. Moreover, the current version does not account for the effects of cohesive sediments and short waves effects in the surf-beat mode of

XBeach is accounted only by empirical formulae. Thus, the review of the current knowledge on the modelling of breach initiation and breach growth leads to the first research question:

1. *To which extent the morphodynamic prediction performance of the XBeach model under overwash and breaching conditions can be improved through the implementation of new physical effects that have not yet been accounted for in the current model version (e.g. grain-stabilization effect)?*

Answering this research question is indeed one of the core tasks of this PhD study. The planned improvements of XBeach are summarised in Table 2.1 under Task 1. These suggestions include the necessity to address two model limitations: (i) grain-stabilization effect and (ii) wave shape and nonlinearity effects on the sediment transport rate. These two limitations are thought to be urgent because they are the most relevant to sediment stirring and transport and might be the reasons behind the commonly reported overestimation problem of the sediment transport rates in XBeach for extreme flow conditions.

Table 2. 1: Current Knowledge gaps/limitations and planned improvements/extensions

Task	Title	Knowledge Gaps / Limitations	Planned improvements / Extensions
Task 1	XBeach improvement	Barrier material and cohesive sediment (See Section 2.5.1)	Not addressed in this study
		Limitations related to bed friction (See Section 2.5.2)	Not addressed in this study
		Vegetation effect on coastal erosion and sediment entrainment (See Section 2.5.3)	Not addressed in this study
		Depth averaged computations (See Section 2.5.4)	Not addressed in this study
		1.1 Effect of phase-averaged computations (of short waves in the surf-beat mode of XBeach) on sediment stirring and transport (See Section 2.5.5)	Planned: the model of Van Thiel de Vries (2009) in Eq. 2.6 which indirectly account for the effect of shortwaves' nonlinearity on sediment transport, will be improved.
		Hindered erosion by the dilatancy effect (See Section 2.5.6)	Implemented by De Vet (2014)
		Effect of high sediment concentrations on fall velocity (See Section 2.5.6)	Implemented by De Vet (2014)
		Bed slope effect on incipient sediment motion (See Section 2.5.6)	Implemented by De Vet (2014)
		1.2 Grain-stabilization and soil compaction effect on sediment transport (See Section 2.5.7)	Planned: the concept of grain-stabilization will be introduced, formulated and integrated into the formulation of XBeach so that overestimated sediment transport might be reduced.
		longshore variability of soil strength (See Section 2.5.8)	Not addressed in this study, but implementing the Grain-stabilization effect might open the way toward accounting for this effect.
Task 2	Coupling inundation and breaching models	Breaching and induced inundation are often modelled separately (see Section 2.6.2)	Testing the applicability of XBeach in modelling breaching and induced inundation in a single XBeach model.
Task 3	Coupling breaching, inundation and infiltration models	3.1 Predicting reliable inland discharges for further simulation of flood-induced SWI is lacking.	Examining the feasibility of utilising the XBeach groundwater module to simulate the SWI and identifying the most coupling approaches for modelling breaching, inundation and SWI.
		3.2 Natural remediation time after SWI events is too long without implementing suitable mitigation measures	Identifying and testing a suitable mitigation measure(s) to shorten long remediation intervals

Since the final target of this PhD study is to predict the implications of flooding induced by extreme storm surges for groundwater contamination, the modelling of coastal flood propagation in the hinterland is essential in order to calculate the extent and depths of the inundation as shown in Fig 2.22.

Therefore, it is needed to couple one of the common inundation models (e.g. River-2D of Steffler and Blackburn 2002) with XBeach. Alternatively, XBeach might be used to simulate both breaching and induced inundation in a single model as suggested in *Implications* 5 and 7. The latter combination simplifies the flow and facilitates the automatic transfer of the results from breach modelling to flood modelling. This suggestion leads to the following research question:

2. *Is the XBeach model capable of simulating the inundation induced by a barrier breaching instead of applying another inundation model, so that both processes are simulated in a single XBeach model rather than the current modelling approaches which address breaching and inundation separately?*

The tentative answer to this question, based on the results of this systematic review, is yes, XBeach may work as an inundation model. Indeed, it operates the same hydrodynamic equations as the common inundation models with only minor modifications (Beevers et al. 2016; Hartanto et al. 2011). However, the final answer to this question is the second main research task in this PhD study (Table 2.1 under Task 2). In the case of a negative answer, the coupling of XBeach with another inundation model such as River-2D represents an alternative solution in this phase.

To study the implications of coastal floods for groundwater contaminations, the coupling of one of the common infiltration/solute transport models such as HGS or SEAWAT (see Chapter 7) with the selected inundation and breach models would be required. Alternatively, the groundwater module of XBeach might be used for that purpose, thus providing the advantage of modelling the breaching, induced inundation and the subsequent SWI in a single model system. Hence, following the results of the review related to SWI modelling leads to the third research question:

3. *Is the XBeach model capable of simulating, in addition to breaching and flood propagation, salt water intrusion (SWI) by utilising its groundwater module, and if it is not the case, what are the alternative approaches to properly simulate a coastal barrier breaching, induced flooding and subsequent SWI?*

To answer this research question, the physical processes, as well as the governing equations of SDSWI, need to be compared to the governing equations of the groundwater module of XBeach. In addition, the modelling approaches for SDSWI events in previous studies (e.g. Yang et al. 2013, 2015a; b) need to be analysed. As a result, a proper modelling approach can be proposed and one of these studies can be reproduced using the proposed modelling approach. Moreover, possible structural mitigation measures to reduce long remediation intervals of contaminated aquifer after a coastal flood event can be proposed and evaluated. The flowchart (Fig 2.25) show how and where the previous research tasks will be integrated into the processes and modelling framework.

2.8.2 Specification of objectives

The tentative objectives for the PhD study are defined in Section 1.2. Based on the previous summary of the knowledge gaps and the research needs, the specific objective of the study can be specified more precisely as follows (see also Bendoni et al. 2016):

1. Evaluating the performance skill of the current XBeach model by means of available large-scale tests for dune erosion performed by LWI in 2013 (hereafter called GWK-tests). As a result, reasons for the overestimation problem of XBeach can be identified through the reproduction of the GWK-tests and possible model improvements can be better identified.
2. Improving the XBeach model (i) through improving the model of Van Thiel de Vries (2009) (Eq 2.6), which indirectly account for effect of waves nonlinearity on sediment transport (Task 1.1 in Table 2.1), and (ii) through introducing the grain-stabilization concept and implementing its effect in the formulation of XBeach, so that overestimated sediment transport might be reduced (Task 1.2 in Table 2.1). This also includes extensive testing and validation of the improved model through diverse case studies from different coastal environments.
3. Testing the applicability of XBeach for combined modelling of the breaching and the induced flooding, including extensive testing and validation of XBeach for the combined modelling through synthetic and real breaching and inundation cases (Task 2 in Table 2.1).

4. Studying the possibility of using the groundwater module of XBeach in modelling SDSWI and identifying the possible modelling approaches. This might also include the identification of possible mitigation measures to shorten long natural remediation intervals (Task 3.1 in Table 2.1).
5. Applying the overall modelling approach to a pilot site, including testing of the most suitable mitigation measure for SDSWI (Task 3.2 in Table 2.1)

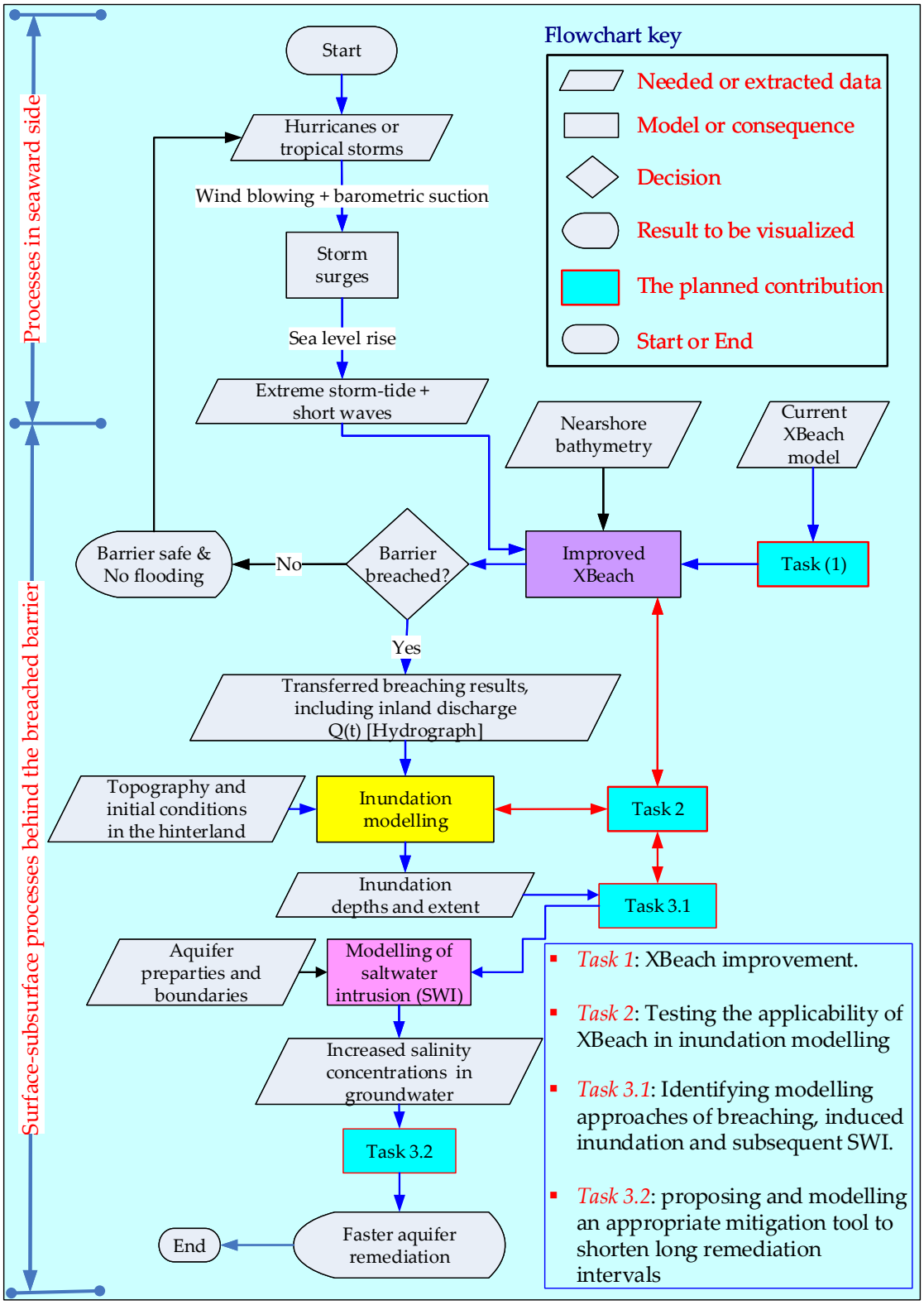

Fig 2. 25: Flowchart for processes and planned research tasks in the framework of this study.

2.8.3 Specification of methodology

In order to achieve the aforementioned specific objectives, each objective is addressed in a separate phase as schematized in Fig 2.26. Thus, each phase is addressed in a separate chapter as the following:

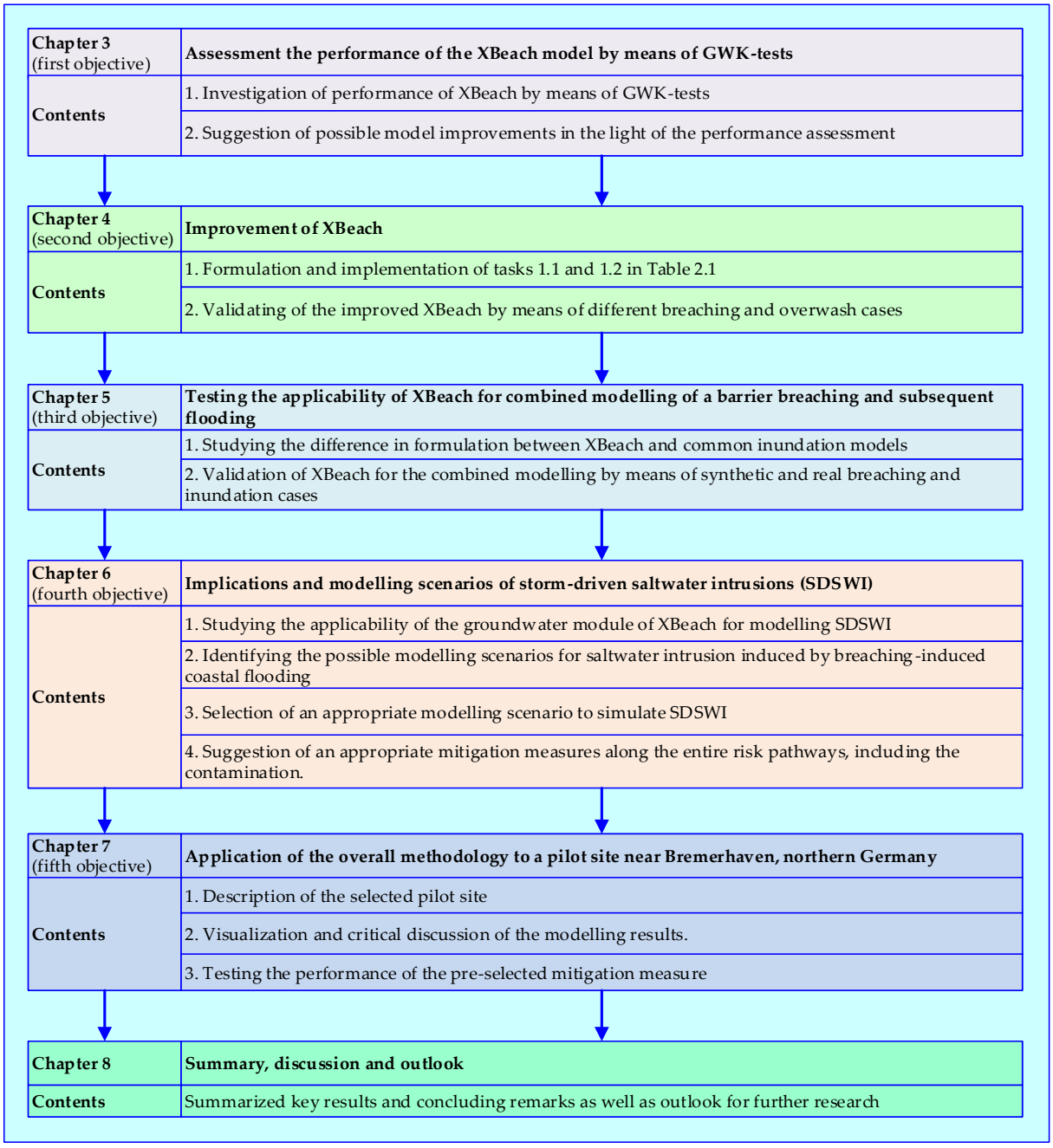

Fig 2. 26: Specified methodology of the of the PhD study and organisation structure of the rest of the thesis.

In chapter 3, the first objective is addressed through assessing the performance of the XBeach model by means of GWK-tests for dune erosion. In the light of these experiments, the model capabilities are investigated and possible model improvements are introduced.

In chapter 4, the second objective is addressed through introducing improvements of the XBeach model in order to treat the overestimation problem of the erosion rates during extreme storm surges. In this context, the XBeach code is improved (i) through improving the model of Van Thiel de Vries (2009)(Eq 2.6), which indirectly account for effect of wave nonlinearity on sediment transport, and (ii) through introducing the grain-stabilization concept and implementing its effect in the formulation of XBeach, so that overestimated sediment transport are reduced. Moreover, the improved XBeach is

validated by means of three cases for dune erosion, for barrier breaching as well as for a barrier island erosion and overwash under an extreme storm surge event.

In chapter 5, the third objective is addressed through testing the applicability of XBeach for modelling both the breaching and the induced flood propagation. Thus, another validation is performed to test the applicability of XBeach for the combined modelling by means of synthetic and real breaching and inundation cases.

In chapter 6, the fourth objective is addressed through elaborating possible modelling scenarios of the three processes (breaching, induced inundation and subsequent SWI). As a result, an appropriate modelling approach is selected to draw the implications of storm-surge-driven coastal floods for groundwater contamination. Based on the latter implications, appropriate mitigation measures are suggested to shorten the long remediation time after a SDSWI. Finally, the most suitable measure is selected and applied to mitigate storm-driven saltwater intrusion in a selected pilot site.

In chapter 7, the fifth objective is addressed through applying the overall modelling methodology to a pilot site near Bremerhaven, Germany. The selected mitigation tool from chapter 6 is applied to mitigate possible salt water intrusion owing to coastal floods and to shorten long remediation intervals.

Chapter 8 summarises the key results and concluding remarks. In addition, suggestions for a further development of the overall modelling methodology or any part of its individual components are provided.

3 Investigation of the XBeach model performance using GWK-tests

This chapter‡‡ aims at examining the performance of the XBeach model, which is selected in Chapter 2 as the most appropriate modelling tool to simulate coastal erosion and breaching of coastal barriers by considering the hydro-geo-morphodynamic interactions at the sea/land boundary. Model performance is examined in this chapter using a unique database from large-scale model tests for dune erosion (hereafter called GWK-tests), which were performed in 2013 by Leichtweiß-Institut (LWI) in the Großer Wellenkanal (GWK) of the Forschungszentrum Küste (FZK), a joint coastal research centre of both universities Hannover and Braunschweig. In fact, it is important to examine whether and to which extent the selection of the XBeach model in chapter 2 is justified before starting with any further XBeach improvement/developments in the following chapters. Therefore, the numerical reproduction of the GWK-tests is appropriate to examine the performance of XBeach for the prediction of wave-induced dune erosion under extreme storm surge conditions. Moreover, such reproduction is also important to identify more precisely the possible limitations of XBeach to capture the processes, which are relevant to the morphological changes in beach/dune systems. Therefore, this chapter starts first with a brief description of the GWK-tests followed by the experimental setup in GWK and the numerical model setup in XBeach. The outcomes of the GWK-tests and the numerical simulations are comparatively analysed in order to possibly identify the need for further XBeach improvements.

3.1 Description of the GWK-tests

The GWK-tests were performed in 2013 to physically simulate the erosion from the seaward side of the sand dunes in the western zone of the Wangerooge Island, northern Germany (Fig 3.1).

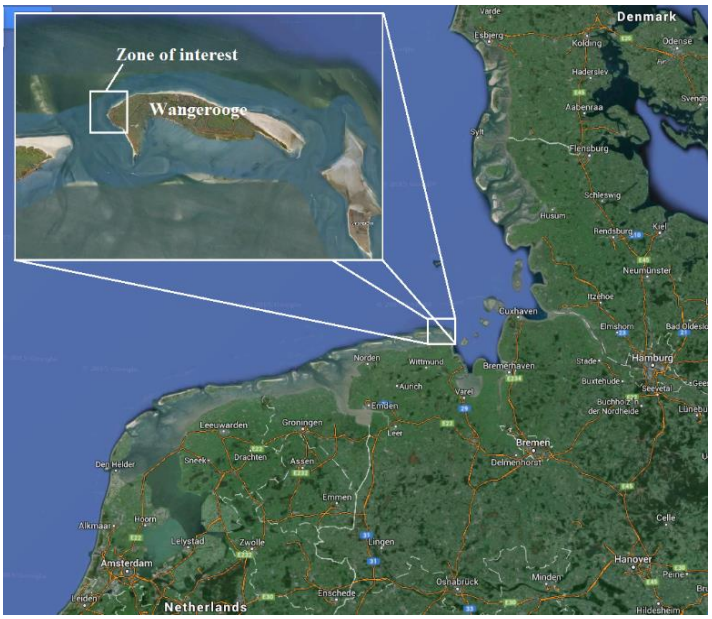

Fig 3. 1: Wangerooge Island, northern Germany: the western part of Wangerooge is exposed to coastal erosion during extreme storms from the North Sea [https://www.google.de/maps].

Despite its protection by shore protection works (e.g. revetments and seawalls) against erosion as shown in Fig 3.2, the western zone of Wangerooge Island is subject to permanent morphological

‡‡ More details of this chapter reported in:
Elsayed, S. M.; Oumeraci, H. (2015): Breaching of coastal barriers under extreme storm surges and implications for groundwater contamination: *Assessment of the XBeach Model Performance under Storm Surges using GWK-Data*. Internal Report no 1072/17, Leichtweiß-Institut for Hydraulic Engineering and Water Resources, TU Braunschweig, Braunschweig, Germany, 133 p.
Freely available at:
https://www.researchgate.net/publication/316351876_Assessment_of_the_XBeach_Model_Performance_under_Storm_Surges_using_GWK-Data

Moreover, the final outcomes of this chapter are part of the following journal paper:
Elsayed, S.M.; Oumeraci, H. (2017): Effect of beach slope and grain-stabilization on coastal sediment transport: An attempt to overcome the erosion overestimation by XBeach. Coastal Engineering, volume 121, Pages 179–196, http://dx.doi.org/10.1016/j.coastaleng.2016.12.009.

changes from sand dunes (dune extension) adjacent to the revetments (Oumeraci et al. 2014). Therefore, the purpose of the GWK tests was to understand the erosion processes induced by the impact of storm waves on the front face of the sand dune extension. Moreover, the tests aimed at selecting and testing an appropriate solution, which is able to prevent/reduce the dune erosion, especially under extreme storm surge events. Therefore, the distance between the existing revetments and a planned dune line that provides a minimum erosion of the Wangerooge dunes is estimated.

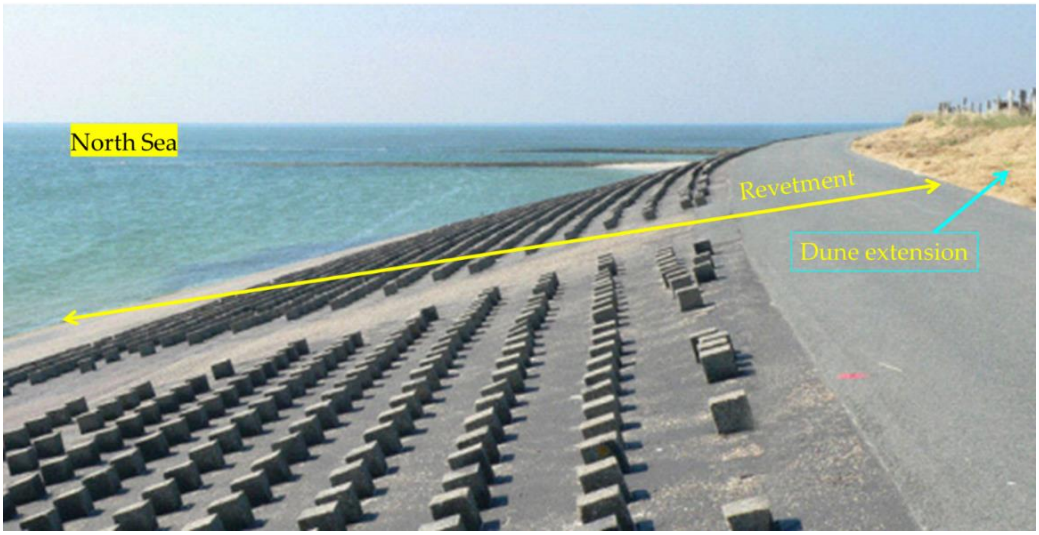

Fig 3. 2: Revetments at western Wangerooge, in front of a sand dune prone to erosion under extreme storm events.

(a) Large-scale test in GWK for coastal dune erosion	(b) Wave generator in GWK
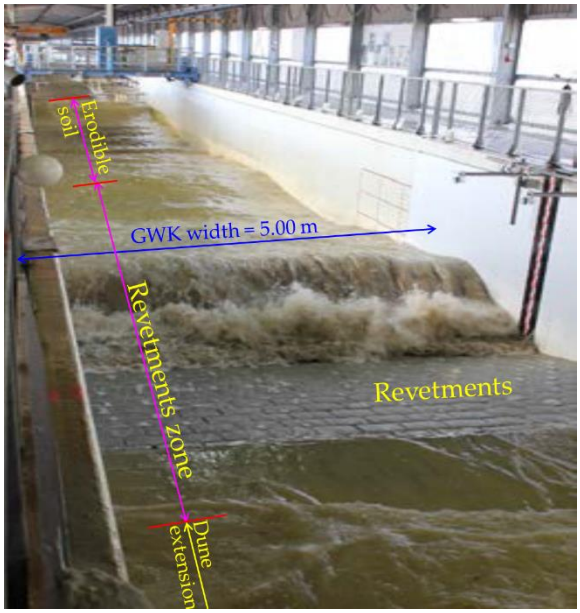	

Fig 3. 3: Large Wave Flume (GWK) in Hannover: (a) GWK-test of coastal dune erosion in Wangerooge and (b) wave maker in GWK.

The GWK-tests were performed using the results of site investigations for the wave conditions and their dominant directions. The latter investigations are briefly summarised in German by Oumeraci et al. (2014) and in English by Elsayed and Oumeraci (2015a). Moreover, the tests were based on preliminary tests in the Twin-wave flume of the Leichtweiß-Institute für Wasserbau (LWI) with a scale of 1:15, so that the best modelling situation for the GWK tests is chosen without considerable efforts

and time. The length of the flume is 310 m while the width and the depth of the flume are 5 m and 7 m, respectively. The wave generator (Fig 3.3.b) is equipped with a hydraulically driven shaft engine with an output of 900 kW, which can move horizontally with a maximum stroke of ± 2.10 m. The flume can be used to generate maximum heights of regular or irregular waves up to 2 m, solitary waves up to 1.5 m and focused (breaking) waves up to 3 m.

Considering GWK dimensions, the considered scale for GWK-tests is 1:3, which is five times the scale of the preliminary physical model in the LWI flume. Froude's similarity is considered for scaling the real conditions to the lab conditions in GWK. In fact, such large-scale tests allow the modeller to use natural sediments without or with significantly reduced scale effects.

3.2 Physical model setup in GWK

The large-scale experiments were performed on five cross-shore profiles in GWK (Fig 3.4) subject to wave conditions as specified in Table 3.1. Each profile consists of three main zones: erodible sand foreshore (green), revetment zone (magenta) and erodible sand dune extension (yellow).

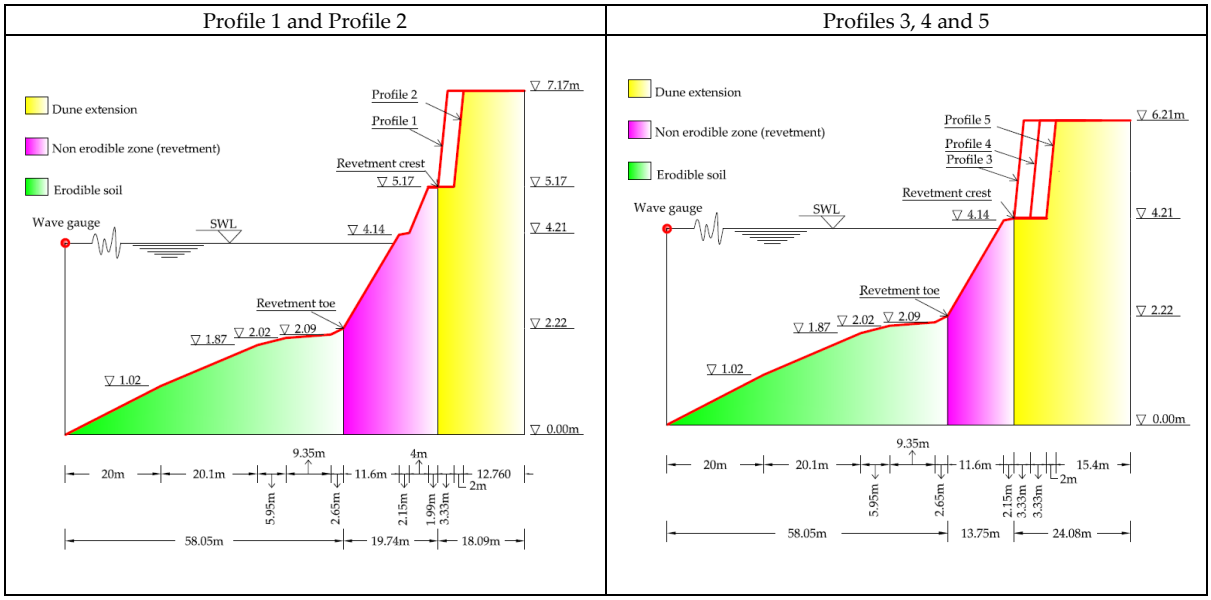

Fig 3. 4: Cross-shore profiles tested in GWK (all levels and dimensions are in meters and level 0.00 represents the flume bottom): left panel shows profiles 1 and 2 while right panel shows profiles 3, 4 and 5; differences among profiles in both panels, separately, lie in the offset of the dune front.

The erodible foreshore has the same levels and dimensions in the five tested profiles. However, the revetment zone and the dune extension differ. The revetment zone in profiles 1 and 2 has the same dimensions and levels, while for profiles 3, 4 and 5 the same dimensions and levels prevail, but different from those in profiles 1 and 2. For all profiles, the dune extension with a front slope 1:1 is built behind the revetment crest as shown in Fig (3.5.a). The dune front starts at level 5.17 m for profile 1 (level 0.00 represents the flume bottom). In profile 2, the dune extension also starts at level 5.17 m, but the dune front has an offset as shown in Fig (3.5.b) of 3.33 m behind the revetment crest. The dune extension for profiles 3, 4 and 5 starts at level 4.21 m and has no dune offset for profile 3 (Fig 3.5.a), but both profiles 4 and 5 have offsets of 3.33 m (Fig 3.5.b) and 6.66 m (Fig 3.5.c), respectively.

The tests aimed at understanding the effect of different dune offset on the erosion of the dune extension zone. Moreover, they aimed at testing the effect of different overtopping rates on the dune erosion, where variable overtopping rates are estimated using the empirical model EurOtop of Pullen et al. (2007) based on varying the water depth in the flume. In summary, 17 GWK tests are performed considering the test conditions in Table 3.1 whilst the dune erosion is measured using a 3D scanner after each individual laboratory test.

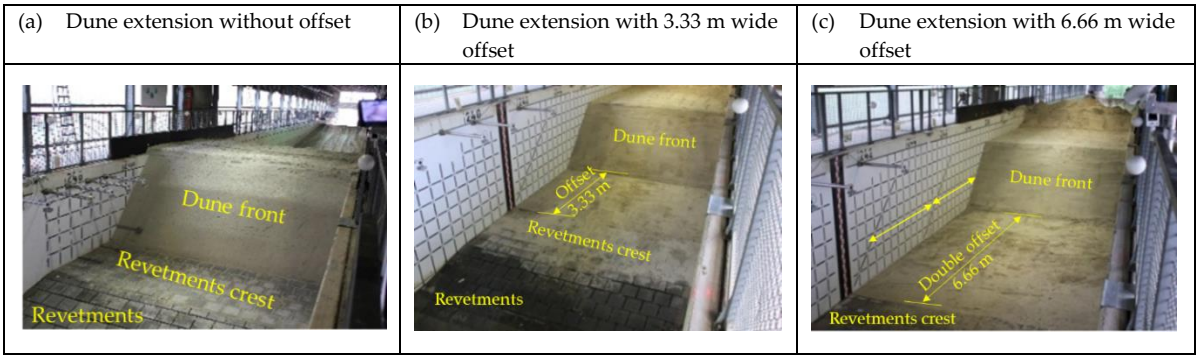

Fig 3. 5: Physical model setup in GWK: dune extension with a front slope of 1:1 is built behind the revetment crest with (a) no offset for profiles 1 and 3, (b) with offset of 3.33 m width for profiles 2 and 4, and (c) with double offset of 6.66 m width for profile 5.

Table 3. 1: Test conditions for dune erosion in GWK and in XBeach

GWK Test No.	Cross-shore profile No	Overtopping rate	Water depth (SWL)	Wave type	Test duration		XBeach test No.
[-]	[-]	q_{nom} [l/(s·m)]	[m]	[-]	[s]		[-]
Test 01	Profile 1	1.92	3.66	Wave spectrum (irregular waves) with significant wave height of 1.1 m and peak period of 6.6 s	5740		XB1
Test 02	Profile 1	<1.92	3.40		6702		XB2
Test 03	Profile 1	1.92	3.66		5740		XB1
Test 04	Profile 1	16.35	4.00		6705		XB3
Test 05	Profile 1	192	4.50		2151	6492	XB4
Test 06					2156		
Test 07					2185		
Test 08	Profile 2	16.35	4.00		6632		XB5
Test 09	Profile 3	423	4.00		2328	6979	XB6
Test 10					2316		
Test 11					2335		
Test 12	Profile 4	423	4.00		2311	6393	XB7
Test 13					1782		
Test 14					2300		
Test 15	Profile 5	423	4.00		2309	8908	XB8
Test 16					2308		
Test 17					2291		

In Table 3.1, Test 01 is for instance performed on profile 1. The water depth (SWL) in the flume is 3.66 m, the planned overtopping rate is 1.92 l/s/m, the test duration is 5740 s and the generated waves have a significant wave height of 1.1 m with a peak period Tp (the period that gives the peak of the spectrum) of 6.6 s (wave maker at distance 68 m from the toe of the erodible foreshore). As shown in Table 3.1, some GWK tests (e.g. Test 05 to Test 07) were performed on the same profile without reshaping the dune front to its initial state. Therefore, these tests are also performed in a single XBeach test. In the last column of Table 3.1, the XBeach test number corresponding to the GWK test(s) is specified (e.g. GWK test 01 corresponds to XBeach test XB1 while GWK tests 05 to 07 correspond to the single XBeach test XB4). Moreover, GWK Tests 01 and 03 have the same conditions and are therefore reproduced only by single XBeach test, which is XB1.

The dune extensions adjacent to the revetments as shown in Fig 3.5 are prone to seaward erosion induced by the waves running up and overtopping the revetments, which make these dunes in the collision/impact regime of Sallenger (2000) as described in Fig 2.7. The dune erosion, as noticed in GWK, may take different forms (Fig 3.6): (i) cracks followed by slides, (ii) grooves, furrows and sagging, (iii) peeling and flaking, or (iv) overhangs (Oumeraci et al. 2014). Form (i) represents the most common form that initiates due to dune toe erosion and induced instabilities derived by gravity force. Form (ii) mainly occurs in the case of partial overtopping of dunes. Thus, given sufficient time, the grooves and rills deepen with successive overtopping. In the case of irregularities in dune compaction and/or moisture, form (iii) is more likely. Overhangs (form (iv)) is more common in situation where dune toe is significantly eroded while dune crest is more coherent. The dune erosion from different forms is measured at the end of each individual test using the 3D scanner, which represents a proper and accurate facility for monitoring the erosion at the dune extension zone.

(i) Crack and slides	(ii) Grooves, rills, and sags	(iii) Peeling and flaking	(iv) Overhangs
			

Fig 3. 6: Forms of dune erosion observed in the GWK tests of Wangerooge (Oumeraci et al. 2014).

3.3 Numerical model setup

Though the cross-shore profiles in the GWK tests can be simulated in XBeach as 1D profiles, the GWK tests are reproduced as 2DH models in order to reproduce the same laboratory conditions. Therefore, five topographies are generated, where each topography is defined by x-file, y-file and bed-file that contain the x, y and z-coordinates of the calculation meshes. As a result, grid resolution of 0.2 m is applied to each numerical test. Another five files are generated to specify the hard bed (revetment) zone for each profile. In addition, the same laboratory conditions and boundaries as in GWK are reproduced in XBeach. For instance, the waves in GWK are measured by different wave gauges (see Oumeraci et al. (2014) or Elsayed and Oumeraci (2015a) for further details). However, the readings of the installed wave gauge above the toe of the erodible foreshore (Fig 3.4) is used only to feed XBeach by the offshore wave boundary condition after performing the wave reflection analysis by the software L~davis (analysis software developed by LWI). Table 3.2 summarises the main parameters used in the parameter file of XBeach in order to reproduce the same conditions and boundaries of the physical models in GWK.

The sediment sizes are obtained from the distribution curve of the sand used in the flume. Based on the median grain size D_{50}, the bed friction coefficient c_f is calculated. Because the flume has sidewalls that prevent lateral water flow, lateral boundaries are selected as impermeable walls. Moreover, the SWL values in Table 3.1 are assigned to each XBeach test. Furthermore, the measured waves at the wave gauge shown in Fig 3.4 is assigned to XBeach after performing the reflection analysis (i.e. incident wave spectrum) using a formatted variance-density spectrum file, defined in XBeach using instat = 6 or vardens. The other XBeach hydrodynamic and morphodynamic parameters are set at default values.

Table 3. 2: Main parameter settings and boundary conditions for the reproduction of GWK tests in XBeach

Parameter	Value	Note
D50	0.16 mm	Median grain size
D90	0.275 mm	D_{90} grain size
front	1	Absorbing-generating and weakly-reflective front side as 2D inflow boundary
left	1	Side wall as impermeable lateral boundary
right	1	Side wall as impermeable lateral boundary
back	2	Absorbing-generating and weakly-reflective back side as 2D outflow boundary
instat	6	Formatted variance-density spectrum file with records from wave gauge in Fig 3.4 after performing the reflection analysis is used as offshore wave boundary.
lateralwave	Neumann	Neumann boundary is a lateral wave boundary on both lateral sides of the model
c_f	0.00062	Non-dimensional friction coefficient (based on D50).
form	2	Sediment transport is calculated according to the formulation of Van Rijn (2007a; b)-Van Thiel de Vries (2009)
morfac	10	Factor in Exner equation for the bed update in XBeach (Eq 4.3) which is often used to accelerate calculations of morphological evolution
tstop	Table 3.1	Simulation time in XBeach = time duration of GWK test(s)

3.4 Assessment of XBeach performance based on simulations outcomes

The numerical models of GWK tests are run using a compiled version of XBeach (revision no 4812). The results, in general, showed a relatively reasonable prediction capability for both the scour behind the revetment and the frontal dune erosion. Moreover, they showed that XBeach is capable of simulating the transition zones between hard (the revetment zone) and mobile beds (the dune extension). However, results also showed a better prediction performance with lower overtopping rates (e.g. Test XB3 in Fig 3.8) than with higher overtopping rates (e.g. Test XB8 in Fig 3.9).

According to Pender and Karunarathna (2013), Sutherland et al. (2004) and Van Rijn et al. (2003), the accuracy of the post-storm profiles is usually assessed using the Brier Skill Score (BSS) and the root-mean-square error (RMSE). The BSS and the RMSE measures for comparing observed and simulated post-storm profiles are given as follows:

$$BSS = 1 - \left(\frac{\langle (z_p - z_m)^2 \rangle}{\langle (z_b - z_m)^2 \rangle}\right) \quad \& \quad RMSE = \sqrt{\langle (z_p - z_m)^2 \rangle} \tag{3.1}$$

The angled brackets in Eq. 3.1 indicate the average of N readings of the bed levels along the cross-shore profile, z_p is the predicted profile from XBeach, z_m is the observed post-storm profile and z_b is the initial (pre-storm) profile. BSS is in fact a common statistical indicator for the prediction skill relative to a baseline prediction, which is used in almost all morphological studies by XBeach. However, it has some limitations. For instance, it cannot account for the migration direction (e.g. for a bar) because it just evaluates whether the computed bed level at specific time is closer to the actually observed bed level at the same time than the initial bed level or not. Moreover, BSS can be extremely sensitive to small changes for low values of the denominator (Othman et al. 2014; Sutherland et al. 2004), which may result in large negative scores for the case of model overprediction. Therefore, to avoid such drawbacks, Othman et al. (2014) reported that the BSS can be used in absence of other skill scores that produce only positive numbers. For the same reason, Van Rijn et al. (2003) suggested the use of further statistical indicators together with the BSS in order to partially overcome the BSS limitations. Given that the BSS is a common indicator in most XBeach studies, the RMSE is used as a further statistical indicator as recommended by Van Rijn et al. (2003). According to Van Rijn et al. (2003), the model performance classification is as follows: BSS < 0 bad fit, BSS = 0 - 0.3 poor fit, BSS = 0.3 - 0.6 reasonable/fair fit, BSS = 0.6 - 0.8 good fit and BSS = 0.8 - 1.0 excellent/best fit. In fact, similar ranges cannot be provided for the RMSE but lower values of RMSE indicate better fit.

To get an idea of how different predicted profiles can be for different BSS ranges, Fig 3.7 provides an example for the BSS ranges for an exemplary profile. The profiles (initial, predicted and observed) are considered linear and BSS values are calculated based on readings of the bed levels at the profiles ends (i.e. N = 2), where one of the ends is considered non-movable. Thus, Fig 3.7 shows that the highest the BSS value is the nearest the predicted profile to the observed profile and the more far from the initial profile. In addition, Fig 3.7 shows that the range of excellent BSS is quite wide so that a BSS for a predicted profile with 0.9 can be quite far from the observed profile even though it is within the range of excellent/best fit.

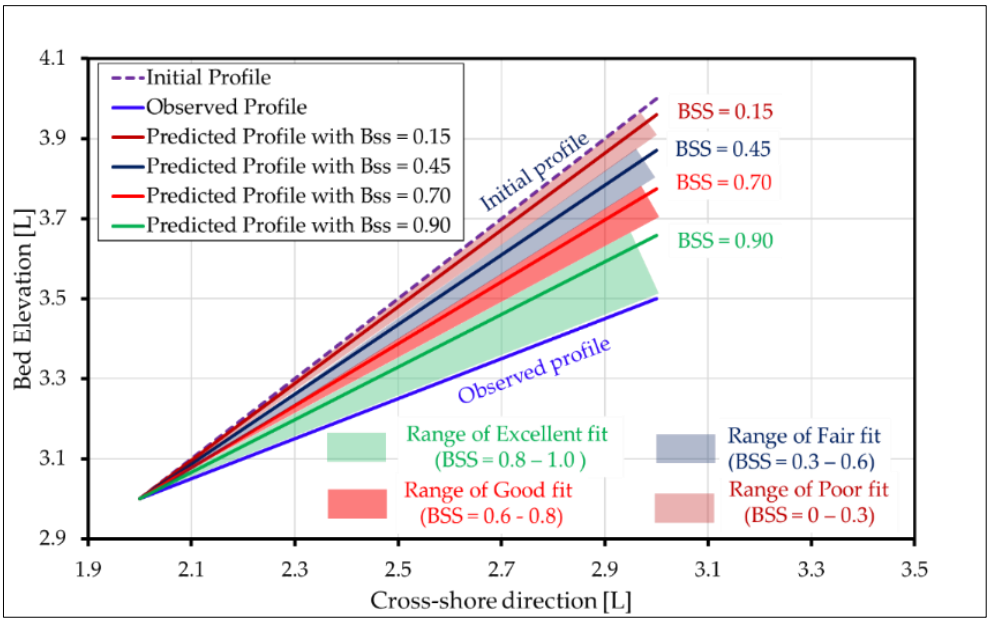

Fig 3. 7: Example of BSS ranges for an exemplary linear profile of one movable end; BSS values and ranges are calculated by considering N = 2.

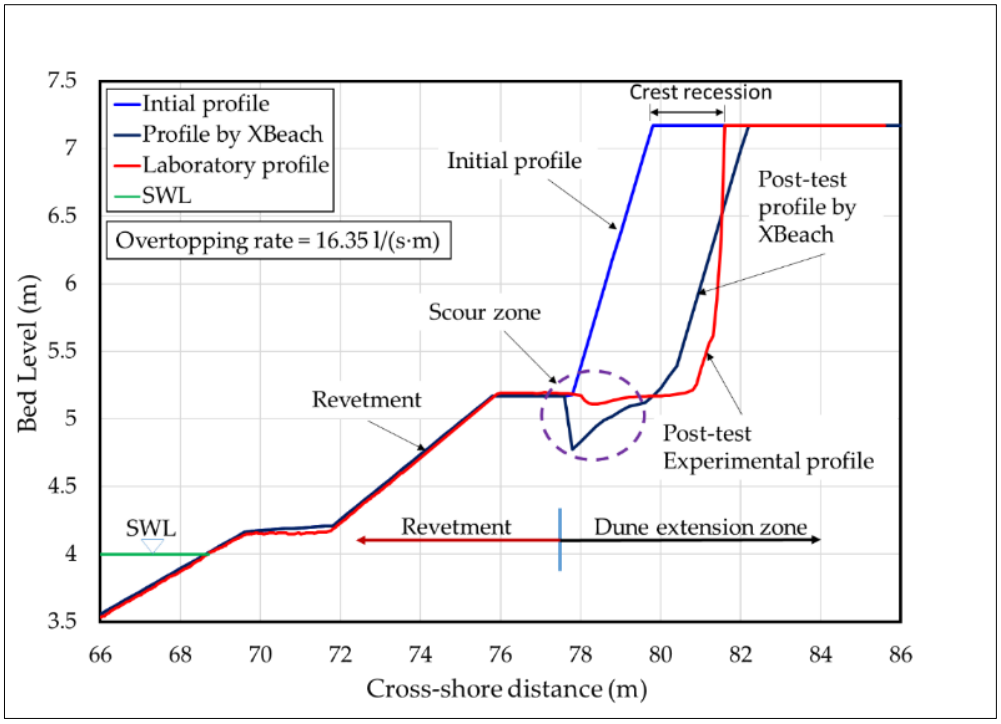

Fig 3. 8: Measured (GWK test 04) and calculated (XBeach test XB3) cross-shore profiles after 6705 s of wave action with a lower overtopping rate qnom = 16.35 l/(s·m); BSS and RMSE are calculated for the cross-shore distance x (76 m ≤ x ≤ 83 m) showing that BSS = 0.915 and RMSE = 0.30 m.

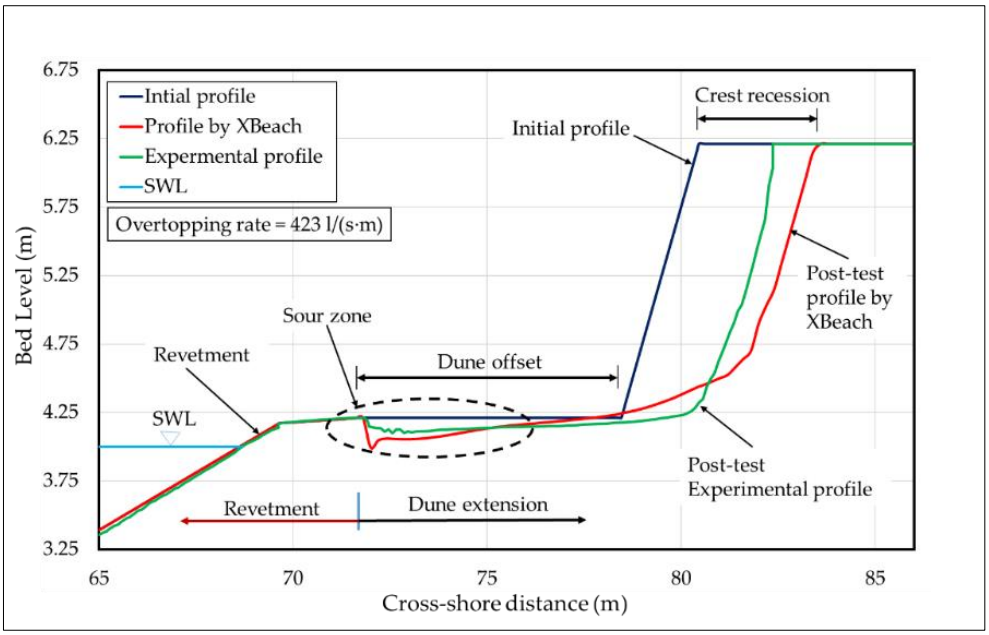

Fig 3. 9: Measured (GWK tests 15-17) and calculated (XBeach test XB8) cross-shore profiles after 8908 s of wave action with a higher overtopping rate qnom = 423 l/(s·m); BSS and RMSE are calculated for the cross-shore distance x (70 m ≤ x ≤ 85 m) showing that BSS = 0.68 and RMSE = 0.38 m.

When applying both accuracy indicators in Eq 3.1 to the test XB3 (Fig 3.8), which is characterised by lower overtopping rate q_{nom} =16.35 l/(s·m), BSS value of 0.915 (excellent fit) and RMSE value of 0.30 m are obtained for the cross-shore distance x (76 m ≤ x ≤ 83 m). However, for the test XB8 (Fig 3.9), which is characterised by higher overtopping rate q_{nom} = 423 l/(s·m), the BSS decreases to 0.68 (good fit) and the RMSE increases to 0.38 m (70 m ≤ x ≤ 85 m). These values confirm that the prediction capability of XBeach decreases with higher overtopping rates, which are mainly accompanied by higher flow velocity as often reported in the literature (e.g. Bisschop et al. 2010; Van Rhee 2007, 2010; De Vet 2014). As shown in Fig 3.10, this conclusion is verified by comparing the observed and the modelled crest recession for all 17 GWK tests in Table 3.1.

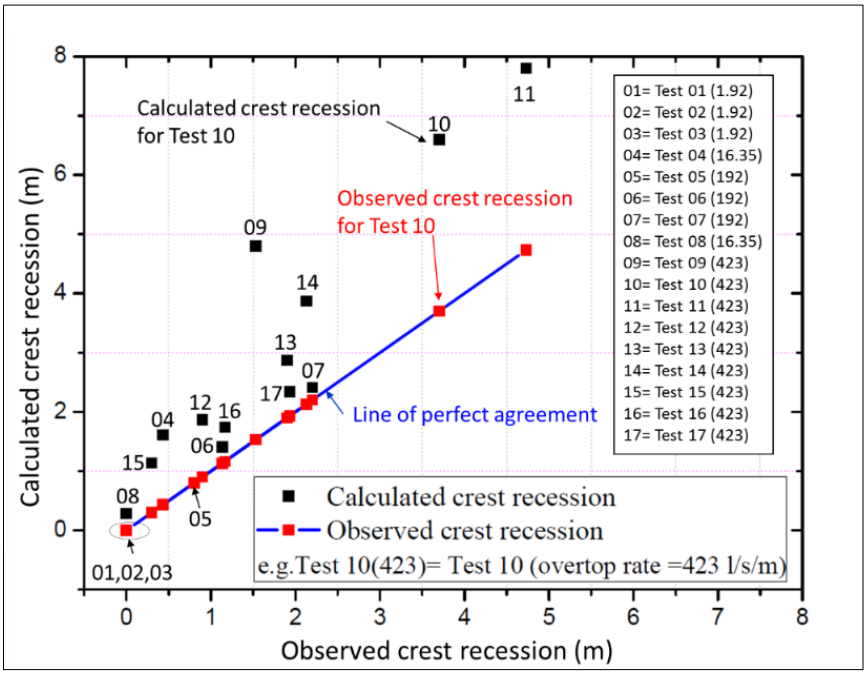

Fig 3. 10: Modelled vs observed crest recessions for the GWK tests 01-17 with different overtopping rates (q_{nom} = 1.92 - 423 l/(s.m)) and different dune offsets widths (0 – 6.66 m).

3.5 Summary and discussion of the results

In this chapter, the performance of XBeach is examined using the 17 GWK tests for dune erosion at Wangerooge Island, Germany. The reproduction of the seventeen laboratory tests by the surf-beat mode of XBeach showed that XBeach overestimates the erosion and thus the deposition volumes. This overestimation becomes particularly significant for very large overtopping rates on coastal barriers, which are commonly induced by extreme storm surges. Both the crest recession (Fig 3.10) and scour size behind the revetment crest (e.g. Fig 3.8 and 3.9) are overestimated by 73 % in average. However, the mismatch between the observed and calculated profiles vanishes with lower overtopping rates (e.g. GWK test 01-03) and also with increasing distance of the dune offset from the revetment crest (e.g. GWK test 08). With increasing overtopping rate from 1.92 l/(s.m) in GWK tests 01-03 to 16.35 l/(s.m) in GWK test 04, the overestimation increases. Therefore, the overestimation is more likely and larger under higher overtopping rates and narrower dune offsets from the revetment crest (e.g. GWK test 09-11). By increasing the dune offset and fixing the overtopping rate (e.g. GWK test 12-17), the overestimation decreases.

Based on these results the following conclusions may be drawn:

(i) XBeach is a suitable model for simulating coastal erosion, especially under low overtopping rates on the coastal barriers, thus justifying the selection of XBeach for dune erosion.

(ii) XBeach, however, overestimates the erosion volumes under very large overtopping rates on coastal barriers. Such overestimated results represent the motivation for proposing, implementing and testing further physically-based improvements to overcome the erosion overestimation, before using it for barrier breaching.

In order to improve the prediction capability of morphological changes by XBeach, the following processes associated with sediment stirring need to be examined and implemented in the model so that the over-predicted erosion rates can be reduced with an improved XBeach model in the next chapter:

(i) Wave nonlinearity effect on sediment transport, which is described in XBeach by a calibration factor for the time-averaged flow depending on the wave skewness and asymmetry

(ii) Excessive in-situ critical shear stress as compared to that predicted by the common Shields criterion for incipient sediment motion (Shields 1936). Thus, omitted effects in Shields criterion (e.g. grain-stabilization) need to be accounted for in order to get reliable erosion rates.

The priority of examining these two processes arises from the need to solve the overestimation of the erosion rates throughout examining the processes that govern the sediment stirring in XBeach so that reliable coastal erosion and breach dimensions can be achieved and hence reliable inland discharges through breaching induced inlets can be calculated. In fact, these two processes are the only processes that control calculations of sediment transport in XBeach. Other model limitations such as the bio-stabilization effect of vegetation are of lower priority for the interest of this study because non-vegetated zones of any barriers undergo often more erosion and breaching as compared to vegetated zones as the bio-stabilization effect in vegetated zones strengthen these zones and enhances their resilient against erosion (Bendoni 2015).

4 Improvement of sediment stirring modelling in XBeach

The outcomes of the previous chapter showed that the XBeach model overestimates the erosion rates particularly under significant overtopping rates on coastal barriers, which is often the case during extreme storm conditions (De Vet 2014). This chapter[§§], therefore, aims at investigating the reasons behind such overestimation in order to improve the prediction capability of XBeach through the implementation of new physical processes. More specifically, this chapter revolves around the following research question (see section 2.8.1).

- *To which extent the morphodynamic prediction performance of XBeach under overwash and breaching conditions can be improved through the implementation of new physical processes and effects that have not yet been accounted for in the current model version?*

In fact, the hydrodynamics and morphodynamics of XBeach were extensively calibrated and validated against (1D) flume experiments (e.g. Van Dongeren et al. 2009; Roelvink et al. 2009; Van Thiel de Vries 2009) and some (2DH) field cases (e.g. Roelvink et al. 2009): the model showed qualitatively a good agreement with measured cross-shore measurements of dune erosion and overwash. However, the overwash morphology was validated for the first time by McCall (2008) and McCall et al. (2010) using the 2DH field case Santa Rosa Island under Hurricane Ivan (see section 4.3.3 below). Such hurricane events often result in significant overtopping rates and large flow velocities, especially through breach induced inlets (Bisschop et al. 2010, 2016). The results of the Santa Rosa simulations have shown that XBeach substantially overestimates the erosion volumes and consequently the washover volumes (McCall 2008; McCall et al. 2010; De Vet 2014). As reported by McCall et al. (2010) and De Vet (2014), the overestimation of the erosion rates for the specific Santa Rosa case is certainly due to the limitations of the morphodynamic module of XBeach to reproduce sediment transport with sufficient accuracy rather than to the limitations of the hydrodynamic module. In fact, various studies (e.g. Daly et al. 2012; Deltares 2015a; b; Roelvink et al. 2009; De Vet 2014) reported that XBeach is generally capable of predicting hydrodynamics properly. In some cases, however, the sediment transport rates are overestimated, especially during extreme storm surge conditions where significant overtopping rates and high flow velocities are expected (as the case in GWK-tests in chapter 3). For the latter reason, some artificial and physically based sediment transport limiters are introduced in XBeach as aforementioned in section 2.5.6, so that the transport rates induced by the high-velocity flow are properly simulated (McCall et al. 2010; Terlouw 2013; De Vet 2014). However, the use of these limiters does not provide a general solution for the overestimation problem. In fact, this approach resulted in an improved prediction performance of XBeach for some cases while it becomes worse in some other cases (Elsayed and Oumeraci 2017a); i.e. approaches based on limiters do not solve fully and satisfactorily the overestimation problem. Therefore, there is an urgent necessity to address the overestimation problem using a more physically-based approach. Thus, this chapter is devoted to the implementation of two new model improvements in the current XBeach model as a contribution to the solution of the overestimation problem and to the validation of the improved model. Therefore, the theoretical background of the current XBeach code related to the two new planned improvements is first briefly introduced in section 4.1. The two proposed improvements are then formulated in section 4.2. The validation of the improved model is performed in section 4.3 using three test cases: dune erosion, barrier breaching as well as erosion and overwash of a barrier island under an extreme storm surge event. Finally, a summary of key results is provided in sections 4.4.

[§§] More details of this chapter reported in:
Elsayed, S. M.; Oumeraci, H. (2016): Breaching of coastal barriers under extreme storm surges and implications for groundwater contamination: *Improvement and Extension of the XBeach Model to Account for New Physical Processes*. Internal Report no 1073/17, Leichtweiß-Institut for Hydraulic Engineering and Water Resources, TU Braunschweig, Braunschweig, Germany, 117 p.
Freely available at:
https://www.researchgate.net/publication/315819318_Improvement_and_Extension_of_the_XBeach_Model_to_Account_for_New_Physical_Processes

Moreover, the final outcomes of this chapter are part of the following journal paper:
Elsayed, S.M.; Oumeraci, H. (2017): Effect of beach slope and grain-stabilization on coastal sediment transport: An attempt to overcome the erosion overestimation by XBeach. Coastal Engineering, volume 121, Pages 179–196, http://dx.doi.org/10.1016/j.coastaleng.2016.12.009.

4.1 Theoretical background of sediment transport calculations in XBeach

XBeach solves the nonlinear shallow water equations (NLSWEs), including the capabilities for time-varying wave action balance, roller energy balance and the advection-diffusion equation (Roelvink et al. 2009). A full explanation of the hydrodynamic formulation can be found in Deltares (2015a) and Roelvink et al. (2010). However, in the following, the focus will be on the sediment transport calculations, advection-diffusion equation and the effects of wave nonlinearity on coastal sediment transport.

4.1.1 Sediment transport formulation in the current XBeach model

Different sediment transport equations are implemented into XBeach (revision 4812) to calculate bed, suspended and total sediment loads that allow flexibility in modelling different types of environment. These are the Soulsby (1997) and the Van Rijn (2007a; b; c; d) formulations, modified by Van Thiel de Vries (2009). Model user selects one out of these formulations to determine the bed boundary condition (equilibrium sediment concentration C_{eq}) for the depth-averaged advection diffusion of Galappatti and Vreugdenhil (1985).

$$\frac{\partial dC}{\partial t}+\frac{\partial dCu^E}{\partial x}+\frac{\partial dCv^E}{\partial y}+\frac{\partial}{\partial x}\left(D_h d\frac{\partial C}{\partial x}\right)+\frac{\partial}{\partial x}\left(D_h d\frac{\partial C}{\partial y}\right)=\frac{d(C_{eq}-C)}{T_s} \quad (4.1)$$

Eq (4.1) shows that the mass-balance of suspended sediment in flowing water can be expressed in the form of a partial differential equation that describes the processes of convection, turbulent diffusion and sediment entrainment/deposition in terms of the local sediment concentration. In Eq (4.1), C represents the depth-averaged sediment concentration which varies on the wave-group time scale, D_h is the sediment diffusion coefficient and d is the water depth while u^E and v^E are the Eulerian wave-induced flow velocities in cross-shore and longshore directions, respectively. u^E and v^E are defined as the short-wave-averaged velocity observed at a fixed point and are computed from the hydrodynamic module of XBeach, which as discussed in section 2.4.2 solves a Generalized Lagrangian Mean (GLM) form of the NLSWEs (Andrews and McIntyre 1978; Walstra et al. 2000). The entrainment of sediment is represented by an adaptation time T_s (the elapsed time for C to reach C_{eq}), which is given by a simple approximation based on local water depth d and sediment fall velocity w_s as in Eq (4.2). A small value of T_s corresponds to nearly instantaneous sediment response.

$$\mathrm{T}_s = max\begin{cases} f_{T_s}\frac{d}{w_s} \\ T_{s,min} \end{cases} \quad (4.2)$$

Where f_{T_s} is a correction and calibration factor to account for the fact that the mass-balance for a uniform suspended sediment of fall velocity w_s is determined based on depth-averaged flow conditions (Beevers et al. 2016; Galappatti and Vreugdenhil 1985; Roelvink et al. 2015; De Vet 2014) (default value of f_{T_s} is 0.1) and the minimum adaptation time $T_{s,min}$ is 0.5 sec by default (Roelvink et al. 2015). The entrainment or deposition of sediment is determined by the mismatch between the depth-averaged sediment concentration C and the equilibrium concentration C_{eq} that represents the source term in Eq (4.1).

The differential equation for the advection-diffusion of sediment is solved to obtain C using a finite difference approach and a first order upwind scheme, with the water depths from previous time steps and the corresponding velocities at the updated time step (Beevers et al. 2016; Deltares 2015a; Roelvink et al. 2010). As a result, the bed update is calculated based on continuity considerations of the sediment (Exner Equation):

$$\frac{\partial z_b}{\partial t}=-\frac{f_{mor}}{1-n}\left(\frac{\partial q_{s_x}}{\partial x}+\frac{\partial q_{s_y}}{\partial y}\right) \quad (4.3)$$

Where z_b represents bed level, f_{mor} is a morphological factor added to the Exner equation to speed up the calculation, parameter n represents the porosity of the bed. q_{s_x} and q_{s_y} are the sediment transport

rates in cross-shore and longshore directions, respectively, that are calculated based on the depth-averaged concentration C and the advection and dispersion fluxes as:

$$q_{s_x} = dCu^E + D_h d\frac{\partial C}{\partial x} \qquad \text{with} \qquad q_{s_y} = dCv^E + D_h d\frac{\partial C}{\partial y} \tag{4.4}$$

Where q_{s_x} and q_{s_y} are the volume flux of sediment, excluding pores, through a cross-section perpendicular to the axis indicated by the subscript while water depth d and flow velocities u^E and v^E are calculated from the NLSWEs.

Many studies (e.g. De Vet 2014; Vousdoukas et al. 2012) reported that the prediction of equilibrium sediment concentration C_{eq} is better using Van Rijn-Van Thiel formulation than using the Soulsby-Van Rijn formulation. However, C_{eq} is calculated from the outcomes of both formulations as follows

$$C_{eq} = max\begin{Bmatrix} min\left(C_{eq,b}, \frac{1}{2}C_{max}\right) + min\left(C_{eq,s}, \frac{1}{2}C_{max}\right) \\ 0 \end{Bmatrix} \tag{4.5}$$

Where C_{max} is a user-defined parameter (By default 0.1 m^3/m^3) while the equilibrium sediment concentrations $C_{eq,b}$ and $C_{eq,s}$ represent, respectively, the bed and suspended loads contribution in the total equilibrium concentration C_{eq} and are calculated according to Soulsby-Van Rijn formulation as follows

$$C_{eq,b} = \frac{A_{sb}}{d}\left(U_{stirring} - U_{cr}\right)^{2.4} \qquad \text{with} \qquad C_{eq,s} = \frac{A_{ss}}{d}\left(U_{stirring} - U_{cr}\right)^{2.4} \tag{4.6}$$

Where $U_{stirring}$ is the depth-averaged sediment stirring velocity, U_{cr} is the critical stirring (threshold) flow velocity for sediment movement that is based on Shields curve (Shields 1936) and A_{sb} and A_{ss} are the bed and suspended load coefficients, respectively (see e.g. Deltares (2015a) for details). If the Van Rijn-Van Thiel formulation is selected instead of Soulsby-Van Rijn formulation, then $C_{eq,b}$ and $C_{eq,s}$ take the form

$$C_{eq,b} = \frac{A_{sb}}{d}\left(U_{stirring} - U_{cr}\right)^{1.5} \qquad \text{with} \qquad C_{eq,s} = \frac{A_{ss}}{d}\left(U_{stirring} - U_{cr}\right)^{2.4} \tag{4.7}$$

The critical velocity in Eq. (4.7) is computed as a weighted summation of the separate contributions of currents U_{cr_c} based on Shields curve (Shields 1936) and waves U_{cr_w} based on Komar and Miller (1975)

$$U_{cr} = \alpha U_{cr_c} + (1-\alpha)U_{cr_w} \tag{4.8}$$

Where α is a weighting factor based on whether the long wave stirring is turned on or not? The stirring velocity $U_{stirring}$ is defined as in Eq (4.9) for both Soulsby–Van Rijn and Van Thiel-Van Rijn formulations.

$$U^2_{stirring} = \begin{cases} (u^E)^2 + (v^E)^2 + 0.018\frac{u^2_{rms}}{c_d} & \text{(Soulsby– Van Rijn)} \\ (u^E)^2 + (v^E)^2 + 0.64\, u^2_{rms} & \text{(Van Thiel – Van Rijn)} \end{cases} \tag{4.9}$$

c_d is a drag coefficient and u_{rms} is the root-mean-squared orbital velocity or the at-bed short wave orbital velocity that is obtained from the wave group varying wave energy using the linear wave theory. $U_{stirring}$, in addition, can be represented in terms of effective Shields parameter θ, median sediment size D_{50}, relative density of sediment s ($\rho s/\rho$), gravitational acceleration g and non-dimensional friction coefficient C_f as follows.

$$U^2_{stirring} = \theta\frac{gD_{50}(s-1)}{C_f} \qquad \text{with} \qquad c_f = \sqrt{g/C^2_{ch}} \quad \text{or} \quad c_f = \sqrt{\frac{gn^2}{d^{\frac{1}{12}}}} \tag{4.10}$$

Where C_f can be calculated based on the roughness coefficient of Chezy c_{ch} or Manning n as in Eq (4.10). The critical stirring velocity U_{cr} is mainly a function of the sediment properties (see e.g. Deltares (2015a) for the details). However, it can also be expressed as a function of the critical Shields parameter θ_{cr} as follows:

$$U^2_{cr} = \theta_{cr}\frac{gD_{50}(s-1)}{C_f} \tag{4.11}$$

4.1.2 Effect of wave nonlinearity on sediment transport in the current XBeach model

In XBeach, one of the most important aspects of wave-induced sediment transport and cross-shore profile evolution is the mechanism through which asymmetric short waves transport sediment onshore to counteract the effects of gravity in the form of offshore sediment transport under wave rundown (Van Geer et al. 2014; Roelvink and Reniers 2012). Other return current effects, e.g. undertow, is indirectly included in XBeach through the depth-averaged flow equation (Reniers et al. 2004; Roelvink and Reniers 2012). Indeed, a key parameter for cross-shore sediment transport under breaking and near-breaking waves is the wave shape and the induced shape of the near-bed wave orbital velocity (Abreu et al. 2010; Brinkkemper 2013; Hsu and Hanes 2004; Mora 2015). Generally, a harmonic velocity field (Fig 4.1; dashed lines) will result in no net cross-shore sediment transport because both the time history of flow velocity (Fig 4.1.a) and acceleration (Fig 4.1.b) are symmetric with respect to the positive and negative phase. However, a skewed velocity field (Fig 4.1; solid lines) can cause a net cross-shore transport of sediment (that moves onto the onshore direction).

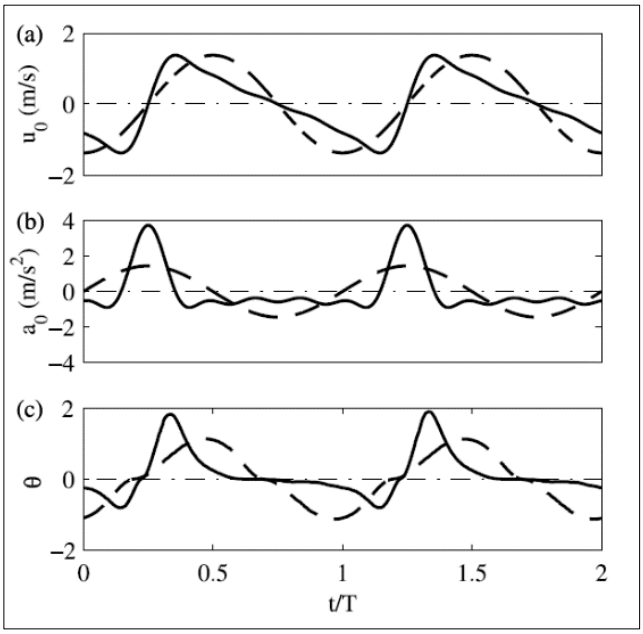

Fig 4. 1: Sediment transport under saw-tooth forcing (solid curve) and single sinusoidal forcing (dashed curve) of wave periods T = 6.0 s. (a) free-stream velocity, (b) free-stream acceleration, and (c) non-dimensional bed shear stress (Hsu and Hanes 2004)

XBeach (surf-beat mode) considers the wave energy of short waves as averaged over their length, and hence does not directly simulate the wave shape (Deltares 2015a; De Vet et al. 2015). By other words, XBeach does not explicitly compute short intra-wave processes since it only calculates the shortwave energy balance and does not contain phase information of the short waves (Van Geer et al. 2014; Smallegan et al. 2016). However, wave shapes gradually change when they propagate to the nearshore (see Fig 2.8) due to the combined effect of wave shoaling, breaking and nonlinear interactions (Brinkkemper 2013; Mora 2015). As waves propagate from deep water onto beaches, the water surface elevation becomes increasingly nonlinear due to the amplification of the higher harmonics. As a result, the time histories of both near-bed flow velocity and acceleration also become asymmetric; i.e. the skewness (velocity skewness) and asymmetry (acceleration skewness) also increase. Skewness is defined as the relative difference between the larger orbital velocities under the wave crest and the lower orbital velocities under the wave trough while asymmetry is defined as the relative measure of the larger accelerations between wave trough and crest as compared to the smaller accelerations between wave crest and trough (Fuhrman et al. 2009; Hsu and Hanes 2004). The increase in skewness and asymmetry has important implications for the wave-induced net cross-shore sediment transport as shown in Fig 4.1 as it results in an increase of onshore sediment transport. In order to indirectly

account for these changes of the wave shape within XBeach, Van Thiel de Vries (2009) proposed a skewness and asymmetry discretization model that takes the following form

$$u_a = \gamma_{ua} u_{rms}(S_k - A_s) \tag{4.12}$$

Besides the sediment transport under the effect of depth-averaged flow, the model of Van Thiel de Vries in Eq (4.12) adopts a net flow velocity u_a that stirs sediment to transport onshore under effect of nonlinear waves, where the values of wave skewness S_k and wave asymmetry A_s are calculated using either the formulation of Van Thiel de Vries (2009) or the formulation of Ruessink et al. (2012). As a result, the flow velocity u_a can be calculated as a function of S_k, A_s, u_{rms} and a calibration factor γ_{ua} as in Eq (4.12). In case of or on the locations where waves are linear (symmetric), u_a vanishes because both S_k and A_s equal zero. However, with highly nonlinear waves, higher values for u_a are expected since the difference between S_k and A_s is considerable. Consequently, higher values for u_a will result in higher onshore sediment transport (Deltares 2015a; Nederhoff et al. 2015). The parameter γ_{ua} is defined in XBeach by the keyword *facua* (*fac*tor for u_a) and has a default value of 0.1. It represents in fact one of the most important parameters in XBeach as it is the only parameter mostly affecting the net cross-shore sediment transport (Bugajny et al. 2013; Vousdoukas et al. 2012). Therefore, many studies (e.g. Nederhoff 2014; Splinter and Palmsten 2012; De Vet et al. 2015; Vousdoukas et al. 2012) reported that *facua* might be one of the reasons behind the overestimation problem by the current XBeach model that usually needs to be increased (than the default value 0.1) in order to achieve better prediction of the erosion rates. Higher values for *facua* would increase u_a. As a result, sediment transport due to wave nonlinearity would accordingly increase in the onshore direction, thus resulting in a reduction of the over-predicted erosion rates. The latter is possible because u_a is used in both the advection-diffusion Eq (4.1) and in the sediment transport Eq (4.4) by replacing the Eulerian velocities u^E and v^E by $(u^E + u_a \sin\theta_m)$ and $(v^E + u_a \cos\theta_m)$, respectively, where θ_m is the angle of wave incidence with respect to the cross-shore direction. With the latter replacements, it is expected that net onshore sediment transport increases by increasing *facua* and u_a accordingly. Therefore, the success of the application of XBeach strongly depends on how precisely important parameters (e.g. *facua*) are calibrated (Evangelista et al. 2017; Vousdoukas et al. 2012).

4.1.3 Effect of onset of sediment motion on over-predicted erosion in the current XBeach model

Some studies (e.g. Harley et al. 2016; McCall et al. 2010; Muller et al. 2016; Pender and Karunarathna 2013; Terlouw 2013) attempted to overcome the overprediction of the erosion volumes by XBeach, especially under overwash and breaching conditions by avoiding the sediment sheet flow. For this purpose, an upper limit for the sediment stirring flow velocity $U_{stirring}$ was fixed by setting the effective Shields parameter $\theta \approx 1.0$ in Eq (4.10) since $\theta = 1.0$ represents the minimum value for incipient sediment sheet flow conditions. Despite the success of this approach to reduce the over-predicted erosion and deposition sediment volumes, it fails to provide a physically-based justification for setting an upper limit to the stirring flow velocity. More recent studies (e.g. De Vet 2014) attempted to overcome this problem by increasing the critical Shields parameter θ_{cr} in Eq (4.11), rather than setting the limit $\theta \approx 1.0$ for the effective Shields parameter in Eq (4.10). The increase of θ_{cr} increases the critical stirring velocity U_{cr} and thereby reduces the difference between $U_{stirring}$ and U_{cr} in Eq (4.6) and/or Eq (4.7), which finally means less sediment transport and reduction of the overestimated erosion by XBeach. Therefore, De Vet (2014) attempted to increase θ_{cr} by implementing in XBeach the dilatancy effect proposed by Van Rhee (2007, 2010). However, the validation cases in the study of De Vet (2014) did not show the same behaviour when sediment transport is hindered by the latter effect. In some cases, the erosion was so strongly reduced which means that the calculated value underestimates the actually observed value (e.g. the case of Zwin Dam, see section 4.3.2), while in other cases the reduced erosion was not sufficiently reduced to achieve a good agreement with the observed erosion (e.g. the Santa Rose Island case, see section 4.3.3). These and further similar cases showed the necessity to introduce a more appropriate approach for the reduction of the erosion by explicitly considering the

grain-stabilization effect of the sediment particles on incipient motion, which might hinder the inception of sediment motion and reduces over-predicted erosion rates as will be discussed in section 4.2.2.

4.2 Proposed improvements for sediment stirring calculations in XBeach

In order to improve the prediction capability of morphological evolution by XBeach, processes associated with sediment stirring (e.g. wave nonlinearity effect and onset of sediment motion) are investigated and better represented in an improved version of XBeach so that over-predicted erosion rates are reduced based on physical means. The latter was possible by introducing two new model modifications: the first is related to the effect of bed (beach) slope on wave nonlinearity and thus on sediment transport while the second is related to the grain-stabilisation effect on the onset of sediment motion as respectively described in the following two subsections.

4.2.1 Bed slope effect on wave nonlinearity and sediment transport

During extreme storm surges, cross-shore winds strongly affect the location of the break point, the breaking-wave height and wave shape (i.e. skewness and asymmetry). In fact, wind increases the shoaling wave energy at discrete multiples of the primary frequency and has a significant effect on the wave shape at both a deeper and shallower shoaling locations (Feddersen and Veron 2005). High energy waves in deep water evolve toward the shore, where their steepness increase and their shape affect the sediment stirring in the nearshore area due to the high nonlinearity (Guedes Soares et al. 2004). In this context, the XBeach calibrations by Vousdoukas et al. (2012) and Nederhoff (2014) revealed the model sensitivity to the flow velocity u_a induced by the wave nonlinearity (Eq 4.12), or more precisely to the related calibration factor *facua* (γ_{ua}), which is defined by Van Thiel de Vries (2009) as a coefficient related to the phase shift between flow and intra-wave sediment concentration. Van Thiel de Vries (2009) suggested a value of 0.1, which is the default for this parameter in XBeach. However, Vousdoukas et al. (2012) and Nederhoff (2014) reported that beaches of steeper slopes require higher values of *facua* in order to improve the prediction capability of XBeach. Moreover, Bugajny et al. (2013) reported that *facua* represents the most important parameter in XBeach, because it is the only parameter which affect the results most. Increasing this parameter results in fact in higher velocity u_a and subsequently in more onshore sediment transport that counteracts the offshore sediment transport induced by wave rundown. Therefore, increasing the calibration factor γ_{ua} would result in a significant reduction of the erosion which is generally over-predicted by the current XBeach code.

Both Vousdoukas et al. (2012) and Nederhoff (2014) reported that a relationship might exist between the seaward slope steepness and the calibration parameter *facua*, which needs to be implemented in XBeach. However, neither Vousdoukas et al. (2012) nor Nederhoff (2014) attempted to determine this relation. For this purpose, a sensitivity analysis would be needed for the calibration parameter γ_{ua} using XBeach by varying the slope steepness and comparing the observed erosion with the erosion predicted by XBeach. As a result, the value of γ_{au} providing the best fit between the observed and the calculated erosion is selected. Instead of performing such a sensitivity analysis, a mathematical relationship between γ_{au} and the beach slope steepness could be developed and implemented in XBeach based on data from previous literature. The implementation of such a relationship would allow the XBeach user to insert only the value of the average slope steepness in order to get the most appropriate γ_{au}-value for the simulations.

A relation between the average seaward slope steepness (measured perpendicularly to shoreline from the closure depth to the foredune (rise over run)) and *facua* (γ_{au}) is proposed in this study based on the results of the sensitivity analyses performed by Bugajny et al. (2013), Carrion Aretxabala (2015), De Vet et al. (2015), Nederhoff (2014), Splinter and Palmsten (2012) and Vousdoukas et al. (2012). Carrion Aretxabala (2015) applied XBeach to simulate the morphological impact of the Sinterklaas storm on a dune system at Het Zwin (at the borders between The Netherlands and Belgium) where the average slope steepness is 7.85 %. As a result, the best fit of the modelled and observed profiles is

achieved for γ_{au}= 0.15. Nederhoff (2014) applied XBeach to simulate the effect of hard structures on dune erosion and overwash, where the average slope steepness is 9.33%; the best fit is achieved for γ_{au} = 0.25. Moreover, Bugajny et al. (2013) reported that for a beach with slope steepness of 15.79% , a *facua* γ_{au} = 0.5 and for a beach with slope steepness of 14.39%, a *facua* γ_{au} = 0.4 would be required to achieve the best fit. On the other hand, Splinter and Palmsten (2012) used XBeach to simulate the dune erosion of a beach with an average slope steepness of 11.80% and reported that the best fit is achieved for γ_{au} = 0.3. Vousdoukas et al. (2012) found, during the calibration of the XBeach model, that γ_{au} = 0.1 provides the best fit with a 6% slope steepness and γ_{au} = 0.3 provides the best fit with a 8% slope steepness. Furthermore, De Vet (2014) and De Vet et al. (2015) reported that the skewness and asymmetry calibration parameter γ_{au} plays an important role in reducing the overestimation of the erosion volumes of the Fire Island model by XBeach. Therefore, they reported that γ_{au} = 0.2 enhances the prediction capability of the model for an averaged seaward slope steepness of 6.5 %. Table 4.1 summarizes the data related to the average seaward slope steepness and the corresponding γ_{au}-values as extracted from the aforementioned studies. Moreover, either the BSS or the RMSE are also provided as statistical indicators for the best fit.

Table 4.1: Summary of data from previous studies for the relation between the average slope steepness and *facua* parameter, including statistical indicators for best fit.

Study	Average seaward slope steepness S_s = tan β **	γ_{au}-value for best fit	Accuracy indicator
Carrion Aretxabala (2015)	7.85%	0.15	RMSE = 3.80 m
Nederhoff (2014)	9.33%	0.25	BSS = 0.97
Bugajny et al. (2013)	15.79%	0.5	BSS = 0.82
	14.39%	0.4	BSS = 0.54
Splinter and Palmsten (2012)	11.80%	0.3	RMSE = 1.07 m
Vousdoukas et al. 2012))	6.00%	0.1	BSS = 0.40
	8.00%	0.3	BSS = 0.72
De Vet (2014) and De Vet et al. (2015)	6.50%	0.2	BSS = 0.64

** The average seaward slope steepness (S_s = tan β, β represents the average seaward slope angle) of a beach or a coastal barrier is measured perpendicularly to shoreline from the closure depth to maximum run-up point (no overwash case) or to the crest of the coastal barrier in case of wave overtopping (overwash case).

In order to obtain the relation between facua γ_{au} and the average seaward slope steepness ($S_s = tan\beta$), the collected data from the previous studies in Table 4.1 are plotted in Fig 4.2.

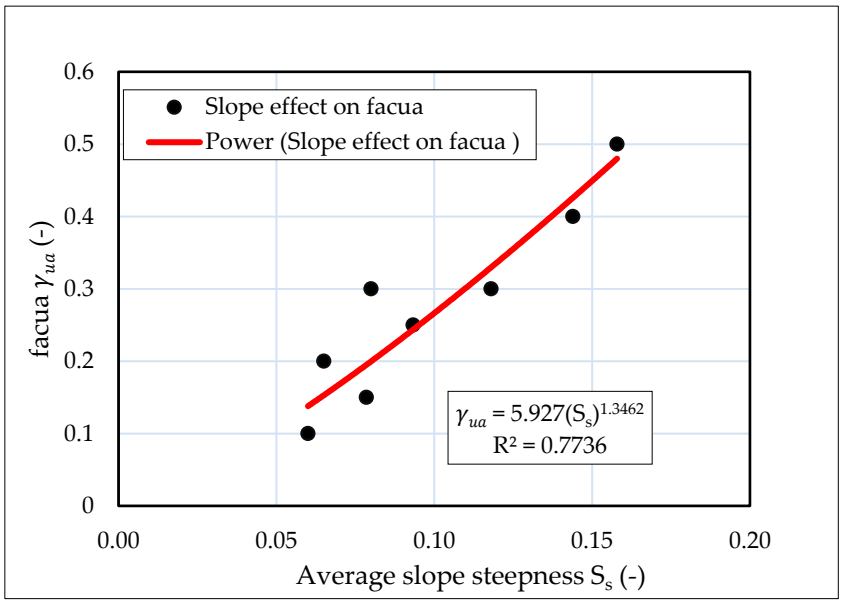

Fig 4. 2: Relation between the average seaward slope steepness and *facua* parameter

The data in Fig 4.2 showed a strong correlation (R = 0.89) when fitted a power function $\gamma_{ua} = aS_s^b$. As a result, the relation between facua γ_{ua}[-] and average slope steepness s_s [-] can be expressed as:

$$\gamma_{ua} = 5.93 s_s^{1.35} \quad (4.13)$$

Eq (4.13), called hereafter "*facua-asabeta*" relationship, indicates that the beach slope has a direct control on the onshore sediment transport induced by the waves skewness and asymmetry. More precisely, Eq (4.13) proves that the phase shift between the intra-wave sediment concentration and flow, represented by the factor *facua*, is significantly affected by the beach slope steepness. Higher phase shift values are expected with steeper slopes as obvious from Fig 4.2. As a result, instead of using the *facua* value $\gamma_{ua} = 0.1$ as proposed by Van Thiel de Vries (2009), γ_{ua} should be determined as a function of the beach slope steepness as proposed in Eq (4.13). Therefore, by considering the latter equation, the skewness and asymmetry discretization model in XBeach, as proposed in Eq (4.12), can be modified as follows:

$$u_a = 5.93 s_s^{1.35} u_{rms} (S_k - A_s) \quad (4.14)$$

Eq (4.13) is implemented in XBeach, after defining a new model parameter called *asabeta* that indicates to the Average Slope Angle beta (β) (see Elsayed and Oumeraci (2015) for the details), where the slope is measured perpendicularly to shoreline from the closure depth to maximum run-up point (when no overwash is expected) or to the crest of the coastal barrier in case of wave overtopping is expected (overwash case). This model improvement allows the XBeach user to insert the value of the average slope angle using the new parameter *asabeta*, so that adequate γ_{ua}-value is simply calculated by the model according to Eq (4.13). Consequently, a proper value for u_a is calculated according to Eq (4.14), which, as discussed in Section 4.1.2, affects both the sediment entrainment/deposition in Eq (4.1) and total transport rates in Eq (4.4).

4.2.2 Grain-stabilization effect on the inception of sediment motion

The experiments of Shields (Shields 1936), which build the basis of the Shields approach for the calculations of U_{cr} in XBeach, were carried out with unidirectional flow over a plane bed of uniform sediment with small grain-interlocking. Therefore, it is believed that the classical Shields concept for the inception of motion does not account for the grain-interlocking effect and the soil texture effect, which are more pronounced for natural mixed-grain-size sediment beds than for uniform sediment beds. Therefore, a large part of the erosion overestimation by XBeach is assumed to be attributed to the underestimation of the critical Shields parameter for incipient sediment motion. In other words, there are unaccounted forces in the formulation of the critical Shields parameter (e.g. the uprooting force to overcome the sediment interlocking). In fact, this assumption is in line with

(i) the studies of Morris (2011) and Özer et al. (2016), who reported that the soil erodibility depends on the soil texture as well as on the compaction energy

(ii) the study of Reid and Frostick (1984) who reported, based on field measurements in Turkey Brook (England), that the shear stress required to initiate particle motion in natural sediment beds is considerably in excess (see Fig 4.3; D_{50} envelope) of that predicted by Shields curve. For instance, the values of the effective shear stress measured by Reid and Frostick (1984) for incipient bedload were consistently higher, ranging from 1.2 to 6.2 times the common critical shear stress values predicted by Shields curve.

Reid and Frostick (1984) attributed this excess to the mutual interference of bed sediment particles. Therefore, the latter studies (Morris 2011; Özer et al. 2016; Reid and Frostick 1984) ensure that the critical shear stress calculated based on Shields curve is underestimated as long as sediments are mutually interlocked and stabilised under compaction/consolidation effect. This might result in the over-predicted erosion rates by XBeach.

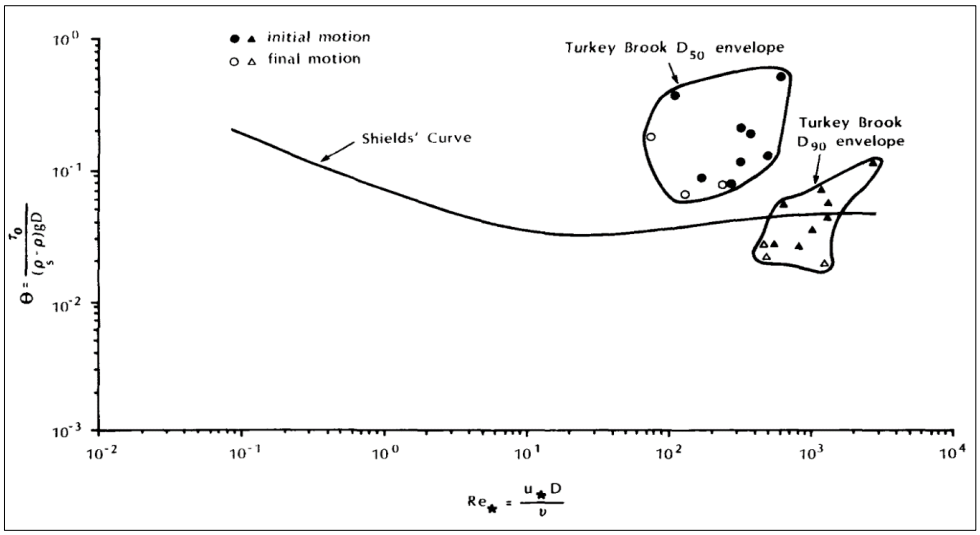

Fig 4. 3: Shields threshold criterion plotted against grain Reynolds Number for Turkey Brook. Initial and final motions were higher than that predicted by Shields thus Shields curve is more applicable if D_{90} of the sampled bedload is taken as representative of particle size (Reid and Frostick 1984).

As other sources for grain-stabilizations, Nowell et al. (1981) reported that marine fine-grained sands are mainly stabilised by biological effects that result in increasing the critical shear stress for incipient sediment motion by 2 to 3 times the values predicted by the Shields curve. The latter is generally valid for sediment of particle Reynolds number $Re_* \leq 1$ (Re_* is the ratio of inertial forces on sediment particle to viscous forces: $Re_* = u_*.D/\nu$ where u_* is shear velocity, D is the grain diameter and ν is the kinematic viscosity). Other studies (e.g. Cha 2012; Nickling and Ecclestone 1981) reported that marine sand in general might be connected by chemical (salty) connections that increase the shear stresses required to initiate the sediment motion. Therefore, the overestimation of the erosion rates by XBeach can partially be attributed to the omission of the effects of diverse grain-stabilizing effects such as the interlocking, biological and/or chemical (salty) stabilizations on critical bed shear stresses for incipient sediment motion.

Despite the lack of processes based models to determine the aforementioned grain-stabilizing effects, the additional shear stress required to account for these effects can be implemented to XBeach by amplifying the critical stirring velocity U_{cr} using an amplification factor γ_{pi} as follows

$$U_{cr}^2 = \frac{\theta_c(s-1)gD_{50}}{c_f} \rightarrow U_{cr_{pi}}^2 = \frac{\theta_{cpi}(s-1)gD_{50}}{c_f} \rightarrow U_{cr_{pi}} = \gamma_{pi} U_{cr} \rightarrow \theta_{c_{pi}} = \gamma_{pi}^2 \theta_c \quad (4.15)$$

where γ_{pi} is a new calibration FACtor for the grain-stabilization and Particle Interaction effect (hereafter called "*facpi*") that considers the increase of the shear stresses required to initiate the sediment motion in case of interlocking, biological and/or salty connections among the sediment particles, $\theta_{c_{pi}}$ is an amplified critical Shields parameter that takes the grain-stabilization into account, $U_{cr_{pi}}$ is the depth averaged critical velocity after considering the grain-stabilization effect. Therefore, the proposed modification affects Eqs. 4.6 and 4.7 that are rewritten below accordingly using Eqs 4.16 and 4.17, respectively.

$$C_{eq,b} = \frac{A_{sb}}{d}\left(U_{stirring} - \gamma_{pi}U_{cr}\right)^{2.4} \;\&\; C_{eq,s} = \frac{A_{ss}}{d}\left(U_{stirring} - \gamma_{pi}U_{cr}\right)^{2.4} \quad (4.16)$$

$$C_{eq,b} = \frac{A_{sb}}{d}\left(U_{stirring} - \gamma_{pi}U_{cr}\right)^{1.5} \;\&\; C_{eq,s} = \frac{A_{ss}}{d}\left(U_{stirring} - \gamma_{pi}U_{cr}\right)^{2.4} \quad (4.17)$$

These modifications are implemented in XBeach by defining a default value for *facpi* $\gamma_{pi} = 1.0$ for the cases without any grain-stabilization effect. However, values larger than 1.0 will definitely reduce the mismatch between $U_{stirring}$ and U_{cr} so that equilibrium concentrations C_{eq} in Eq 4.16 and 4.17 are reduced, which reduces the depth averaged concentrations calculated by Eq (4.1) and hence the total sediment load calculated by Eq (4.4). As a result, over-predicted erosion rates can be reduced.

It is common in morphological evolution models for coastal environments (e.g. XBeach) and for fluvial environments (e.g. Basement of Vetsch et al. 2015) that loose soil beds and hard beds (e.g. revetments and rocky beds) are simulated. Sediment entrainment from loose soil beds is often based on Shields criterion while, in hard beds, sediment entrainment has to be deactivated. However, there is no modelling tool that can yet properly predict sediment entrainment from bed types between compacted to highly compacted beds. The factor *facpi* represents an attempt to do that through an increase of the critical Shields parameter to account for grain-stabilisation effect. Future research could, therefore, attempt to establish physically-based predictors for the calibration factor *facpi* based on soil properties (e.g. median grain size and void ratio as a measure of the compaction degree of sandy soils). Because the value of *facpi* depends on the mutual interference of bed sediment particles, compaction state, concentration of soluble salts and the biological state at the considered study site, model calibrations are crucial in this phase in order to estimate real value for *facpi* as discussed in the following validation cases.

4.3 Test cases for model validation

In order to test the effect of the proposed XBeach improvements in the simulation results by XBeach, three test cases are selected:

(i) GWK tests for dune erosion from the seaward side, which are discussed in chapter 3,
(ii) Zwin dam test for dune breaching (Bakker et al. 1996; Roelvink et al. 2009; De Vet 2014; Visser 1998), and
(iii) Santa Rosa case for barrier island erosion and overwash under a hurricane event (McCall 2008; McCall et al. 2010; De Vet 2014).

The selection of these test cases is based on:

(i) the (partial) availability of pre- and post-storm data to validate the model with the two new extensions,
(ii) the consideration of all possible regimes for testing the proposed model improvements; thereby a dune erosion case (first case), a breaching case (second case) and a barrier island overwash and inundation case (third case) are selected, and
(iii) considering the cases that did not show the same behaviour with the attempts in the previous studies for overcoming the erosion over-prediction by XBeach.

As an example for the latter selection criterion, Zwin dam breach width was significantly underestimated when the artificial limiter for effective Shields parameter is activated while recent physically-based improvements by De Vet (2014) were unable to satisfactorily solve the problem. In contrast, overestimation of erosion and overwash volumes at Santa Rosa Island was possible to be overcome through only the latter artificial limiter whilst no physically-based limiter was able to even improve the prediction capability of XBeach for this case. The details of these three test cases are discussed in the following subsections.

4.3.1 Large-Scale Dune Erosion Tests in GWK

The XBeach dune erosion test XB8 corresponding to GWK tests 15-17 (see chapter 3) represents an adequate means for examining the effect of the proposed improvements on the performance of XBeach. The properties of the sand of the coastal dune and further test conditions are provided in sections 3.3 (Table 3.2). These tests are selected as being representative of the 17 GWK tests in chapter 3 since they have the maximum dune offset. In addition, they are subject to the highest overtopping rates and thus represent more extreme and complex conditions. Consequently, seven new runs for XB8 are performed with the improved model by considering the same model parameters and boundary conditions as in Table 3.2. In the first run, only the dilatancy effect of De Vet (2014) is considered, while in the second run, the *facua-asabeta* relationship is applied for an average slope angle of 4.41^0 (obtained from the GWK model dimensions) and the grain-stabilization effect is not considered by simply setting γ_{pi} = 1.0. In the third run, both dilatancy effect and average slope angle effect are considered besides setting γ_{pi} = 1.0. In the fourth run, an increase of the critical stirring velocity (U_{cr}) by 10% (due to grain-

stabilization) is applied besides considering the average slope angle effect. Similarly, in runs 5 - 7, besides the average slope angle effect, an increase of critical stirring velocity by 20%, 50% and 100% is respectively considered, which are attributed to the grain-stabilization effect. The increases of the critical stirring velocity in runs 4 - 7 were possible by setting γ_{pi} = 1.1, 1.2, 1.5 and 2.0, respectively. The results are shown in Fig 4.4.

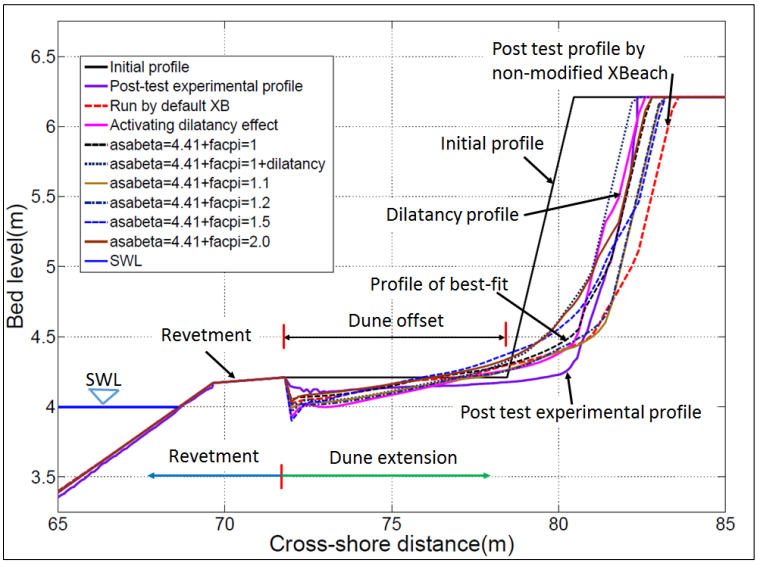

Fig 4. 4: Results of testing the modified XBeach code by considering dune erosion test XB8 (zoom in the dune extension zone)

The non-modified XBeach model results in an overestimation of the erosion volume with a BSS = 0.68 as aforementioned in section 3.4. When the dilatancy effect is activated, the BSS increases to 0.92. However, the dilatancy activation results in underestimation of the frontal dune erosion and overestimation of the scour behind the revetment crest as clearly shown in Fig 4.5.

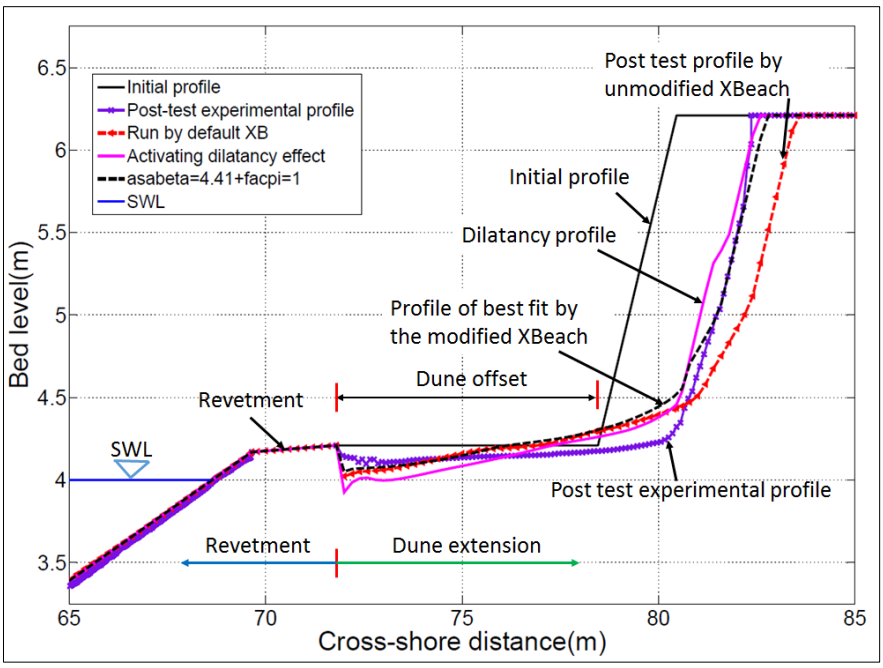

Fig 4. 5: Results of testing the modified XBeach code, including a comparison between the profile of best fit and the dilatancy profile.

The best fit (BSS = 0.983) is achieved without activating the grain-stabilization or the dilatancy effects, simply by assigning the correct value of the skewness and asymmetry calibration parameter

facua using the average slope angle β (asabeta = 4.41^0). When activating both the dilatancy effect and the *facua-asabeta* relationship, the erosion volume is significantly underestimated that results in a reduction of the BSS value to 0.715. Small values for the grain-stabilization effect (*facpi* = 1.1 and 1.2), besides assigning the correct value of *facua* results in a considerable over-prediction of the erosion volumes. This is because increasing the critical Shields parameter using the parameter *facpi* hinders both onshore directed sediment transport, induced by wave skewness and asymmetry effects, and offshore directed sediment transport induced by wave rundown effect. With higher *facpi* values, the overestimation decreases until an underestimation is reached with *facpi* of 2.0 since the increase of the critical Shields parameter hinders the sediment transport onshore and offshore and could, therefore, result in underestimated erosion rates.

Based on the previous analysis, it can be said that the overestimation problem in XB8 was neither due to the grain-stabilization nor to the dilatancy effects, but simply because of the non-assignment of a proper value for the parameter *facua*. Once a proper *facua* value is assigned using the new implementation of the *facua-asabeta* relationship, the overestimation problem is overcome with a BSS = 0.983, thus highlighting the massive importance of including the *facua-asabeta* relationship to XBeach. The latter score can be improved more by adopting other XBeach parameters such as *wetslp*, which is the critical avalanching slope under water (i.e. wet avalanching slope). However, *wetslp* is out of the scope of the verifications of the improved XBeach, but its effect can be seen, for instance, in Vousdoukas et al. (2012) and/or in Berard et al. (2017).

4.3.2 Zwin Dam Breaching Test

An artificial earthen dam was constructed in the mouth of the tidal inlet of Zwin, which is located on the border between the Netherlands and Belgium (see also section 5.4). The test represents a full-scale dam breach experiment that was performed on the 7th of October 1994 to validate the breaching model BRES (Dutch for breach) of Visser (1998). Therefore, the test is well documented in Dutch by Bakker et al. (1996) and in English by Visser (1998). The dam was constructed from sand of a median grain diameter D_{50} of 0.3 mm with a crest height of 3.3 m + NAP (Dutch datum; NAP is the Dutch abbreviation form of MSL), a crest width of 8 m, a landward slope of 1:3, a seaward slope of 1:1.6 and alongshore length of 250 m (Bakker et al. 1996; Roelvink et al. 2009; De Vet 2014; Visser 1998). Though the breach width at the narrowest point was the main measure, this test was used in the study of Roelvink et al. (2009) to validate XBeach capability to simulate barrier breaching under water overtopping. Moreover, it was also used by De Vet (2014) to validate his implementation of the dilatancy effect to XBeach.

In order to initiate a breach under overtopping conditions, an initial breach (pilot channel, see Fig 4.6) was enforced at the middle of the dam having a depth of 0.8 m, a bottom width of 1 m and side slopes of 1:1.6. This pilot channel was enforced to ensure that the breach is initiated at this location. The level of the surrounding seabed was about 0.7 m + NAP, while the mean tidal prism of the Zwin was about 350,000 m^3. The experiment was performed under calm conditions and the water elevation was the main driver for the breaching process, i.e. there was no wave action. The breach developed to a width of 41 m within one hour after the breach initiation, where eroded sediment from the landward side of the dam under overtopping effect is deposited inside the tidal inlet. During that time, the evolution of the breach width is measured.

The Zwin dam test was reproduced in XBeach by Deltares (2015b) and Roelvink et al. (2009), using a non-uniform grid with grid sizes gradually varying from 0.5 m near the breach to approximately 50 m far away from it. The median grain diameter D_{50} of the bed material was set to 0.3 mm in accordance with the prototype test conditions for the artificial dam. The results showed that XBeach overestimates the final breach width (Deltares 2015b). As a first attempt to overcome this over-prediction, De Vet (2014) limited the critical Shields parameter at 1.0 to prevent sediment sheet flow conditions. However, this artificial limiter led to significantly worse predictions than without any limiter (Fig 4.7). As a result, De Vet (2014) applied in a further attempt the dilatancy effect, which resulted in an underestimation of the breach width by 20%.

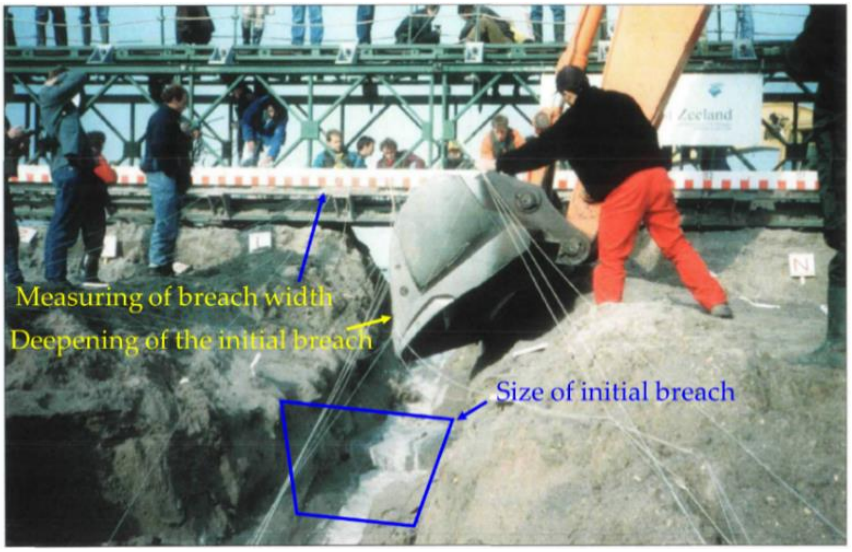

Fig 4. 6: Zwin dam breach initiation, after Bakker et al. (1996).

In order to examine the effect of the grain-stabilization effect, the Zwin dam model is run again six times using the improved model with considering the same model parameters of De Vet (2014). Because the test was performed under calm conditions, no waves are considered in the numerical model and therefore the new implementation of the skewness and asymmetry calibration parameter *facua* (*facua-asabeta* relationship) cannot be examined using this test. Out of the six new runs, the first run considered no model modifications (default settings) while in the second run, the erosion is hindered by activating the dilatancy effect. Runs from 3 - 6 considered (without the dilatancy) *facpi* γ_{pi} = 1.1, 1.3, 1.5 and 2.0, respectively. As a result, the computed breach widths obtained from the numerical runs are compared to the observed breach widths as shown in Fig 4.7.

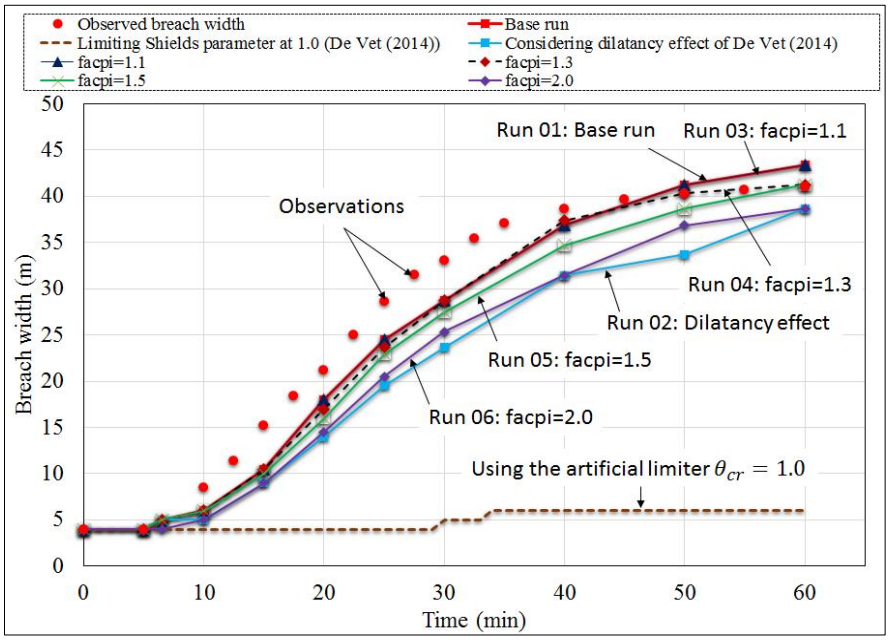

Fig 4. 7: Zwin Dam Breaching Test: Temporal evolution of breach width for the different runs.

Consistent with De Vet (2014), the first run (Base run), with default settings, showed that XBeach overestimates the final breach width by 5.9%. Moreover, applying the dilatancy effect in the second run resulted in an underestimation of the breach width by 5.7%. Using *facpi* of 1.1, results showed no enhancement of the prediction capability of XBeach as compared to the base run. However, the best fit between the final breach widths is achieved when the grain-stabilization parameter *facpi* is set $\gamma_{pi} = 1.3$.

This is also shown for run 04 with a determination coefficient R^2 and a RMSE obtained from the comparison between the observed and the computed breach widths (Table 4.2). From the outcomes of runs 5 and 6, the higher values of *facpi* result in a reduction of the breach width as shown in Fig 4.7.

Table 4. 2: Statistical indicators for the simulation of Zwin breach width evolution using different *facpi* values.

Run	description	R^2	RMSE (m)
1	default settings (Base run)	0.9880	2.77
2	dilatancy activated	0.9776	5.84
3	facpi = 1.1	0.9881	2.77
4	facpi = 1.3	0.9897	2.73
5	facpi = 1.5	0.9866	3.59
6	facpi = 2.0	0.9821	5.14
7	Artificial limiter ($\theta = 1$)	0.8587	21.95

The lowest R^2 and the highest RMSE values obtained from the comparison between the observed and computed breach widths are achieved in run 7 using the artificial limiter followed by run 2 with the dilatancy effect activated. However, the highest R^2 and the minimum RMSE are achieved for run 4 with $\gamma_{pi} = 1.3$ that ensures the grain-stabilization role in hindering the erosion when setting a proper value for *facpi*. In other words, the overestimation of erosion volumes can be attributed to the underestimation of the critical stirring velocity U_{cr} by 23% or, more specifically, to the underestimation of the critical Shields parameter by 40.83% $\left(U_{cr} = f\left(\sqrt{\theta_{cr}}\right)\right)$. This underestimation can be interpreted by the non-consideration of the grain-stabilization effects in the Shields curve as discussed in section 4.2.2.

Applying the grain-stabilization effect using a proper value for *facpi* has allowed predicting the final breach width better than the default settings and even better than the recent development by De Vet (2014), which proves that the parameter *facpi* was indeed capable of hindering the erosion. The too slow reaction of the model at the beginning in most of the cases means that some among the diverse user defined parameters of XBeach (e.g. the critical slopes for avalanching) need to be calibrated in order to achieve better results at the beginning.

4.3.3 Dune overwash and erosion at Santa Rosa Island

The studies of McCall (2008) and McCall et al. (2010) were the first studies for the validation of XBeach using a 2DH case for the dune erosion and overwash at Santa Rosa Island, Florida, the USA under Hurricane Ivan. A barely vegetated sandy section (D_{50} = 0.2 mm) of the barrier island (Fig 4.8) is chosen that showed a significant morphological response to the storm, which was recorded using a high-quality pre- and post-storm LIDAR (Light Detection and Ranging) data. According to McCall et al. (2010), Hurricane Ivan was the largest of five hurricanes that struck the US coast in 2004, resulting in massive damages. Santa Rosa Island is a wave-dominated, narrow barrier island between the Gulf of Mexico and the Santa Rosa Sound on the Northern Florida Panhandle. The island is aligned approximately east–west with a length of almost 85 km. The width of the island varies between 150 m and 1000 m. The westernmost tip of the island is approximately 50 km from the location of landfall of Hurricane Ivan. During Hurricane Ivan, large stretches of Santa Rosa Island were overwashed (washover deposit depths up to 1.5 m with multiple breaches on the westernmost tip).

McCall (2008) and McCall et al. (2010) applied XBeach to a 2 km stretch of Santa Rosa Island between Pensacola Beach and Navarre Beach, which is part of the Gulf Islands National Seashore (Fig 4.8). These studies were based on two LIDAR surveys of the study area that were carried out before and after Hurricane Ivan (Fig 4.9).

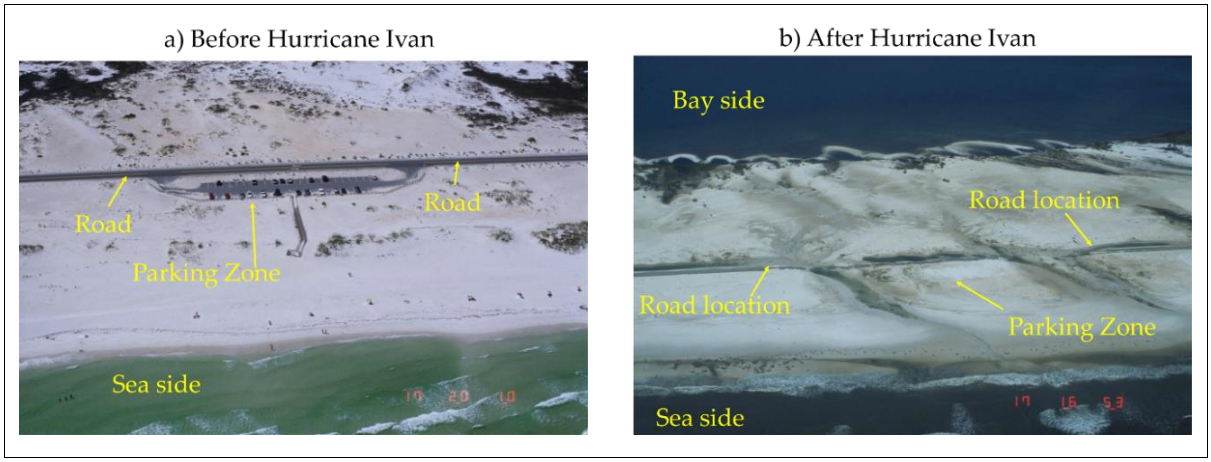

Fig 4. 8: Aerial photo for the study site in Santa Rosa Island before (a) and after (b) Hurricane Ivan, after McCall (2008)

A grid spacing in the longshore direction is set to 20 m whilst the grid spacing varies from 2 m across the barrier island to 29 m on the offshore boundary. The wave and tide boundary conditions are hindcasted as shown in Fig 4.10 based on the available data from two tidal stations. As a result, the offshore wave boundary is described by JONSWAP shaped spectra.

The significant wave height H_s varies from 2.5 m to 7.0 m, where the temporal evolution of H_s is centred symmetrically around the peak of the surge. The peak wave period at the offshore boundary decreases during the storm from 20.0 s to 10.0 s to reflect the frequency dispersion of the hurricane-generated waves in the wave hindcasting model (McCall et al. 2010). Moreover, the surge level, both offshore and behind Santa Rosa Island, varies in the simulation from high astronomical tide 0.30 m + MSL to 1.75 m + MSL.

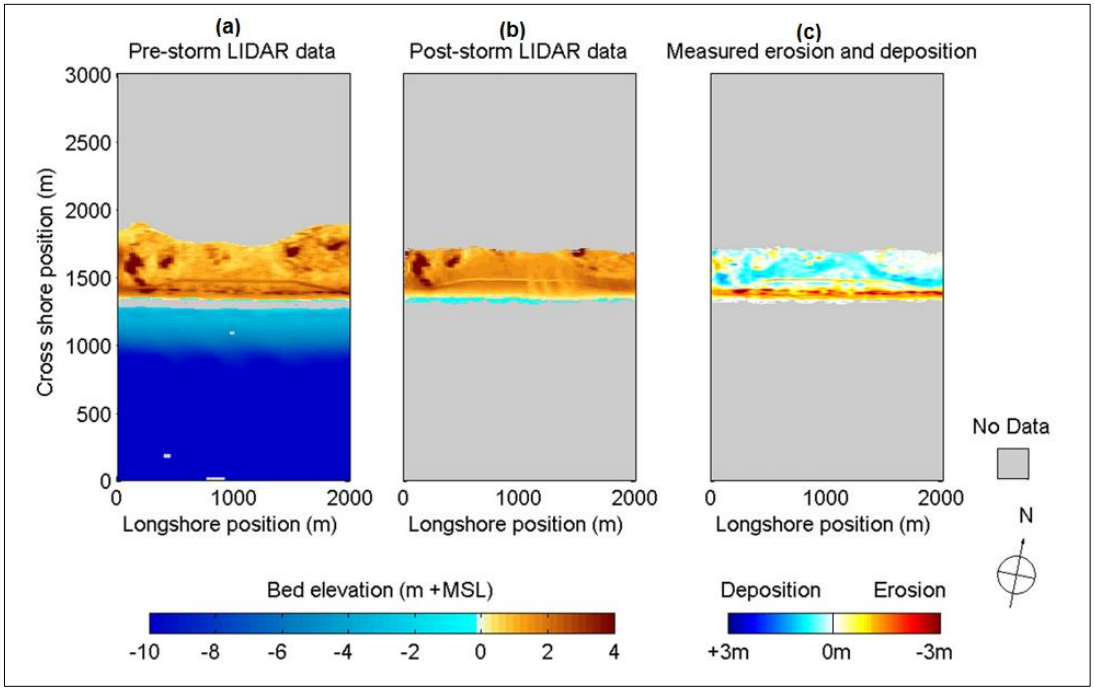

Fig 4. 9: LIDAR-measured bed elevation of the study site: (a) before Hurricane Ivan, (b) after Hurricane Ivan and (c) erosion–deposition plot based on the pre- and post-storm LIDAR data (McCall et al. 2010).

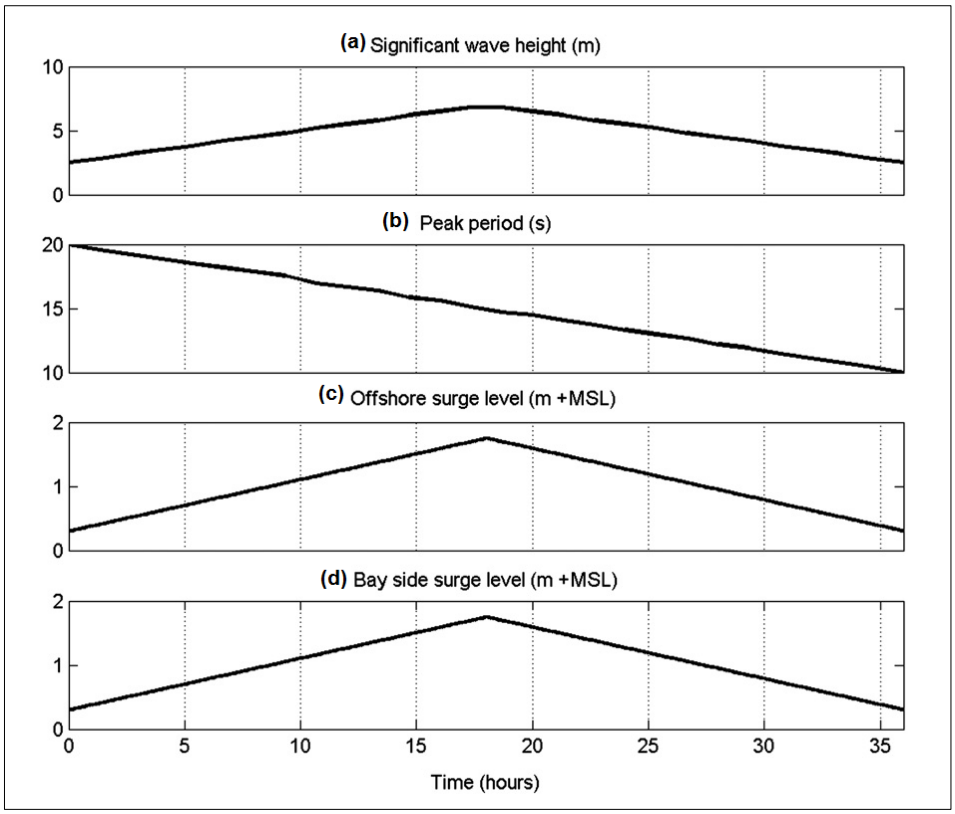

Fig 4. 10: Model boundary conditions: (a) significant wave height, (b) peak wave period on the offshore boundary, (c) surge level on the offshore and (d) surge level on the bay side (McCall et al. 2010).

The duration of the storm is set to 36 h, based on the duration of high energy wave conditions. For the first 6 h of the simulation by McCall et al. (2010), the barrier island is supposed to be in the collision/impact regime since the surge level and wave heights are low and the level due to combined surge and wave run-up does not exceed the crest of the foredunes. Therefore, the morphological response is limited primarily to the erosion of the foredunes and deposition in the nearshore area. The second stage of the simulation running from approximately 6th to 12th hour, where the regime is overwash. During this time, the surge level and wave height increase, leading to run up and overwash. Further erosion of the foredunes takes place, including small amounts of erosion and deposition on the bay side of the barrier. From the 12th hour onwards, the combined surge level and wave setup exceed the height of the foredunes, which are already reduced in height by the preceding phases of the storm, leading to inundation overwash, which results in significant erosion from both dune front and foredune and thereby deposition in the bay side.

McCall (2008) and McCall et al. (2010) reported that XBeach over-predicts the erosion and washover volumes for Santa Rosa by 200% that results in BSS = − 2.69. They, however, were able to overcome this over-prediction by limiting artificially the effective Shields parameter to 1.0, leading to BSS = 0.74. De Vet (2014) reached the same conclusion, though he attempted to overcome the overestimation of the erosion volumes by implementing the dilatancy effect, rather than through artificial limiters. However, the results showed that the erosion and overwash volumes are still overestimated with BSS = - 4.64, which means that the overestimation of the erosion volumes remains even after the recent implementation of De Vet's improvements. In order to overcome the erosion overestimation considering the proposed improvements in Section 4.2, the Santa Rosa model is run again ten times using the same model parameters and boundary conditions of McCall et al. (2010). The first run is performed without hindering the erosion (i.e. using the default settings of XBeach). As a result, the outcomes showed significant overestimation of the erosion and overwash volumes as reported by McCall (2008), McCall et al. (2010) and De Vet (2014), resulting in bad BSS = -2.69 and high RMSE = 1.43 m as reported in Table 4.3.

Table 4. 3: BSS and RMSE for the different attempts to overcome the erosion overestimation at Santa Rosa Island

Run	Properties	BSS	RMSE (m)
1	default settings	-2.690	1.430
2	asabeta = 1.15 + facpi = 1	-3.480	1.550
3	asabeta = 1.15 + facpi = 5	-2.258	1.324
4	asabeta = 1.15 + facpi = 5.8	0.695	0.405
5	asabeta = 1.15 + facpi = 6.0	0.719	0.389
6	asabeta = 1.15 + facpi = 6.2	0.759	0.360
7	asabeta = 1.15 + facpi = 6.5	0.781	0.343
8	asabeta = 1.15 + facpi = 7.0	0.799	0.329
9	asabeta = 1.15 + facpi = 7.1	0.827	0.305
10	asabeta = 1.15 + facpi = 7.2	0.816	0.314

In order to examine the effect of the *facua-asabeta* relationship, the average seaward slope angle *asabeta* is estimated to 1.15^0 and assigned to XBeach in the second run, while *facpi* is set at 1.0. Since *asabeta* $=1.15^0$ results in a *facua* value of 0.03 rather than 0.1 in the first run, less onshore sediment transport under nonlinear waves on the seaside is simulated, thus resulting in a higher overestimation of the erosion volumes. As a result, the BSS decreases to - 3.48 and the RMSE increases to 1.55 m. In runs 3 – 10 (see Table 4.3), *asabeta* is fixed at 1.15^0 while the value of *facpi* is increased until the highest BSS (0.827) and the lowest RMSE (0.305 m) are achieved for *facpi* = 7.1 in Run 9 (see Fig 4.11 for the outcomes of this run). Higher values for *facpi* result in lower BSS and higher RMSE because the erosion is hindered more than required.

By comparing Fig 4.9 (observations) with Fig 4.11 (predictions), one may notice that the overestimation of the erosion is overcome by setting a proper value of the grain-stabilization effect using the new parameter *facpi*. The cross-shore cross-sections shown in Fig 4.12 provides a clearer visualisation of the enhancement of the prediction performance of the model with the new improvements. Fig 4.12 shows also the significant overestimation of the erosion and overwash volumes by the non-improved XBeach. When using the improved model, the prediction capability increases by assigning proper values for the new parameters *asabeta* and *facpi*.

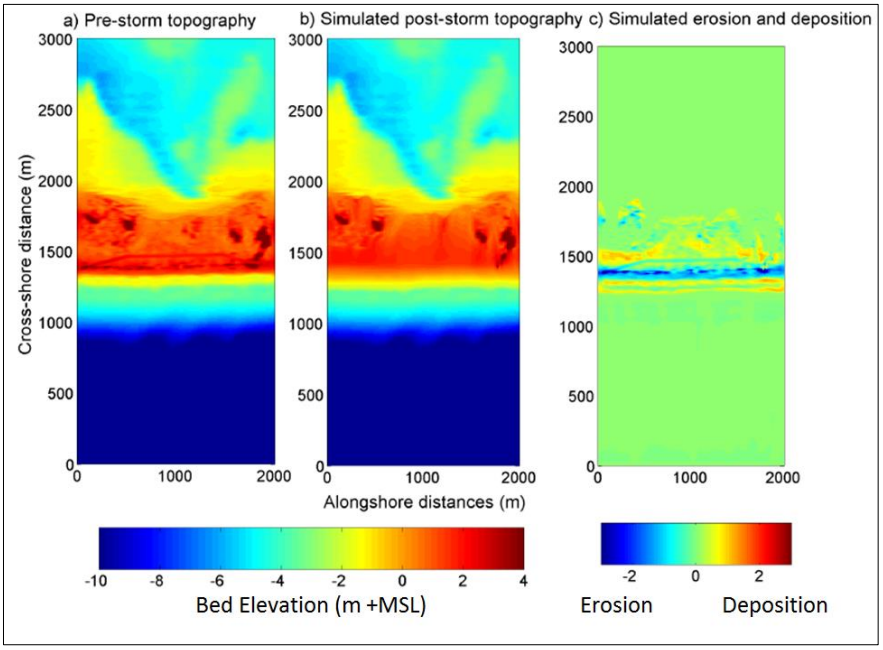

Fig 4. 11: Plan view of Pre- and post-storm simulated topographies as well as the simulated erosion and depositions zones when a very high *facpi* of 7.1 is used to represent the grain-stabilization effect (run 09).

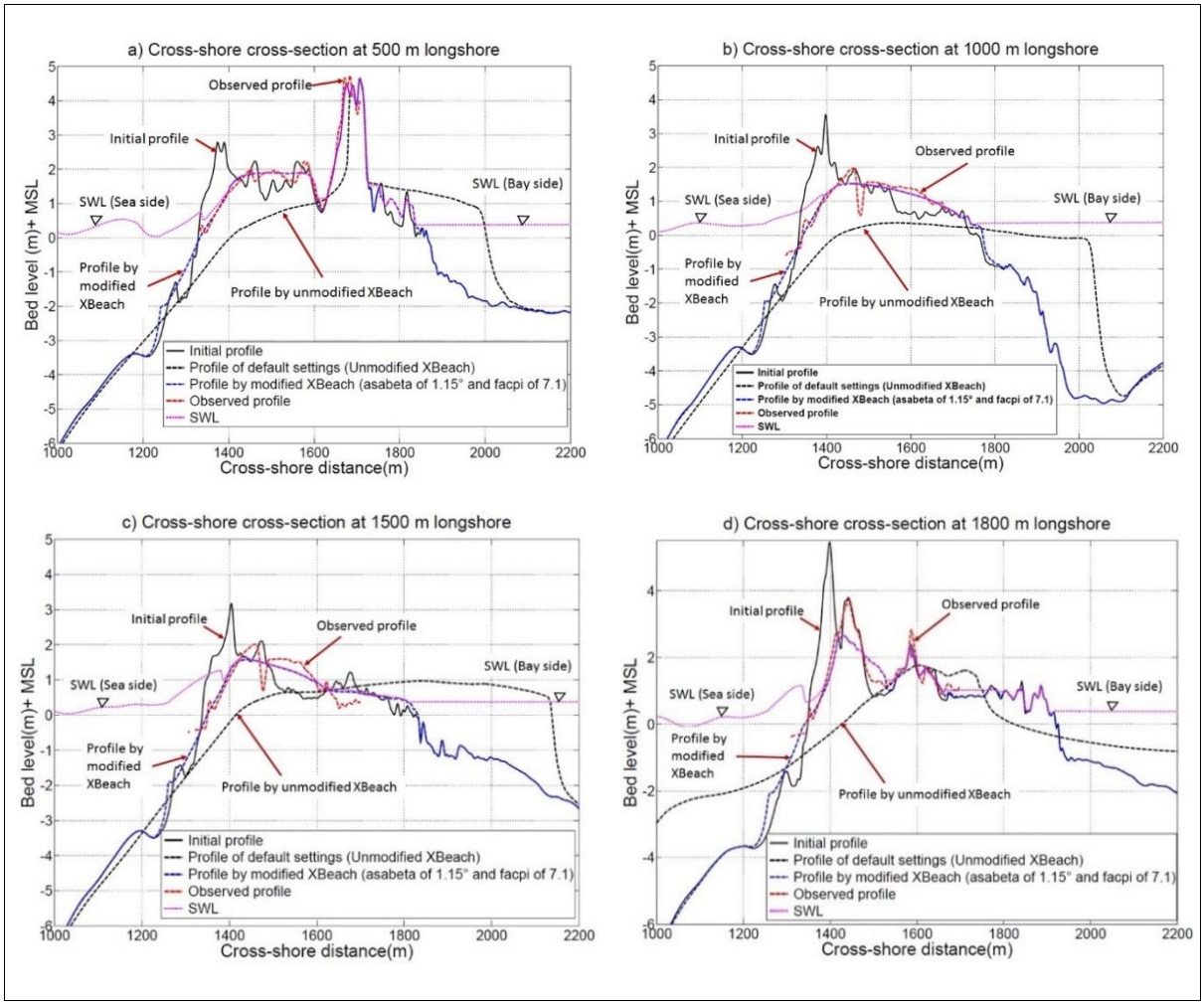

Fig 4. 12: Comparison between final profiles by non-modified and improved XBeach model as well as observed profiles at different cross-shore cross-sections: (a) at 500 m longshore, (b) at 1000 m longshore, (c) at 1500 m longshore and (d) at 1800 m longshore.

The very high value for *facpi* (7.1) means that the critical stirring velocity U_{cr} is amplified 7.1 times, which means that the critical Shields parameter is amplified 50.41 times the value estimated by the common Shields curve. The need for the latter amplification arises from the characteristics of the study area, which contains both longshore road and big parking zone (Fig 4.8). In addition to the hindered erosion by the asphaltic layer in the latter zones, the compaction of soil beneath these zones, which is common in such zones and leads to more particle interlocking and grain-stabilization, also hinders the sediment transport. Therefore, the hindered erosion by such grain-stabilization should be defined to XBeach, as proposed, in order to simulate proper erosion and overwash volumes.

Now it is possible to understand why McCall et al. (2010) were able to fit measured and simulated profiles by using an artificial limiter that fixes the effective Shields parameter to a threshold value $\theta_{max} = 1.0$ that cannot be exceeded even if the flow velocity is higher. Indeed, they were not preventing the sediment sheet flow, but they were limiting the difference between the effective and the critical Shields parameter $(\theta - \theta_c)$ by fixing the effective one θ at 1.0. The same difference can indeed be achieved physically by increasing the critical Shields parameter θ_c. The latter approach is in fact more appropriate because it can be interpreted by the grain-stabilization effect while the artificial limiter suggested by McCall et al. (2010) is more difficult to interpret.

4.4 Summary, discussion and implications of the results

In this chapter, the reasons for the overestimation of the erosion and overwash volumes by the XBeach model under storm wave conditions are explored. It is found that the main two reasons for the overestimation are:

(i) the effect of wave nonlinearity on sediment transport or more specifically the calibration factor *facua* for the time-averaged flow due to wave skewness and asymmetry,

(ii) the considerable excess of the actual shear stress required to initiate the sediment particle motion in the case of interlocked and compacted soils as compared to that predicted by Shields curve.

The first contribution of this study to overcome over-predicted erosion volumes by XBeach is related to reason (i) mentioned above and consists of developing a new relationship (called "*facua-asabeta*") between the calibration factor *facua* for the net flow due to wave skewness/asymmetry and the seaward average slope angle β measured perpendicularly to shoreline from the closure depth to the foredune. The new relationship is derived from the results of sensitivity analyses to the *facua* factor recently carried out in previous studies. Thus, this relationship is implemented in XBeach so that proper *facua* value can be calculated based on assigned β. The second contribution is related to reason (ii) mentioned above and consists of amplifying the critical shear stress required for incipient sediment motion according to Shields curve using an amplification factor γ_{pi} (called "*facpi*"). This factor is also implemented in XBeach in order to account for grain-stabilization effects (e.g. interlocking, chemical and biological stabilizations) as a measure for soil resistance to erosion.

The performance of the improved XBeach model was examined for three selected test cases. The selection was mainly based on the need to separately test the effect of the proposed improvements on (i) frontal dune erosion (section 4.3.1), (ii) sand barrier breaching (section 4.3.2) and (iii) dune overwash and erosion (section 4.3.3). It is noticed that for all test cases, the default XBeach settings result in significant overestimates of the erosion rates. However, this overestimation is overcome using the proposed improvements using two new parameters: *asabeta* and *facpi*. Table 4.4 summarises the values of *asabeta* and *facpi* which are used to achieve the best fit between the measured and simulated profiles.

Table 4. 4: Values of the new parameters *asabeta* and *facpi* used in this chapter to overcome the overestimation of erosion and overwash volumes.

Test case	*asabeta* (deg)	*facua* (-)	*facpi* (-)	D_{50} (mm)	Soil state
Frontal Dune erosion (GWK tests)	4.41^0	0.188	1.0	0.16	Disturbed soil with low compaction density (artificial dune)
Sand barrier breaching (Zwin dam)	Not applicable	Not applicable	1.3	0.3	Disturbed soil low compaction density (artificial dam)
Sand barrier overwash and erosion (Santa Rosa Island)	1.15^0	0.03	7.1	0.2	Undisturbed soil with high compaction density (natural barrier)

Table 4.4 represents rather a rough guide for recommended *facpi* values. The values of *asabeta* and the associated *facua* values are excluded from this guide because they can respectively be calculated based on the bathymetry change and the proposed *facua-asabeta* relationship (Eq 4.13). Therefore, there is no need to activate the sediment grain-stabilization effect in the case of artificial dunes/barriers made of sand with finer grain sizes (D_{50} = 0.16 mm) like for the GWK tests, where the soil is loose and the grain stabilization effects are negligibly small. For sand with coarser sediment sizes with D_{50} = 0.3 mm, *facpi* can be set to 1.3 as long as the soil compaction density is low like for the Zwin dam case. In the case of a natural coastal barrier, e.g. Santa Rosa Island, the grain-stabilisation effects might be determinant thus significantly affecting the results. In fact, the soil is undisturbed, possibly consolidated resulting in strongly interlocked sediments. In such cases, *facpi* in the order of 7.1 should be used with a median grain size in the order of 0.2 mm. The need for the parameter *facpi* arose from the fact that the Shields criterion for incipient motion is no longer applicable in the case of undisturbed and highly compacted soils.

It is also important to stress the importance of using the proposed *facua-asabeta* relationship (see Section 4.2.1) to properly simulate the effect of wave skewness and asymmetry on sediment transport because, under all the flow regimes of Sallenger (2000), XBeach is very sensitive to the parameter *facua* and the *facua-asabeta* relationship (Eq 4.13) enables to estimate the proper *facua* value. As a result, net onshore sediment transport under wave skewness and asymmetry effect can properly be simulated which might solve the overestimation problem.

Despite the success in overcoming the overestimation of the erosion/overwash rates and volumes using the two proposed improvements of the XBeach model, the following recommendations for future improvements are provided:

(i) The proposed *facua-asabeta* relationship (Eq 4.13) is obtained based only on eight data points obtained from previous studies based on different conditions. Therefore, this relationship needs to be further tested and possibly improved in the light of new experiments.

(ii) Instead of simply using the recommended values for the parameter γ_{pi} (*facpi*) in Table 4.4, it might be preferable to build Shields-like curves that account for the grain-stabilization effect. These curves could be determined from the results of systematic simulations for several real study cases. The relation between the median grain size, the compaction energy and the parameter *facpi* that provides the best fit between the measured and simulated profiles can finally be obtained.

Based on the analysis presented in this chapter it can be reported that the soil resistance (grain-stabilization effect) represents one of the main factors governing coastal erosion, coastal morphology and breach development. Higher values for *facpi* indicate indeed higher soil resistance due to grain-stabilization. In this chapter, a uniform grain-stabilization parameter is applied to reduce the over-predicted erosion by XBeach by using a unique value for *facpi* in each model run. However, a spatially varying grain-stabilization could be implemented to XBeach in future studies for barrier breaching by defining spatially variable *facpi* that can be assigned to the model as a matrix containing different *facpi* for each cell of the computational grid. In this way, the spatially varying soil resistance could be considered to improve the prediction capability of breach location and dimensions. As a result, the interaction between soil resistance, longshore variability of hydraulic loads and longshore variability of barrier topography can be considered in future XBeach simulations as recently suggested in Elsayed and Oumeraci (2016b, 2017a).

5 Combined modelling of coastal barrier breaching and inundation using the improved XBeach code

Coastal floods induced by breaching/overtopping of coastal barriers under extreme storm surges represent a multi-scale problem governed by a complex interaction between a variety of hydrodynamic and sediment-related processes at different time and spatial scales (Christensen et al. 2013; Elsayed and Oumeraci 2016b). However, and as aforementioned in section 2.6, the present modelling of a barrier breaching and the induced inundation is often based on modelling these two processes separately, thus ignoring the strong interaction between them. Therefore, combined modelling of such successive and strongly coupled processes is crucial. Rather than developing the coupling between two different models, this chapter*** presents diverse attempts to use the same hydro-geo-morphodynamic model system (XBeach) to simultaneously simulate both coastal barrier breaching/overflow and subsequent coastal inundation. More specifically, this chapter aims at answering the second PhD research question (see section 2.8.1), which is repeated here as follows:

- *Is XBeach able to properly simulate the coastal inundation induced by barrier breaching, so that both breaching and inundation are simulated in a single model, instead of the current approaches modelling separately breaching and inundation with two different models?*

In order to clearly answer this research question in the following sections and to assess the performance of XBeach, in terms of inundation modelling, the following specific tasks need to be addressed:

- Comparison of the equations/assumptions underlying XBeach and the current 1D and 2D inundation models.
- Comparison of the results from XBeach and another 1D inundation model (e.g. the Hydrologic Engineering Center's River Analysis System HEC-RAS of Brunner 2016) to simulate the inundation of a synthetic cross-shore cross-sectional profile.
- Comparison of the results from XBeach and another 2D inundation model (e.g. River-2D of Steffler and Blackburn 2002) in simulating the inundation of a 2DH synthetic case study.
- Comparison of the results from XBeach with the flood extent and water depths observed in a real case study.

The outcomes of these comparisons are crucial. Therefore, the applicability of XBeach for coastal inundation, i.e. outside its more common types of application in near shore hydro-morphodynamics, needs to be tested comprehensively before applying it to simulate together both barrier breaching and subsequent inundation. This may open the way to a greater number of XBeach users beyond the current applications, including further hydraulic and morphological problems in fluvial and coastal environments (see also Beevers et al. 2016; Hartanto et al. 2011). Moreover, such an examination also enables assessing the current approach for modelling coastal inundation (i.e. one-way coupling between an overtopping/breaching model and another inundation model) as compared to the proposed approach using XBeach to simulate both overtopping/breaching and subsequent inundation in combination. The following section addresses the differences in the equations/assumptions underlying XBeach and common inundation models, while the other sections summarise the results of XBeach applications for the combined modelling of barrier breaching and coastal inundation. The key outcomes and their implications are drawn in the concluding section.

*** More details of this chapter reported in:
Elsayed, S. M.; Oumeraci, H. (2016): Breaching of coastal barriers under extreme storm surges and implications for groundwater contamination: *Application of XBeach in Coastal Flood Propagation*. Internal Report no 1074/17, Leichtweiß-Institut for Hydraulic Engineering and Water Resources, TU Braunschweig, Braunschweig, Germany, 126 p.
Freely available at:
https://www.researchgate.net/publication/315739116_Application_of_XBeach_in_Coastal_Flood_Propagation

Moreover, the final outcomes of this chapter are part of the following journal paper
Elsayed, S.M.; Oumeraci, H. (2016): Combined Modelling of Coastal Barrier Breaching and Induced Flood Propagation Using XBeach. Hydrology. Spec. Issue Floods Landslide Predict. 3, 34. doi: 10.3390/hydrology3040032. http://www.mdpi.com/2306-5338/3/4/32

5.1 Equations/assumptions underlying flood propagation models

The circulation of water in oceans, seas and rivers is 3D process, which is usually analysed using the 3D continuity equation and the 3D Navier–Stokes equations. The latter equations are obtained, respectively, from mass and momentum conservation principles. However, circulation in flumes, flooded straight roads, estuaries, rivers and cross-shore coastal profiles can be simplified and simulated using a 1D version of the continuity and momentum equations which are known as Saint-Venant equations (Saint-Venant 1871). For modelling nearshore hydrodynamics, and often also coastal flooding and inland inundation, the vertical velocity component in the full 3D Navier–Stokes equations can be neglected. As a result, the so-called (2D) shallow-water equations are obtained, which is the case of the CFD module of XBeach and the common 2D inundation models (e.g. River-2D, Telemac-2D). Therefore, in the following subsections, the 1D and 2D governing equations of flood propagation as compared to the governing equations of XBeach are briefly outlined, including the underlying assumptions. The comparison enables the capability of XBeach in modelling coastal inundation to be assessed, besides its proved capability of modelling nearshore hydro-morphological processes.

5.1.1 1D inundation models

Surface runoff, flood wave propagation and inundation extent can be simulated using one-dimensional hydraulic models (e.g. HEC-RAS) of compound channels or straight streets (Abderrezzak et al. 2009), using Saint Venant equations (Saint-Venant 1871). The latter equations are derived by considering the unidirectional equilibrium of a control volume of incompressible fluid based on the assumptions of hydrostatic pressure distribution and fully turbulent flow. The balance of the discharge (mass) in and out the control volume enables the continuity equation (Eq 5.1) to be derived, while the balance of forces within this control volume enables the derivation of the momentum equation (Eq 5.2) in the form of accelerations balance, including inertial (local + convective), pressure, gravity and friction accelerations (Lin et al. 2006).

$$\frac{\partial Q}{\partial x} + \frac{\partial A}{\partial t} = 0 \tag{5.1}$$

$$\underbrace{\underbrace{\underbrace{\frac{\partial u}{\partial t}}_{\text{Local acceleration}} + \underbrace{u.\frac{\partial u}{\partial x}}_{\text{Convective acceleration}}}_{\text{Inertial force term}} + \underbrace{g.\frac{\partial d}{\partial x}}_{\text{Pressure force term}} + \underbrace{g.S_0}_{\text{Gravity force term}}}_{} = \underbrace{g.S_f}_{\text{Friction force term}} \tag{5.2}$$

Q (x,t) is the discharge $[m^3/s]$, x is the longitudinal distance along the flow direction [m], A is the flow cross-sectional area $[m^2]$, t is time [s], u is the depth-averaged unidirectional flow velocity in the flow direction [m/s], g is the gravitational acceleration 9.81 $[m/s^2]$, d is the water depth [m], S_o is the bottom slope [-] and S_f is the bed friction slope [-] (for the fully turbulent flow, the bed friction slope can be described by $S_f = u^2/(C_{ch}^2 * R_H)$, where C_{ch} is the Chezy coefficient $[m^{\frac{1}{2}}/s]$, R_H is the hydraulic radius [m]). The numerical solution of Eqs. 5.1 and 5.2 enables simulating unidirectional unsteady flows (see e.g. Elsayed and Oumeraci 2016a). For instance, the 1D model HEC-RAS solves these equations using the finite difference method by utilizing the four point implicit (box) method of Szymkiewicz (1996). Moreover, these equations can be coupled with morphological solvers to simulate flow-induced unidirectional sediment transport (e.g. HEC-RAS can calculate the sediment transport potential using simple formulae such as the formula of Meyer-Peter and Müller (1948) (see e.g. Pender et al. 2015)).

As 1D models require fewer data and less computational effort than 2D flood models, which often require refined representation of topography and local hydraulic effects (e.g. complex flow patterns and abrupt hydraulic transitions), they are preferred where the hinterland takes a flame-like shape (e.g. valley, channel and straight street) and can be described by a sequence of cross-sections. However, for complex topographies, 1D models are no more applicable, so that 2D inundation models, as discussed in the next section, will be required.

5.1.2 2D inundation models

Two-dimensional inundation models (e.g. River-2D) can provide data essential for risk assessment, such as flow depths and velocity fields at every grid point in a plane. They indeed solve a two-dimensional version shallow-water equations (Lin et al. 2006; Steffler and Blackburn 2002; Vetsch et al. 2015), which are commonly known as the nonlinear shallow water equations NLSWEs, throughout a horizontal discretization of bed topography. The NLSWEs have indeed several typical applications besides describing flood propagation such as describing river flows, tidal flows, tidal mixing, residual currents, storm surges, flow around structures, dam-break waves, coastal flows and tsunamis (Vreugdenhil, 2013), where the short-wave behaviour and the induced radiation stresses are often inputted as external forces in the shallow-water equations as the same case in the surf-beat model of XBeach (see section 2.4 and section 5.1.3). The NLSWEs are often derived by integrating the 3D Navier-Stokes equations over the water depth. However, they can also be derived directly by considering the bi-directional horizontal equilibrium of a control volume of incompressible fluid based on the assumptions of hydrostatic pressure distribution and fully turbulent flow. Thus, continuity equation (Eq 5.3) can be obtained by the mass balance in the control volume while two momentum equations (Eqs 5.4 and 5.5) in the form of accelerations balance can be obtained by the force balance within the same control volume.

$$\frac{\partial z_s}{\partial t} + \frac{\partial (d.u)}{\partial x} + \frac{\partial (d.v)}{\partial y} = 0 \tag{5.3}$$

$$\frac{\partial u}{\partial t} + u\,.\frac{\partial u}{\partial x} + v\,.\frac{\partial u}{\partial y} - \nu_h\left(\frac{\partial^2 u}{\partial x^2} + \frac{\partial^2 u}{\partial y^2}\right) = \frac{\tau_{sx}}{\rho d} - \frac{\tau_{bx}}{\rho d} - g\,.\frac{\partial z_s}{\partial x} \tag{5.4}$$

$$\underbrace{\underbrace{\underbrace{\frac{\partial v}{\partial t}}_{\text{Local acceleration}} + \underbrace{u\,.\frac{\partial v}{\partial x} + v\,.\frac{\partial v}{\partial y}}_{\text{Convective acceleration}}}_{\text{Inertial force term}} - \underbrace{\nu_h\left(\frac{\partial^2 v}{\partial x^2} + \frac{\partial^2 v}{\partial y^2}\right)}_{\text{Transverse Shear stresses term}} = \underbrace{\frac{\tau_{sy}}{\rho d}}_{\text{surface shear stresses term}} - \underbrace{\frac{\tau_{by}}{\rho d}}_{\text{Friction forces term}} - \underbrace{g\,.\frac{\partial z_s}{\partial y}}_{\text{pressure forces term}} \tag{5.5}$$

z_s is the water surface level [m], z_b is the bed level [m] so that the water depth $d = z_s - z_b$, u and v are the depth-averaged flow velocities per meter width [m/s] in x- and y- directions, ν_h is the horizontal eddy viscosity coefficient $[m^2/s]$ and ρ is the water density $[kg/m^3]$. τ_{sx} and τ_{sy} are the components of the surface shear stresses $[N/m^2]$ while τ_{bx} and τ_{by} are the components of the bed shear stresses $[N/m^2]$, where $\tau_{bx} = \rho g.d.S_{fx}$ and $\tau_{by} = \rho g.d.S_{fy}$. The friction slope terms s_{fx} and s_{fy} depend on the bed shear stresses that are assumed to be related to the magnitude and direction of the depth averaged velocities and a dimensionless bed friction coefficient c_f as follows.

$$\tau_{bx} = \rho.g\,.d.s_{fx} = c_f.\rho.u.\sqrt{u^2+v^2} \qquad \text{with} \qquad \tau_{by} = \rho.g\,.d.s_{fy} = c_f.\rho.v.\sqrt{u^2+v^2} \tag{5.6}$$

5.1.3 XBeach as an inundation model

As mentioned in section 2.4, the surf-beat mode of XBeach represents a coupled stochastic (phase-averaged) spectral wave model for storm-induced waves and nonlinear shallow water model for infragravity waves (Roelvink et al. 2009, 2015). Therefore, this XBeach mode describes short-wave processes in a stochastic manner, solving the phase-averaged wave action equation of Holthuijsen et al. (1989) based on empirical formulations calibrated to field or laboratory data (Buckley et al. 2014). However, the infragravity wave motions and mean flows induced mass-flux and the subsequent (return) flow are modelled in a deterministic manner based on mass and momentum conservation laws, solving the NLSWEs using a finite difference scheme, where the short waves induced radiation forces (F_x and F_y $[N/m^2]$) are input as external source term on the NLSWEs as in Eqs 2.1 to 2.3, which are repeated as follows (Eqs 5.7 to 5.10)

$$\frac{\partial z_s}{\partial t} + \frac{\partial (d\,.\,u^L)}{\partial x} + \frac{\partial\,(d\,.\,v^L)}{\partial y} = 0 \tag{5.7}$$

$$\frac{\partial u^L}{\partial t} + u^L.\frac{\partial u^L}{\partial x} + v^L.\frac{\partial u^L}{\partial y} - \nu_h\left(\frac{\partial^2 u^L}{\partial x^2} + \frac{\partial^2 u^L}{\partial y^2}\right) = \frac{\tau_{sx} - \tau_{bx}^E}{\rho d} - g.\frac{\partial z_s}{\partial x} + \frac{F_x}{\rho d} \tag{5.8}$$

$$\frac{\partial v^L}{\partial t} + u^L.\frac{\partial v^L}{\partial x} + v^L.\frac{\partial v^L}{\partial y} - \nu_h\left(\frac{\partial^2 v^L}{\partial x^2} + \frac{\partial^2 v^L}{\partial y^2}\right) = \frac{\tau_{sy} - \tau_{by}^E}{\rho d} - g\,.\frac{\partial z_s}{\partial y} + \frac{F_y}{\rho d} \quad (5.9)$$

Comparing Eqs 5.7 to 5.9 with the NLSWEs for any common inundation model (Eqs 5.3 to 5.5), two main differences can be noticed: (i) the representation of the depth-averaged velocities u and v and (ii) the short wave induced forces F_x and F_y.

In the NLSWEs (Eqs 5.7 to 5.9), most of the terms are formulated in terms of the Lagrangian velocities (superscript L), which are defined as the distance a water particle travels in one wave period divided by this period. Only the bed shear stresses (Eq 5.10) are formulated in terms of the Eulerian velocities (superscript E) and defined as the short-wave-averaged velocity observed at a fixed point.

$$\tau_{bx}^E = c_f \rho u^E \sqrt{(1.16u_{rms})^2 + u^{E^2} + v^{E^2}} \quad \text{with} \quad \tau_{by}^E = c_f \rho v^E \sqrt{(1.16u_{rms})^2 + u^{E^2} + v^{E^2}} \quad (5.10)$$

Where c_f is another dimensionless bed friction coefficient equivalent to that in Eq 5.6 $\{c_f = \sqrt{(g/(C_{ch}^2))} = \sqrt{((gn^2)/d^{1/12})}\}$, n is the Manning coefficient $[s/m^{\frac{1}{3}}]$. The root-mean-squared orbital velocity u_{rms} [m/s] is the short wave orbital velocity that is at bed obtained from the wave group varying wave energy using linear wave theory (Sultan 1992) as:

$$u_{rms} = \frac{\pi H_{rms}}{T_{rep}.\sqrt{2}.sinh(k(d+\delta.H_{rms}))} \quad (5.11)$$

Where T_{rep} is the representative wave period [s], H_{rms} is the root-mean-square wave height [m], k represents the wave number $[m^{-1}]$ and δ states what fraction of the wave height should be added to the water depth in order to account for the wave nonlinearity effect on u_{rms} (Roelvink et al. 2015).

The NLSWEs of the common inundation models (e.g. River-2D) are formulated in terms of the Eulerian frame of reference only, i.e. all the velocities in Eqs 5.3 to 5.5, for instance, are represented by the Eulerian frame of reference in contrast to XBeach, which mixes between the Eulerian and Lagrangian frames. The latter represents one of the main differences between XBeach and any other inundation model. However, this difference vanishes if the shortwave energy is fully dissipated through the transition from the coastal zone to the hinterland. As a result, the formulation of the bed shear stresses in XBeach (Eq 5.10) yields to that in Eq 5.6, which is the formulation of the bed shear stresses in several inundation models (e.g. River-2D or BASEMENT-2D of Vetsch et al. (2015)). XBeach has, therefore, a more generic representation of the bed shear stresses and the depth-averaged velocities, which is known as Generalised Lagrangian Mean (GLM). The GLM approach unambiguously splits a motion into a mean part (Eulerian) and an oscillatory part (Lagrangian), providing a mixed Eulerian–Lagrangian description for the flow field for wavy water surfaces but appointed to fixed Eulerian coordinates. Therefore, the GLM approach does not suffer from the strong drawback of the Lagrangian specification of the flow field – following individual fluid parcels – that Lagrangian positions which are initially close gradually drift far apart (Andrews and McIntyre 1978). In the Lagrangian frame of reference, it, therefore, becomes often difficult to attribute Lagrangian-mean values to some location in space while a pure Eulerian frame of reference (as in the common flood propagation models) omits the oscillation induced by wavy water surfaces. According to Andrews and McIntyre (1978) and Walstra et al. (2000), the GLM approach applies to any problem, whose governing equations are given in Eulerian form (e.g. common inundation models), with a more thorough representation of the real processes (e.g. the GLM approach provides a far more direct route to wave dissipation mechanism than does the conventional Eulerian-mean description).

The wave induced forces F_x and F_y represent the second basic difference between XBeach and any other inundation model. The magnitude of these forces depends mainly on the wave energy in deeper water. A significant part of this energy is dissipated due to wave breaking and bed friction effects as well as due to wave diffraction through breach-induced inlet (e.g. Ambrosio and Siegle 2014). When using XBeach as an inundation model, the flood propagation in the hinterland may be affected by the non-dissipated part of wave energy, i.e. the wave-induced forces might still have considerable values in the hinterland that would affect the propagation kinematics and inundation depths. However, this rest of wave energy is expected to be rapidly dissipated in the hinterland under the bed friction effect.

As a result, the terms of the short wave-induced forces in Eqs 5.8 and 5.9 would vanish quickly in the hinterland and become identical to Eqs 5.4 and 5.5, which are the momentum equations for the state of the art inundation models. The latter means that XBeach utilizes more generic equations that can simulate the hydrodynamic under wavy and non-wavy water surfaces. Therefore, XBeach can be applied in both coastal and fluvial environments (Beevers et al. 2016; Hartanto et al. 2011). In fluvial environments, velocities are usually described by the Eulerian form of the NLSWEs. As a result, XBeach can simulate the hydrodynamics in the nearshore area and the hinterland with the capability of simulating the induced morphodynamics, including soil avalanching.

The most interesting feature in the morphodynamic part of XBeach is the inclusion of a soil avalanching algorithm that accounts for the slumping of sandy material (see section 2.2.2 item ii) from the dune face to the foreshore or from the breach sides to inside the breach (see e.g. Evangelista et al. 2015; Swartenbroekx et al. 2010; Wainwright and Baldock 2015). Avalanching is implemented in XBeach by introducing a critical bed slope steepness for both dry and wet areas. It is considered that inundated areas are much more prone to slumping. Therefore, two separate critical slopes for dry and wet points are used, which are by default 1.0 and 0.3, respectively. In fact, the default value for the dry slope (1.0) satisfies the equilibrium profile of Vellinga (1982). According to Roelvink et al. (2009), the latter slope must be seen as an average slope after dune erosion, where some stretches may exhibit vertical slopes and other drier parts may have slumped further. On the other hand, the default value for the underwater critical slope (0.3) is much lower and was estimated based on the maximum underwater slope that was observed at the Het Zwin breach test (see section 4.3.2 and section 5.4 in below). When these critical slopes are exceeded, the material is exchanged between the adjacent cells to the amount needed to bring the slope back to the critical slope.

The previous capabilities of XBeach make it eligible as a very appropriate inundation model besides being a breaching model with well-proved capabilities. Therefore, XBeach can be used as a breaching and inundation model in combination rather than using two decoupled models to simulate barrier breaching and subsequent coastal flooding. In the following sections, the performance of XBeach is tested

(i) against the results from the 1D inundation model HEC-RAS by the US Army Corps of Engineers (Brunner 2016) and the 2D inundation model River-2D by the University of Alberta, Canada (Steffler and Blackburn 2002) based on a 1D and 2D synthetic test cases, respectively and

(ii) against an experimental test case in the field for the breaching of the Het Zwin dam and the subsequent flood propagation (Visser 1998).

The selection criteria of the 1D model HEC-RAS and River-2D as verification codes to examine the applicability of XBeach for flood propagation are threefold: (a) they are freely available software, (b) they are widely tested and applied as flood propagations, and (c) they respectively utilize the full terms of the 1D and 2D Saint-Venant equations (Saint-Venant 1871) as discussed in section 5.1 and therefore no approximations are introduced in both models; i.e. they are full dynamic wave models solve the full terms of the momentum equations without any approximation. In both 1D and 2D synthetic test cases, XBeach is applied over a single calculation grid to simulate nearshore processes, induced overtopping, overwash and/or breaching as well as flood propagation in the hinterland. Nevertheless, the application of HEC-RAS and River-2D is limited only to examine the XBeach performance for flood propagation in the hinterland, where the inland discharge computed from XBeach at the landward toe of the coastal barrier is used as an upstream input to the inundation models HEC-RAS or River-2D. Therefore, both inundation models simulate the hydrodynamics over a grid containing only the topography of the shore/hinterland.

5.2 Validation of XBeach as a 1D inundation model using a synthetic cross-shore profile

5.2.1 Test programme and validation procedure

In order to validate first the 1D version of XBeach for the combined modelling of the overtopping/overwash and the induced coastal flooding, the synthetic cross-shore profile in Fig 5.1.a is considered. For this purpose, XBeach is applied in the nearshore seaward of the dune toe to obtain the time-dependent inland discharge Q(t) at the landward toe of the dune which is used as an upstream boundary condition for the 1D inundation model HEC-RAS (Fig 5.1.b) that is limited to the hinterland only. The results obtained from XBeach applied as a 1D inundation model in the hinterland are finally compared to the outcomes from HEC-RAS. In fact, the separate modelling of barrier overtopping/breaching and induced inundation is the commonly used approach as discussed in section 2.6 (see also Gallien 2016; Gallien and Guza 2015). However, XBeach is introduced here for the combined modelling, as theoretically justified in section 5.1, so that the transfer of boundary conditions from one model to another can be avoided and the limitations of the separate modelling can be identified.

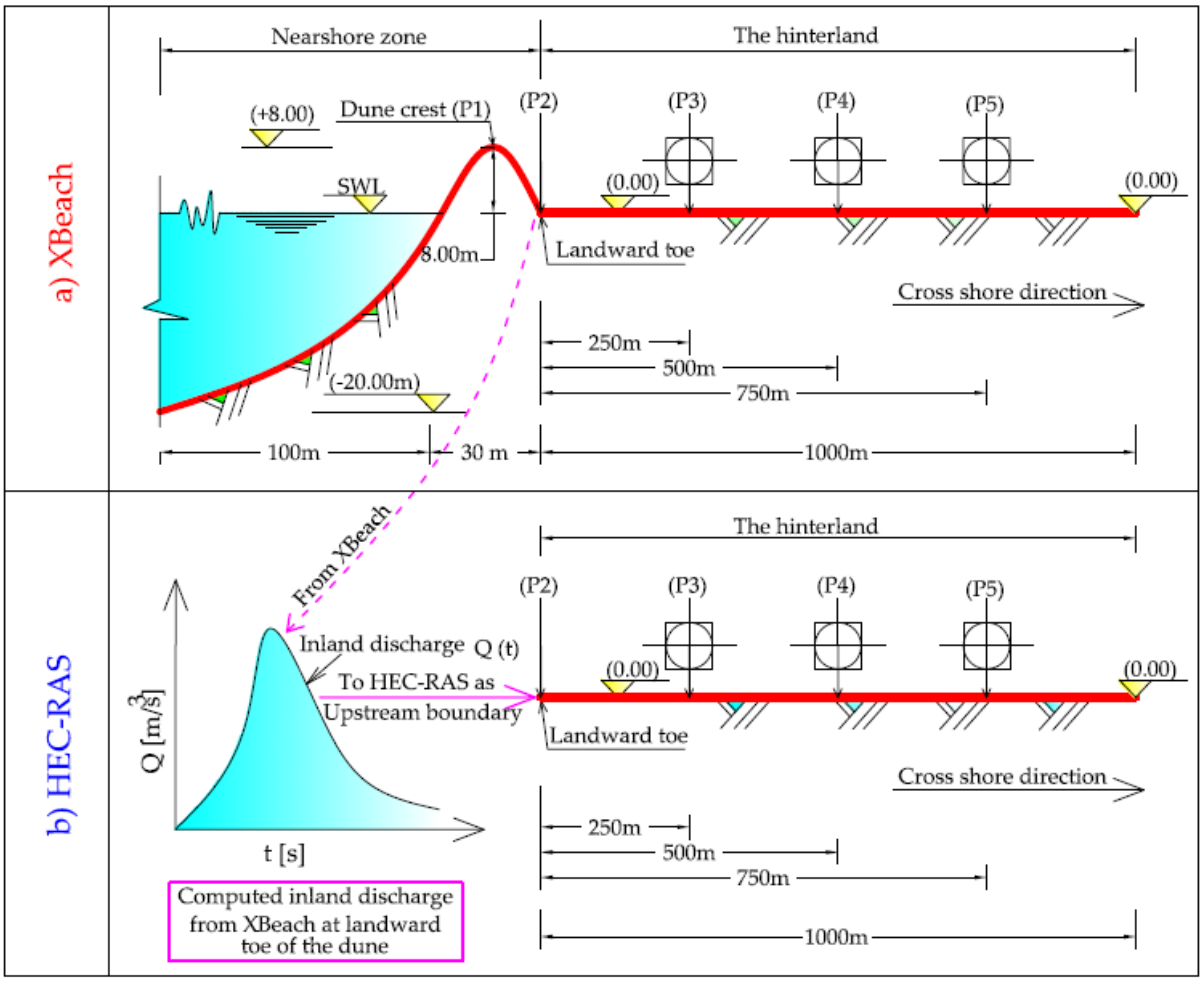

Fig 5. 1: Test case 1: 1D synthetic cross-shore profile (a) 1D synthetic profile used in XBeach to simulate a 1D overwash event and the induced flood propagation in the hinterland and (b) the inland discharge Q(t) is computed from XBeach at point P2, where Q(t) serves as inflow boundary condition for the HEC-RAS inundation model for the hinterland. The outcomes of the inundation from XBeach and HEC-RAS are compared at reference points P3, P4 and P5.

The cross-shore profile in Fig 5.1.a represents a numerical wave flume with a width of 5.0 m (alongshore) and a length of 1130 m. The cross-shore profile consists of three main cross-shore stretches:

a 100-m sea stretch, a 30-m sandy dune stretch and 1000 m hinterland stretch, where the dimensions and levels of each stretch are shown in Fig 5.1 (not to scale). In the sea stretch, the bed level varies from -20.00 m at offshore to 0.00 at the shoreline. The base width and the height of the dune are, respectively, 30.0 m and 8.0 m, where the height is measured from zero sea water level SWL (Mean SWL) as a datum. A 1.0 km flat stretch is added to the landward toe of the dune to represent the profile extent in the hinterland. The main parameters and boundary conditions used within XBeach to simulate this profile are shown in Table 5.1, while all other XBeach parameters (see Roelvink et al. 2015) are kept by the default of XBeach.

The bed is considered non-erodible (hard bed) in the hinterland stretch of 1000 m and erodible in the nearshore zone stretch of 130 m extending from the landward toe of the dune to offshore, with a uniform median grain size of 2 mm. The cross-shore spatial step (dx) is considered regular of 2 m length. For both the coastal zone and the hinterland, a Manning coefficient n = 0.03 $[m^{-1/3}.s]$ is assumed to account for bed friction. The storm-induced waves (low-frequency waves) are represented by a Joint North Sea Wave Project (JONSWAP) spectrum with Hs = 1.5 m (significant wave height) and Tp = 6.6 s (peak period). Moreover, the wave direction is considered perpendicular to the coastline while the water flow outside the hinterland stretch in the downstream direction is permitted.

Table 5. 1: Main parameters and boundary conditions used in XBeach for the analysis of the 1D synthetic profile (Fig 5.1.a).

Parameter	Value	Meaning	Note
D50	2 mm	Median grain size	
dx	2m	Cross-shore spatial step	Regular spatial step
dy	5m	Profile width	
Bedfriction	*n*	Manning parameter (selected as representative for the bed friction)	
bedfriccoef	0.03 $m^{-1/3}$.s	Value of Manning coefficient	This value is generalised over the whole model
instat	4 or jons	Standard JONSWAP spectrum is selected as an upstream wave boundary condition	The selected spectrum coefficients are: *Hs* (significant wave height) =1.5 m and *Tp* (peak period) = 6.6 s
front	0	Absorbing-generating weakly-reflective boundary is used as a 1D inflow boundary	
back	1	Absorbing-generating weakly-reflective boundary is used as a 1D outflow boundary	
left	1	Impermeable wall is a lateral flow boundary	Left side wall of the numerical wave flume
right	1	Impermeable wall is a lateral flow boundary	Right side wall of the numerical wave flume
lateralwave	Neumann	Neumann boundary is a lateral wave boundary in both lateral sides	The alongshore gradient of the wave energy is zero at the lateral boundaries
asabeta	11.3^0	Average slope angle accounts for the beach slope effect on wave nonlinearity	See chapter 4
facpi	1	Grain-stabilization effect is not considered	See chapter 4
form	2	Sediment transport is calculated according to the formulation of Van Rijn (2007a; b)-Van Thiel de Vries (2009)	See Roelvink et al. (2015)
tstop	3600s	Simulation time	
tint	1s	Output time step	

During a storm surge event of 1.0 hour, it is assumed that the SWL rises from level zero (0.00 m) as a long wave resulting from the combination of both metrological surge and astronomical tide effects. Two scenarios for the formation of this long wave are considered, where each scenario represents a hydraulic load case (Fig 5.2):

(i) *Load case 1 (LC1)*: represents, in addition to the wave action described by a JONSWAP spectrum, a sudden sea level rise from 0.00 m to +5.00 m where the latter level persists over the entire storm duration (rectangular shape) and

(ii) *Load case 2 (LC2)*: represents, in addition to the wave action described by a JONSWAP spectrum, a linear sea level rise from 0.00 m to 6.00 m within half of the storm duration followed by a linear decrease at the same rate to level 0.00 m within the other half (triangular shape).

These load cases represent rather simple hydraulic loading which enable the understanding of the induced erosion and inundation processes. Moreover, the effect of different hydraulic loading can be assessed. The first load case is quite simple and represents a stationary sea level rise for a short interval of time whilst the second load represents a simple variation of the sea level and might be comparable with real storm-surges-induced sea level variations.

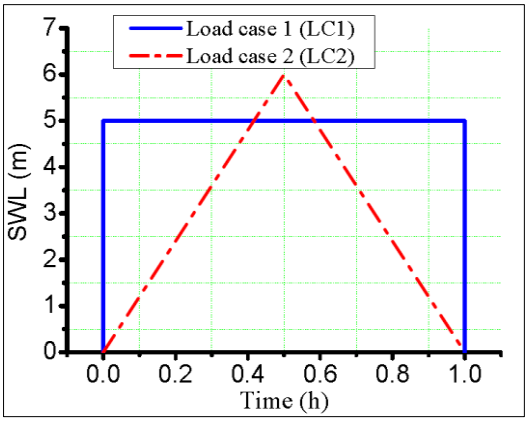

Fig 5.2: Synthetic cases of the rise of the sea level (SWL) under the effects of both meteorological and astronomical tides during the simulation interval (1.0 hour).

The hinterland stretch (Fig 5.1.b) is modelled in HEC-RAS using the inland discharge of water and sediment calculated from XBeach at the landward toe of the dune as upstream boundaries. In addition, the same modelling conditions of the synthetic profile by XBeach are considered in the HEC-RAS model. For instance, the lateral flow is prevented by impermeable walls and levee boundaries (boundaries to prevent the lateral flow) in both XBeach and HEC-RAS models, respectively. Moreover, five measuring points (P1-P5), as shown in Fig 5.1, are set as reference points in the XBeach model while three of them (P3-P5) are considered for comparison of the outcomes from XBeach and HEC-RAS. The results of this comparison are presented in section 5.2.2.

5.2.2 Validation results

The synthetic profile in Fig 5.1.a is simulated in XBeach under both the rectangular (LC1) and triangular (LC2) loads as described in Fig 5.2. The results of these simulations are presented in sections 5.2.2.1 and 5.2.2.2, respectively. As a result, the inland discharges of both water and sediment are calculated in section 5.2.2.3 at the dune's landward toe. The latter discharges are used as upstream boundary conditions for the inundation model HEC-RAS by considering only the hinterland in section 5.2.2.4. As a result, the computed water levels and flow velocities by both XBeach and HEC-RAS are compared.

5.2.2.1 Bed profile and water level evolution under load case LC1 by XBeach

Under load case 1 (rectangular evolution of sea level with wave action) as defined in Fig 5.2, the dune is totally overwashed so that seawater can propagate into the hinterland. Fig 5.3 shows the evolution of both bed level and water level in both sea and hinterland.

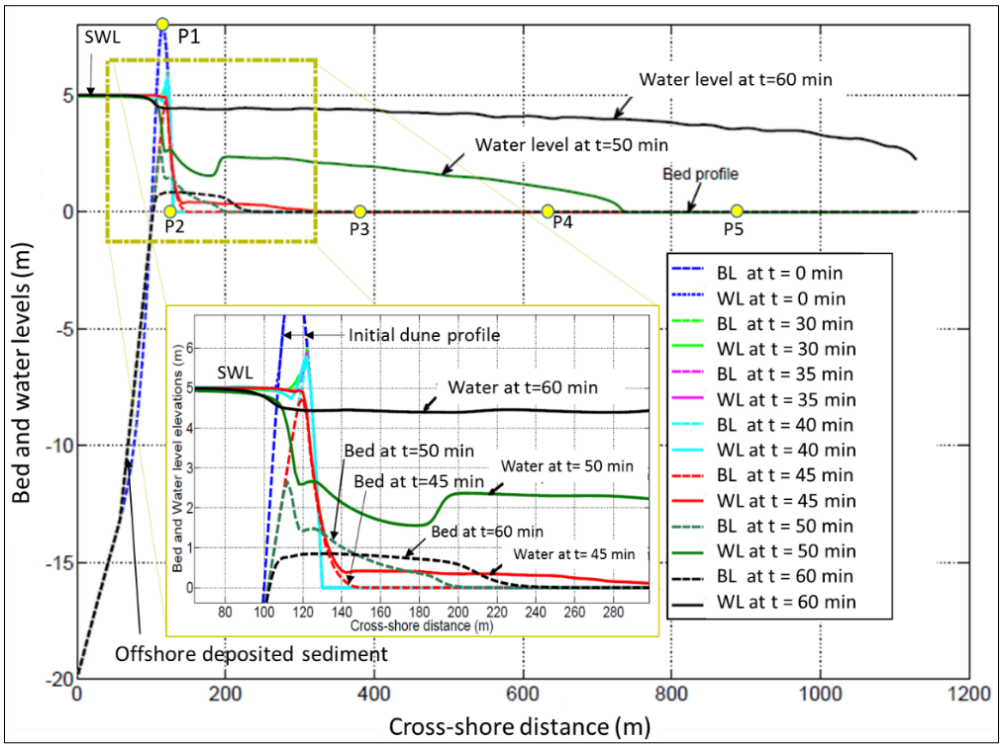

Fig 5. 3: Evolution of the bed level (BL) and water level (WL) for the synthetic profile in Fig 5.1.a under load case LC1 as defined in Fig 5.2.

A seaward erosion of the dune, which is accompanied by a seaward avalanching, is observed. It develops up to 30 min, resulting in a progressive lowering of the dune crest from level +8.00 m at the start of the simulation to level +6.00 m, which means that the dune was under the collision regime of Sallenger (2000); i.e. a regime during extreme events, at which the frontal seaward face of a coastal barrier is subject to collision by breaking waves as well as to wave run up and run down. The eroded sediment transported under the run-down effect deposits offshore. Because of the dune crest lowering during the first 30 minutes to level +6.00 m, the sea waves overtop the dune, causing landward erosion. The overtopping phase extended over a duration of ca. 15 min (from 30 min to 45 min). During this phase, the dune crest is lowered ca. 1 m more, thus allowing seawater to overflow the eroded dune. The overflow phase extended until the simulation end, where significant morphological changes occurred during this phase, resulting in a complete damage of the dune and in sediment deposition behind the dune. As a result, a significant amount of seawater flows inland inducing hinterland flooding. For both overtopping and overflow regimes, the dune works like a broad-crested weir with a movable crest, where a free flow (i.e. no backwater effect) is noticed during the overtopping phase and at the beginning of the overflow phase. This movable crest weir becomes submerged with the time marching, which results in the formation of a hydraulic jump downstream the dune (see the water surface at t = 50 min in Fig 5.3). The hydraulic jump indicates the flow transition from supercritical flow over the dune (Froude number >1) to subcritical flow (Froude number <1) behind it. The length of the hydraulic jump varies with the height of the dune and vanishes when the water level in the hinterland (behind the dune) becomes almost equal to the SWL.

5.2.2.2 Bed profile and water level evolution under load case LC2 by XBeach

The difference with LC1 (rectangular) is the variation of the SWL, which for LC2 (triangular) is linearly increased from level 0.00 m to level +6.00 m within 30 minutes and then linearly decreased at the same rate to level 0.00 m after 1.0 hour (see Fig 5.2). Fig 5.4 shows the evolution of both bed and water levels under LC2.

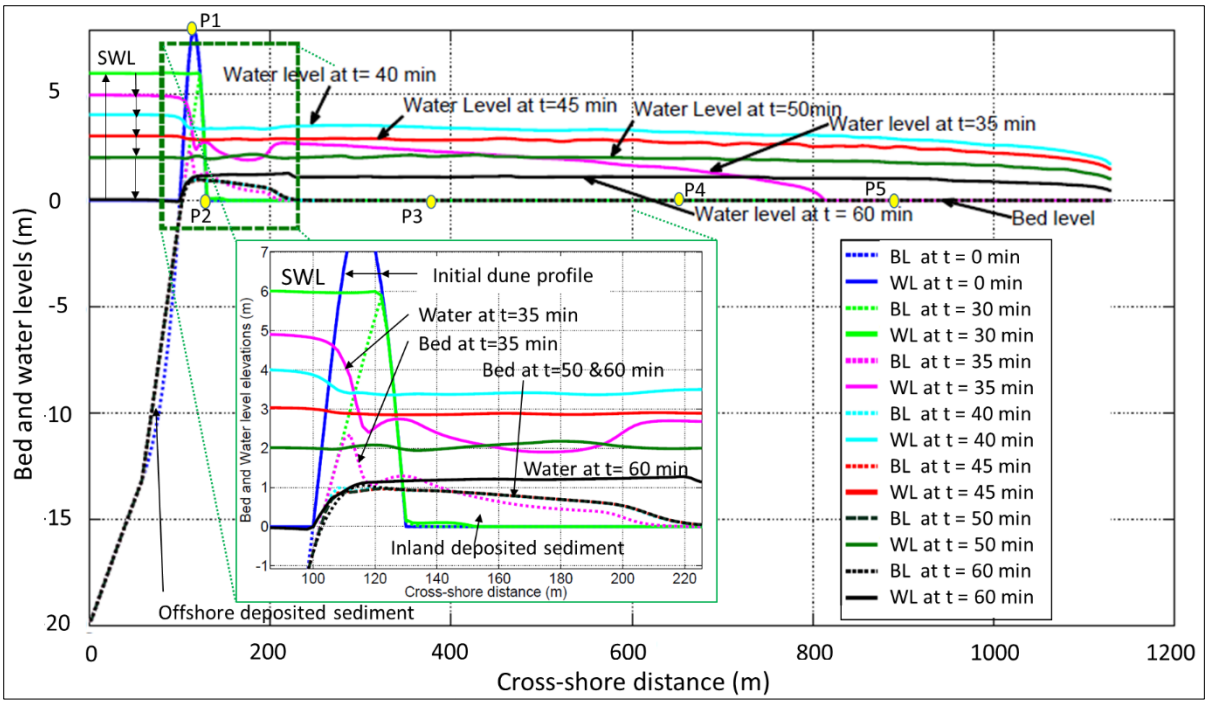

Fig 5. 4: Evolution of the bed level (BL) and water level (WL) for the synthetic profile in Fig 5.1.a under load case 2 (LC2) as defined in Fig 5.2.

Similar to the behaviour under the rectangular load case, seaward erosion is preliminarily developed resulting in dune crest lowering. This crest lowering is followed by wave overtopping at approximately 27.5 min. At this time, both SWL and dune crest are approximately at the same level. However, the waves overtop the dune followed by overflow. During overflow, the dune behaves like a broad-crested weir, resulting in a supercritical flow over the dune and a subcritical flow behind it. Between these two flow regimes, a hydraulic jump is visible from the water level at t = 35 min (Fig 5.4). With the time marching (from t = 40 min onwards), the dune behaves like a submerged weir. However, the decrease of the SWL reduces the difference between the water levels in front and behind the dune and thus the inland flow velocity decreases and the hydraulic jump vanishes. Moreover, the SWL becomes lower than the water level in the hinterland at the end of the simulation time. However, the overwash and inundation processes, in general, are faster under the triangular load case (LC2) than under the rectangular one, which means that the form of the hydraulic load affects the speed of both the erosion and the inundation processes.

5.2.2.3 Water and sediment inflow discharges to the hinterland

Though XBeach doesn't provide a direct estimation of the inland flow rate, the outputs (flow velocity and water depth) can be exploited to calculate the flow rate over the crest of a coastal barrier and/or through a breach induced inlet. The inland discharge per meter q(t) over the dune can simply be calculated at either the barrier crest or at the landward toe of a barrier (e.g. P1 and P2 in Fig 5.3 or 5.4, respectively) using the products of the Eulerian velocity vector $u^E(t)$ at these locations and the local water depth vector $d(t)$ at the same locations. However, the inland discharge calculation at the dune crest (i.e., at P1) is not favoured due the high mobility (erosion) of the dune crest. In fact, the seaward avalanching results in lowering of P1 until it falls under the collision regime. In such situation, discharges at the point P1 are often counted by negative values as long as P1 has fallen beneath wave run-down. During wave rundown, the Eulerian velocity and the discharge are directed offshore and thus have negative values. Such negative values must be avoided when passing the inland discharge to another propagation model (e.g. HEC-RAS) to be used as an upstream boundary for the flood propagation in the hinterland by such models. Therefore, calculating the inland discharge at the

landward toe (e.g. at P2) is preferred. Fig 5.5 shows a comparison between the computed inland water and sediment discharges under both load cases LC1 and LC2.

The erosion process and thus the induced hinterland inundation take place earlier under the triangular load case LC2 (inundation start at t ≈ 1650 s = 27.5 min) than under the rectangular load case LC1 (inundation start at t ≈ 2400 s = 30 min). However, the peak discharge is higher under LC1 than LC2. In contrary, the sediment discharge under LC2 has a higher peak as compared to LC1. Moreover, the ratio between the sediment to water inflows under LC2 is almost 1%. This ratio decreases under LC1 because more sediment is directed offshore during the collision regime under LC1 than under LC2.

Fig 5.5, in addition, shows that the sediment transport peaks precede the flow peaks under both LC1 and LC2. The sediment transport potential depends, in addition to the sediment characteristics, on the bed shear stress, which is higher as long as both the discharge and the steepness of the landward slope of the dune are sufficiently high. Therefore, the steeper slope of the dune landward face at the beginning of the overtopping is associated with higher gravity forces on the sediment, so that a lower water discharge Q is required for sediment mobility and transport. This additional gravity effect is higher on the sediment than on water (due to density difference) and might thus result in higher sediment discharge as compared to those under the effect of the peak water discharge. As a result, the sediment discharge peak (i.e., the peak of the sediment transport potential) develops earlier than the water discharge peak. These rather counter-intuitive results are consistent with the result of Worni et al. (2014), who compared the temporal evolution of the water discharge with that of the bed shear stress during the entire breaching process. In fact, their comparison shows that the peak of the latter occurs before the water discharge peak. When the overwash progresses, the steepness of the dune landward slope decreases (see Figs 5.3 and 5.4) and the sediment transport potential decreases accordingly. On the other hand, the flow peak is reached, especially in these weir-like cases, when the sea level over the dune crest reaches its maximum. The latter condition might be achieved at a later stage of the overtopping process when the slope of the dune landward face becomes milder. At this stage, the sediment discharge is lower as compared to that at the beginning of the overtopping. Therefore, the water discharge peak might be reached later than the peak of the sediment discharge as shown in Fig 5.5. In the case of a breach, the lateral feeding of sediment by avalanching from the lateral sides of the breach-induced channel would result in inseparable water and sediment peaks as depicted in Fig 5.13.

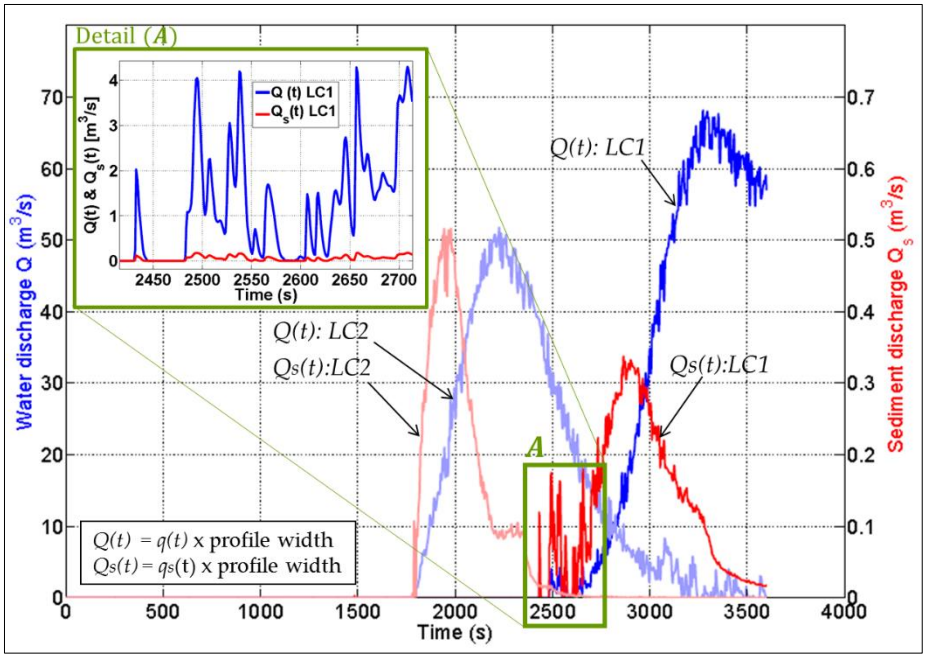

Fig 5. 5: Calculated inflow discharge to the hinterland at P2 of both seawater Q (measured from LHS axis) and sediment Qs (measured from RHS axis); blue and red colours refer to Q and Qs, respectively; dark colours indicate outcomes under the rectangular load case (LC1) while light colours indicate outcomes under the triangular load case (LC2); Detail (A) shows Q and Qs under LC1, both drawn using one vertical scale.

5.2.2.4 Comparison of inundation depths and flow velocities obtained from XBeach and HEC-RAS

The HEC-RAS model is used as a benchmarking inundation model to compare the obtained hinterland inundation against the one by XBeach. The same model set-up (e.g. bed friction) and boundary conditions are applied in the HEC-RAS model as it is as in XBeach (see Elsayed and Oumeraci (2016a) for further details). Moreover, both the water and sediment discharges in Fig 5.5 are used as upstream boundaries to the HEC-RAS model. The sediment transport in the HEC-RAS model is calculated using the formula of Meyer-Peter and Müller (1948). As a result, comparison of the temporal evolution of water profiles in the hinterland stretch by both HEC-RAS and XBeach are shown in Figs 5.6 and 5.7 for the rectangular and triangular load cases, respectively.

In Fig 5.6, the water levels at times 45 and 50 min from both HEC-RAS and XBeach are almost convergent, thus providing a first indication of the capability of XBeach applied as an inundation model. However, HEC-RAS provides higher water levels at times 54 and 60 min, where the difference is larger upstream than downstream the hinterland stretch. The higher water levels by HEC-RAS at the hinterland inlet can be attributed to the effect of the upstream boundary. In fact, by feeding HEC-RAS by the inflow hydrographs computed from XBeach, only the mass is transferred properly, but not the momentum; i.e. the inland discharge alone is not enough as inflow boundary condition for HEC-RAS as it lumps both the variation of water velocity and water depth at the hinterland inlet together in one information, which is the inland discharge. Therefore, the variation of the flow velocity at the hinterland inlet would also be required as another inflow boundary condition, so that the model can correctly calculate the water level at the hinterland inlet based on both the imposed hydrograph and flow velocity.

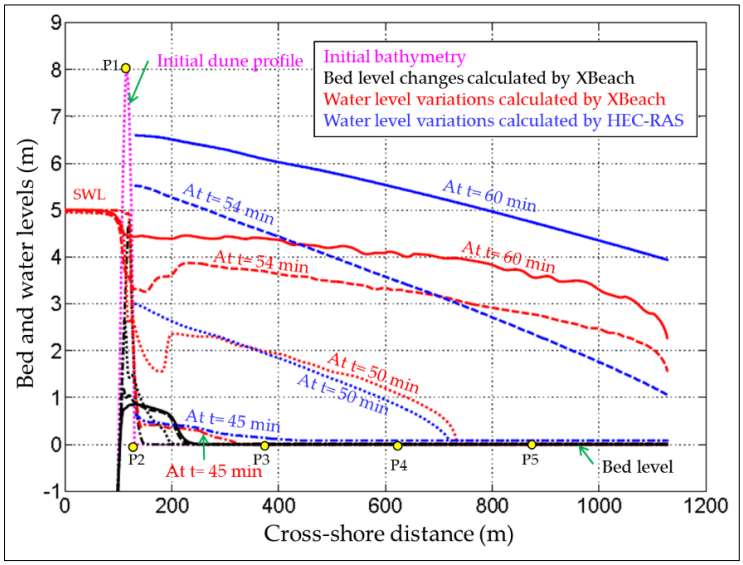

Fig 5. 6: Comparison of water levels calculated by both HEC-RAS and XBeach (1D) at times 45, 50, 54 and 60 min under the rectangular load (LC1).

Since there is no possibility to feed the inland velocity to HEC-RAS as another inflow boundary condition, HEC-RAS calculates the water level at the model inlet based on the incoming discharge and the local bed slope. As a result, with this flat and horizontal bed, HEC-RAS assumes that the flow at the hinterland inlet is always subcritical, which is only appropriate at the beginning of the inundation. The latter might explain why the water levels converge at times 45 and 50 min. At the beginning of the overflow phase, the flow over the dune and at P2 is supercritical, while it is subcritical according to HEC-RAS. This might explain why HEC-RAS provides higher water levels at times 54 and 60 min. The higher water depth at the hinterland inlet results in providing lower values for the associated flow velocity. As a result, the HEC-RAS model cannot reproduce the hydraulic jump at the model inlet. The higher water depth at the inlet leads to a general increase of the water depths as well as a general decrease of the flow velocity at the points P3, P4 and P5 as shown in Fig 5.8.

Similarly, the water levels in Fig 5.7 under LC2 provide the same behaviour as under LC1. At 35 min, the water levels are convergent since the upstream boundary has yet no significant effect. Afterwards, HEC-RAS provides higher water levels due to the effect of the upstream boundary. Fig 5.9 also shows the temporal evolutions of the water depths and velocities at the measuring points P3, P4 and P5 under LC2.

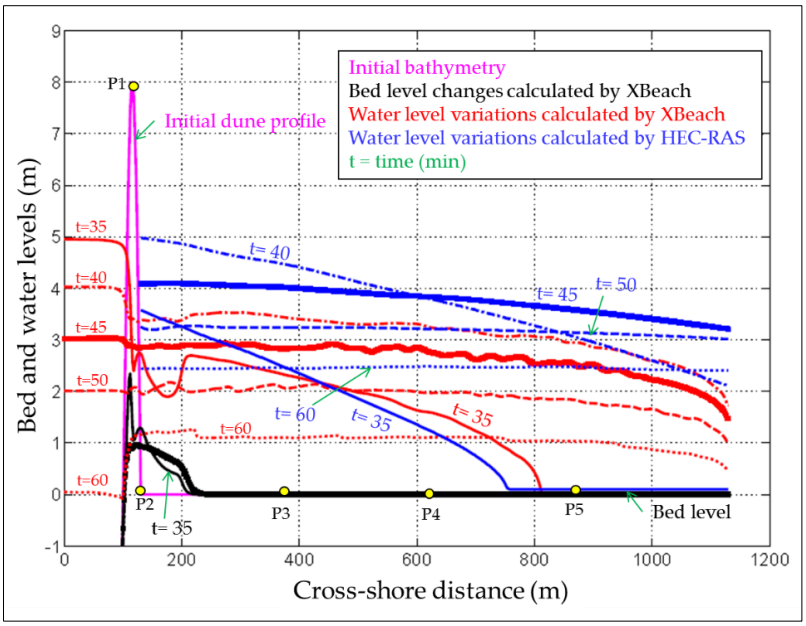

Fig 5. 7: Comparison of water levels calculated by both HEC-RAS and XBeach (1D) at times 35, 40, 45, 50 and 60 min under the triangular load (LC2).

In Figs 5.8 and 5.9, the water depths from HEC-RAS and XBeach increase by the same rate at the inundation start, but the increasing rates from XBeach become lower than those from HEC-RAS by 30 to 40 % due to the upstream boundary effect in which the difference increases at the nearer points to the upstream boundary. The higher increase of the water depths in HEC-RAS as compared to those in XBeach may explain why the depth-averaged velocities from HEC-RAS are lower than those from XBeach by 30 to 40%.

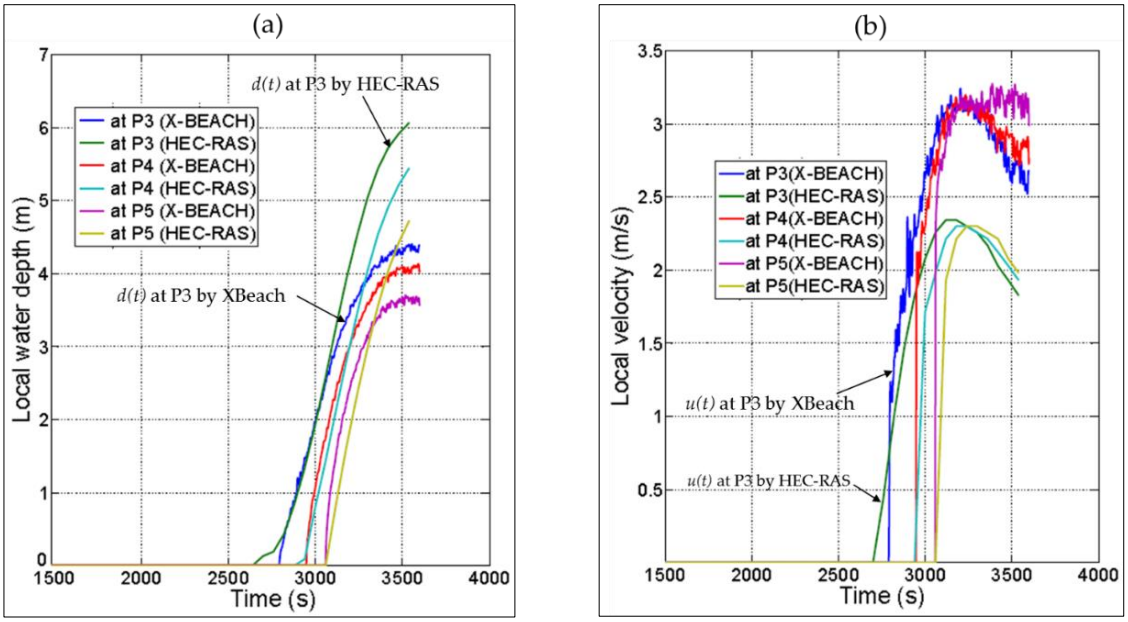

Fig 5. 8: Comparison of local water depths (a) and local depth-averaged velocities (b), calculated by both HEC-RAS and XBeach (1D) at the measuring point P3, P4 and P5 under the rectangular load (LC1).

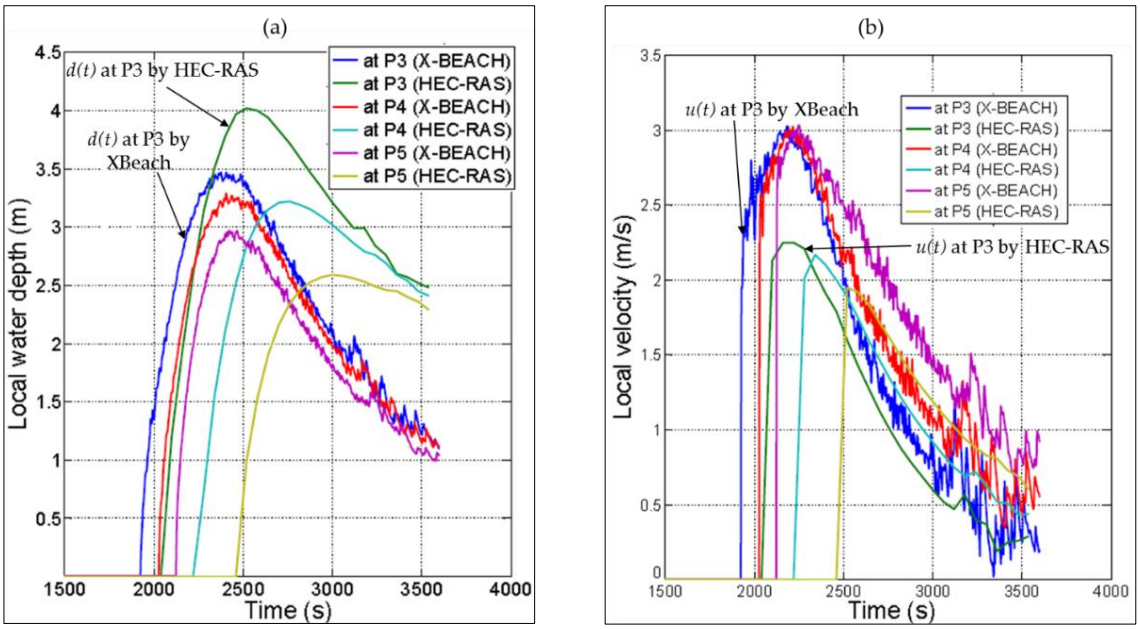

Fig 5. 9: Comparison of local water depths (a) and local depth-averaged velocities (b), calculated by both HEC-RAS and XBeach (1D) at the measuring point P3, P4 and P5 under the triangular load (LC2).

Remark 5.1: Summary of comparative analysis between 1D coupled and decoupled approaches

The comparative analysis of the water depths, velocities and flood extent in the hinterland due to barrier breaching as obtained from XBeach and those obtained by the benchmarking 1D inundation model HEC-RAS have revealed the following limitations of the uncoupled modelling of breaching and subsequent inundation:

(i) The use of hydrograph Q(t) as inflow conditions to the common inundation models is in line with the mass conservation principle, but the flow velocity v(t) which cannot be accounted for in the inflow conditions is also crucial as it provides together with Q(t) the momentum;

(ii) Higher estimates for the flood extent and water depths, mainly because of lumping both the variation of water velocity and water depth through the breach together in one information (hydrograph Q(t)) which lead to unfulfillment of the momentum conservation when transferring the flow from the breaching model to the inundation model (in some cases this may even lead to physically wrong water levels as shown in Figs 5.6 and 5.7)

5.3 Validation of XBeach as a 2D inundation model using 2D synthetic coastal zone

5.3.1 Test programme and validation procedure

The coastal zone (1130 x 1000 m) in Fig 5.10 represents a synthetic 2DH case study. This zone is also divided into three main stretches as described above in section 5.2.1. In the 100-m sea stretch, the bed level varies from -20.00 m offshore to 0.00 m at the shoreline.

The dune has a fixed base width of 30 m, while the crest level varies linearly in alongshore from level + 8.00 m at the dune centre to + 12.00 m at the lateral edges of the considered zone, i.e. the dune crest and thus its side slopes vary alongshore. This longshore variability of the dune dimensions is assumed in order to attempt getting a breach initiation at the lowest point of the dune crest. The hinterland is considered flat and horizontal with 0.00 m-bed level. However, it contains six regular buildings of 10 m height and horizontal dimensions of 100 x 48 m. These buildings are set in order to check the capability of XBeach to simulate building effects on the flood propagation.

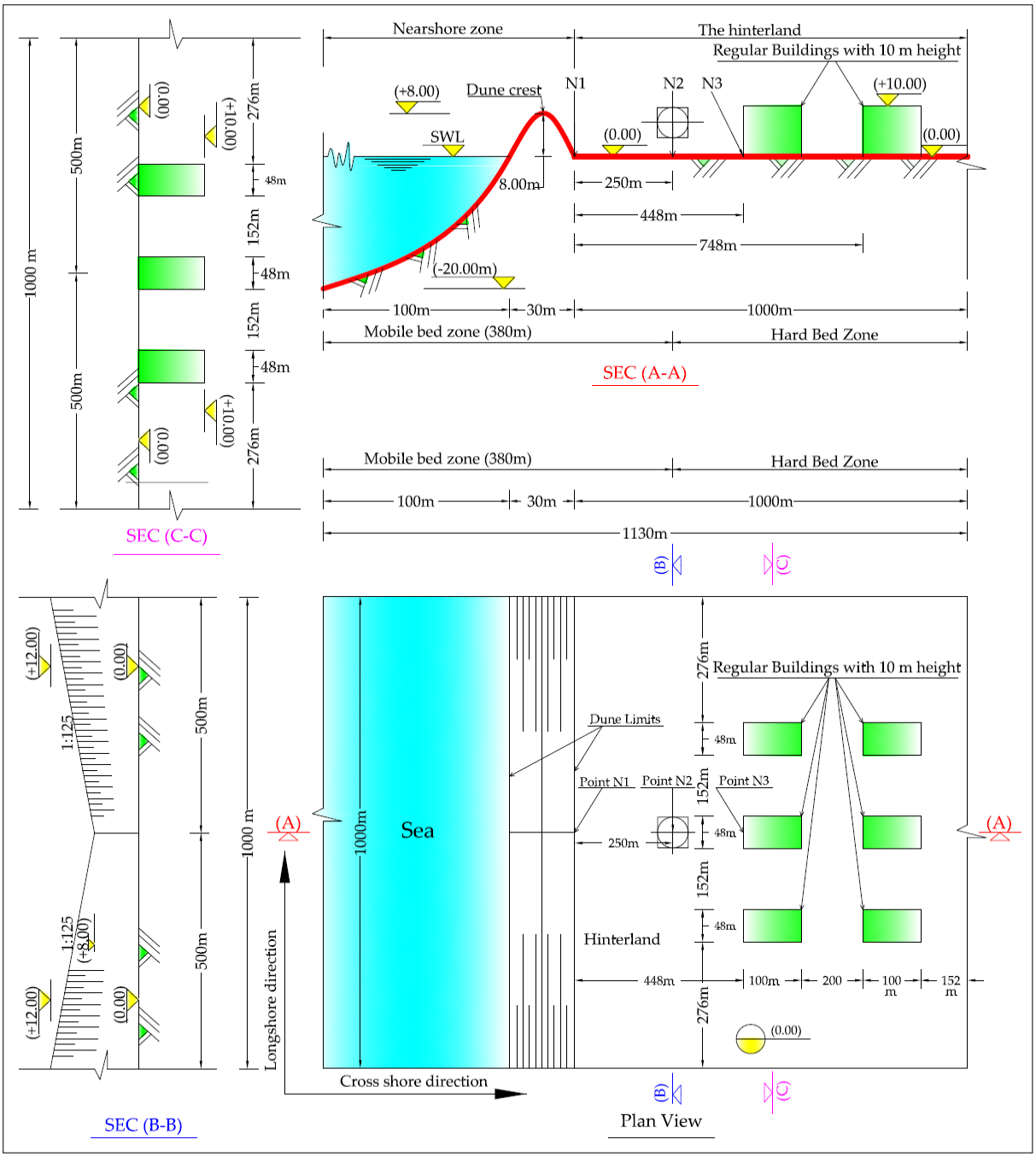

Fig 5. 10: Test case 2: Synthetic 2DH case study showing the sea, the dune, and the hinterland, including the building locations in the hinterland, sections A-A (cross-shore cross-section), B-B and C-C (alongshore sections) show the important details (all dimensions and levels are set in metre and not to scale).

Three points N1, N2, and N3, as shown in Fig 5.10, are set as reference points in XBeach. Moreover, three cross-sections are provided in Fig 5.10 to illustrate the details of the considered coastal area: the first is Sec A-A that passes through the lowest crest of the dune and thus the mid of two buildings, while the second and third cross-sections are alongshore sections that pass, respectively, through the measuring point N2 (sec B-B) and through the middle of the first seaside row of the buildings (sec C-C).

The bed is considered erodible in both sea and dune stretches. Moreover, a stretch of 250 m of the hinterland adjacent to the dune is also considered erodible, while the rest of the hinterland is considered non-erodible (Hard bed as shown in Fig 5.10). Because the buildings are simulated in XBeach as ground elevations, the bed in the building zone and the buildings themselves are considered non-erodible. For

the mobile bed zones, a median grain size of 2 mm is assumed. The bed friction is set by using an assumed Manning coefficient n = 0.03 $[m^{-1/3}.s]$, which is considered uniform over the entire model.

Similar to the hydraulic loads in the previous synthetic case (section 5.2.1), the wave direction is considered perpendicular to the coastline and the storm-induced waves are represented through the model by a JONSWAP spectrum with Hs = 1.5 m and Tp = 6.6 s. The JONSWAP option in XBeach generates alongshore varying time series of the wave energy on the basis of a specified analytical 2D JONSWAP-type spectrum. As a result, the JONSWAP spectrum imposes XBeach to stochastically generate short-crested waves, with variable wave height in the longshore direction. The longshore variability of the wave height (or generally the alongshore variability of the hydraulic load) means alongshore varying wave impact (wave collision by breaking waves), alongshore varying wave run up and run down, and accordingly alongshore varying erosion. During a storm surge event of 1.0 hour, it is assumed that the SWL rises from zero level (0.00 m) as a long wave resulting from the combination of both metrological surge and astronomical tide effects. The formation of the sea level is assumed to take the rectangular form shown in Fig 5.2. The whole zone in Fig 5.10 is simulated in XBeach considering the same parameters and boundary conditions in Table 5.1 except those shown in Table 5.2.

Table 5. 2: Main parameters and boundary conditions used in XBeach for the analysis of the 2D synthetic coastal area (Fig 5.10)

Parameter	Value	Meaning	Note
front	1	Absorbing-generating weakly-reflective boundary is used as a 2D inflow boundary	
left	0	Neumann boundary is a lateral flow boundary	Neumann means that gradient of the lateral outflow is zero
right	0	Neumann boundary is a lateral flow boundary	
back	2	Absorbing-generating weakly-reflective boundary is used as a 2D outflow boundary	
lateralwave	Neumann	Neumann boundary is a lateral wave boundary in both lateral sides of the model	
dy	2m	The spatial step in the longshore direction	Regular spatial step
morfac	10	Factor in Exner equation to accelerate the calculations of the morphological evolution	See Eq 4.3
tstop	5400s	Simulation time	
tint	5s	Output time step	

The flood propagation in the hinterland zone is simulated in River-2D over a calculation mesh containing the topography of the hinterland only and considering the inland discharge through the expected breach(es), computed from XBeach as inflow boundary. The grid of the River-2D model is designed so that the distance between the grid nodes is in the range from 8 m to 12 m. The former lower limit (8 m) is chosen to avoid model instabilities during high flow velocity regimes, while the latter (12 m) is chosen so that four nodes can be generated along the shorter dimension (48 m) of the buildings in Fig 5.10. In order to compare the flood extent and kinematics in the hinterland, the same simulation circumstances of XBeach are applied to the River-2D model. For instance, water outflow outside the hinterland zone in downstream and lateral directions is permitted where Neumann lateral flow boundaries are considered. Moreover, the same constant values for bed friction (n = 0.03 $[m^{-1/3}.s]$) and eddy viscosity ($\nu_h = 0.1\ [m^2/s]$) are applied in both XBeach and River-2D models. The results of this comparison are shown in section 5.3.2.

5.3.2 Validation results

The synthetic study case in Fig 5.10 is simulated in XBeach under load case LC1 as defined in Fig 5.2. The results of the breach and flood propagation simulation are analysed in section 5.3.2.1. The water and sediment inflow discharges to the hinterland are obtained in section 5.3.2.2. Consequently, the water discharge is used as an upstream boundary condition for the inundation model River-2D,

including only the topography of the hinterland in section 5.3.2.3, so that the performance of XBeach in the hinterland can be examined by comparing its outcomes with River-2D outcomes.

5.3.2.1 Breach and flood propagation results from XBeach for load case LC1

XBeach is applied to simulate both the breaching of the coastal barrier in Fig 5.10 as well as the induced inundation, considering the rectangular load case LC1 (Fig 5.2) in addition to the JONSWAP spectrum that represents the offshore wind waves. Fig 5.11 shows the model set-up in XBeach as well as the induced breaches, inundation and sediment deposition in the form of sediment fans behind the breaches.

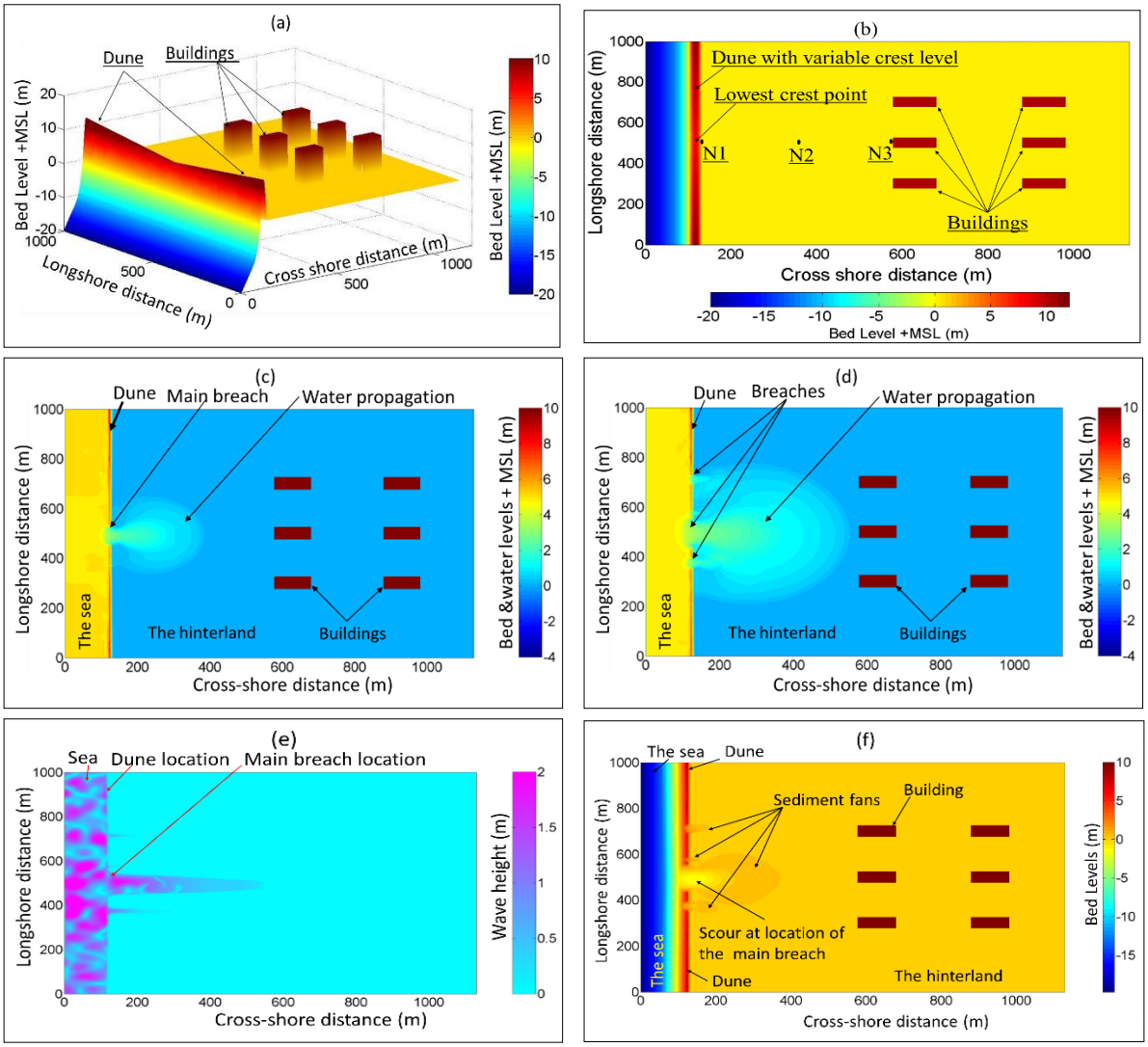

Fig 5. 11: Application of XBeach for the 2D synthetic coastal zone in Fig 5.10, showing: (a) 3D view of the bed levels and the buildings, (b) plan view of the bed levels and building locations, (c) main breach location and inundation extent at t = 45 min, (d) locations of breaches and inundation extent at the storm end (t = 60 min), (e) distribution of the wave height over the model domain at the storm end and (f) morphological changes at the storm end.

The synthetic 2D case in Fig 5.10 is set-up in XBeach considering the longshore variability of the dune dimensions in addition to defining the buildings as higher ground elevations (Fig 5.11.a). The spatial distribution of the buildings and the locations of the reference points N1, N2 and N3 are shown in Fig 5.11.b. A single breach is developed at almost the lowest point of the crest, resulting in the propagation of seawater in the hinterland as shown in Fig 5.11.c. With the time marching, three other breaches develop around the main breach (Fig 5.11.d). Because of the longshore variability of the dune

crest, only one breach was expected to develop at the lowest point of the dune crest, as already observed at the beginning. Indeed, by assuming longshore homogeneity of the strength characteristics of the barrier, this expectation would be justified only for uniformly distributed hydraulic loading alongshore (i.e. with long-crested waves or without any waves). In the case of long-crested waves over a uniformly distributed bathymetry alongshore, one breach might only be expected at the lowest point of the dune crest, since the hydraulic load is uniformly distributed alongshore and, thus, erosion, offshore avalanching and the induced lowering of the dune crest are also uniformly distributed alongshore. In this case, the lowest point of the dune crest would indeed represent the potential location of a unique breach. In the case of short-crested waves (alongshore varying hydraulic loads), which represent the real sea state, the hydraulic load is non-uniformly distributed alongshore (Fig 5.11.e), resulting in wave focusing at local zones in front of the dune. As a result, the erosion, offshore avalanching and the induced lowering of the dune crest may also vary alongshore, which might result in multiple breaches. Because a standard JONSWAP spectrum is used throughout XBeach for wave generation, short-crested waves with alongshore varying time series of the wave energy are generated, so that erosion and offshore avalanching are also varying alongshore, thus leading to multiple breaches. Consequently, the location of incipient breaching is not only a function of the longshore variability of the dune characteristics but also depends on the longshore variability of the hydraulic load. Fig 5.11.e shows an example for the variability of the wave height over the model domain at the storm end (t = 1.0 hour) and shows that part of the energy is diffracted through the breach induced inlet. In addition, Fig 5.11.f shows that the breaching process results in a significant scour at the location of the main breach as well as in sediment deposition behind the breaches, forming sediment fans.

5.3.2.2 Water and sediment inflow discharges to the hinterland

As mentioned in Table 5.2, the longshore spatial step (dy) is set at 2 m, which means that the 2D model of the considered coastal zone is divided into 500 cross-shore stretches (longshore extend = 1000 m). The total inflow discharge Q(t) over the dune and through the breach induced inlets is obtained by summing all the discharges calculated for each stretch separately at the landward toe of the barrier. Of course, several dune zones are not overtopped, especially those at the lateral edges of the model (Fig 5.11.d), which means that there is no necessity to calculate all the discharges at the landward toe of the barrier for all stretches. However, the inland discharge is calculated for the 500 stretches by following the illustrated approach in Fig 5.12.

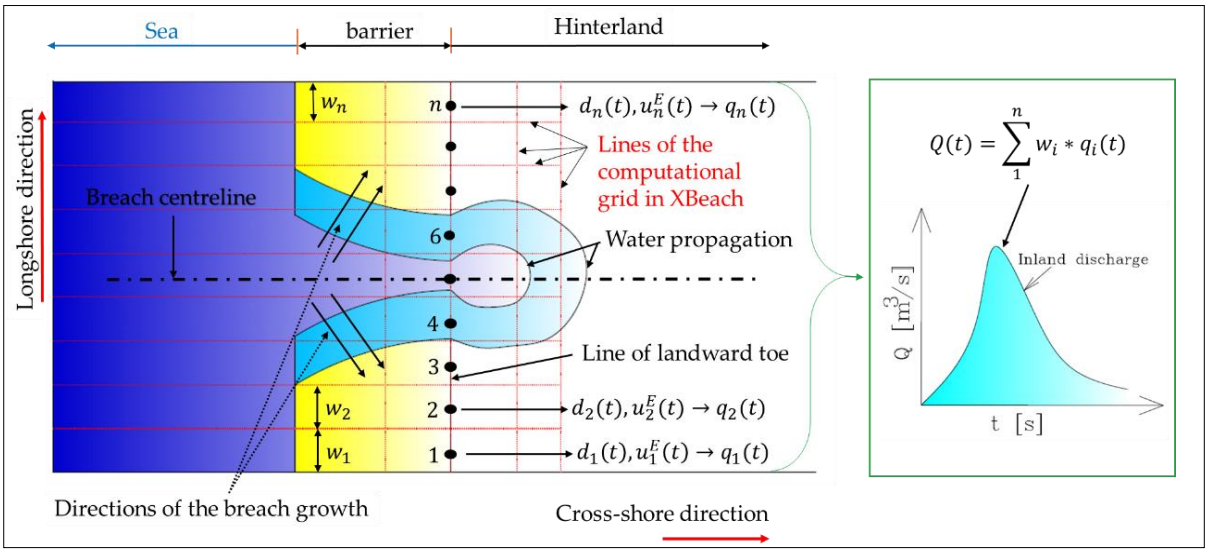

Fig 5. 12: Approach for the calculation of the inland water discharge Q(t) through a breach using XBeach, n = number of longshore stretches, w_i represents stretch width, d_i and u_i^E are the local water depth and Eulerian velocity at dune landward toe of each stretch (schematic).

The breaching process results in significant amounts of sediment transport with the water inflow to the hinterland. Therefore, the inland sediment discharge $Q_s(t)$ is also calculated from the outcomes of XBeach using the same approach for calculating the inland water discharge Q(t); i.e., the sediment transport rate over the toe of each individual stretch out of the 500 stretches is calculated separately. As a result, the total inland sediment discharge $Q_s(t)$ through summation of the calculated individual q_s-values is obtained. Fig 5.13 shows the inland discharge of both water and sediment calculated at the landward toe of the dune.

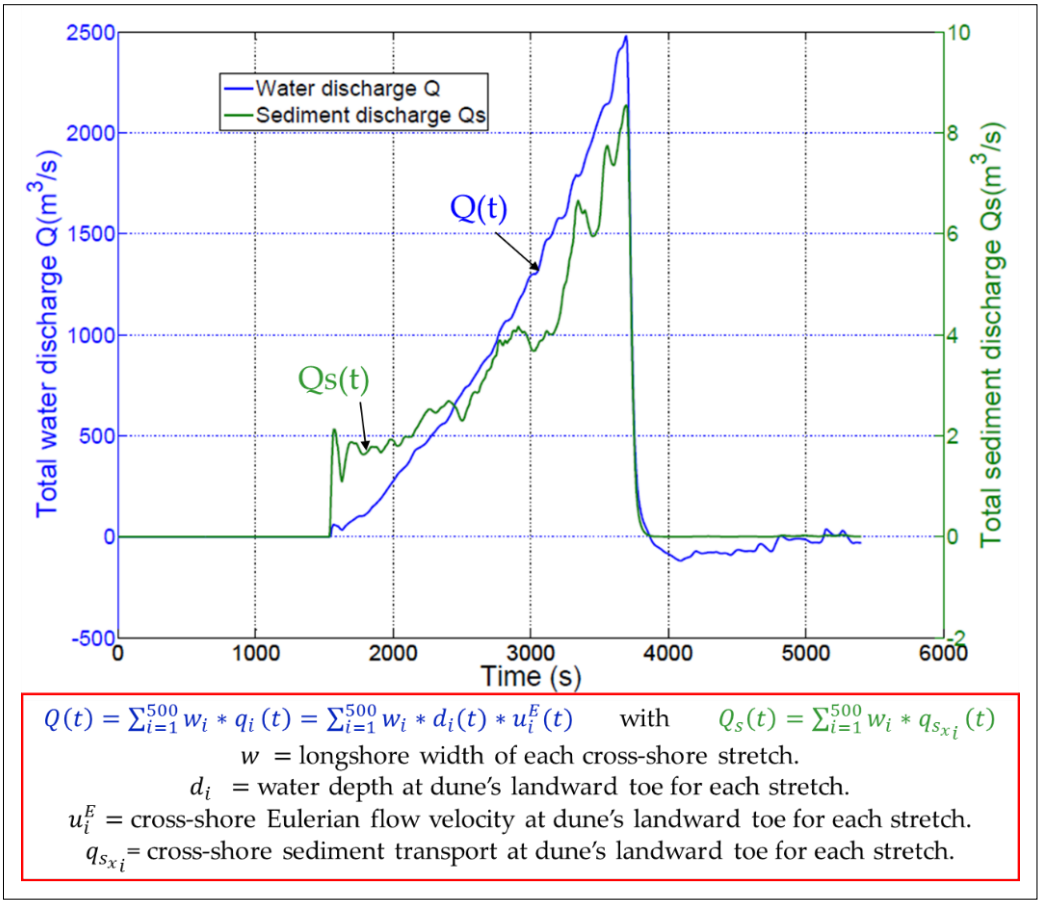

$Q(t) = \sum_{i=1}^{500} w_i * q_i(t) = \sum_{i=1}^{500} w_i * d_i(t) * u_i^E(t)$ with $Q_s(t) = \sum_{i=1}^{500} w_i * q_{s_{x_i}}(t)$

w = longshore width of each cross-shore stretch.

d_i = water depth at dune's landward toe for each stretch.

u_i^E = cross-shore Eulerian flow velocity at dune's landward toe for each stretch.

$q_{s_{x_i}}$ = cross-shore sediment transport at dune's landward toe for each stretch.

Fig 5. 13: Total inland discharge of water (Q) and sediment (Q_s) calculated at the landward toe of the dune under the rectangular load case (LC1).

The significant amounts of salt water flowing inland shown in Fig 5.13 indicate how crucial the breaching process is for the possible contamination of coastal groundwater (see chapter 6). For instance, the inland discharge started from zero at the breach initiation phase and increased steadily to reach approximately 2500 m^3/s at the storm end. The water stopped flowing inland after one hour only because the storm is ended. Due to the sudden decrease of the SWL from +5.00 to 0.00 m after 1.0 hour, the inland discharge is suddenly decreased; it is counted by negative values, which means that part of the water in the hinterland flows back to the sea after the storm end (ebbing condition; see Fig 2.15). The sediment transport rate increases with the flow and stops suddenly with the storm end, which means that the breach would steadily enlarge and deepen as long as the water is flowing inland through the breach. The fluctuations of the sediment hydrograph $Q_s(t)$ in Fig 5.13 might be explained by the avalanching effect, where the avalanched soil from the lateral sides of the breach represents a pulse-like feeder of sediment. In fact, soil suddenly avalanches in the form of headcut (soil blocks; see Fig 2.14.c) when the breach side slopes exceed the critical slope for avalanching, resulting in such fluctuations.

5.3.2.3 *Comparative analysis of inundation modelling results from XBeach and River-2D*

In this 2D case, the River-2D model is used as a benchmarking inundation model to compare the obtained hinterland inundation against the one by XBeach. The same simulation conditions (e.g. bed friction and eddy viscosity) and boundaries are applied in the River-2D model as in XBeach (see Elsayed and Oumeraci (2016a) for further details). In addition, buildings are defined in the River-2D model as internal no flow boundaries (impervious blocks). Because River-2D calculates the flood propagation without sediment transport, only the inflow water discharge Q(t) from Fig 5.13 is used as upstream input to the River-2D model while the sediment inflow discharge $Q_s(t)$ is omitted. In addition, the size of the inflow inlet is fixed at the final size of the four breaches in Fig 5.11.d since the development of the breaches dimensions over the simulation time cannot be assigned to River-2D. The flood extent calculated by River-2D at t = 45 min as well as at the storm end (t = 60 min) are shown in Fig 5.14.a and b, respectively.

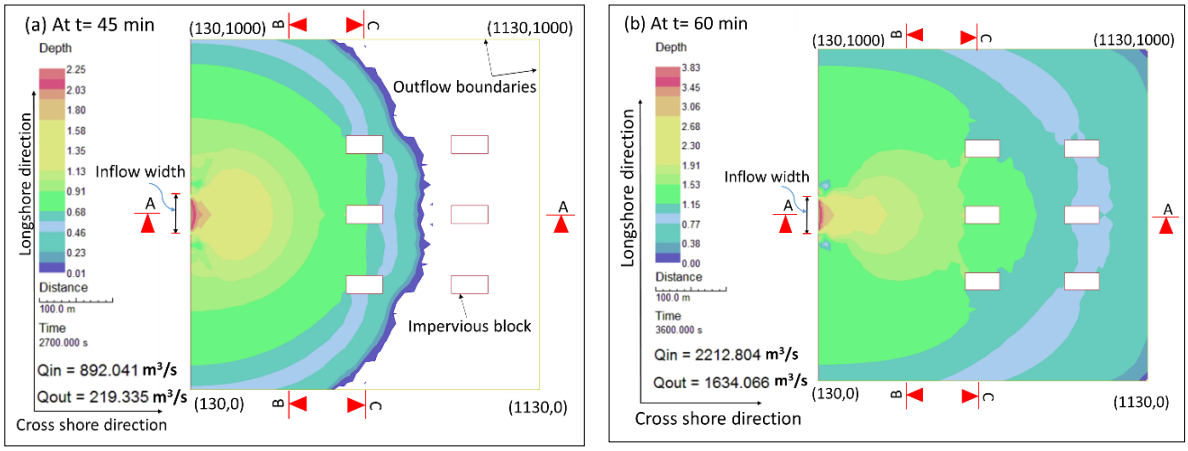

Fig 5. 14: Flood extent and water depths calculated by River-2D: (a) at t = 45 min and (b) at storm end (1.0 hour), both under the rectangular load case (LC1).

Fig 5.14, in addition, illustrates the water depths in the hinterland as well as the instantaneous inflow (Q_{in}) and outflow (Q_{out}) discharges through the model inlet as well as through both the lateral and downstream boundaries, respectively. Moreover, Fig 5.14 visualises the contribution of buildings to the attenuation of the flood propagation in the hinterland. However, when comparing the flood extents calculated by River-2D in Fig 5.14.a and 5.14.b with their counterparts by XBeach in Fig 5.11.c and 5.11.d, respectively, a substantial difference in the flood extents and water depths can be noticed. Fig 5.15 provides comparisons between the temporal evolution of water depths by XBeach and River-2D at sections A-A, B-B and C-C. The three cross-sections show that the flood extent and water depths by River-2D have higher values as compared to those by XBeach. Such higher values can be attributed to two reasons:

(i) Assigning the inflow to River-2D through a fixed width (see Fig 5.14) while omitting the evolution of the breach size dimensions as generated by XBeach. Such a fixed inflow width results in wider estimates of the flood extent from the beginning to the end of the simulation.

(ii) By passing the inflow hydrograph to River-2D, which lumps both the variation of water velocity and water depth through the breach(es) together in one information, the momentum conservation principle is omitted, resulting in subcritical inflow behind the model inlet, which is in contrast to reality. In order to account for the momentum conservation, the variation of the flow velocity through the breach(es) would also be required as another inflow boundary condition, so that the model (River-2D) can correctly calculate the water level at the hinterland inlet based on both the imposed hydrograph and flow velocity.

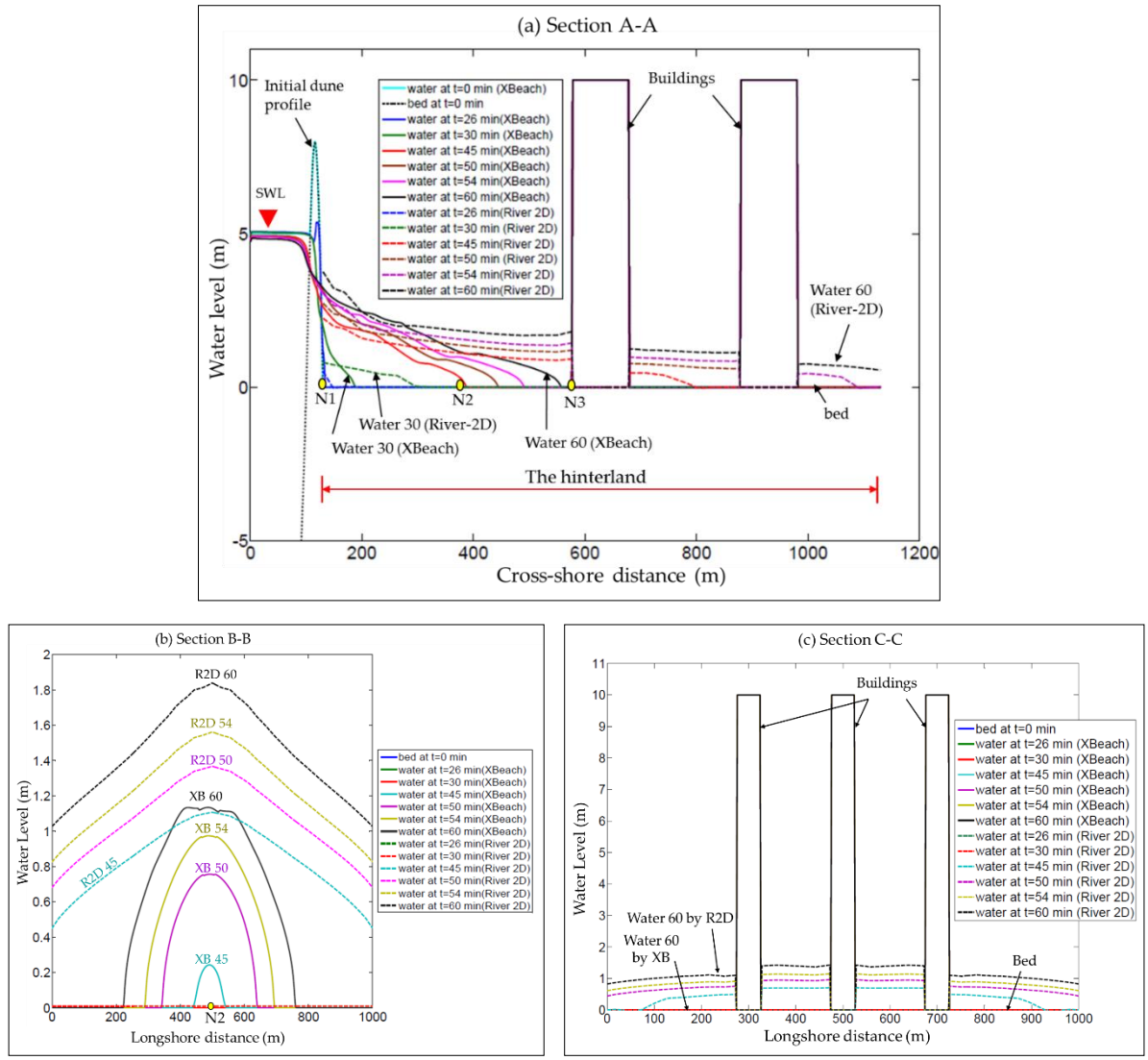

Fig 5. 15: Comparison of the temporal evolutions of water depths by XBeach and River-2D at t = 26, 30, 45, 50, 54 and 60 minutes at (a) Sec A-A, (b) Sec B-B and (c) Sec C-C, showing higher predictions of water depths and flood extent by River-2D at all sections.

The higher values for the flood extent and depths by River-2D results in lower values for the flow velocity from River-2D as compared to XBeach. For instance, Fig 5.16 shows a comparison of the flow velocities at the reference points N1, N2 and N3, reveals lower estimates for the flow velocity from River-2D.

The modelling approaches, using two models separately (overtopping/breaching model for the inflow conditions and CFD model for the subsequent inundation), is not favoured for the following reasons: "manual" transfer of the inflow boundary conditions by considering only mass conservation and omitting momentum conservation, in addition to the non-consideration of the evolution of the inflow width in the common inundation models (see Fig 5.14). This generally results in higher estimates of the flood extent and depths and sometimes even in non-realistic water levels as shown in Fig 5.7 and 5.8, where the water levels at the hinterland inlet exceed the SWL. Therefore, a combined modelling of coastal barrier breaching and induced inundation using XBeach is preferred. For this purpose, a validation of XBeach is performed using the case study of the Het Zwin dam breach as in the following section.

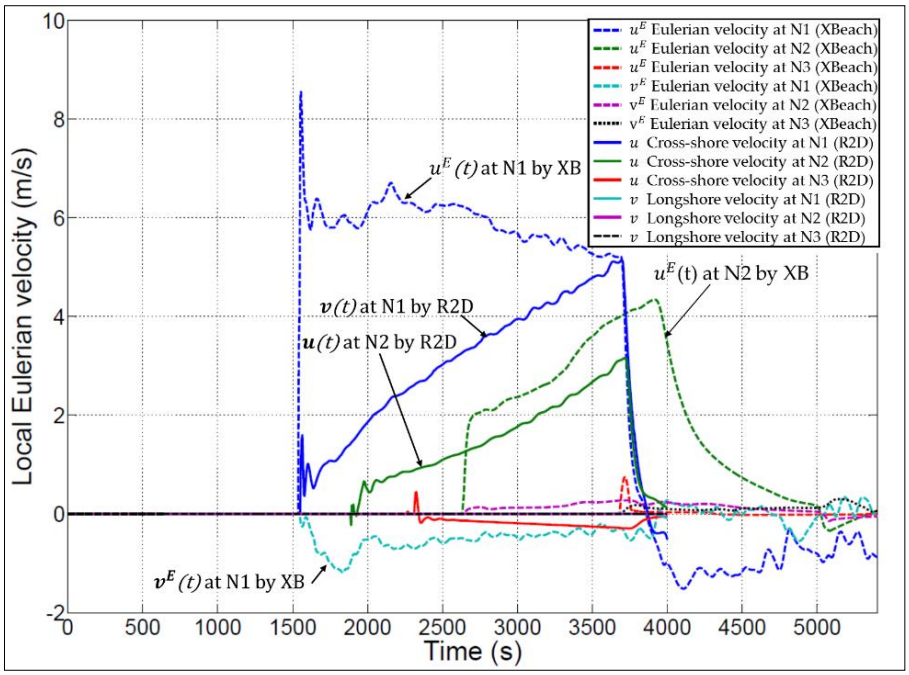

Fig 5. 16: Comparison of flow velocities obtained from XBeach and from River-2D at the reference points N1, N2 and N3 for load case LC1.

Remark 5.2: Summary of comparative analysis between 2D coupled and decoupled approaches

The comparative analysis of the water depths, velocities and flood extent in the hinterland due to barrier breaching as obtained from XBeach and those obtained by the benchmarking 2D inundation model River-2D have revealed the same limitations of the 1D uncoupled modelling of breaching and subsequent inundation (*Remark 5.1*) in addition to the following limitation:

(i) No account of the evolution of the inflow width in the common inundation models.

5.4 Validation of XBeach using the real dam breaching case of Het Zwin

5.4.1 Test programme and validation procedure

More details of the Het Zwin dam breaching case as shown in in Fig 5.17 and which was induced by overflow provided in section 4.3.2. During the field experiment for the breaching of the Het Zwin dam, the mean tidal range at Zwin was around 2.85 m. Therefore, the mean tidal prism of the Zwin was about 350,000 m^3. To ensure that the breach is initiated at a certain location, an initial breach was enforced in the middle of the dam (Sec X-X in Fig 5.17.a) having a depth of 0.8 m, a bed width of 1 m and side slopes of 1:1.6. The level of the surrounding seabed was about 0.7 m + NAP and the experiment was performed under calm conditions (i.e., no waves and no wind). Therefore, the water elevation was the main driver for the breaching process. As a result, the breach developed to a width of 41 m within one hour after the breach initiation. In addition to measuring the temporal evolution of the breach width, the water levels above the NAP and flow velocities were also measured during the experiment at both up- and downstream the dam using five measuring stations MS1 to MS5 (Fig 5.17.b).

Considering the model dimensions in Fig 5.17, the Zwin dam test was reproduced in XBeach by Roelvink et al. (2009), using a non-uniform grid with grid sizes gradually varying from 0.5 m near the breach to approximately 50 m far away from it. The median grain diameter D_{50} of the bed material was set to 0.3 mm in accordance with the prototype test conditions for the artificial dam. In order to achieve the same volume of the tidal prism, Roelvink et al. (2009) defined the volume of the tidal prism using a prismatic profile, so that the mean tidal prism remains the same (350,000 m^3).

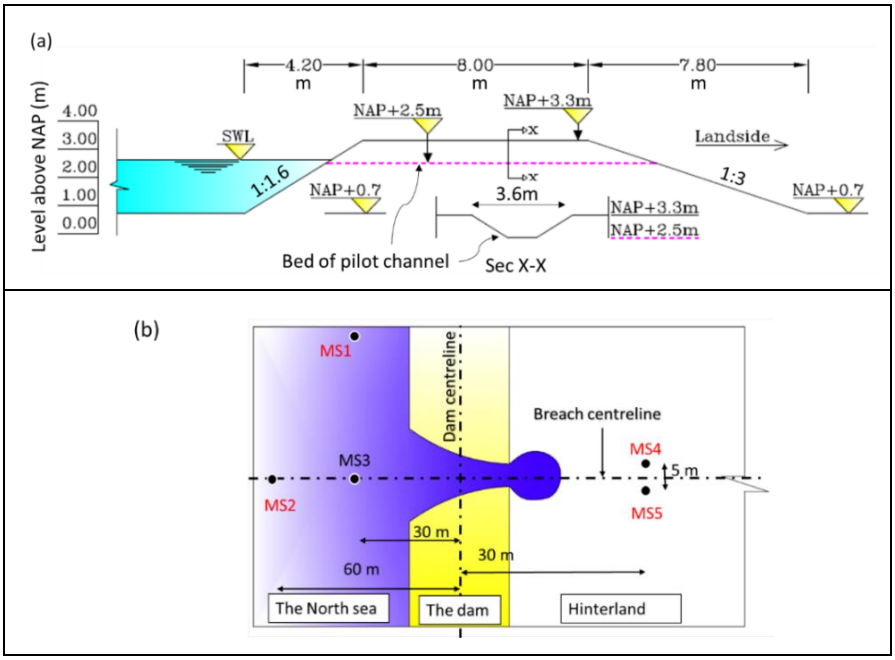

Fig 5. 17: Test case 3: The 1994 dam at Het Zwin: (a) dimensions of the dam and the enforced pilot channel (sec X-X), (b) locations of the measuring stations, after Visser (1998).

Though the experiment was performed under calm conditions and though the tidal prism is replaced by an equivalent prism, this experiment is still appropriate to validate the application of XBeach for the proposed combined modelling of breaching and the induced flood propagation based on:

(i) The comparison between the observed and calculated breach widths to assess the capability of XBeach as a breaching model.

(ii) The comparison between the observed and modelled water depths and flow velocities at the measuring stations MS4 and MS5 (located behind the dam) to show that XBeach can correctly predict the water depths and flow velocities in the hinterland.

(iii) The comparison between the volume of the tidal prism and the total inflow discharge to prove that XBeach can calculate the flood extent correctly.

The breaching model of Roelvink et al. (2009) is run again using the default setting in addition to the model settings in Table 5.3, which represent the difference between this simulation and Roelvink's simulation. The validation results are presented in section 5.4.2.

Table 5. 3: Main parameters used XBeach for the analysis of the breaching of the Het Zwin dam and the induced flooding

Parameter	Value	Meaning	Note
facpi	1.3	Grain-stabilization effect is considered by increasing the critical stirring velocity by 30%	See chapter 4 and/or Elsayed and Oumeraci (2017a)
form	2	Sediment transport is calculated according to the Van Rijn (2007a; b)-Van Thiel de Vries (2009)	See Roelvink et al. (2015)

5.4.2 Validation results

The real overflow-induced breaching case of the 1994 artificial dam at Het Zwin (Fig 5.17) was reproduced in XBeach by Roelvink et al. (2009). In this study, Roelvink's breach simulation model is run again considering the model settings in Table 5.3. The measured SWL at the measuring station MS2 (Fig 5.17.b) is assigned to the model as the seaward hydraulic load, and no wave action is considered. The dam breach results are presented in sections 5.4.2.1 while section 5.4.2.2 presents a comparison of the observed and modelled water depths and flow velocities at the measuring stations in Fig 5.17.b. Section 4.3.3 provides the calculations of the inland discharge as well as a comparison of the total inland volume and the mean tidal prism at Het Zwin.

5.4.2.1 *Reproduction of the Zwin dam breach by XBeach*

The dam breach case at Het Zwin is a field breaching test induced by overflow; i.e. the breach development is only induced by a landward erosion of the dam. Figs 5.18.a and 5.18.b present the breach development in cross-shore and longshore directions, respectively. Moreover, Fig 5.18.c presents a comparison of the observed and simulated breach widths.

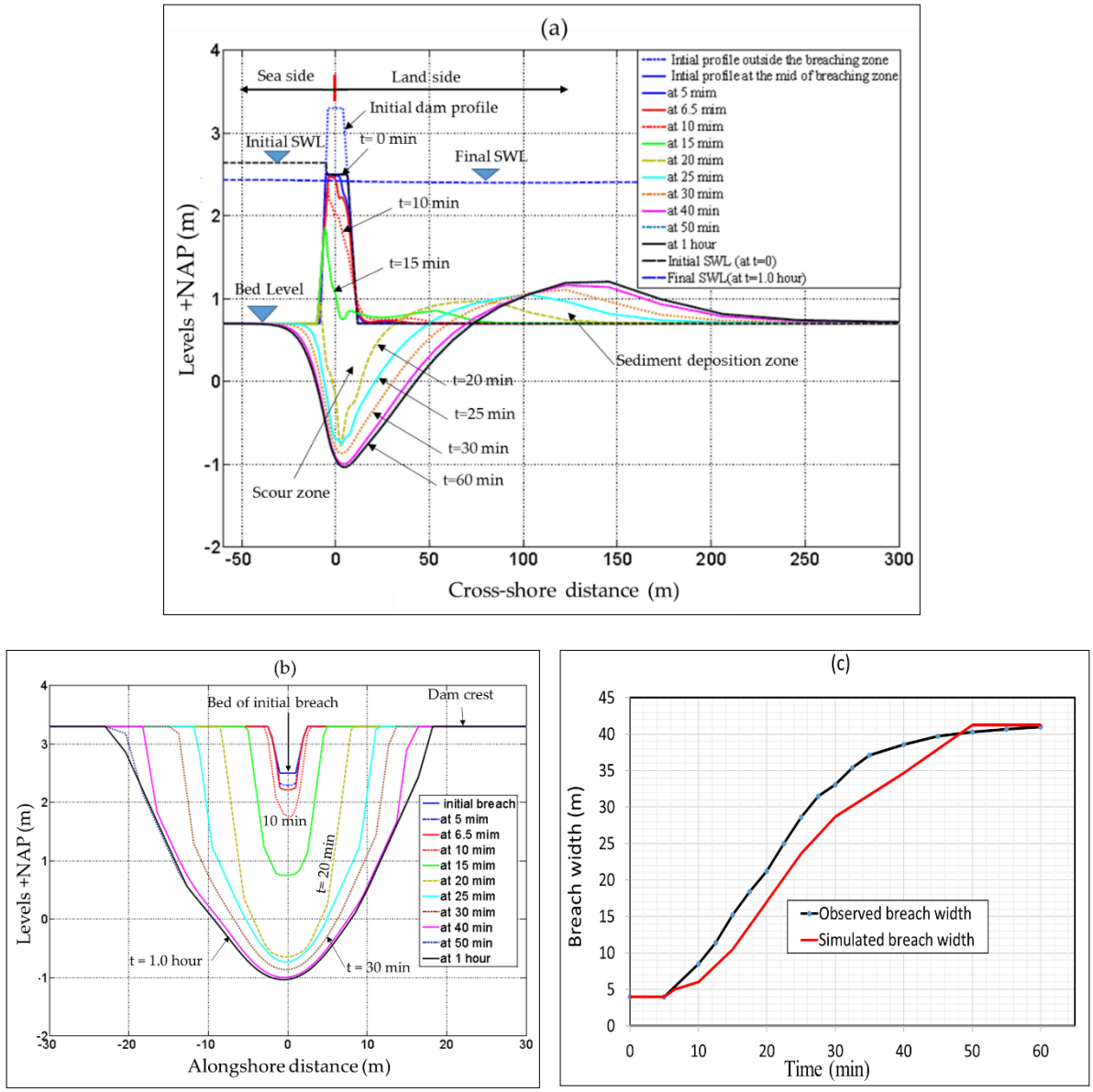

Fig 5. 18: Reproduction of Het Zwin breach by XBeach: (a) breach development in cross-shore direction, (b) breach development in longshore direction and (c) simulated vs observed breach width evolution.

Due to the overflow, the landward side of the dam erodes, causing a crest lowering at the breach location as well as an avalanching of the lateral sides of the breach. With the time marching, the dam body at the breach location is totally overwashed. The overwash phase is followed by scouring at the breach location and sediment deposition behind the dam (Fig 5.18.a). The avalanching algorithm in XBeach enables simulating the lateral development of the breach induced channel (Fig 5.18.b). The breach process extent until filling the tidal prism (i.e. until the water levels in front and behind the dam become equal). The high correlation, as well as the relatively low root, mean square error RMSE between the observed and simulated breach widths demonstrates the capability of XBeach as a breaching model ($R^2 = 0.98$ and RMSE = 2.73 m). A comparison of these statistical indicators with the

calculated by Roelvink et al. (2009) is presented in chapter 3 (Table 4.2) and Elsayed and Oumeraci (2017a).

5.4.2.2 *Observed vs computed water depths and flow velocities at Het Zwin dam breach*

The comparison of the observed and simulated water depths and flow velocities at different points indicated in Fig 5.17.b are shown in Fig 5.19.

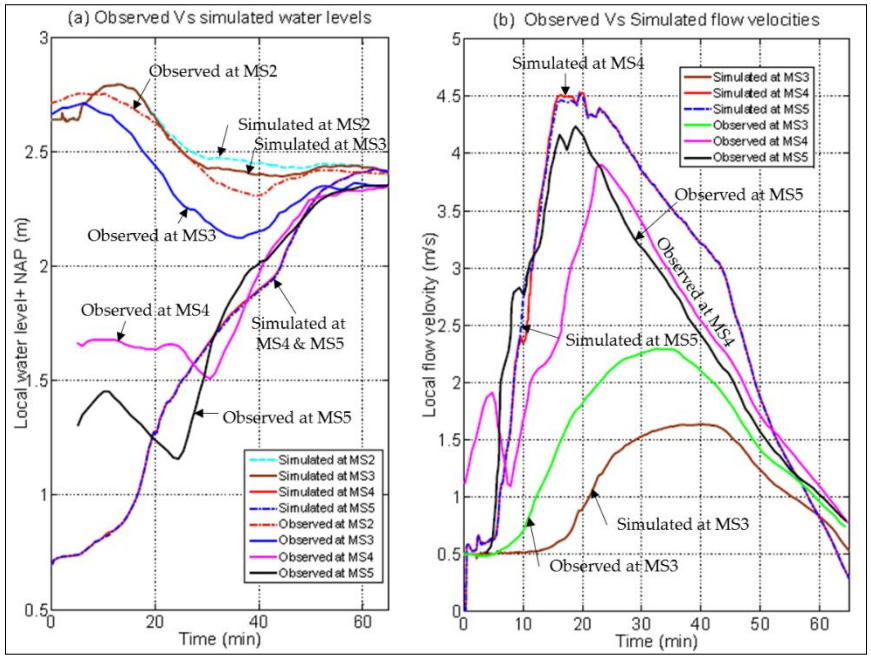

Fig 5. 19: Observed vs computed (XBeach) water depths and flow velocities at different measuring stations in Fig 5.17.b.

At t = 0 (time of pilot channel enforcement), about 10 min prior to maximum water level, the water level at the seaside was 2.72 m + NAP (see observed water level at MS2). At t = 10 min, a water level of 2.75 m + NAP is reached. For the remainder of the test, which has a total duration of 1.0 hour, the water level decreases to 2.4 m + NAP. After 1.0 hour, the water level behind the breach equals the sea level and the breach stops growing. Because of the water flow in the landside, the water level at MS4 and MS5 increases dramatically until reaching the sea level and the flow velocity at these points increases until reaching the peak velocity after 20 min, then both decrease because the breaching process becoming increasingly slower until it stops. The comparison between the observed and simulated flow velocities and water depths in Fig 5.19 illustrates the relatively good prediction capability of XBeach. The peak flow velocities at MS4 and MS5 are overestimated by 6 to 15 % while it is underestimation by ca. 30% at station MS3. The latter deviations from the observed values could be attributed to the difference between the observed and simulated breach dimensions. In fact, this may be explained by the calculated narrower breach width at the start of the breach as shown in Fig 5.18.c, which results in a higher flow velocity through the breach and thus at the measuring stations MS4 and MS5. This justification is confirmed by the fact that the narrower breach width will allow less inland flow rates and therefore less simulated versus observed flow velocity at MS3. Nevertheless, these overall comparisons in Fig 5.19 still demonstrate the capability of XBeach to properly calculate the flow velocity and water depth at any local point in the hinterland. For future improvements, the prediction capability of the breach dimensions will definitely lead to a better prediction of the flow velocity and water depth in the hinterland.

5.4.2.3 *Water discharge through the dam breach*

The 2DH model of the Zwin dam was discretized into 101 cross-shore stretches in the longshore direction (e.g. Fig 5.12). These stretches have variable widths that vary from 0.5 m at the breach location

to approximately 50 m far away from the breach (see e.g. Elsayed and Oumeraci (2016a). In order to calculate the total inland discharge through the breach-induced channel, the inland discharge should be calculated over the 101 cross-shore stretches using the same schematic approach in Fig 5.12. As a result, the water inflow discharge q_i is calculated for each of the 101 cross-shore stretches in Fig 5.20.a, which shows that the dam was overtopped at only five cross-shore stretches at the beginning of the simulation. With the time marching, many other stretches are also overtopped due the lateral growth of the breach. The summation of the inflow discharges q_i in Fig 5.20.a provides the total inflow hydrograph Q(t) as shown in Fig 5.20.b. Q(t) is zero at t = 0 (time of pilot channel enforcement) and increases to 161 m^3/s after 40 min and reduces again to zero because the water levels at the upstream and downstream dam sides become equal. The area under the water discharge curve in Fig 5.20.b represents the total volume of the inflow water (total volume = 308430 m^3). Such volume depends on the polder area of the tidal inlet as well as on the sea water level; i.e. with higher sea water levels, higher inflow volumes are expected. The latter volume is near to the value of the mean tidal prism (350000 m^3), thus indicating the XBeach capability to predict the flood extent properly. The difference between the total inland volume (308430 m^3) and the mean tidal prism (350000 m^3) can be attributed to the difference of the mean tidal level (2.85 m + NAP) to level 2.40 m + NAP at the end of the breaching process (see Fig 5.19.a). Such decrease in the sea water level decreases the capacity of the tidal inlet.

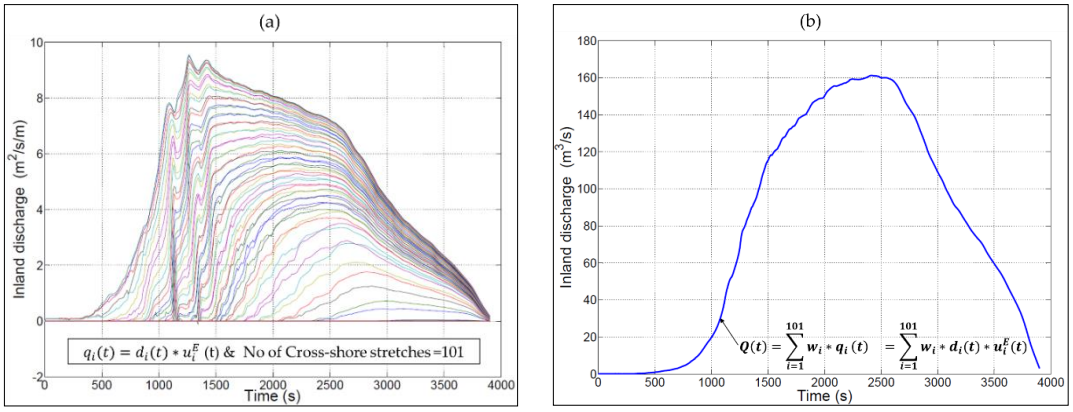

Fig 5. 20: Water discharge calculation through the Zwin dam breach (a) discharges qi over the 101 cross-shore stretches and (b) total inland discharge Q(t).

The comparison between the observed and the calculated (i) breach widths in Fig 5.18.c and (ii) water depths and flow velocities (Fig 5.19) as well as the comparison between the volume of the tidal prism and the calculated total inland discharge demonstrate the capability of XBeach to properly calculate the breach development together with the resulting water depths, flow velocities and flood extent in the hinterland. These results, therefore, support the suitability of applying XBeach for the combined modelling of barrier breaching and subsequent inundation.

Remark 5.3: Effect of breach growth on flood kinematics in the hinterland

The too slow reaction of the Zwin model at the beginning as shown in Fig 5.18.c means that there are some of the many user defined parameters of XBeach (e.g. the critical slopes for avalanching) that need to be calibrated in order to achieve better results at the beginning. The narrower breach dimensions at the beginning result in a higher flow velocity through the breach and thus at the measuring stations MS4 and MS5 in the hinterland. For the same reason, less inland flow rates and therefore less simulated versus observed flow velocity at MS3 are obtained. This indeed highlights the importance of the temporal development of the breach dimensions on the flood propagation in the hinterland.

5.5 Summary, discussion and implications of the results

In this chapter, diverse attempts have been presented to apply the hydro-morphodynamic model XBeach as an inundation model and a breaching model in combination rather than using two decoupled

models to simulate coastal barrier breaching and the induced flooding. The comparative analyses of (i) the results from the current modelling approach, applying separately an overtopping/breaching model to calculate the inflow hydrograph Q(t) and a common inundation NLSWEs-based model, such as HEC-RAS and River-2D, using Q(t) as inflow boundary condition at the barrier to simulate the flood propagation in the hinterland, and (ii) the results of XBeach applied to simulate together both breaching and subsequent inundation, have clearly demonstrated the advantages of the latter modelling approach. In fact, among the available open-source hydro-morphodynamic models, XBeach is the most appropriate tool for the latter approach. Indeed, in addition to solving numerically the same governing equations (NLSWEs) as the other common inundation models, XBeach has the following capabilities and advantages:

(i) XBeach can generate realistically the sea conditions through generating alongshore varying time series of wave energy (alongshore varying hydraulic loads), where the effect of waves is introduced as a source term in the NLSWEs;

(ii) the CFD module can simulate, in combination, wave overtopping and overflow processes, the flow through the developing breach, and the subsequent coastal inundation processes in a single simulation;

(iii) the morphodynamic module can properly calculate sediment transport and the resulting morphological changes and also includes a soil avalanching algorithm making XBeach capable to properly simulate the evolution of barrier breaching.

The comparative analysis of the water depths, velocities and flood extent in the hinterland due to barrier breaching as obtained from XBeach and those obtained by the two benchmarking 1D and 2D inundation models HEC-RAS and River-2D have revealed the following limitations of the uncoupled modelling of breaching and subsequent inundation:

(ii) The use of hydrograph Q(t) as inflow conditions to the common inundation models is in line with the mass conservation principle, but the flow velocity v(t) which cannot be accounted for in the inflow conditions is also crucial as it provides together with Q(t) the momentum;

(iii) Higher estimates for the flood extent and water depths, mainly because of lumping both the variation of water velocity and water depth through the breach(es) together in one information (hydrograph Q(t)) which lead to unfulfillment of the momentum conservation when transferring the flow from the breaching model to the inundation model (in some cases this may even lead to physically wrong water levels as shown in Figs 5.6 and 5.7);

(iv) No account of the evolution of the inflow width (see Fig 5.14) in the common inundation models.

These limitations are overcome by the combined modelling of breaching and subsequent inundation using XBeach, as demonstrated by the afore-described results of the dam breach case in the Het Zwin. In fact, the results have demonstrated a new promising application of XBeach and its potential for modelling together both dune breaching and subsequent flood propagation in coastal zones. As a CFD model using an NLSWEs solver coupled with a morphodynamic model, which includes a soil avalanching module, XBeach has the capability to integrally simulate coastal inundation induced by extreme storm surges with the advantage of reproducing the mutual interaction between hydrodynamics (e.g. flow in the breach channel) and morphodynamics, including soil avalanching (e.g. breach development). An attempt has been to demonstrate the advantage of this combined modelling approach using a single hydro-morphodynamic model (XBeach) instead of the current approach using two decoupled models. In fact, the proposed modelling approach using XBeach showed a good agreement between the flow velocities and water depths observed in the real case study of the Het Zwin (sand) dam breach. In contrast, the flood extent and flow depths predicted by the decoupled modelling approaches are up to 40% larger than the observed values.

Moreover, the outcomes of this chapter have demonstrated that dune breach initiation is not only a function of the longshore variability of the dune topography (e.g. crest level) but also a function of

the longitudinal variability of the hydraulic load as a result of wave transformation due to the longshore variability of the foreshore morphology mutually interacting with the waves (see Fig 5.11). This might explain why many breaches developed where they were not expected. By adding the residual resistance of the dune material (Elsayed and Oumeraci 2017a; Morris 2011; Özer et al. 2016) to these triggering factors of breach initiation, the prediction of the breaching process becomes much more complex. In fact, the longshore variability of the resistance of the dune material may be caused by the presence of weak spots (e.g. bioturbation) or zones of less interlocked sediments and less consolidated soils (see Fig 2.20). The latter type of longshore variability is not implemented in the proposed model. Thus, it will remain, besides the longshore variability of the hydraulic loads, one of the biggest research challenge. Nevertheless, it can be drawn that dune breach initiation is a function of:

(i) the longshore variability of the dune topography (e.g. crest level),
(ii) the longitudinal variability of the hydraulic load (e.g. wave focusing) and
(iii) the longshore variability of the residual resistance of the dune (e.g. weak spots due to bioturbation or low soil consolidation).

The latter two triggering factors are highly uncertain and may thus decrease the predictability of the potential breach locations. Fig 5.21 illustrates how these triggering factors affect breach initiation. Moreover, it also indicates that the highest uncertainties are expected for the case where the hydraulic load, the topography and the resistance of the dune all together are varying alongshore. In fact, XBeach does not yet account for the spatial variability of the residual resistance of dunes, so that this might represent a candidate topic for further development of XBeach.

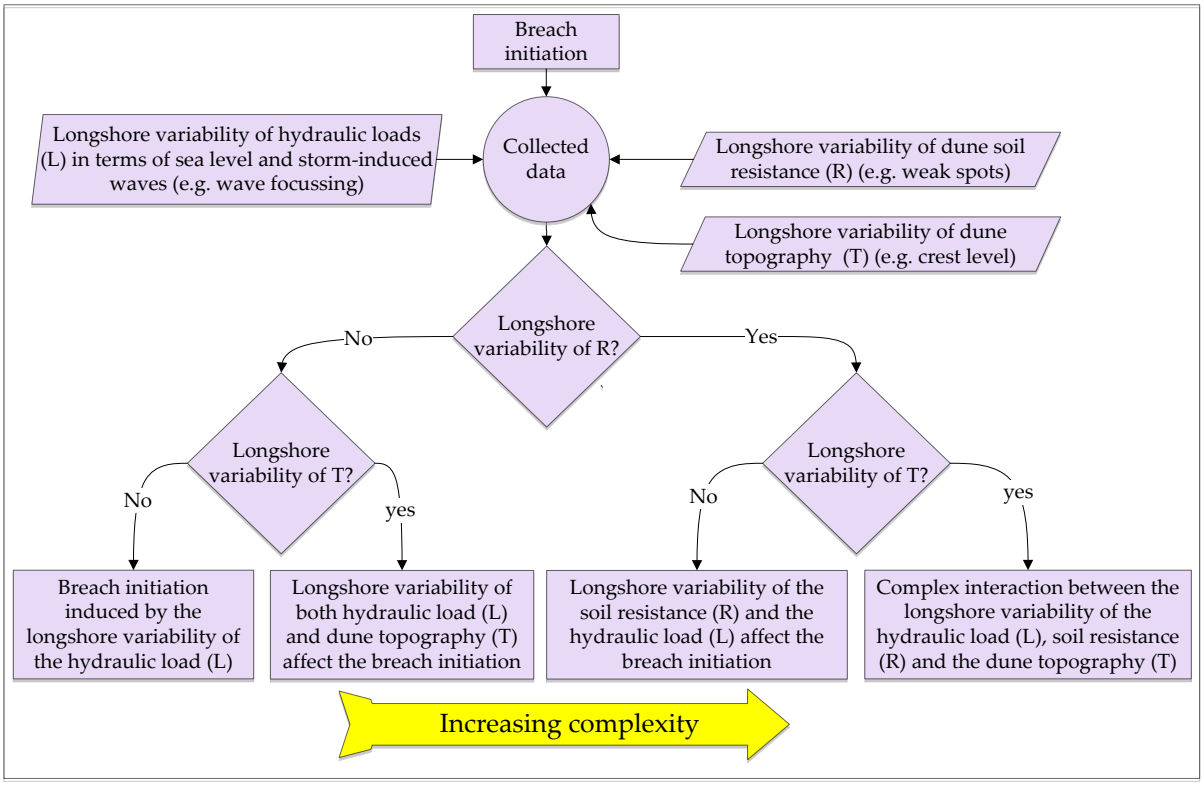

Fig 5. 21: Triggering factors associated with longshore variability for breach initiation along a dune.

It is common in urban flood studies to utilise methods by which the residential areas within the flood-prone zone is set at a very high roughness value in an attempt to account for the influence of obstacles to the flow such as buildings and fences (Van Drie et al. 2008). This issue has also been briefly discussed in this chapter. Thus, two possibilities might be considered in the inundation modelling with XBeach: setting very high roughness values or defining higher ground elevations at the obstacle locations. In this chapter, the latter option is applied; the higher ground elevations at the obstacle locations are specified to be hard and impermeable in order to avoid any erosion and/or avalanching.

However, in the River-2D model, the buildings are treated as impervious internal boundaries. Such internal boundaries facilitate the treatment of complex building geometries, which are difficult to be treated in XBeach as it uses a structured grid form of quadrilateral cells. The latter grid type might not be flexible enough to represent complex building geometries. For further development of XBeach, it is suggested to examine an unstructured grid option in order to avoid very fine grids.

6 Implications of coastal floods for groundwater contamination: Modelling scenarios and mitigation measures

In regions of limited surface water availability, groundwater resources are extremely important since they are often intensively used for drinking, domestic, irrigation or industrial purposes (Abdullah 2017; Barlow and Reichard 2010). Irrigational demands from aquifers, in general, account for ca. 70 % of the world's freshwater usage (Narayan et al. 2007; Siebert et al. 2010; Walther et al. 2014). Most of these demands are withdrawn from coastal aquifers due to the fact that more than 60% of the world's population lives within 100 km of coastlines (Neumann et al. 2015; Yang et al. 2013). The latter might explain why coastal aquifers have a special weightiness as freshwater sources, especially with the really limited surface water availability in coastal zones (Oude Essink 2001). Demographic studies suggest that the latter percentage (i.e. the 60%) will increase to 75% by 2020 (Kalaoun et al. 2016), which might lead to an overexploitation of the freshwater aquifers. Besides the latter effect on aquifers in coastal areas as well as in atoll islands, extreme storm surges and tropical storms are among the main indirect threats since any subsequent coastal flood might be a real source of coastal aquifers contamination (see e.g. Holding and Allen 2015; Williams 2010; Yang et al. 2013, 2015a; b). Therefore, coastal barriers such as dunes, dykes and other engineered structures are often required. However, during extreme storm surges, overtopping waves and/or floods resulting from breaching of coastal barriers may still be a threat, as they can induce, in addition to direct damages, long-term damages and losses (see, e.g., Steyer et al. 2007; Villholth and Neupane 2011; Williams 2010). The most important long-term effect of coastal floods is salt water intrusion (SWI) into coastal aquifers induced by the vertical infiltration of the salt water behind overtopped/breached coastal barriers, thus resulting in salty groundwater. In fact, saltwater inundation during extreme events has a substantial impact on the dynamics of the coastal aquifers as well as on the salinity distribution in such aquifers (Violette et al. 2009; Werner et al. 2013; Yang et al. 2013, 2015a; b). Even a moderate storm surge event may significantly affect the usability of coastal aquifers (Holding and Allen 2015; Wilson et al. 2011). Therefore, it is important to understand the effects of storm surges and the induced hinterland inundation on ensuring high water quality from coastal aquifer. Currently, only very few research studies are available to assess the effect of storm surges on groundwater systems. Nevertheless, and as aforementioned in sections 2.7 and 2.8.1, the recent studies (e.g. Yang et al. 2013, 2015a; b; Yu et al. 2016b) lacks a proper breaching/overtopping model to estimate inland discharges during extreme events, which might result in incorrect estimates of the contamination extent and accordingly incorrect estimates of the elapsed time for the natural remediation to reach again the pre-flooding conditions. In addition, these studies are limited to the determination of the time interval for the natural remediation process (NRP) of coastal aquifers after a SWI event, which is significantly slow, taking from 3 to 20 years according to Violette et al. (2009) and Yang et al. (2013). Even in the recent studies, no structural mitigation measures are proposed to shorten such long remediation intervals.

In chapter 5, the XBeach model is successfully applied to integrally simulate the mutual interaction between storm-induced barrier breaching/overtopping and the subsequent surface propagation of the flooding water, while omitting the subsurface flow (i.e. the infiltration process) and the accompanied salinity increase of the originally fresh aquifers. This chapter[†††], however, is directed toward considering the subsurface flow and toward studying the possibility of coupling the three processes (i.e. breaching, surface runoff, subsurface flow). Moreover, an attempt is made to examine suitable structural mitigation measures to shorten the long remediation intervals after a storm-driven saltwater

[†††] More detail of this chapter can be found in the progress report:
Elsayed, S. M.; Oumeraci, H. (2017): Breaching of coastal barriers under extreme storm surges and implications for groundwater contamination: *Implications of coastal floods for groundwater contamination*. Internal Report no 1075/17, Leichtweiß-Institut for Hydraulic Engineering and Water Resources, TU Braunschweig, Braunschweig, Germany, 101 p.
Freely available at:
https://www.researchgate.net/publication/316459814_Implications_of_coastal_floods_for_groundwater_contamination
Moreover, the outcomes of this chapter are part of a submitted paper:
Elsayed, S.M.; Oumeraci, H. (2017): Modelling and management of storm-driven saltwater intrusion in freshwater aquifers: The case of near Bremerhaven, Germany. Submitted for publication in the INECEP summer school book, published by Cuvillier Verlag Publisher, Germany.

intrusion (SDSWI) event. Therefore, the main goal of this chapter is to address the third research question of this PhD study (see section 2.8.1) which is repeated as follows

- *Is the XBeach model capable of simulating, in addition to breaching and flood propagation, the SWI process by utilising its groundwater module?*
- *And if it is not the case, what are the alternative approaches to properly simulate a coastal barrier breaching, the induced flooding and the subsequent SWI?*
- *In addition, what are the most suitable structural mitigation measures to shorten the long natural remediation intervals after SDSWI events, which are reported in many studies (e.g. Yang et al. 2013, 2015a; b)?*

In order to clearly answer these questions, the following specific issues will be addressed in the following sections.

- The physical processes, as well as the governing equations of SDSWI will be summarised and compared to the governing equations of the groundwater module of XBeach.
- The modelling approaches for SDSWI events in previous studies (e.g. Yang et al., 2015a, 2015b, 2013) will be analysed. As a result, a proper modelling approach can be proposed.
- Possible structural mitigation measures to shorten long remediation intervals of contaminated aquifers after coastal flood events will be proposed in order to evaluate the most proper one in chapter 7 based on available data for a pilot site near Bremerhaven, northern Germany.

6.1 Modelling of water flow and contaminant transport in porous media

Saline water is water that contains a significant concentration of dissolved salts (mainly sodium chloride NaCl) and is commonly known as salt water. Salinity is an important factor that affects the usability of waters due to its influence on many aspects associated with the chemical and biological processes in natural waters (Bear and Cheng 2010; Cheng and Ouazar 2016; Kresic 2006). Seawater typically has a salinity of around 35‰ (35000 mg/l), although lower values are typical near coasts where rivers pour fresh water off the sea/ocean (around 25‰ according to Yang et al. 2013). Therefore, saline water cannot be used for drinking, irrigation and industrial purposes. In fact, the guidelines of the World Health Organization (WHO) for drinking-water quality (WHO 2011) and the European water framework directive (Kaika 2003) consider water as usable for the latter purposes if the salt concentration is less than 0.5‰ (500 mg /l).

Freshwater in aquifers, in general, are formed by rainwater percolation into the substrate and/or by seepage (conductance) from freshwater bodies. Therefore, the natural input to groundwater is conductance from surface water, which is known by recharge, while the natural outputs from groundwater are natural springs and seepage to streams (e.g. seas) in the form of a seaward directed flow (also known as submarine fresh groundwater discharge SFGD). The latter flow represents a natural remediation of coastal aquifers (Chui and Terry 2012; Narayan et al. 2007; Post et al. 2013) as it continuously dilutes contaminants (e.g. salt) and transports them seaward as shown in Fig 6.1. Nevertheless, such a natural remediation process (NRP) of contaminated aquifers may take many years after an SDSWI event before reusing the aquifers for subsistence purposes (Chang and Clement 2013; Elsayed and Oumeraci 2017b; Illangasekare et al. 2006; Yang et al. 2013, 2015a; b).

In fact, the intrusion of seawater into aquifers is a complex hydrodynamic process associated with the motion of fresh and salt waters with different properties. Moreover, aquifers under SDSWI events represent very complex and highly dynamic hydrological systems with diverse interacting physical processes: (i) variability of saturated flow above and beneath the phreatic line, (ii) spatiotemporal variations of fluid density; the polluted water (sea water) being denser than the ambient groundwater, thus favouring the process of vertical percolation (driving mechanism for flow described by pressure gradients as well as by density gradients), (iii) tidal fluctuations in the nearshore zone (see e.g. Levanon et al. 2016; Li et al. 2004; Robinson et al. 2014), (iv) possible open wells that represent a very fast pathway for contamination of the subsurface due to their direct contact with groundwater and (v) surface runoff

of the overtopping/breaching-induced flooding. The latter process is often represented by the nonlinear shallow water equations (NLSWEs) while the first two processes (i) & (ii) depend on the degree of soil saturation as discussed in the following subsections.

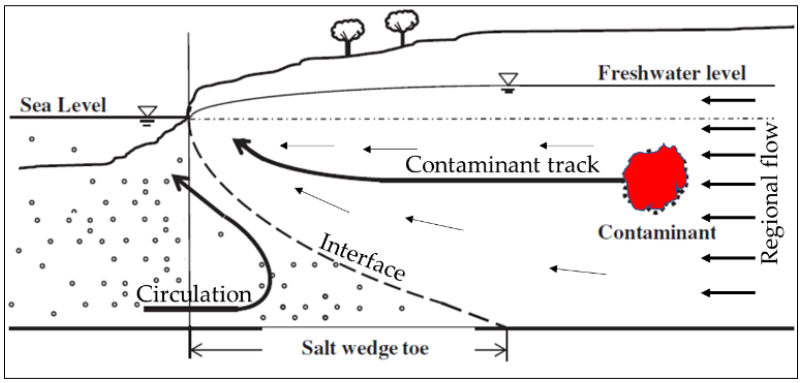

Fig 6. 1: Cross-shore conceptual model illustrating a contaminant transport process occurring in a coastal groundwater system due to seaward directed flow, after Chang and Clement (2013).

6.1.1 Flow in the unsaturated zone above the phreatic line

The unsaturated zone, also called “vadose zone” ("vadose": Latin for "shallow"), is the zone located between the land surface and the groundwater table (GWT). The pores in the vadose zone are filled with water and air, so that pore pressure (p_w) is equal to atmospheric pressure (p_a) at the GWT, while $p_w < p_a$ above the GWT and $p_w > p_a$ beneath the GWT (see Fig 6.2).

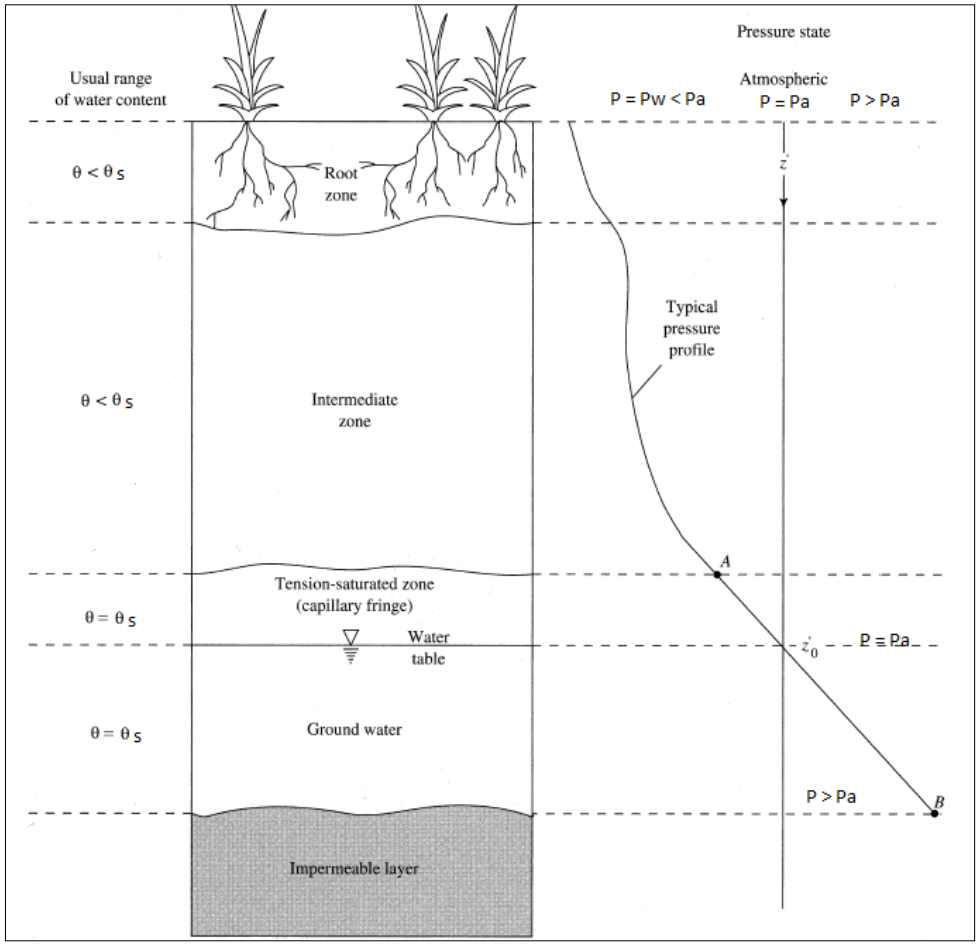

Fig 6. 2: Designation of hydrologic soil profile horizons. Note that this figure is idealised and that one or more of these horizons may be absent in a given situation (Dingman 2015).

The vadose zone plays an inextricable and crucial role in surface water infiltration, chemicals migration, soil moisture storage and the rate of groundwater recharge (Barbu and Ballestero 2015). For instance, with thicker vadose zones, a larger amount of salt water might be collected during coastal flooding events (Holding and Allen 2015). However, when the vadose zone has a low hydraulic conductivity, the migration of salt into the subsurface is slow and may limit the amount of salt water entering the system from inundation (Yang et al. 2015b). Though the pressure head is positive (> Pa) below the GWT and increases with depth as shown in Fig 6.2, the vadose zone is characterised by negative fluid pressure (suction) head, which is lower than the atmospheric pressure (Bear and Cheng 2010; Kresic 2006). Therefore, the flow in the unsaturated zone is governed by two main parameters, namely: (i) the change in the total potential hydraulic head $h(\vartheta)$ along the flow path (head (h), which is equal to the elevation of the water table measured from a reference datum, e.g. an assumed base of the aquifer or the mean sea level MSL) and (ii) the unsaturated hydraulic conductivity $K(\vartheta)$. However, both parameters depend on the volumetric water content θ in the porous medium; both change in time and space as the soil becomes more or less saturated in response to water input and output, e.g., due to infiltration and evapotranspiration (Therrien et al. 2010; Therrien and Sudicky 1996). The unsaturated hydraulic conductivity $K(\vartheta)$ is always lower than the saturated hydraulic conductivity K_s because of the presence of air in the voids, and it increases with saturation increase. Quantification of flow processes in the unsaturated zone is therefore more complex than in the saturated zone. In fact, it requires the determination of $h(\vartheta)$ and $K(\vartheta)$, which are constant in the saturated zone because the soil is saturated and the water content is constant over time at any specific location.

Water flow in variably saturated soils is traditionally described using the mass conservation equation of Richards (Richards 1931) as follows:

$$\frac{\partial \vartheta}{\partial t} = \frac{\partial}{\partial z}\left[D(\vartheta)\frac{\partial \vartheta}{\partial z} + K(\vartheta)\right] = \frac{\partial}{\partial z}\left[K(h)\left(\frac{\partial h}{\partial z} + 1\right)\right] \quad (6.1)$$

where $\partial\vartheta$ is the change in volumetric moisture content [-]; ∂t is the time interval for analysis [T]; ∂z is the space interval [L]; $K(\vartheta)$ or $K(h)$ is hydraulic conductivity [L/T] so that $D(\vartheta)$, the soil water diffusivity function [L^2/T], is defined as $D(\vartheta) = K(\vartheta).dh/d\vartheta$; h is the soil water pressure head or matric potential [L]. Eq 6.1 reflects the fact that the temporal change of the water content in a porous medium is a function of the unsaturated hydraulic conductivity $K(\vartheta)$ and matric potential $h(\vartheta)$. Therefore, functions for both parameters need to be first defined. In fact, these parameters are usually described using empirical relationships based on the residual water content ϑ_r and the saturated water content ϑ_s in which ϑ_r specifies the maximum amount of water in soil that will not contribute to liquid flow because of blockage from the flow paths or strong adsorption onto the solid phase. These empirical relationships are specific for each soil and highly nonlinear for a given soil.

Most of the hydrogeological codes for variably saturated flow (e.g. HydroGeoSphere, HYDRUS and SUTRA) solve a modified 3D form of Richards Equation (Botros et al. 2012; Therrien et al. 2010; Therrien and Sudicky 1996) that take the form:

$$\frac{\partial \vartheta}{\partial t} = \frac{\partial}{\partial x}\left[K(h)\frac{\partial h}{\partial x}\right] + \frac{\partial}{\partial y}\left[K(h)\frac{\partial h}{\partial y}\right] + \frac{\partial}{\partial z}\left[K(h)\left(\frac{\partial h}{\partial z} + 1\right)\right] + \sum \Gamma \pm Q \quad (6.2)$$

Where $\sum \Gamma$ represents the volumetric fluid recharge rate [$L^3\ L^{-3}\ T^{-1}$] and the volumetric fluid exchange between the porous medium and wells, if any. Therefore, the term $\sum \Gamma$ has a positive value in the case of feeding the porous medium. Q represents the fluid flux per unit volume from a source (positive) or a sink (negative) to the porous medium system and is specified from the boundary conditions [$L^3\ L^{-3}\ T^{-1}$].

6.1.2 Flow in the aquifer zone beneath the phreatic line

The flow in the saturated zone (aquifer zone) can be described by Richards equation considering the saturation condition under the phreatic line (section 6.1.1) or using a generalised 3D-form of Darcy law (Tek 1957), which is known as the groundwater flow equation through porous media (also known as equations of variable density flow in porous media):

$$\frac{\partial}{\partial x}\left(K_{sx}\frac{\partial h}{\partial x}\right)+\frac{\partial}{\partial y}\left(K_{sy}\frac{\partial h}{\partial y}\right)+\frac{\partial}{\partial z}\left(K_{sz}\frac{\partial h}{\partial z}\right)+\sum\Gamma\pm Q=S_s\frac{\partial h}{\partial t} \quad (6.3)$$

where K_{sx}, K_{sy} and K_{sz} are values of hydraulic conductivity at saturation along the x, y, and z coordinate axes, which are assumed to be parallel to the major axes of hydraulic conductivity $[LT^{-1}]$. The hydraulic conductivity ($K_s = p.g\rho/\mu$) depends on soil properties (e.g. permeability p $[L^2]$) and fluid properties (e.g. density ρ $[M/L^3]$ and absolute (dynamic) viscosity μ $[L^2/s]$). h in Eq 6.3 is the hydraulic head $[L]$ measured from reference datum (mainly the MSL), S_s is the specific storage of the porous material $[L^{-1}]$ that represents the change in aquifer storage in the form of the volume of water released from storage per unit change in head (h) per unit volume of aquifer. Eq 6.3 describes groundwater flow under non-equilibrium (transient) conditions in a heterogeneous and anisotropic medium. Therefore, it is the main governing equation in many numerical codes for modelling groundwater flow (e.g. Modflow, Visual Modflow and Feeflow).

6.1.3 Contaminant transport in porous media

Contaminant transport in a variably saturated groundwater system can be simulated using mass conservation equations for the contaminant substance known as the advection-dispersion equations of contaminant transport. Such equations take the following general form in three dimensions:

$$\vartheta\frac{\partial C}{\partial t}=\underbrace{-\frac{\partial(v_i C)}{\partial x_i}}_{\text{Advection term}}+\underbrace{\frac{\partial}{\partial x_i}\left(\vartheta.D_{ij}.\frac{\partial C}{\partial x_j}\right)}_{\text{Dispersion term}}+\underbrace{R_c}_{\text{Source/sink term}} \quad \text{with i, j = 1, 2, 3} \quad (6.4)$$

Where C is the dissolved concentration of the solute $[ML^{-3}]$; x_i is the distance along the respective Cartesian coordinate axis $[L]$; v_i is the seepage or linear pore water velocity $[L/T]$; D_{ij} is the dispersion coefficient tensor $[L^2/T]$; R_c is sources or sinks term $[ML^{-3}T^{-1}]$. The hydrodynamic dispersion coefficient D_{ij} tensor, which describes the combined effect of mechanical dispersion and molecular diffusion, is given by Scheidegger (1960) as follows

$$D_{ij}=\underbrace{\frac{(D_L-D_T)v_i v_j}{v}+D_T v\delta_{ij}}_{\text{Mechanical dispersion}}+\underbrace{D}_{\text{Molecular diffusion}} \quad (6.5)$$

Where D_L and D_T are longitudinal and transverse dispersivities, respectively; v is the magnitude of pore water velocity; δ_{ij} is the Kronecker delta (δ_{ij}= 1 if i = j, and δ_ij = 0 otherwise) and D is molecular diffusion. Knowledge of water content ϑ and water flux density v_i in Eq 6.4 is obtained from solutions of Richards equations (Eq 6.2) in the unsaturated zone or Darcy equations (Eq 6.3) in the saturated zone. Therefore, contaminant transport cannot be solved without solving first the groundwater flow field of the system under study.

The advection term in Eq (6.4) is responsible for translating the solute field by moving the solute with the flow velocity without changing the shape of the contaminant plume at all. The dispersion term describes the combined effect of mechanical dispersion and molecular diffusion as defined by Eq 6.5 (Abd-Elhamid 2010; Botros et al. 2012). The molecular diffusion describes the spreading of a solute plume through the spread of particles in random motion from regions of higher concentration to regions of lower concentration. However, mechanical dispersion reflects the fact that not everything in the porous medium moves at the average water flow speed; some paths are faster, some slower, some longer, some shorter, which results in a net spreading of the solute plume that looks very much like a diffusive behaviour (Scheidegger 1960).

Based on the advection-dispersion equation (Eq 6.4), the modelling tools of SWI can be divided into two categories (Kalaoun et al. 2016; Kourakos and Mantoglou 2015):

(i) *Sharp-interface models*: assume that seawater and fresh water are separated without mixing (e.g. Sharp of Essaid 1990). Thus, sharp interface models consider only advective transport processes whilst dispersion is neglected, and

(ii) *Variable-density models*: take into consideration the existence of a mixing zone between seawater and freshwater and therefore they require aquifer parameters that are difficult to estimate such as dispersivity.

Though the sharp interface models do not account for hydrodynamic dispersion, they allow the development of solutions that are useful for understanding SWI and for solving real-world problems (Gaaloul et al. 2012). However, it is well known that instead of sharp interface between freshwater and saltwater there is a transition zone since both fluids are miscible. Even if salt water is a conservative and nonreactive solute and SWI represents a stable configuration of density-driven flow and solute transport, modelling such phenomenon remains a challenge due to diverse difficulties (e.g. handling large-scale models with sufficiently high resolution, accounting for heterogeneity of hydraulic parameters and estimating effective hydraulic parameters).

Remark 6.1: Is XBeach capable of simulating saltwater (SWI) by using its groundwater flow module?

Though XBeach, which simulate both breaching and subsequent inundation, has a groundwater flow module solving the 3D Darcy equation (Eq 6.3) like the USGS Modflow groundwater model (see e.g. McCall 2015), it cannot yet simulate contaminant transport because it does not yet include the advection-dispersion equations (Eq. 6.4). The latter might represent a candidate topic for further development of XBeach so that it will be able to simulate coastal barrier breaching, induced inundation, groundwater flow and subsequent SWI in a single model. Meanwhile, it is necessary to look for alternative approaches to properly simulate all these processes in an integral manner. For the latter purpose, available groundwater flow and SWI intrusion models are examined in section 6.2. Thereby, in section 6.3, a brief overview of the applications of such models to simulate previous storm-driven saltwater intrusion (SDSWI) events is introduced. As a result, possible coupling approaches between XBeach and a suitable intrusion model are discussed in section 6.4.

6.2 Brief overview of groundwater models for contaminant transport

Contaminant transport models, including the SWI models, can be categorised into three broad categories: physical, analytical and numerical. Of these three model categories, numerical models are by far the most commonly used (Kumar 2016). Physical models consist of miniature physical analogy of the geology and/or hydrology of the situation under study. Similarity laws are applied to satisfy miniature analogy for both dimensions and loads, groundwater heads and flows being measured directly (Anderson et al. 2015). Analytical models involve solving equations where a definite closed answer is reached at the end of the calculations, offering a very simplified version of the real problem and facilitating significantly the computations. For instance, Ghyben-Herzberg principle (Herzberg 1901) is a typical simplified analytical model that states that seawater can penetrate far into freshwater aquifers and the occurrence depth of salt–fresh water interface is around 40 times greater than the freshwater level in an unconfined aquifer.

Numerical groundwater models describe the groundwater flow and transport processes using the aforementioned mathematical equations (section 6.1) that are solved using suitable numerical techniques and based on certain simplifying assumptions. These assumptions typically involve the direction of flow, the geometry of the aquifer, the heterogeneity or anisotropy of soil or bedrock within the aquifer as well as the contaminant transport mechanisms. Because of the simplifying assumptions embedded in the mathematical equations and the many uncertainties in the values of data required by the model, a model must be viewed as an approximation and not as an exact duplication of field conditions. Groundwater models, however, even as approximations, are useful for several applications. The applicability or usefulness of a model depends on how closely the mathematical equations approximate the physical system being modelled.

For groundwater development variations, protection and remediation, the available predictive numerical models might be divided into two main categories (Fig 6.3):

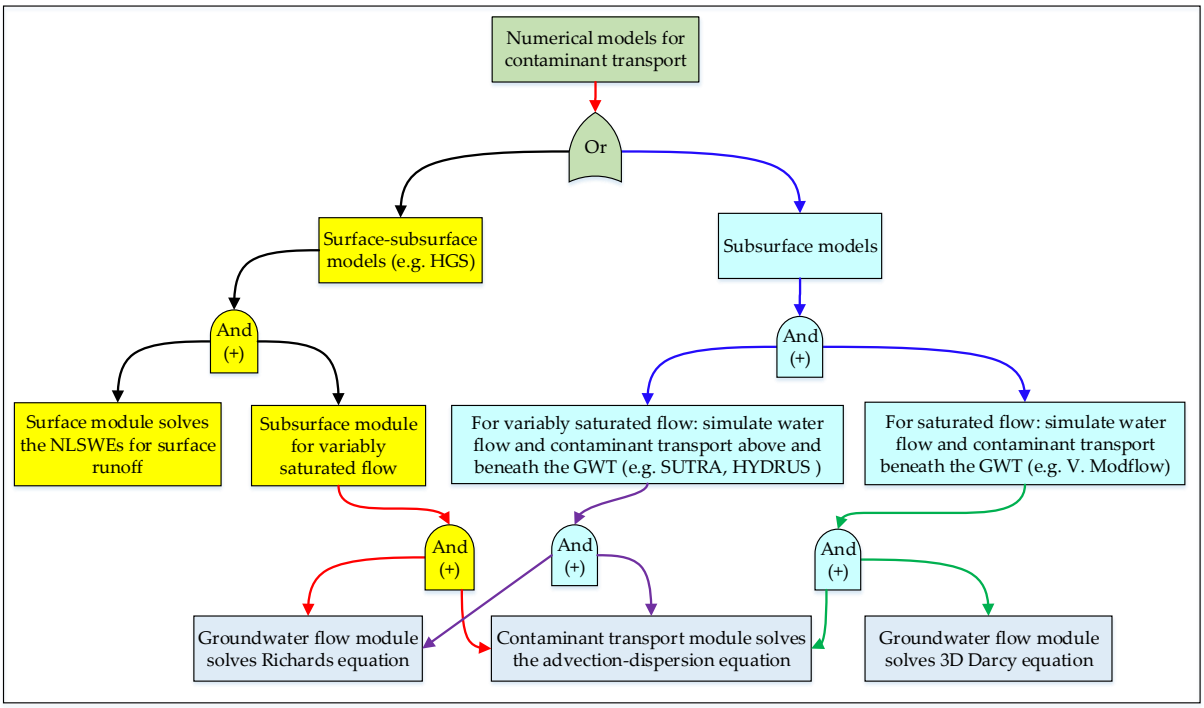

Fig 6. 3: Classifications of numerical models for contaminant transport in porous media.

(i) *Surface-subsurface models* (see e.g. Brunner and Simmons 2012; Furman 2008; Maxwell et al. 2014; Tian et al. 2016; Yu et al. 2016): such models (e.g. HGS) are capable to integrally simulate the whole hydrogeological cycle in both surface and subsurface domains. The surface domain includes processes like surface runoff and wave propagation while the subsurface domain includes infiltration, groundwater flow and contaminants transport.

(ii) *Subsurface models* that simulate only groundwater flow and the induced contaminant transport (e.g. Modflow and Visual Modflow).

In the surface-subsurface models, the surface module is mainly based on solving the NLSWEs. For these particular models, the NLSWEs include an infiltration/exfiltration term in the continuity equation to calculate the conductance rate to the subsurface domain. The latter rate acts as a source term in Richards equation (Eq. 6.2) for the subsurface calculations, which also includes the advection-dispersion equation (Eq. 6.4) to calculate the induced contaminant transport.

The subsurface models, which are the most popular, include two main modules:

(i) *Module for groundwater flow*: solves Eq 6.2 or 6.3 in order to obtain the water content ϑ and flow velocities v_i and

(ii) *Module for contaminant transport*: solves Eq 6.4 using the previous two outcomes from the former module.

Several subsurface flow models (e.g. Modflow and SUTRA) have been developed by the United States Geological Survey (USGS). For instance, Modflow, a finite difference model, is the most widely used, tested and verified code. It has become the industry standard given its versatility and open structure: independent subroutines called ''modules'' are grouped into ''packages'', which simulate specific hydrologic features (Kresic 2006; Kumar 2006). For these reasons, Modflow has also been chosen as a standard code for explaining modelling principles and for solving numerical modelling problems in many textbooks (e.g. Kresic, 2006). Therefore, many graphical user interface (GUI) versions of Modflow have been produced by other institutions. For example, Waterloo Hydrologic Inc. (Waterloo, ON, Canada) has reproduced Modflow under a GUI with the name of Visual Modflow (Surinaidu et al. 2016; Waterloo Hydrogeologic 2015). The second most known model by USGS is SUTRA, which is a

finite element solver of the Richards equation. Therefore, SUTRA can simulate both unsaturated and saturated groundwater flow above and beneath the GWT, respectively. In addition, it can simulate contaminant transport in both latter subdomains with variable density flow. Many other widely used GUI models are commercially available; among them is HYDRUS (Šimůnek et al. 2016), Feeflow (Trefry and Muffels 2007) and Groundwater Modelling System (GMS), which is also a GUI version of the USGS Modflow. Open-source subsurface models are also existing, among them is OpenGeoSys (Kolditz et al. 2012).

The main limitation common to these subsurface codes, including Visual Modflow, is that none of them is capable to also simulate the surface domain (surface runoff of water during a flood event), where salt water is introduced to the hydrologic system. Moreover, most of these models do not account for unsaturated flow and thereby do not simulate the flow in the vadose zone as it is also the case in Visual Modflow. Therefore, surface-subsurface models (e.g. HGS of Therrien et al. 2010) are identified as the most suitable code to simulate the coupled processes because they are fully integrated surface and subsurface models capable of simulating density-dependent flow and solute transport (Holding and Allen 2015). Thus, the hydraulic coupling between the surface and the subsurface domains simplifies the flow and automatically transfer boundary conditions caused by storm surge events to the subsurface.

6.3 Brief review of storm-driven salt water intrusion modelling studies

The study of Kooi et al. (2000) seems to be the first numerical study related to SWI in coastal aquifers due to inundation induced by sea level rise (SLR). They found that a direct inundation of coastal areas owing to the expected SLR within the next 200 years would result in vertical seawater intrusion through a wide high-salinity transition zone (Fig 6.4).

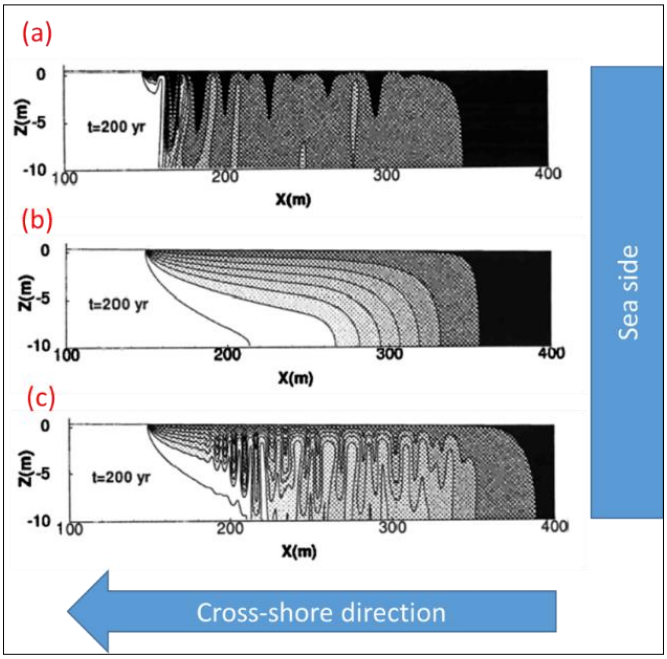

Fig 6. 4: Calculated salinity distribution after 200 years of an SLR scenario for (a) a sandy aquifer, (b) clayey aquifer and (c) clayey layer overlying a sandy aquifer; Salt mass fraction increases with the darkness of shading, after Kooi et al. (2000).

Percolation of salt water takes the form of fingers in the case of highly permeable soils (Fig 6.4.a) while it takes a diffusive form in lowly permeable soils (Fig 6.4.b). Mixable behaviour is determined when a layer of low-permeability soil overlaying a relatively high-permeability aquifer (Fig 6.4.c). Common to the latter three cases is that the underlying shallow groundwater is primarily and initially affected while deeper groundwater is affected later as plumes of infiltrated salt water spread and migrate downwards and laterally back to the sea.

While studying the consequences of an overwash process of a barrier island under a hurricane-driven storm surge event, Anderson (2002) noticed that inundation of barrier islands is a source of instantaneous SWI to the freshwater lenses in such islands that leads to higher water treatment costs. The recharge of the salty water increased salinity concentration from approximately 40 mg/l prior to flooding to nearly 280 mg/l within several weeks of flooding. Though the overwash event was in 1993, the salinity concentrations didn't reach again pre-flooding concentrations by January 1997 (i.e. four years after the inundation event).

After the 2004 tsunami in southern Asia, especially Sri Lanka and India, and Hurricanes Katrina and Rita on 2005, special attention is paid to SDSWI events. Hurricanes Katrina and Rita, for instance, pushed saltwater from the Gulf of Mexico inland into freshwater marsh communities in coastal Louisiana. Such event results in increasing the aquifers salinity in western and eastern coastal Louisiana (Van Biersel et al. 2007; Steyer et al. 2007). Williams (2010) reported that the preliminary estimates of the economic impact from hurricane Katrina to Louisiana agriculture, because of soil salinity increase, were calculated as well over $1 billion dollars. On the other hand, the 26 December 2004 aforementioned tsunami caused widespread destruction and contamination of coastal aquifers across southern Asia. Seawater filled domestic open dug wells and also entered the aquifers via direct infiltration during the first flooding waves and later as ponded seawater infiltrated through the permeable sands that are typical of coastal aquifers. It is estimated that over 40000 drinking water wells in Sri Lanka were either destroyed or contaminated (Illangasekare et al. 2006). Consequently, Illangasekare et al. (2006) determined three principal mechanisms of storm-driven salt water contamination: (i) infiltration of salt water through the vadose zone during inundation; (ii) ongoing infiltration of salt water from depressions that store ponded seawater (see e.g. Yu et al. 2016b) and (iii) transport of salt water through open boreholes and/or trenches, which provide direct access to the aquifer.

To provide a better understanding for the SDSWI through physical modelling, Illangasekare et al. (2006) injected the physical model in Fig 6.5 by salt water (dyed by red colour), where the pre-injection seawater wedge is dyed green, and the pre-injection fresh water flowing from right to left is not coloured.

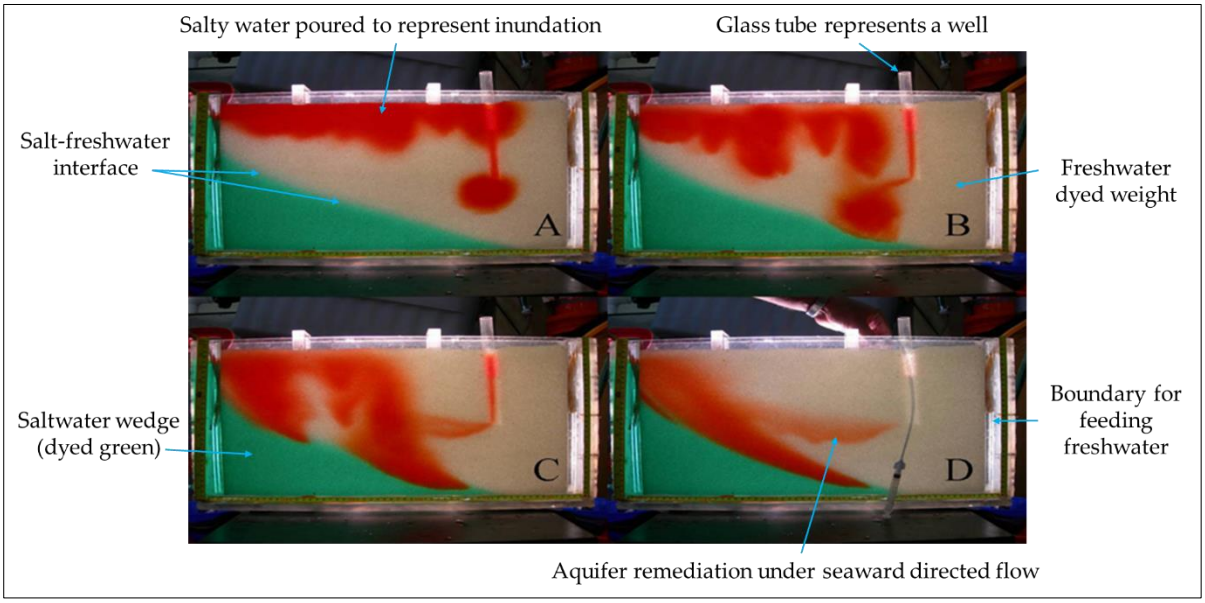

Fig 6. 5: Physical model of salt water injection from top and infiltration into a shallow coastal sandy aquifer at (a) 2, (b) 5, (c) 11, and (d) 19 min; white colour indicates the fresh water, green colour indicates the intrusion owing to the hydraulic connectivity. Seaward-directed flow results in natural remediation of the freshwater (Illangasekare et al. 2006).

Salt water is injected across the top of the aquifer, where the infiltrated salt water is dyed red. Saltwater is also immediately injected into the aquifer through an open borehole (represented by glass tube open

at both ends) that represents a well. The experimental results showed that the surcharged head and an unstable density contrast in the shallow coastal sandy aquifers lead to vertical mixing of salinity within the fresh water. Moreover, the laboratory model demonstrates that within a short period of time the salt water that flooded the well descended as a large finger and contaminated the deeper aquifer. An important observation from the experiments is that salt water (both from surface infiltration and the flooded well) dilute because of mixing with fresh water and move seaward under the seaward-directed flow (see also Fig 6.1). However, diluted salt water remains above the regional seawater interface as the density of both seawater sources decreased because of dilution as they migrated through the aquifer and mixed with fresh water. The study of Van Biersel et al. (2007), ensures indeed Illangasekare's physical model as they reported that water wells are faster risk pathways for the groundwater salinity during storm surges because they feed the ground water by salt water directly.

In another study on the long-term impact of the inundation-induced by the 2004's tsunami in south-eastern India, Violette et al. (2009) reported that the inundation resulted in contamination of groundwater supplies by locally raising salinity from potable levels up to 8320 mg/l, which is approximately one quarter the salinity of seawater. Peak salinity occurred within 1 month after the flood as the saline water infiltrated. The monitoring of observation wells after the inundation event showed that wells at the maximum inland extent of inundation are naturally remediated in less than three months, which is attributed to the horizontal groundwater flow toward the coast that displaced the saline water. However, for a complete natural remediation, by both precipitation-induced recharge and seaward groundwater flow, Violette et al. (2009) reported that natural remediation might take three to seven years. The latter range depends on the hydrodynamic state in the aquifer (e.g. groundwater velocity) as well as meteorological factors such as precipitation intensity, i.e. areas of low recharge experience less flushing, and thereby the contaminated groundwater recovers more slowly. As a result, in regions of high precipitation intensity, faster remediation is expected since the rainfall infiltrates over the affected area and recharges groundwater, accelerating the displacement and dilution of inundation-entrapped saltwater. The latter might explain why the remediation process takes only 26 months and 16 months (for 60% recovery) in the studies of Terry and Falkland (2010) and Bailey and Jenson (2014), respectively, while it extends up to 19 years in the study of Holding and Allen (2015).

With the global awareness of the climate change and expected SLR according to Parry et al. (2007), attention is directed toward the scenario of coastal barrier overtopping/breaching, which might induce catastrophic floods and an SDSWI accordingly. For instance, Yang et al. (2013) studied the effect of storm surge-induced wave overtopping over a two-dimensional vertical (2DV) cross-shore cross-section of a dyke on aquifer salinity through a case study in near Bremerhaven, the North of Germany, using the surface-subsurface model HGS. Using HGS, Yang et al. (2013) estimated that a total of 1045 m^3 of seawater might flow across the dyke during 2.8 h of overtopping (the overtopping period; see section 7.2.2). Therefore, a total of 26 tons of salt is delivered onto the hinterland. Seawater flows as far as 3 km inland on the land surface. Simultaneously, that surface water infiltrates into the aquifer, which is considered homogenous with $Ks = 5 \times 10^{-3}\, m/s$, through the unsaturated soil zone (1 m thickness). As a result, salt plumes develop and move vertically downwards within the unsaturated and saturated zones (Fig. 6.6). However, both the considered precipitation (300 mm/year) and the seaward flow (constant freshwater inflow rate of $q = 6.6 \times 10^{-5}\, m/s$) continuously dilute the infiltrated seawater and transport it back into the sea.

Fig 6.6 presents the distribution of the salt concentration at various times after the onset of the storm surge. After 3 days of the inundation behind the dyke, seawater reached the aquifer behind the dyke, where the maximum salt concentration for human drinking water of 500 mg/l can be found at 16 m depth. After 1-month, numerous plume fingers developed in the aquifer up to 1700 m behind the dyke, and the upper 35 m of the aquifer water is contaminated with a salt concentration of > 500 mg/l. After 1 year, the salt concentration of 500 mg/l has reached the bottom of the aquifer, such that groundwater of the entire aquifer within the distance of 1700 m from the dyke has become unfit for drinking. After 5 years, the horizontal extent of the contaminated aquifer has reduced to 1000 m behind the dyke due to the seaward flow of fresh groundwater. After 10 years, concentrations in most parts of

the aquifer have dropped below 500 mg/l, such that groundwater has recovered to be suitable for drinking. However, natural remediation by the seaward flow of fresh groundwater is relatively slow. Even after 20 years, concentrations greater than 500 mg/l can still be found close to the aquifer bottom.

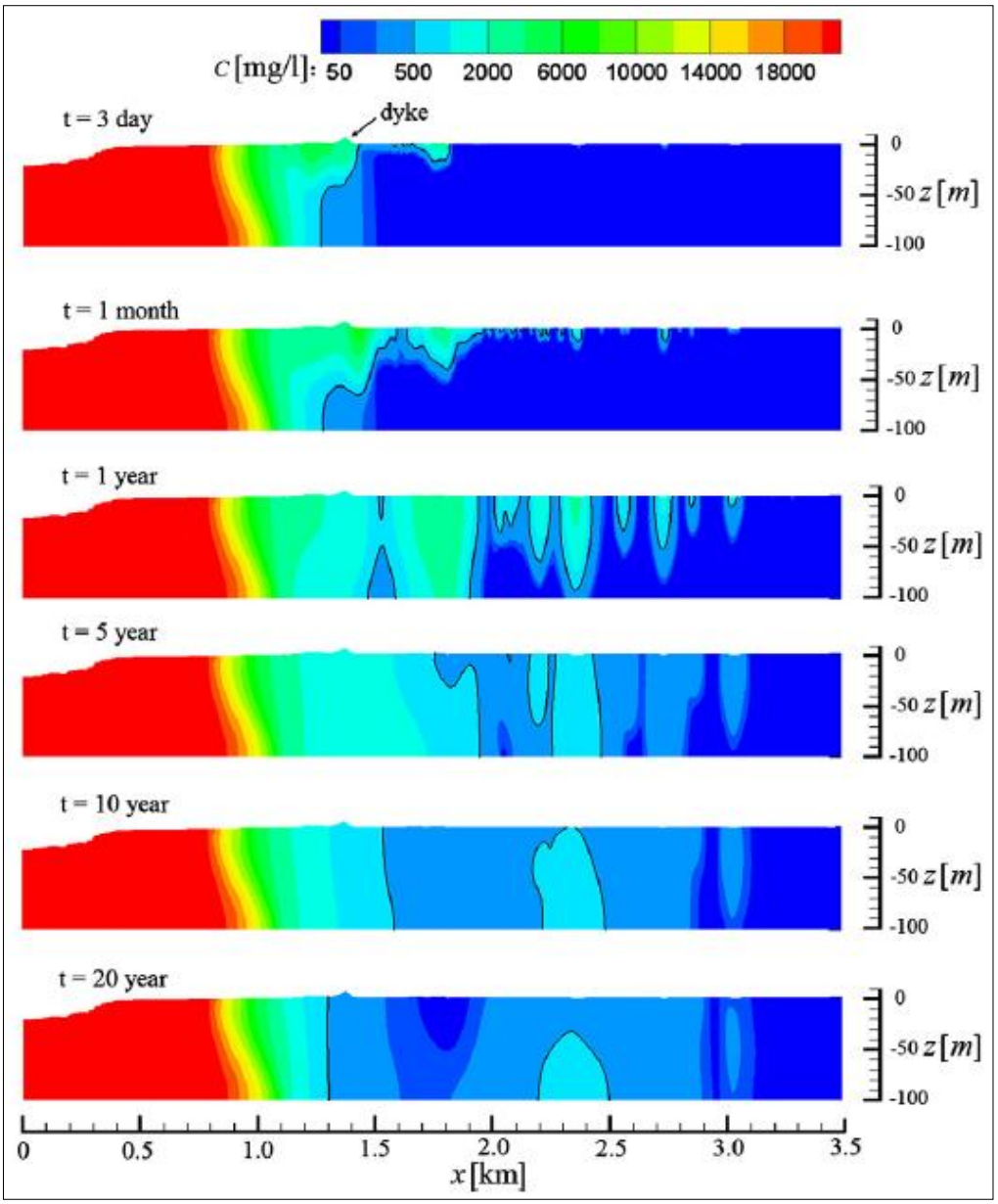

Fig 6.6: Distribution of salt concentration in the coastal aquifer at different times after the storm surge; Black lines are the iso-concentration lines of 500 mg/l (Yang et al. 2013).

In order to study the effect of aquifer heterogeneity on the migration of salt plumes, Yang et al. (2015b) run again the surface-subsurface model of Yang et al. (2013) near Bremerhaven by considering aquifer heterogeneity as described in Fig 6.7.a. With a scenario of total dyke failure (an assumed failure mechanism) during a storm surge event, a total of 2272 m^3 (per meter dyke length) of seawater flowing to the inland. Therefore, a total of 57 ton (per meter dyke length) of salt is delivered onto the hinterland. Seawater flows as far as 7 km horizontally to inland on the land surface. As a result, the salinized area of the aquifer is expanded up to 2050 m landward because of the expansion of inundation extent. The study of Yang et al. (2015b) has also showed that the nature of aquifers heterogeneity has a significant effect on the fate of the salt plumes, which is in line with the laboratory experiments of Vithanage et al. (2012). Moreover, the study showed that the NRP takes more than 20 years as shown in Fig 6.7.b.

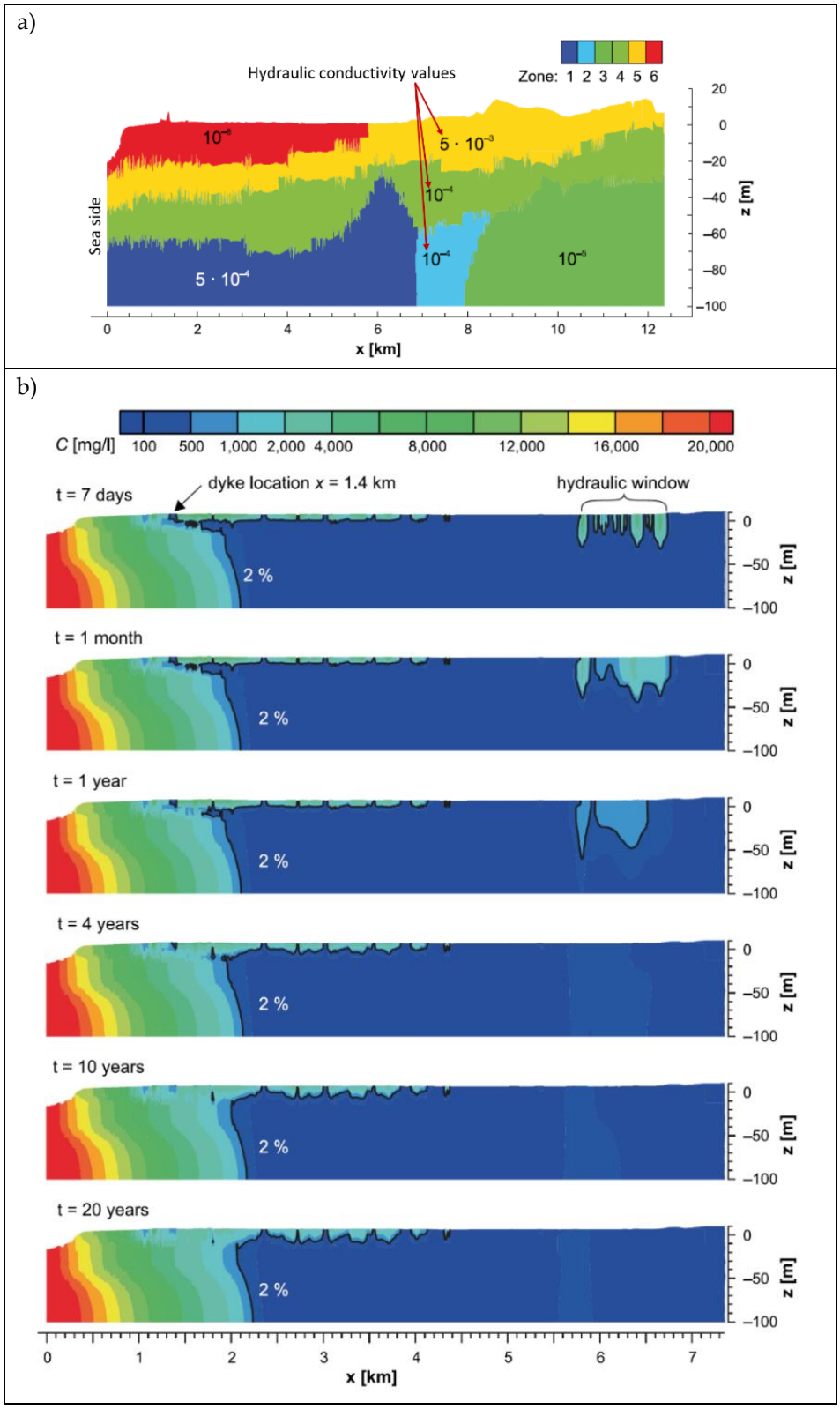

Fig 6. 7: Effect of aquifer heterogeneity on SWI near Bremerhaven: (a) Six different zones of hydraulic conductivity to incorporate geological heterogeneity; Numbers are the hydraulic conductivities [m/s] for each zone, and (b) Distribution of salt concentration in the coastal aquifer of soil heterogeneity described in (a) at different times after the storm surge. Black lines are the 2% salt concentration (500 mg/l) of that in seawater (25000 mg//l) (Yang et al. 2015b).

In a 3D modelling study by Yang et al., (2015a) for the same study area near Bremerhaven, a breach of the dyke is assumed with fixed dimensions (fixed width of 100 m). As a result, the inland discharge

estimated based on this scenario fed the hinterland to calculate the inland flood extent, water depths and the subsequent SWI. This study also reported that the NRP takes more than 20 years. The open channels in the study area are also simulated and showed an important effect on the increase of the contamination extent because they act as preferential pathways for landwards movement of salt water. However, the surface extent of the seawater, and the SWI extent accordingly, may be retreated by the land topography as proved by Yu et al. (2016b).

Remark 6.2: Lessons learnt and modelling gaps from/of previous studies of storm-driven saltwater intrusion (SDSWI)

The most important lessons from previous studies of SDSWI may be outlined as follows:

(i) The natural remediation process (NRP) of an aquifer after a short-term saltwater inundation event is a long-term process that might take decades to reach again the pre-flooding conditions.

(ii) Remediation takes place mainly due to the seaward directed flow that continuously dilates the infiltrated saltwater and move it seaward.

(iii) Aquifer heterogeneity has a significant effect on the fate of the salt plumes and accordingly on the remediation time (Vithanage et al. 2012; Yang et al. 2015b).

(iv) Open channels (e.g. canals and surface drains) might act as preferential pathways for landwards movement of saltwater during coastal flood, thus resulting in an increase of the contamination extent.

Despite the modelling approach used in Yang's studies (see Figs 6.6 and 6.7) to simulate the SDSWI using the surface-subsurface model HGS is well established, Yang's studies suffer the following drawbacks and limitations:

(i) *Omitting the morphological evolution*: Inland discharges induced by overtopping in Yang et al. (2013), by overwash in Yang et al. (2015b), or by breaching in Yang et al. (2015a) were either omit the morphological evolution of the dyke and the induced dyke crest lowering by the overtopping effect (e.g. Yang et al. 2013) or were based on roughly assumed dimensions for the overwash and breach of the dyke (e.g. Yang et al. 2015a; b). The latter assumptions result in non-providing reliable inland discharges. Thereby, the calculated flood extent by the HGS surface module might not be reliable and the SWI calculated by the subsurface module might accordingly inaccurate. Therefore, the surface-subsurface model HGS should be supported by a proper modelling of the morphological evolution.

(ii) *Omitting the short waves*: in the surface module of HGS, short waves are not simulated as the module does not account for them and their induced effects (e.g. breaking, runup, rundown), which are among the main drivers for barrier erosion and breaching (see section 2.2). Therefore, the surface-subsurface model HGS needs also to be supported by a proper module to account for effects of short waves.

(iii) *Omitting the inertial terms in the NLSWEs*: Because of assuming a diffusive wave approximation to facilitate the surface-subsurface coupling (Therrien et al. 2010), the surface module of HGS neglects, while calculating the surface runoff, the inertial terms in the momentum balance in the NLSWEs (see Eq 5.5), which is also another source of inaccurate flood extent and depths. In fact, the inertial terms might be the dominant over the dyke surface during overtopping/overwash/breaching because of the high flow velocity there.

These limitations imply that it is indeed necessary to account for the coupling of breaching, induced inundation and subsequent saltwater intrusion.

6.4 Coupling scenarios for breaching, inundation and saltwater intrusion modelling

Though coastal barrier breaching, induced surface runoff and subsequent saltwater percolation are often hydraulically interconnected, they are traditionally considered as separate systems and are analysed separately. Such separation is partly due to the highly complex nature of coastal aquifers as well as to the difficulties in measuring and modelling the interactions of the involved processes. This might also be explained by the much larger time scale of the groundwater flow and hence SWI as compared to that of the free surface flow. For SDSWI modelling, however, the importance of considering all these processes together in a single model system has become an increasing necessity in order to achieve reliable simulations.

In order to identify an appropriate model tool (in terms of both scope and scale) or at least a systemic modelling approach, which is able to simulate the mutual interactions between the breaching of coastal barriers, the subsequent inundation and the induced vertical intrusion of the seawater to the aquifers, four different coupling scenarios might be considered (Fig 6.8):

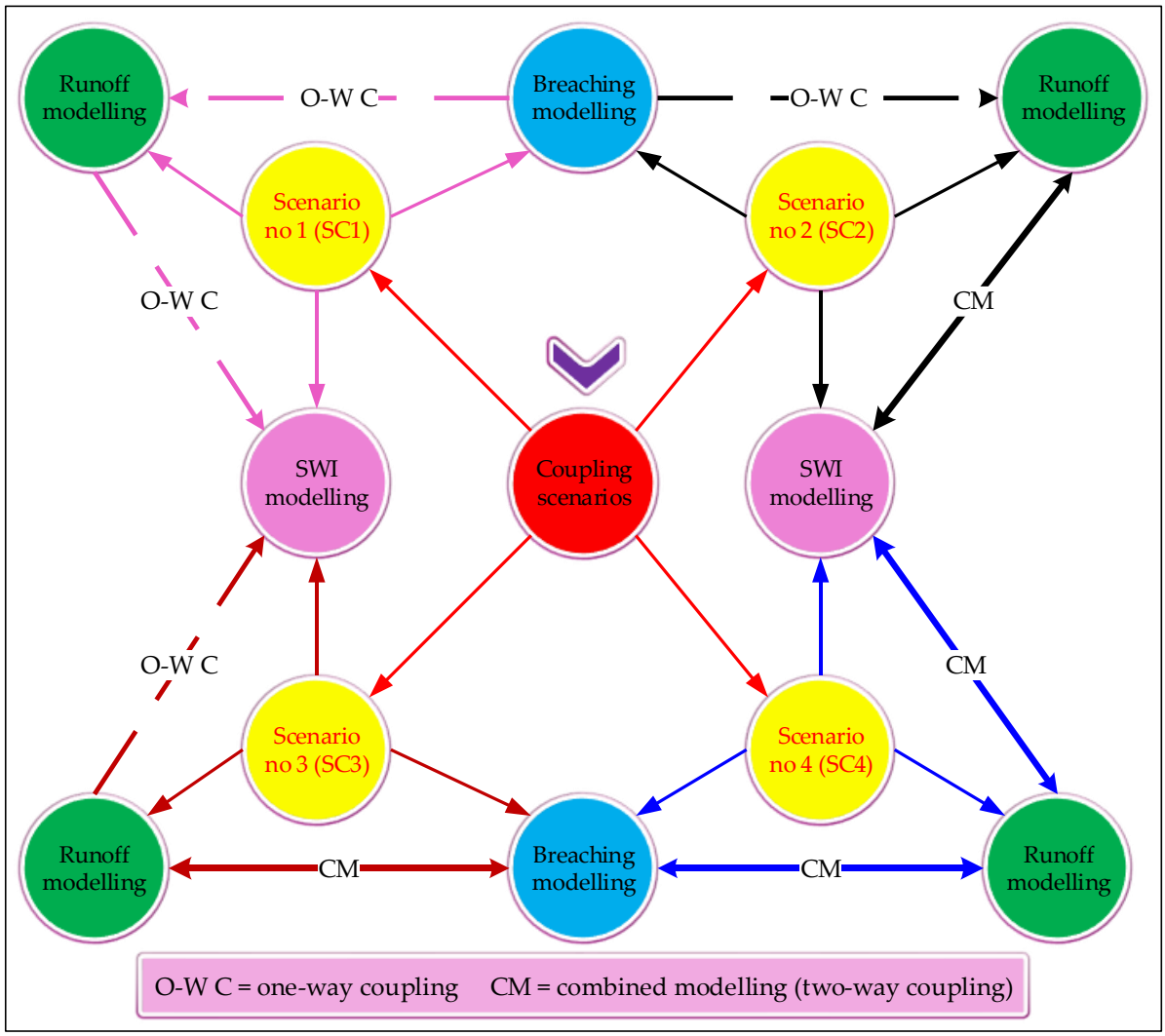

Fig 6. 8: Coupling scenarios among breaching, induced inundation and subsequent saltwater intrusion.

(i) *Scenario no 1 (SC1)*: in this scenario, each process is modelled separately then the outcomes of the breaching model are "manually" transferred to the runoff modelling and so on (one-way coupling approach);

(ii) *Scenario no 2 (SC2)*: in this scenario, the breaching is modelled separately to transfer its outcomes to a surface-subsurface model (e.g. HGS) to simulate the mutual interaction

between surface and subsurface flow. Such approach is almost the one followed in Yang's studies with the difference that the breaching dimensions are roughly assumed (not modelled) so that the calculated inland discharge and subsequent runoff and SWI might be unreliable;

(iii) *Scenario no 3 (SC3)*: here breaching and induced hinterland inundation are modelled in combination to feed a saltwater intrusion model (e.g. SEAWAT) by the breaching-inundation outcomes. For such purpose, the XBeach model can perform the combined modelling as successfully demonstrated in Chapter 5 (see also Elsayed and Oumeraci (2016b));

(iv) *Scenario no 4 (SC4)*: such scenario considers the three processes as a fully coupled by combining the three processes in a single model.

Besides the need to a manual transfer of the boundary conditions from one model to another in SC1, the omission of the mutual interaction among such processes might lead to unreliable outcomes. For instance, Elsayed and Oumeraci (2016b) have shown that the separate modelling of the breaching and the induced inundation might lead to unreliable inundation extent, inundation depths and free surface flow kinematics (see also chapter 5). Therefore, such modelling scenario is unfavourable.

Despite the successful implementation of SC2 in the studies of Yang et al. (2013, 2015a; b), this modelling scenario suffers the weaknesses mentioned at the end of section 6.3 (*Remark 6.2*). To achieve better results based on this scenario (SC2), surface-subsurface models (e.g. HGS) should include a module for the coastal processes and the induced morphological evolution in order to simulate coastal barrier breaching and the resulting inflow conditions at the breach. Coupling scenario SC3 is, therefore, preferable for three main reasons:

(i) The combined modelling of coastal barrier breaching and the induced inundation would result in reasonable inundation extent and water depths as demonstrated in Elsayed and Oumeraci (2016b) (see also chapter 5).

(ii) The splitting of the modelling after the inundation is less critical since both breaching and inundation have the same time scale (often in the scale of days) while the SWI process extends for years. Splitting in this phase would save considerable computational effort.

(iii) The reliability of SWI modelling would be better achieved with SC3 because it is based on a more reliable estimate of flood characteristics than those estimated using SC2.

A single model system for SC4 is not yet available. Though XBeach, which simulate both breaching and inundation, has a groundwater flow module and solving the 3D Darcy equation (Eq 6.3) like the USGS Modflow groundwater model (McCall 2015; McCall et al. 2012), it cannot yet simulate contaminant transport because it does not yet include the advection-dispersion equation (Eq. 6.4). Such scenario, though being computationally costly, might provide a greater potential for future studies.

Remark 6.3: Selection of the most appropriate and feasible modelling approach

A single model for breaching of coastal barriers, induced flooding and subsequent SWI is not yet feasible due to the fact that a breaching and inundation model such as XBeach does not account for subsurface mass transport (e.g. for SWI). On the other side, surface-subsurface models for mass transport (e.g. HGS) do not account for the breaching process. As alternatives, SC2 and SC3 are possible modelling scenarios. Though Yang et al. (2013, 2015a; b) followed the track of SC2, this study will follow the track of SC3 in chapter 7 using the same case study of Yang et al. (2013) in order to achieve more reliable inland discharges, inundation extent and depths. For such purpose, the XBeach model will perform the combined modelling of breaching and inundation while the SWI will be simulated separately using the SEAWAT module of Visual Modflow (see section 7.1).

Despite its incapability to simulate the unsaturated flow through the vadose zone, which represent a major model limitation, the selection of SEAWAT/Visual Modflow is based on the following criteria:

(i) SEAWAT is validated using benchmarks e.g. Elder problem (Elder 1967) and Henry problem (Henry 1964) (see e.g. Elsayed and Oumeraci (2017b) for the verification results).
(ii) Visual Modflow, in addition, is a powerful tool to model and evaluate the effectiveness of different strategies for management and controlling SWI.
(iii) It also includes a river and drainage packages that can respectively simulate the surface-subsurface interaction and drainage from the subsurface (see chapter 7 for more details regarding this point).

Particularly the third selection criterion makes Visual Modflow/SEAWAT more eligible for the purposes of this study than other open source subsurface models such as OpenGeoSys (Kolditz et al. 2012), which are freely available and can easily be programed to include new features. However, due to the time frame of the study, ready to use models (e.g. Visual Modflow/SEAWAT) are preferred. Nevertheless, the application of OpenGeoSys for the same purpose represents a candidate topic for further study. Moreover, being open source code, it might be the most suitable numerical model that can be coupled with XBeach in order to provide a single/coupled model system that can integrally simulate breaching of coastal barriers, induced flooding and subsequent SWI. The validity of source codes of both software might facilitate strong coupling between both models so that XBeach simulate the hydro-geo-morphodynamic over the land surface in both sea and hinterland whilst OpenGeoSys automatically utilizes XBeach outcomes to calculate the subsurface flow and the accompanied solute transport.

6.5 Management of storm-driven salt water intrusion

While large-scale natural disasters (e.g. SWI) cannot be prevented, they can certainly be mitigated through structural and non-structural mitigation measures/tools. In fact, besides being a major limitation for usability of contaminated groundwater for drinking and other subsistence purposes, crops in hinterlands can suffer stress and thereby not grow properly or can die due to intolerance to salt (Faneca Sànchez et al. 2015; Felisa et al. 2013), thus leading to a decrease in the agriculture yield (Fakhruddin 2016; Williams 2010). Given their vulnerability, sustainable management of coastal fresh groundwater reserves is of paramount importance. Moreover, socioeconomic and environmental impacts caused by SWI have claimed the attention of the scientific community worldwide during the last decades (Gaaloul et al. 2012).

Management of coastal aquifers involves decisions regarding the amount of water to be extracted and/or injected into the aquifer (Kourakos and Mantoglou 2015), taking into account the interplay between the conditions of the aquifer and economic, social factors and, in some cases, environmental impacts (Werner et al. 2013). For instance, some studies (e.g. Gaaloul et al. 2012; Kumar 2016) have listed many strategies/approaches for controlling the traditional SWI in coastal aquifer systems, which is either in the form of upconing induced by excessive pumping and/or in the form of landward shifting of the salt-freshwater interface because of a long-term SLR. These strategies include:

1) Reducing pumping from coastal aquifers,
2) Relocating/shifting extraction wells landward,
3) Directly recharging aquifer (primarily surficial aquifers),
4) Freshwater recharge into wells paralleling the coast, creating a hydrodynamic barrier,
5) Creating a trough parallel to the coast by excavating encroaching salt water from wells,
6) Extracting seawater before it reaches wells,
7) Extraction/injection combination and
8) Construction of impermeable subsurface barriers.

Control methods 1 and 2 above are used to reduce the cone of depression by reducing the rate at which water is withdrawn and by spreading wells apart so that concentrated areas of drawdown are avoided. Methods 3 to 5 involve creating a hydrodynamic barrier of fresh water that blocks the further

encroachment of seawater. Extraction techniques, methods 6 and 7, require the use of extraction wells that pump sea water from the aquifer before it can reach freshwater supply wells. Fig 6.9, for instance, shows an Abstraction, Desalination and Recharge (ADR) technique that is suggested by Abd-Elhamid (2010) to mitigate the SWI induced by SLR. Method 8, installing impermeable barriers such as grout and steel sheet piles, is normally limited to areas where the contaminated aquifer is relatively shallow and the subsurface geology allows for a proper seal. Each of these methods can be applied to certain situations and the method used will depend on the specific problem to be solved. Moreover, simulation tools are often used to evaluate the effectiveness of possible decisions.

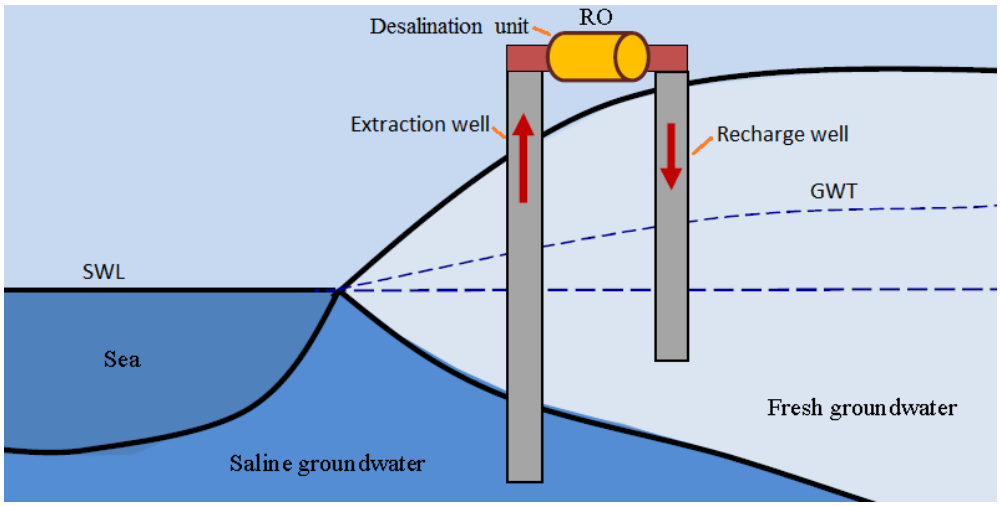

Fig 6. 9: Abstraction, Desalination and Recharge (ADR) technique to control SWI owing to SLR (Abd-Elhamid 2010).

Interestingly, none of the previous traditional techniques for managing common SWI is suitable for managing vertical SWI induced by coastal inundation. For instance, Illangasekare et al. (2006) attempted to overcome SWI induced by the 2004 tsunami in Sri Lanka using widespread pumping of wells to remove seawater. The latter approach was effective in some areas, but over-pumping has led to upconing of the saltwater interface and rising salinity rather than its removal from the upper part of the saturated zone. In addition, the purged well water was often discharged on the land surface close to the wells, allowing the contaminated water to re-enter the aquifer and the wells after vadose zone infiltration.

Rather than do-nothing scenario, which is equivalent to relying on natural remediation, Villholth and Neupane (2011) suggested guidelines for future protection of vulnerable coastal groundwater resources based on the 2004 tsunami experience. Indeed, these guidelines focus on open wells. As open wells easily get contaminated and exacerbate the problem of groundwater salinization, sealed wells are suggested to improve the resilience of the water supply system. In addition, re-enforcing well heads and raising standpipes in the terrain, either by placing them in naturally higher locations or placing them on raised platforms as shown in Fig 6.10 as an option in the case of placing wells outside the flood prone zone is not feasible. Moreover, Kumar (2006) reported that increasing surface sealing in urban areas (roads, roofs, paved areas) reduces the groundwater recharge at the same time, and thereby the vertical percolation of salt water, although it leads to higher storm flow peak discharges in populated areas and in urban drainage networks.

Fig 6.10: Example of 'flood-proofed' water well as a tool to prevent vertical salt water intrusion through wells (Villholth and Neupane 2011).

Despite the importance of the aforementioned mitigation measures, there is still an urgent need for new solutions to mitigate vertical SWI, especially in highly vulnerable coastal zones of intensive usage of groundwater. In fact, SDSWI is a hazard that cannot be mitigated through nonstructural measures such as warning and emergency plans. Therefore, structural mitigation measures are crucial. The best mitigation measure is to make the existing coastal barriers overtopping resistant so that they can cope with extreme overtopping without breaching. For the residual inland discharge due to overtopping, this study suggests using subsurface drainage system (Fig 6.11), especially in flood prone agriculture areas. The drainage, in general, would absorb the contaminated water before reaching the fresh groundwater. However, surface drainage is repulsive since it could enlarge the contamination extent because surface drains would act as preferential pathways for landwards movement of salt water as shown by Yang et al. (2015a) (see also *Remark 6.2*).

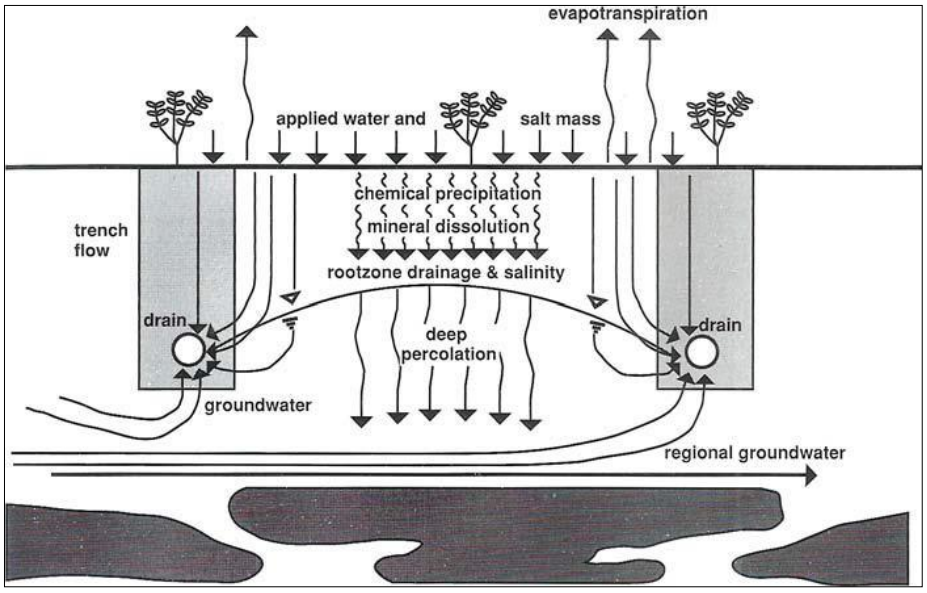

Fig 6. 11: Schematic illustration of the flow of water through soil with respect to salt leaching and root zone drainage (Grismer 1990).

Though the subsurface drainage is a well-established technique to increase the agricultural productivity (e.g. Blann et al. 2009; Fausey et al. 1995), its role in mitigating SDSWI and in shortening long remediation intervals of contaminated coastal aquifers after an SDSWI are not yet investigated. The rest of this study (Chapter 7), therefore, aims among others at exploring the effect of subsurface drainage on aquifers remediation interval after an SDSWI event. The visual Modflow model will be used for this purpose as discussed in *Remark 6.3*. Despite its incapability to simulate the unsaturated flow through the vadose zone, which is a weak point that might affect the modelling outcomes, SEAWAT includes a ready to use drainage package that can be adapted to simulate the subsurface drainage effect. As SEAWAT can implicitly account for the flow through the vadose zone with an acceptable accuracy (Pérez-Paricio et al. 2010; Waterloo Hydrogeologic 2015) through the conductance term as will be discussed in detail in chapter 7, including the drainage package makes SEAWAT the most suitable model for the purposes of this study.

6.6 Summary and discussion of the results

In this chapter, the implications of storm surge-induced barrier overtopping/breaching for coastal aquifer contamination are explored. Vertical saltwater intrusion (SWI) due to coastal inundation may increase the salinity of the originally fresh groundwater, which may significantly reduce the water quality and the environmental values of groundwater, thus possibly hindering any possible sustainable development in coastal zones. In fact, storm- driven saltwater intrusion (SDSWI) can result in widespread aquifer contamination that could last for several years until it gets remediated naturally. Even a moderate storm surge event may significantly affect the usability of coastal aquifers for many years.

SDSWI often starts with a coastal barrier breaching, or even overtopping, inducing inland inundation and subsequent vertical intrusion of seawater in coastal aquifers. Though these processes are naturally continuous and hydraulically interconnected, they are often analysed separately. Such separation is partly due to the highly complex nature of coastal aquifers as well as to the difficulties in measuring and modelling the interactions of the involved processes. In addition, the belief that groundwater flow and hence the SWI have a much larger timescale than that of free surface water flow might explain why these processes have often been modelled separately. However, the importance of considering groundwater flow, SWI and surface flow as fully coupled processes in a single model system has become an increasing necessity in order to achieve reliable simulations.

In this chapter, the feasibility of modelling these three processes in a single model system is addressed. Moreover, the outcomes of previous studies on modelling are summarised. Four different coupling scenarios are identified: (i) separate modelling of breaching of coastal barriers, induced inundation and the subsequent saltwater intrusion, (ii) separate modelling of barrier breaching with surface-subsurface modelling of the induced inundation and the subsequent saltwater intrusion, (iii) combined modelling of the breaching of coastal barriers and the induced inundation with separate modelling of the subsequent groundwater flow and accompanied SWI, and (iv) simulating breaching of coastal barriers, induced inundation and the subsequent saltwater intrusion as fully coupled processes in a single model system. The latter scenario is the most appropriate but not yet feasible. Scenario (i) is not appropriate because the modelling approach omits the hydraulic interconnection among breaching of coastal barriers, induced inundation and the subsequent saltwater intrusion and requires a “manual” transfer of the boundary conditions between the single models. Therefore, only scenarios (ii) and (iii) are considered for a systematic comparative analysis. As a result, scenario (iii) is selected, using XBeach for overtopping/barrier breaching and subsequent coastal flooding, and SEAWAT/Visual Modflow for groundwater flow and SWI in the coastal aquifers.

Most of the previous studies associated with SDSWI are limited to the determination of the time interval for the natural remediation process (NRP) after such events. The latter means that no structural mitigation measures are proposed to control this type of SWI and to shorten long remediation intervals. For the latter purpose, the current approaches for managing SWI are briefly reviewed. Common management strategies are found unsuitable for SDSWI mitigation. Therefore, subsurface drainage

networks are suggested as a management solution. In fact, they can absorb the contaminated water before it reaches the fresh groundwater. In chapter 7, the effect of subsurface drainage on remediation intervals will be investigated using the same case study as Yang et al. (2013).

7 Modelling and mitigating flood-induced saltwater intrusion near Bremerhaven using XBeach and SEAWAT

The main goal of this chapter‡‡‡ is to apply the overall modelling methodology, which is implied by the results of the previous chapter, to a case study near Bremerhaven, Germany. Thus, modelling scenario SC3 as described in section 6.4 and Fig 6.8, is considered to set up the models using existing hydrogeological data and geophysical information from the study of Yang et al. (2013) for the same study area. In this way, breaching/overtopping of coastal barriers and induced inundation of the hinterland can be simulated in XBeach as described in chapter 5 whilst saltwater intrusion (SWI) is modelled separately by the SEAWAT code, which is built in the Visual Modflow graphical interface, so that the outcomes of XBeach are transferred as input data to SEAWAT. Therefore, this chapter starts with a brief outline of SEAWAT /Visual Modflow.

7.1 SEAWAT/Visual Modflow

For simulating SWI, the Visual Modflow 2011.1 graphical interface of Waterloo Hydrologic (Waterloo Hydrogeologic 2015) is applied in this study. Visual Modflow is a finite difference based interface supporting all the most recent public domain and proprietary versions of USGS Modflow, MT3DMS, RT3D and PHT3D for simulating respectively groundwater flow, 3D advective-dispersive multi species transport, 3D reactive transport, and 3D reactive multi-component transport. The transport code MT3DMS is often used to simulate multiphase (immiscible) flow of both liquids and gases that move as separate phases (i.e. without blending) within the subsurface, while the geochemical reactive transport codes RT3D/PHT3D simulate reactions between two or more chemical species. For simulating the conservative (nonreactive) and single phase (miscible) transport of seawater in coastal aquifers, USGS proposes the SEAWAT code, which couples and utilises the USGS numerical modelling programmes Modflow 2000 and MT3DMS, so that three-dimensional variable-density flow (3DVDF) and transport conditions of seawater in coastal aquifers can be simulated.

Besides their applications in many SWI studies (e.g. Ding et al. 2014; Gopinath et al. 2016; Nofal et al. 2014), the key advantage of SEAWAT/Visual Modflow is the inclusion of diverse easy to use boundary condition packages. The most important packages for this study are:

- *Recharge boundary (RCH)*: it is typically used to simulate surficially distributed recharge to the groundwater system.
- *Constant head boundary (CHB)*: it is a time-variant specified-head package used to fix the head value in selected grid cells regardless of the system conditions in the surrounding grid cells. In this way, selected grid cells of constant heads are specified boundary heads that do not change in response to hydrologic stresses. Thus, acting as an infinite source of water entering the system, or as an infinite sink for water leaving the system. This type of boundary is often used to simulate the time-variant seawater level at the seaside boundary or to fix the water table at a user-defined value at the landward boundary.
- *Modflow River Package (RIV)*: it is also a hydraulic head-dependent boundary simulating the surface water/groundwater flow interaction, i.e. it is used to simulate the influence of a surface water body, with a specific concentration, on groundwater flow. Surface water bodies such as rivers, streams, lakes and swamps may either contribute water to the groundwater system or act as groundwater discharge zones, depending on the hydraulic gradient between the surface water body and the

‡‡‡ More detail of this chapter can be found in the progress report:
Elsayed, S. M.; Oumeraci, H. (2017): Breaching of coastal barriers under extreme storm surges and implications for groundwater contamination: Implications of coastal floods for groundwater contamination. Internal Report no 1075/17, Leichtweiß-Institut for Hydraulic Engineering and Water Resources, TU Braunschweig, Braunschweig, Germany, 101 p.
Freely available at:
https://www.researchgate.net/publication/316459814_Implications_of_coastal_floods_for_groundwater_contamination
Moreover, the final outcomes of this chapter are part of a submitted journal paper:
Elsayed, S.M.; Oumeraci, H. (2017): Modelling and Mitigation of Storm-Induced Saltwater Intrusion: Improvement of the Resilience of Coastal Aquifers Against Marine Floods by Subsurface Drainage. Submitted to Environmental Modelling and Software.

groundwater system, in addition to the river conductance to the groundwater system (C_r). This type of boundary will be used in this study to simulate coastal inundation as a vertical SWI source and its effect on groundwater (See Section 7.4.4).

- *Modflow Drain Package (DRN)*: it is also a hydraulic head-dependent boundary designed to simulate the effects of features such as agricultural drains that remove water from the aquifer at a rate (Q_d) proportional to the head difference (Δh) between the head in the aquifer and some fixed head or elevation. Therefore, the DRN package requires information as input for each cell containing this boundary condition such as: (i) the drain head of the free surface of water within the drain, (ii) elevation of the bottom of the drain and (iii) drain conductance (C_d), which is a lumped coefficient describing the head loss between the drain and the groundwater system, so that Q_d is calculated as:

$$Q_d = \mathrm{C_d}\,\Delta h \qquad \text{with} \qquad C_d = K_d A_d / L \tag{7. 1}$$

  where Δh represents the difference between the user-specified boundary head and the model-calculated head near the drain, K_d is a representative hydraulic conductivity for soil surrounding the drain, A_d is a representative drain area and L is the distance between the locations of the user-specified boundary head and the model-calculated head. The DRN package assumes that the drain has no effect if the head in the aquifer falls below the fixed head of the drain. This type of boundary will be adapted in this study to simulate the subsurface drainage effect on the fate of the salt plumes in coastal aquifers (See Section 7.5).
- *Constant concentration boundary*: it acts as a contaminant source providing a solute mass to the model domain in the form of a known concentration. Therefore, this type of boundary is often used to fix the concentration at the sea boundary at a user defined concentration value.
- *Point Source Boundary*: it specifies the concentration of a solute entering or leaving the model through a flow boundary condition grid cell specified in the flow model. Therefore, such boundary is needed to specify the concentration of the intruding solute (saltwater).

These boundaries are used to relate a model domain with the surrounding environment as described below for the case of Bremerhaven

7.2 Study area and available data

The site selected for the case study belongs to the German Bight, which is situated north of Bremerhaven, northern Germany (Fig. 7.1). In the German Bight, increases in wind velocity are expected in the future (Yang et al. 2015a), which may enhance the probability of higher and longer storm surges. The river Weser discharges into the German Bight and the catchment of the lower part of this river incorporates several cities, major ports, a variety of industries as well as agriculture, including livestock farming. The latter makes it crucial to study the impact of possible storm surge event on the sustainable development at this zone of Germany. The discharge of the river Weser results in dilation of the seawater in the North Sea near the study area and thus reduces the average seawater concentration from 35,000 mg/l to 25,000 mg/l (Yang et al. 2013, 2015a). A 12-km long cross shore cross-section is considered, which is perpendicular to the coastline as indicated by the red line in Fig 7.1.a.

The data and further information for the modelling are available from the study of Yang et al. (2013). The study area consists of a two-dimensional vertical (2DV) cross-section of an unconfined coastal aquifer initially saturated with freshwater. The ground surface elevation (Fig 7.2) was obtained from a digital elevation model (DEM) showing that the seaside (west) has a minimum seafloor bathymetry of −20.6 (m.a.s.l.). The inland area is protected by a dyke with a height of 7.3 m.a.s.l., whereas the elevation of the area behind the dyke ranges from 0.5 m.a.s.l. to 14.66 m.a.s.l. A constant domain bottom elevation of −100 m.a.s.l. is used as the aquifer bottom, which is considered impermeable. Groundwater level at the landside boundary was measured to be 4 m.a.s.l. and the effective groundwater surcharge (precipitation minus evapotranspiration) is estimated to be 300 mm/yr.

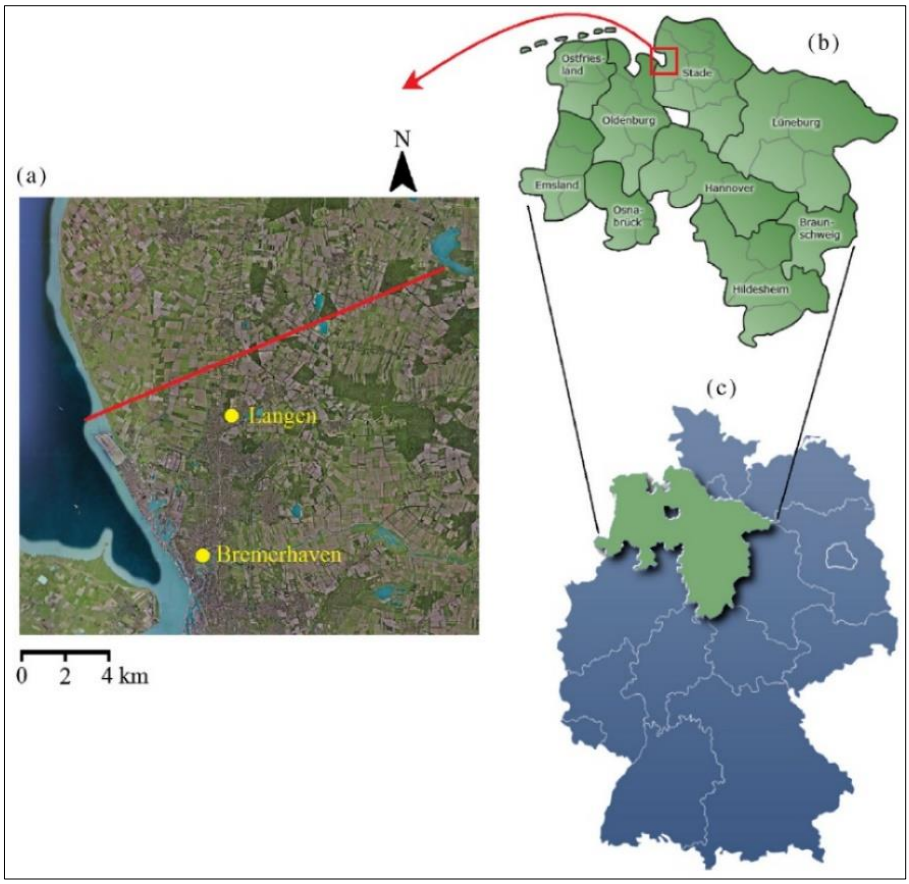

Fig 7.1: Location of the study area: (a) selected cross section near Bremerhaven (red line), (b) state of Niedersachsen (Lower Saxony) and (c) Germany (Yang et al. 2013).

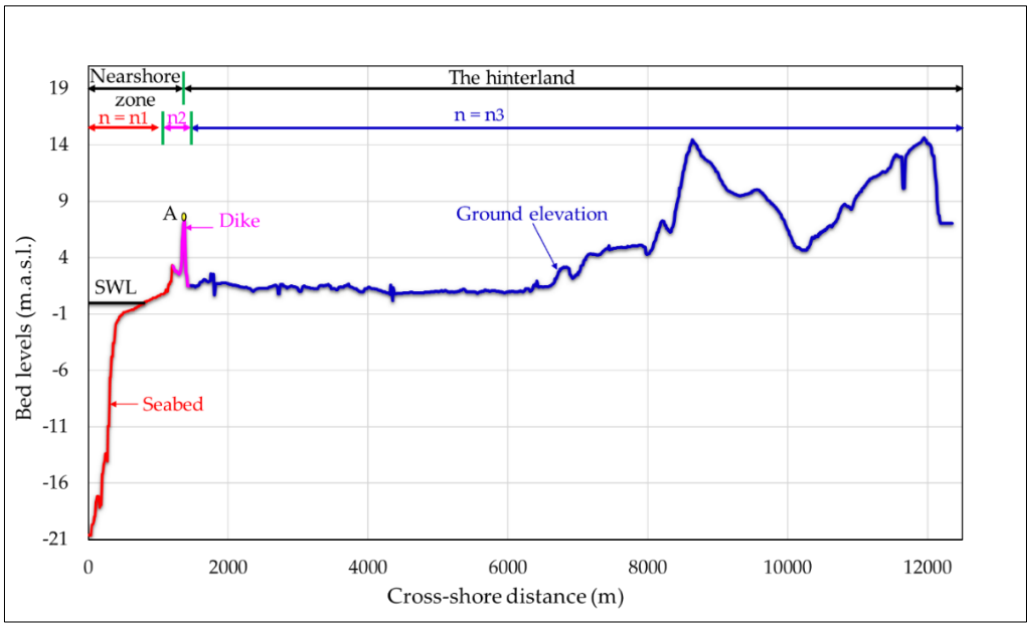

Fig 7.2: Bathymetry and ground elevations above SWL for the considered cross-shore profile near Bremerhaven, Germany (profile is obtained from Yang and Graf). The colours indicate different values for Manning coefficient.

7.2.1 Aquifer parameters

All aquifer parameter values are listed in Table 7.1, which are the same values of Yang et al. (2013). A uniform value for the hydraulic conductivity Ks = 5×10^{-3} m/s (43 m /day) is considered as

representative for the gravel/sand aquifer of the entire domain. In addition, uniform value for the longitudinal dispersivity D_L, the lateral dispersivity D_T and the molecular diffusion coefficient D (see Eq 6.5) are considered by 100 m, 10 m and 10^{-9} m^2 s^{-1}, respectively. Salt concentration in the sea is 25,000 mg/l, which is less than average seawater concentration of 35,000 mg/l in the North Sea because of water dilution by the river Weser. Therefore, seawater density of 1018.3 kg/m^3 is considered representative to the salt concentration of 25,000 mg/l while freshwater (C = 0) density is considered by 1000 kg/m^3. Viscosity is assumed to be independent from salt concentration and hence has a constant value of 1.124 $x10^{-3}$ $kg/m.s$. The aquifer storage parameters are respectively considered by 0.005 m^{-1}, 0.18 and 0.2 for the specific storage, specific yield and the effective porosity n.

Table 7. 1: Parameters of the coastal aquifer near Bremerhaven, northern Germany (same values of Yang et al. (2013)).

Parameter	Value	Unit	Note
Hydraulic conductivity (*Ks*)	5 x 10^{-3}	m/s	
Longitudinal dispersivity (D_L)	100	m	
Transverse dispersivity (D_T)	10	m	
Molecular diffusion (*D*)	1 ×10^{-9}	m^2/s	
Seawater concentration	25000	mg/l	
Saltwater density (ρs)	1018.3	kg/m^3	
Freshwater concentration	0	mg/l	
Freshwater density (ρ)	1000	kg/m^3	
Reference fluid viscosity	1.124 x 10^{-3}	kg/m.s	
Specific storage	0.005	m^{-1}	The volume of water that a unit volume of aquifer releases from storage under a unit decline in groundwater head.
Specific yield	0.18	-	It represents the drainable porosity and indicates the volumetric fraction of the bulk aquifer volume that a given aquifer will yield when all the water is allowed to drain out of it under the gravitational force.
Effective porosity (*n*)	0.2	-	

7.2.2 Storm surge scenario

The impact of a single storm surge event on coastal flow dynamics and on the investigated coastal aquifer is considered. The storm surge results in overtopping flow over the dyke crest (see section 2.2.1.3 item (ii)). Subsequently, sea water floods the hinterland behind the dyke, where the sea water infiltrates into the soil and percolates through the unsaturated zone towards the groundwater table. Therefore, the storm surge event includes the processes of (i) sea level rise, (ii) overtopping and ponding, (iii) sea level dropping and pond reduction and (iv) recovery of aquifer salinity to the initial state (remediation). The considered storm surge (Fig 7.3) induces a maximum sea level rise up to 8.5 m.a.s.l., which is about 1.1 m higher than the dyke crest without consideration of the effects induced by short-waves. The use of the same storm surge curve of Yang et al. (2013) aims at reproducing the same event but with the proposed modelling scenario (SC3) as indicated in Fig 6.8, thus facilitating the compassion of outcomes of this scenario with the outcomes of Yang et al. (2013).

According to the estimations of Yang et al. (2013), the overtopping lasts for 2.8 h and results in a maximum overflow rate of 200 $l\ s^{-1}$ per meter dyke. As reported by Yang et al. (2013), the 200 l/s is the maximum admissible value for overtopping flow according to EurOtop 2007 by Pullen et al. (2007). Thus, a total of 1045 m^3 of seawater overtop the dyke during the 2.8 h of overtopping. It is assumed that the salt concentration of the overflow water is as seawater concentration (i.e. 25,000 mg/l). Therefore, a total of 26125 kg of salt is delivered to the hinterland. In this study, the modelling scenario SC3 (See Section 6.4 and Fig 6.8) is tracked to simulate the naturally successive processes of water overflow, flood propagation and induced saltwater intrusion. In this way, the XBeach model is used to perform the combined modelling of wave overtopping and induced flood propagation as discussed in Section 7.3 below, whilst the vertical infiltration of the flooding seawater to aquifer is discussed in Section 7.4.

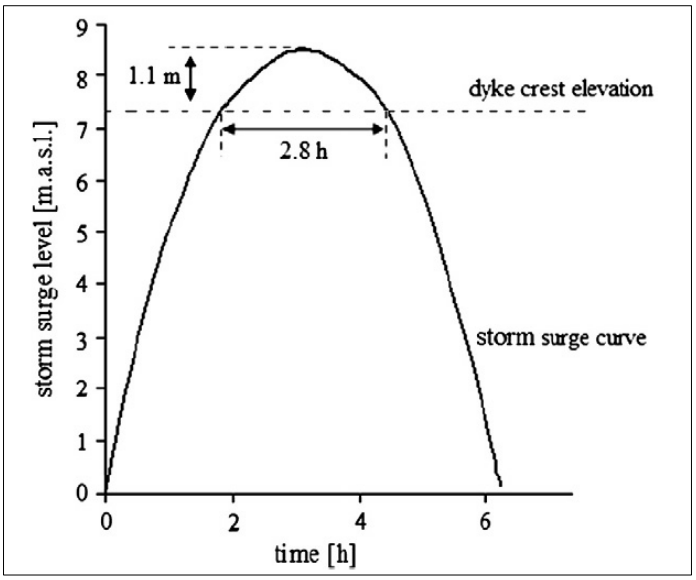

Fig 7. 3: Applied time history of the sea level during a storm surge event for the study site near Bremerhaven: the dashed line represents the elevation of the dyke crest (Yang et al. 2013).

7.3 Combined modelling of water overtopping and induced flood propagation

7.3.1 Model set-up in XBeach

As a first step of the modelling scenario SC3, wave overtopping and subsequent flood propagation are simulated using the hydro-morphodynamic model XBeach (Roelvink et al. 2009). For this purpose, the cross-shore profile in Fig 7.2 is reproduced in XBeach in the form of a numerical wave flume with a width of 1.0 m (alongshore) and a cross-shore length of 12349.2 m. The main parameters and boundary conditions used within XBeach to simulate this profile are shown in Table 7.2, while all other XBeach parameters (see e.g. Roelvink et al. (2015) are kept by the default of XBeach.

Table 7. 2: Main parameters and boundary conditions used in analysing the free surface flow over the cross-shore profile in Fig 7.2 using XBeach.

Parameter	Value	Meaning	Note
D50	1 mm	Median grain size	Obtained from Meilianda et al. (2011)
dx	12.36 m	Cross-shore spatial step	
dy	1.0 m	Profile width	
Bedfriction	n	Manning parameter (selected as representative for the bed friction)	
bedfric coef	Fig 7.2	Values of Manning coefficient	Three values are used as indicated in Fig 7.2
swave	0	Short waves are not considered	
front	0	Absorbing-generating weakly-reflective boundary is used as a 1D inflow boundary	
back	1	Absorbing-generating weakly-reflective boundary is used as a 1D outflow boundary	
left	1	Impermeable wall is a lateral flow boundary	Left side wall of the numerical wave flume
right	1	Impermeable wall is a lateral flow boundary	Right side wall of the numerical wave flume
facpi	1	Grain-stabilization effect is not considered	See chapter 4
form	2	Sediment transport is calculated according to the formulation of Van Rijn (2007a; b)-Van Thiel de Vries (2009)	See Roelvink et al. (2015)
tstop	10 h	Simulation time	
tint	1 s	Output time step	

As presented in Table 7.2, median grain size of 1 mm is considered as the representative median sediment size in the study area. The latter value is obtained from a survey of the study area by Meilianda et al. (2011). The cross-shore spatial step (dx) is considered regular of 12.36 m whilst one longshore spatial step (dy) of 1.0 m is considered. Like Yang et al. (2013, 2015b), three different values for the Manning coefficient (n) are used, as indicated in Fig 7.2, to account for the bed friction of the free surface flow. In other words, the land surface of the considered cross-shore profile is divided into three parts, where different n values are assigned: (i) n_1 for the beach area, (ii) n_2 for the dyke surface area and (iii) n_3 for the area behind the dyke. For the beach area $n_1 = 10^{-7}\ day\ m^{-\frac{1}{3}}$ $(0.00864\ m^{-\frac{1}{3}}.s)$ is selected and behind the dyke $n_3 = 6 \times 10^{-7}\ day\ m^{-\frac{1}{3}}$ $(0.05184\ m^{-\frac{1}{3}}.s)$ is used. Over the dyke, $n_2 = 0.00003\ day\ m^{-\frac{1}{3}}$ $(2.592\ m^{-\frac{1}{3}}.s)$ was calculated so that only maximum inland discharge of 200 l/s is admitted. Yang et al. (2013) considered that the water overflow on the dyke should not exceed an admissible value for overtopping obtained from EurOtop 2007 (page 49). In fact, such assumption is illogical for such overflow case meanwhile it is the reason behind adjusting such very high Manning coefficient (n_2) over the dyke. Because no data are available for the short-wave parameters (e.g. significant wave height and peak period), the short-wave module of XBeach is switched off using the XBeach keyword *swave* = 0. The latter means that many short-wave processes (e.g. wave breaking, run up and run down) are accordingly omitted. Nevertheless, the sea-level rise in Fig 7.3 is considered as the trigger for the overtopping flow process. Though water flow in the hinterland stretch in the downstream direction is permitted, lateral flow is prevented using impermeable wall boundaries as lateral flow boundaries in order to simplify the flow to a 1D flow along the considered cross-shore profile. The model is run for 10 hours using two modelling scenarios as described below while the output time step is considered by 1 s.

Two modelling scenarios for the free surface flow are preliminarily considered: (i) *Morpho-off* scenario considers that no morphological evolution takes place because both the dyke and the beach area are highly protected against coastal erosion and overwash, and (ii) *Morpho-on* scenario considers that the whole study area consents the coastal erosion and the induced morphological evolution. The idea behind these scenarios it to understand the effect of unprotected coastal barriers on coastal flooding and subsequent SWI. The inland discharge q is calculated at the crest of the dyke (Point A in Fig 7.2) showing that the inland discharges for both scenarios are identical as shown in Fig 7.4. Therefore, the same inland water volume (= 2196 m^3) propagates in the hinterland in both scenarios due to this overtopping event. Thus, 54.9 tonnes of salt are supplied to the hinterland. The latter volumes for the inland discharge and salt mass are more than twice the values estimated by Yang et al. (2013) using the surface module of HydroGeoSphere (HGS). Such significant differences arose from the fact that inland discharges calculated by HGS are based on a diffusive wave approximation of the NLSWEs, which ignore the inertial terms in the two momentum equations of the NLSWEs (see Eq 5.5). With the often very high overflow velocities over coastal barriers during overtopping and overflow conditions, omitting the inertial term (local and convective acceleration terms) might reduce inland discharges as the very high flow velocities over the barrier are omitted in the calculation because of the diffusive wave approximation. XBeach, however, uses full terms of the NLSWEs, including the inertial term, and hence accounts for the high flow velocities over the dyke, thus calculating more inland discharges. Bearing on a diffusive wave approximation in the surface calculations of HGS represents indeed one of the weaknesses of Yang's study (see also *Remark 6.2* in section 6.3). In fact, such incorrect estimation of the inland flow rates in Yang's study results in an incorrect simulation of the flood propagation, induced water depths and flood extent as proved by Elsayed and Oumeraci (2016b). Thus, incorrect estimation of flood extent and water depths might also affect the results of the subsurface flow and the contaminant transport.

The identical inland discharges for both simulation scenarios mean that considering the morphological evolution in the *Morpho-on* scenario has no effect on the inland flow for this specific case. The latter becomes clearer from Fig 7.5, which compares the evolution of bed levels and water surfaces along the whole profile.

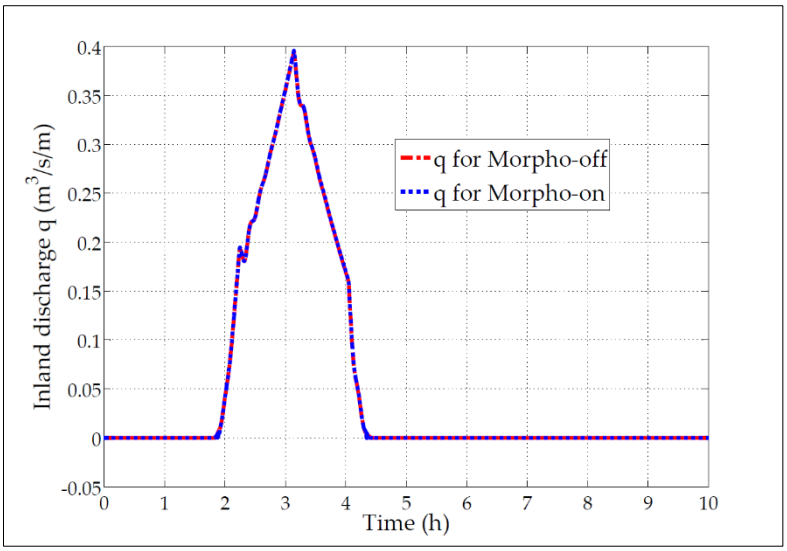

Fig 7. 4: Temporal development of inland discharges *q* calculated at the dyke crest (Point A in Fig 7.2) for both modelling scenarios *Morpho-off* and *Morpho-on* during the 2.8 h dyke overtopping as indicated by the storm surge event in Fig 7.3.

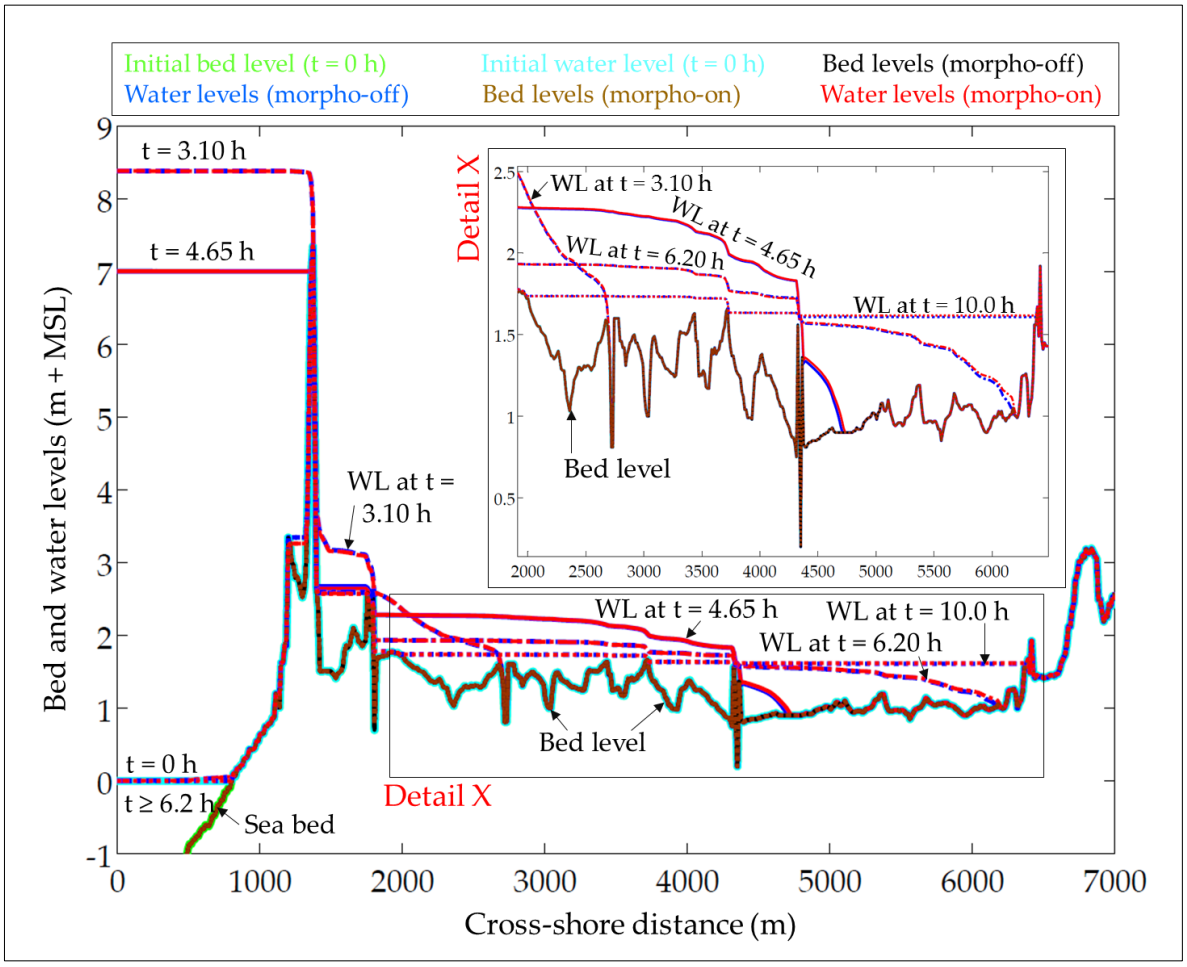

Fig 7. 5: Evolution of the bed level (BL) and water levels (WL) for the cross-shore profile in Fig 7.2 under the effect of the storm surge event in Fig 7.3 with and without considering the morphological evolution.

Fig 7.5 compares the evolution of the bed and water levels for the simulation scenarios *Morpho-on* and *Morpho-off*. It shows that the flood extents for both scenarios are identically increasing with the time marching until water flow is blocked after 10 hours at a cross-shore distance of 6400 m because of the

local increase of the ground elevation at this point. Therefore, the flood extends 5000 m behind the dyke for both simulation scenarios. Water depths along the 5000 m are spatially varying because of the spatial variation of the ground surface. Fig 7.6 clearly shows these variations through comparing the initial (at t = 0 h) and the final (at t = 10 h) bed and water levels for both simulation scenarios.

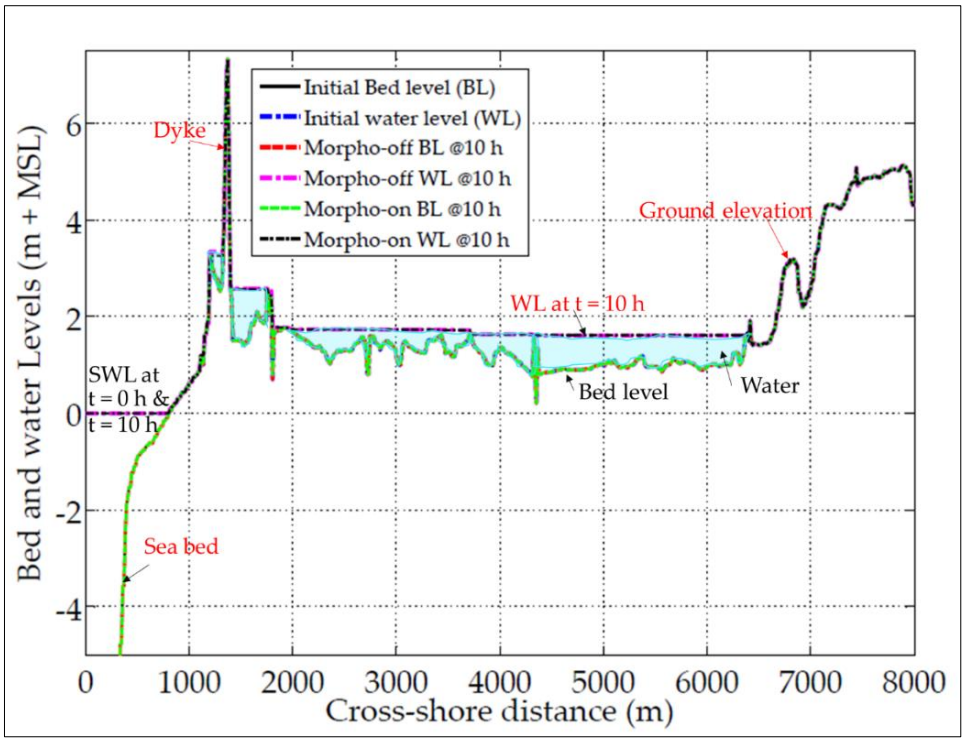

Fig 7. 6: Pre- and post-storm sea, inundation and bed levels at Bremerhaven for both *Morpho-on* and *Morpho-off* scenarios. The flood extends 5 km behind the dyke until water is blocked at a cross-shore distance of 6400 m. Water depths at t = 10 h are spatially varying because of the spatial variation of the ground elevations.

7.3.2 Role of bed friction and hinterland topography

The bed levels in both modelling scenarios show a non-evolutive behaviour, even with the permission of such evolution in the *Morpho-on* scenario. In order to understand the reason behind such a behaviour, a third modelling scenario is performed. The latter scenario is identical to the scenario *Morpho-on* but a unique value for bed friction coefficient is used ($n = n_1 = 0.00864\ m^{-\frac{1}{3}}.s$). This means that the used friction value for the beach area in front of the dyke ($n_1 = 0.00864\ m^{-\frac{1}{3}}.s$) is generalized over the cross-shore profile. Thus, the higher roughness values at the dyke (n_2) and behind it (n_3) are reduced to the value n_1. The idea behind this scenario is to allow higher flow velocities over the dyke crest and behind it by reducing the bed friction. Higher flow velocities definitely stir more sediment, which is transported landwards and deposited behind the dyke. The evolution of the bed and water surface for this scenario is shown in Fig 7.7.

When a lower Manning value is assigned for both the dyke zone and the hinterland, the dyke is totally overwashed, which allows the dyke inundation and induces accordingly higher water depths and wider flood extent behind the dyke. The topography plays indeed an important role in limiting the flood extent because of blocking the water flow at higher ground elevations (see also Yu et al. 2016b). After the storm peak (at t = 3.10 h), the flood extent retreats with the decrease in the SWL and with the induced return of the water to the sea (ebbing/recession conditions). However, part of the flood water is stored in the depressions as shown in Fig 7.7. Now, for the *Morpho-on* scenario, it is clear that the high Manning value at the dyke zone ($n_2 = 2.592\ m^{-\frac{1}{3}}.s$) limits the flow velocity over the dyke to be always under the threshold value for the onset of sediment motion as described by the Shields criterion (Shields 1936). As a result, no morphological evolution takes place with *Morpho-on* scenario as this is

the case for the *Morpho-off* scenario. This is indeed the reason why both *Morpho-on* and *Morpho-off* scenarios provide identical outcomes for the flood extent and water depths. The latter in fact reflects the significant importance of identifying proper values for the bed friction.

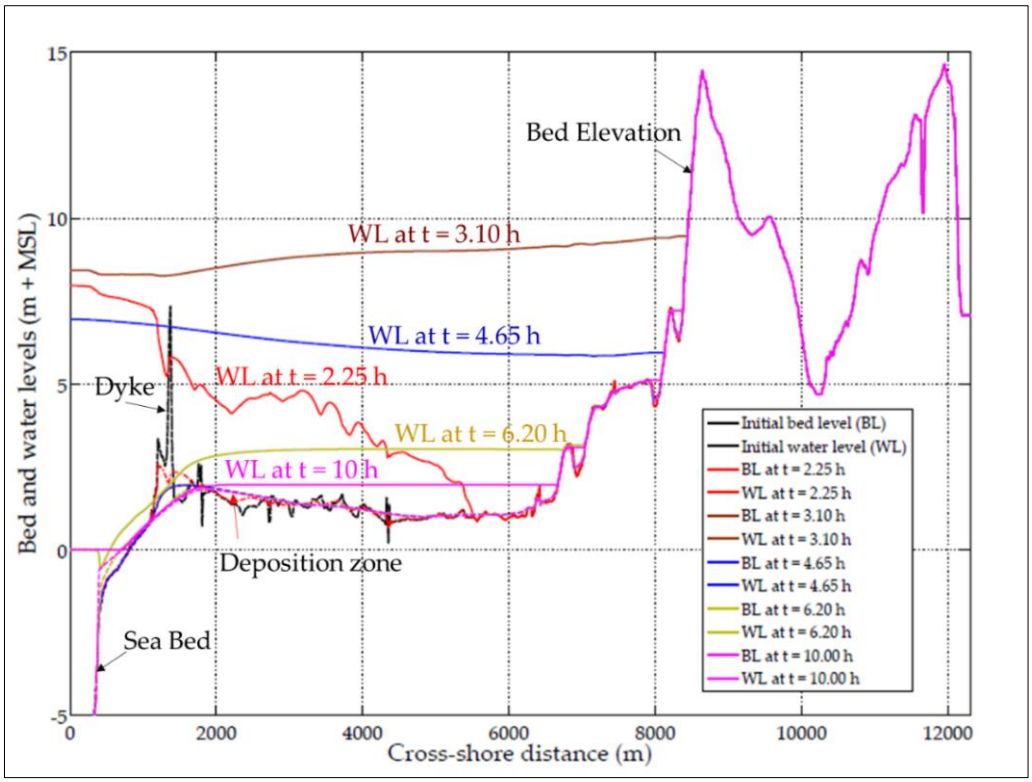

Fig 7. 7: Evolution of bed and water levels during the overtopping event near Bremerhaven for the scenario of using uniform and low bed roughness coefficient over the entire shore profile (beach, dyke and hinterland).

7.3.3 Outcomes of the combined modelling of overtopping flow and inundation using XBeach

The temporary rise of the sea level due to the storm surge event as shown in Fig 7.3 results in overtopping flow of the dyke near Bremerhaven. The overtopping discharges develop as indicated in Fig 7.4. Such an overtopping event does not induce any morphological changes because of the assumed high bed friction over the dyke surface whilst it results in a flood propagation in the hinterland. The flood extent expands with time marching until it reaches 5 km behind the dyke after 10 hours. After this extent, the water flow in the downstream direction is blocked by a local rise in the ground elevation as shown in Fig 7.6. The water depths during such a flood event vary spatiotemporally as shown in Fig 7.8 because of the temporal variation of the inland flow rates and the spatial variation of the ground elevations.

Table 7.3 summarises the main outcomes of the combined modelling of the overtopping flow and the flood propagation using XBeach, including a comparison with the outcomes of Yang et al. (2013) for the same study area.

Table 7. 3: Comparison of the main outcomes of analysing water overtopping and flood propagation using XBeach with the outcomes of Yang et al. (2013).

Outcome	This study	Yang et al. (2013)
Overtopping volume (m^3)	2196	1045
Max. overtopping rate ($l\ s^{-1}$)	~ 400	200
Accompanied amount of salt (tonnes)	54.9	26.125
Flood extent behind the dyke (km)	5.0	1.6

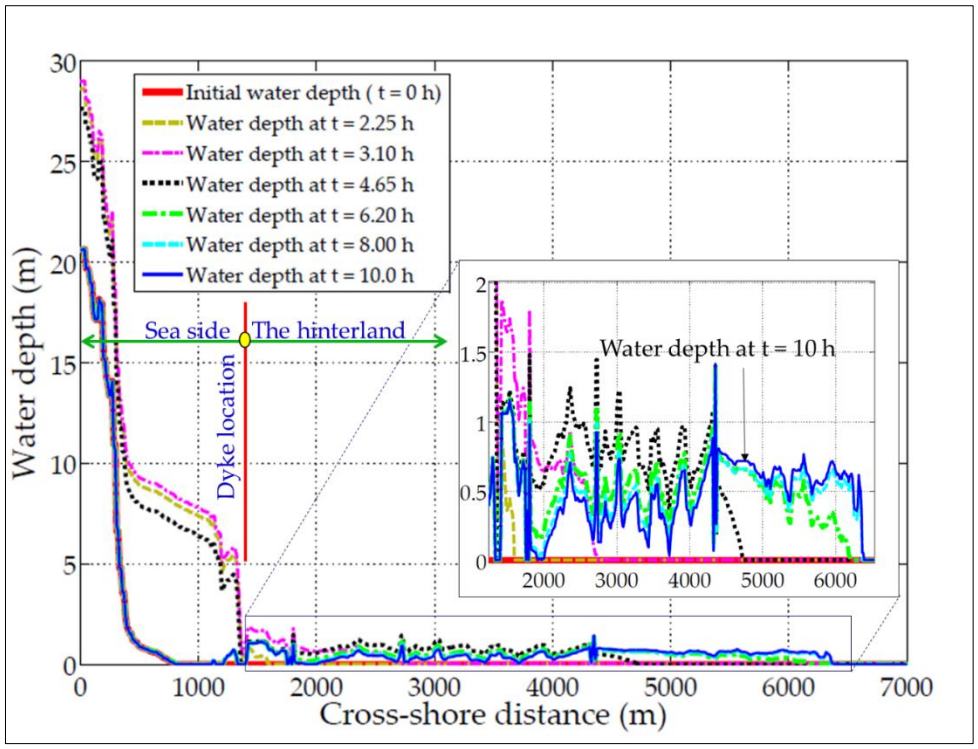

Fig 7. 8: Temporal and spatial variations of the water depths in front and behind the dyke at near Bremerhaven owing to the sea level rise scenario in Fig 7.3.

The outcomes in Table 7.3 show that the use of the surface module of HydroGeoSphere (HGS) in the study of Yang et al. (2013) to estimate the inland discharge results in quite different values for overtopping rates and volumes. Accordingly, flood extent and water depths are also different. Such difference returns in fact to the diffusive wave approximation in HGS that omits the inertial terms in the NLSWEs of HGS which are dominant over the dyke because of the high flow velocities there. However, to provide an opinion on which model calculates better the inland discharge and to assess the extent of the archived improvements, observed data are certainly needed. The different estimates of the inland discharge do not affect only the surface flow but it also affects the saltwater intrusion process and the natural remediation intervals as discussed in the following section.

7.4 Modelling storm-driven saltwater intrusion near Bremerhaven using SEAWAT

Regulations related to groundwater development, contaminant source identification and aquifers remediation require first to specify the modelling hypotheses required for the formulation of the conceptual SDSWI model for the selected aquifer near Bremerhaven as described below.

7.4.1 Modelling hypotheses and conceptual SDSWI model for the selected site

The aim of modelling the SWI induced by the aforementioned inundation event near Bremerhaven is threefold:

(i) studying the distribution of the saltwater in the aquifer in addition to determining the maximum subsurface extent of the contaminant after the inundation event,

(ii) estimating the natural remediation interval that is needed for the aquifer to get remediated naturally, and

(iii) proposing a suitable mitigation measure to shorten the natural remediation time.

For this purpose, the water depths at the time of maximum flood extent in Fig 7.8 (i.e. at t =10 h) need to be transferred to the SEAWAT model of the aquifer. Nevertheless, the water depths along the flood extent spatially vary due to the spatial variation of the ground elevation. Therefore, to simplify the analysis some modelling hypotheses need to be addressed as follows:

(i) Tidal fluctuations in the sea can be omitted and hence a stable sea level of 0.00 m can be considered as the mean sea level (MSL);

(ii) All water overtopping the dyke will infiltrate into the aquifer along the flood extent, which means that no evaporation is considered during the percolation time;

(iii) The infiltration during the flood propagation, i.e. before flood water gets standing (interval of 10 h), can be omitted;

(iv) The standing water, after the interval of 10 hours, infiltrates into the aquifer by a rate depending on both the hydraulic head difference and the conductance rate from the land surface to the GWT. This will be performed using the Modflow RIV package as will be discussed later in Section 7.4.4;

(v) The inland flow (2196 m^3) is uniformly distributed along the flood extent of 5 km as shown in Fig 7.9, which means that a water depth h = 0.44 m averaged over the flood extent - and not the spatially varying water depth - is considered as the external head causing the vertical intrusion of saltwater. This substitution aims at simplifying the input head to the saltwater intrusion model.

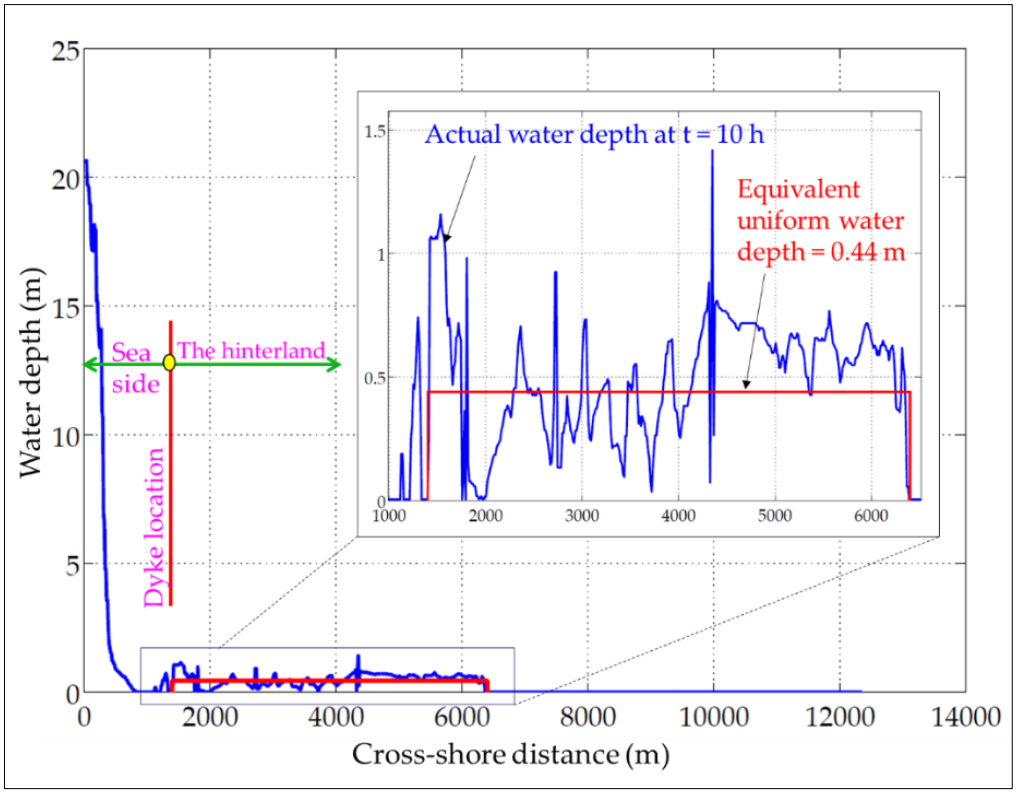

Fig 7. 9: Substitution of the spatially variable water depth h(x) in the hinterland by a water depth (h = 0.44 m) averaged over the entire flood extent (5 km) for simplifying the input head to the saltwater intrusion model.

Using the aforementioned hypotheses as well as the model data from Section 7.2, the conceptual model of the aquifer can be drawn as shown in Fig 7.10. A constant domain bottom elevation of −100 m.a.s.l. is used as the aquifer bottom, which is assumed impermeable. At the seaside, a constant water head (h = 0 m) and a constant salt concentration (C = 25000 mg /l) with seawater density ρ_s = 1018.3 kg/m^3 are considered as indicated in Table 7.1. At the landside boundary, a constant water head (h = 4 m) and a constant concentration (C = 0 mg /l) are also considered, but with a freshwater density ρ = 1000 kg/m^3. Along the ground surface, from the shore line to inland, an effective surcharge is considered with 300 mm/yr, which represents a feeding source of freshwater. Another external load (vertical saltwater intrusion) is considered along with the 5-km flood extent behind the dyke, which

represents the contamination source at the ground surface (Fig 7.10). The aquifer properties (e.g. hydraulic conductivity, porosity, etc.) are assigned using the values in Table 7.1.

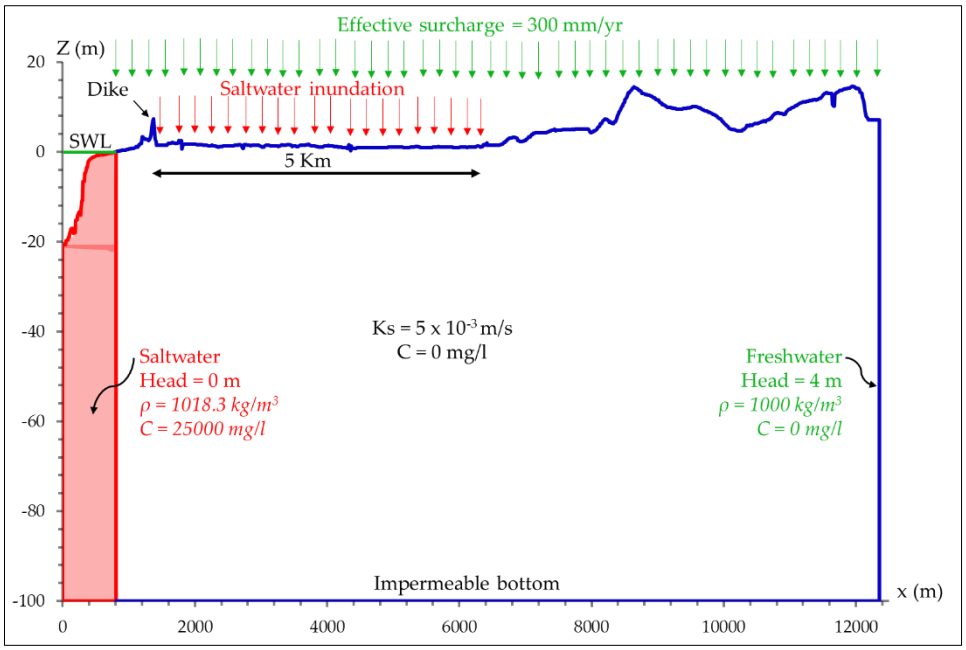

Fig 7. 10: Conceptual model for storm-driven saltwater intrusion (SDSWI) in the selected aquifer near Bremerhaven: Red colour indicates seawater inflow with saline concentration (C) equals saline concentration in seawater while green colours indicate freshwater inflow with C = 0.

7.4.2 Numerical model setup in Visual Modflow

The conceptual SDSWI model from Fig 7.10 of the aquifer near Bremerhaven is set up in Visual Modflow using 500 columns in X-direction ($\Delta x = 24.6\ m$), 1 row in Y-direction ($\Delta y = 1.0\ m$) and 24 layers as shown in Fig 7.11.

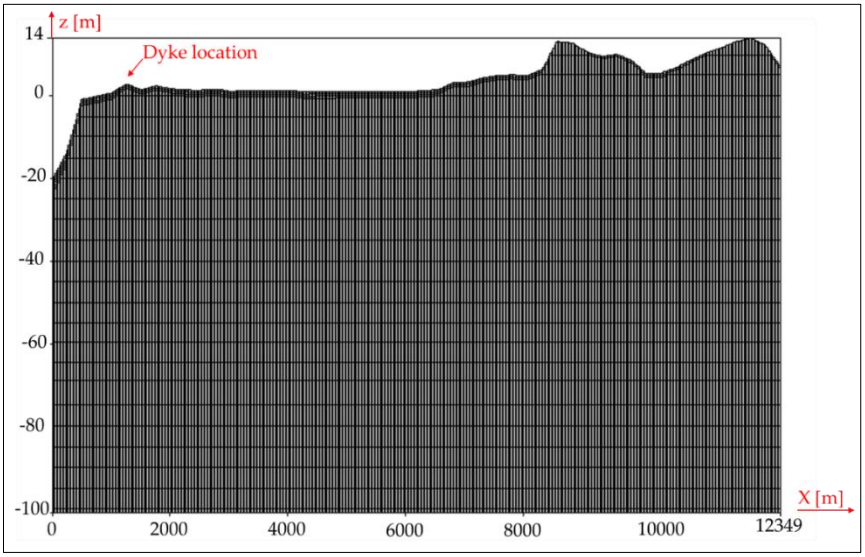

Fig 7. 11: Setup of Bremerhaven aquifer model in Visual Modflow: Grid setup

The layers' thicknesses are small near the ground surface while they have uniform thicknesses of 5 m downwards. Because Modflow utilises rectangular meshes, the ground surface, especially the dyke zone, cannot be reproduced with a sufficient accuracy. For each cell (prism), the aquifer properties in Table 7.1 are assigned. For instance, a kx, ky and kz value of 0.005 m/s is assigned for each cell to represent a homogenous soil of hydraulic conductivity equals 0.005 m/s. After assigning the aquifer

properties (i.e. hydraulic conductivity, porosity…etc.), two initial conditions are defined. Frist, the initial water head in the aquifer is set at 0.25 m above the reference level, which is the mean sea level (0.00 m.a.s.l). This initial head is roughly chosen as an initial condition for the head in the aquifer. Second, the initial salt concentration in the aquifer is set at 0 mg/l except at the seaside boundary it is set at 25000 mg/l. The other boundary conditions are defined in Fig 7.10. For instance, constant water head boundaries of 4.00 m and 0.00 m are defined at the landward and seaward boundaries, respectively. Applying this model, two modelling situations are considered: (i) pre-storm conditions and (ii) storm and post-storm conditions. The details of these two situations are summarised in the next sections below.

7.4.3 Modelling pre-storm conditions

This phase can be considered as "warm-up" phase of the model in order to eliminate the effect of initial conditions. For this purpose, the model is run for ten years so that the time for the flow and transport to reach a steady state can be determined. Therefore, the model is run by considering the same boundary conditions in Fig 7.10 without considering the saltwater inflow from the upper boundary. The system reaches the steady state after three years (1095 days) as visible from Fig 7.12, which displays the mismatch between inflow (q_{in}) and outflow (q_{out}) rates to/from the aquifer. The net flow becomes almost stable after 1095 days with a value of 0.26 m^3/day.

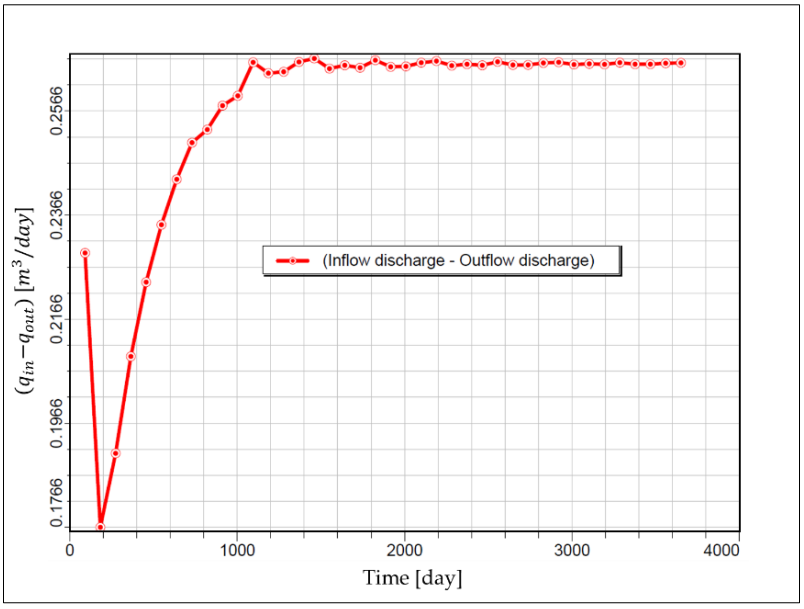

Fig 7. 12: Net flow rates from/to the aquifer under the considered boundary conditions in Fig 3.14 without the vertical saltwater intrusion: a steady state is reached after 1095 days.

The stable net flow after three years means that the water budget in the investigated aquifer is stable (i.e. inflow = outflow +/- change in storage). This, therefore, means that the change in storage has reached a constant value and that the flow in the aquifer has reached a steady state. The latter becomes clearer from Fig 7.13, which displays the head distribution in the aquifer after 3 months, 1 year, 3 years and 10 years, respectively.

As shown in Fig 7.13, the water heads in the aquifer range from h = 4.0 m.a.s.l. at the landward boundary to h = 0.0 m.a.s.l. at the seaside boundary. The part of the soil above the GWT is partially saturated while the uppermost part is almost dry. The equipotential head contours shift seaward with time marching (see Fig 7.13 panels a and b) until they become stationary after three years as can be noticed by comparing panel (c) with panel (d) in Fig 7.13. Such stationary equipotential contours mean that the system reached a steady state. The elapsed time to reach the steady state (3 years) depends indeed on the assigned initial conditions. Therefore, further the initial conditions from the real

conditions in the aquifer, the more time elapsed to reach a steady state. The latter means that defining different initial conditions will definitely result in different time interval until reaching a steady state.

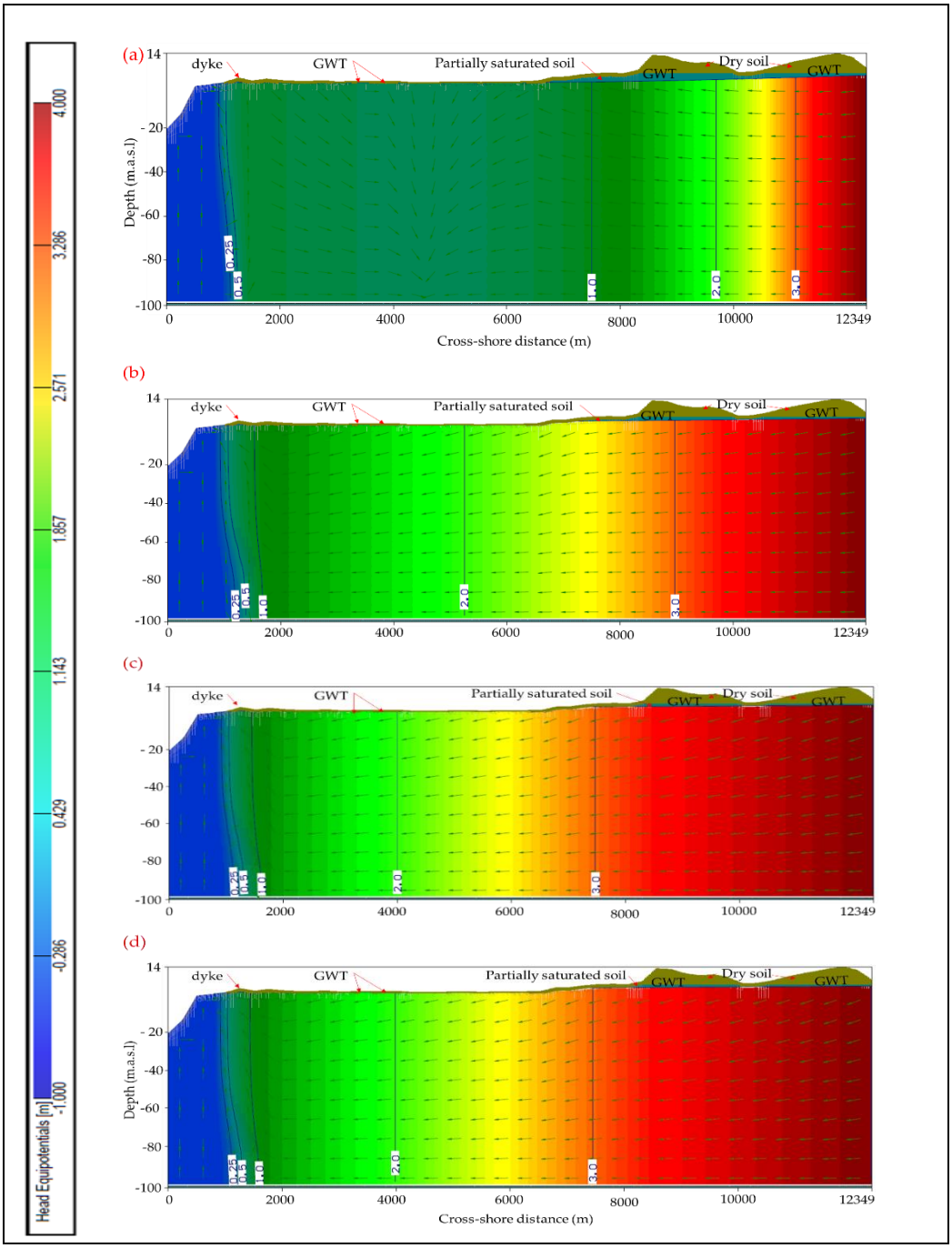

Fig 7. 13: Head distribution (equipotential heads above m.a.s.l) and flow field in Bremerhaven aquifer after (a) 3 months, (b) 1 year, (c) 3 years and (d) 10 years, all under the effect of 4.0 m and 0.0 m constant heads at the landward and seaward boundaries, respectively. Arrows represent the flow directions from the landward to seaward. Equipotential head contours (m) are stationary after 3 years (c and d) because the system reaches a steady state.

Despite the flow of freshwater in the seaward direction as shown in Fig 7.13, the salt water intrudes laterally into the aquifer to the landward direction because of being heavier than freshwater. Saltwater intrusion reaches the equilibrium condition after 290 days (< 1 year). This equilibrium condition represents the position when the mismatch between the source mass (salt entering the freshwater aquifer) and the sinking mass (salt leaving the aquifer) becomes stationary (see e.g. Oz et al. 2014). Such

a situation is indicated in Fig 7.14, showing after 290 days a constant mismatch between the accumulative amount of salt entering the aquifer through the seaside boundary (represented by the red curve) and the accumulative mass of salt leaving the aquifer through the same boundary after the dilation process (the green curve). In fact, saltwater intrudes laterally through the seaside boundary and recirculates after the dilatation process to leave the aquifer through the same boundary. The net mass (brown curve in Fig 7.14) represents the mass of the salt remaining in the aquifer after the recirculation.

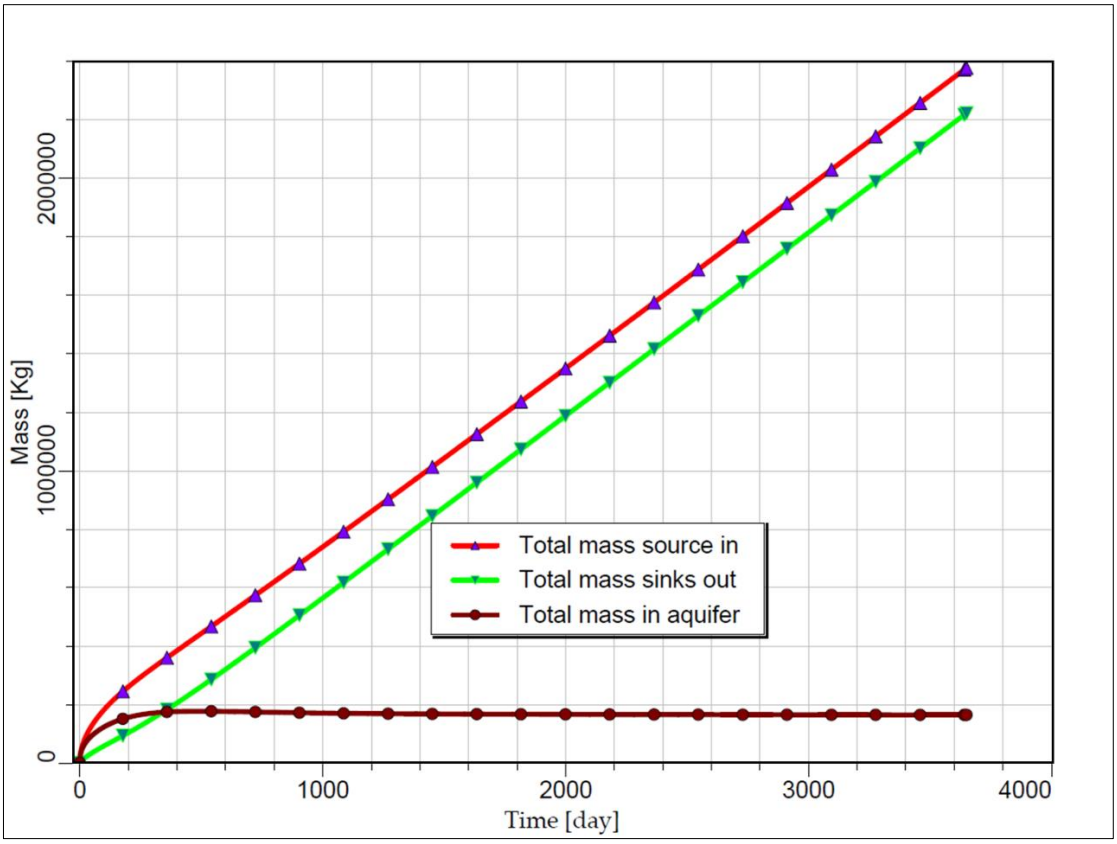

Fig 7. 14: Accumulative salt masses entering the aquifer as a source in (red curve), leaving the aquifer as a sink out (green curve) and accumulative salt mass remaining in the aquifer (brown curve). The latter mass curve represents the mismatch between the former two masses and it is stationary after 290 days because the system reaches an equilibrium state.

As shown in Fig 7.14, the net mass (brown curve) is constant after 290 days which means that the salt-freshwater interface (represented by the 50% isoconcentration contour as shown in Fig 7.15) becomes stationary after 290 days because the net mass (source in - sink out) in the aquifer is constant.

The salt distribution in Bremerhaven aquifer due to the lateral intrusion in Fig 7.15 shows that the salt is migrating landward with the time marching. The latter is quite clear by comparing panels (a) and (b), which show a landward migration of the 50 % [corresponding to $C = \frac{(C_{seawater} - C_{freshwater})}{2} = \frac{25000-0}{2} = 12500$ mg/l], 2% (C = 500 mg/l) and 0% (C = 0.01 mg/l) isoconcentration contours in panel (b) than the same contours in panel (a). The system reaches the aforementioned equilibrium situation after 290 days, which might explain why the 50 % and 2% isoconcentration contours become stationary as shown by comparing panels b, c and d of Fig 7.15. Nevertheless, the 0% contour is still migrating landward with the time marching. The zone in the right of the latter contour line is purely freshwater without any dissolved salts. Therefore, it is the safest zone for pumping. The 2% isoconcentration contour corresponds to the maximum allowable dissolved salts in drinkable water according to the standards of the World Health Organisation (WHO 2011) and the European water framework directive (Kaika 2003). Therefore, any pumping from the zone at the right side of the 2% isoconcentration contour

could also be possible. Of course, the farther the pumping well is from the 2% contour line in the landward direction, the more usable the extracted water and also the better to avoid further intrusions and upconing in the case of excessive pumping.

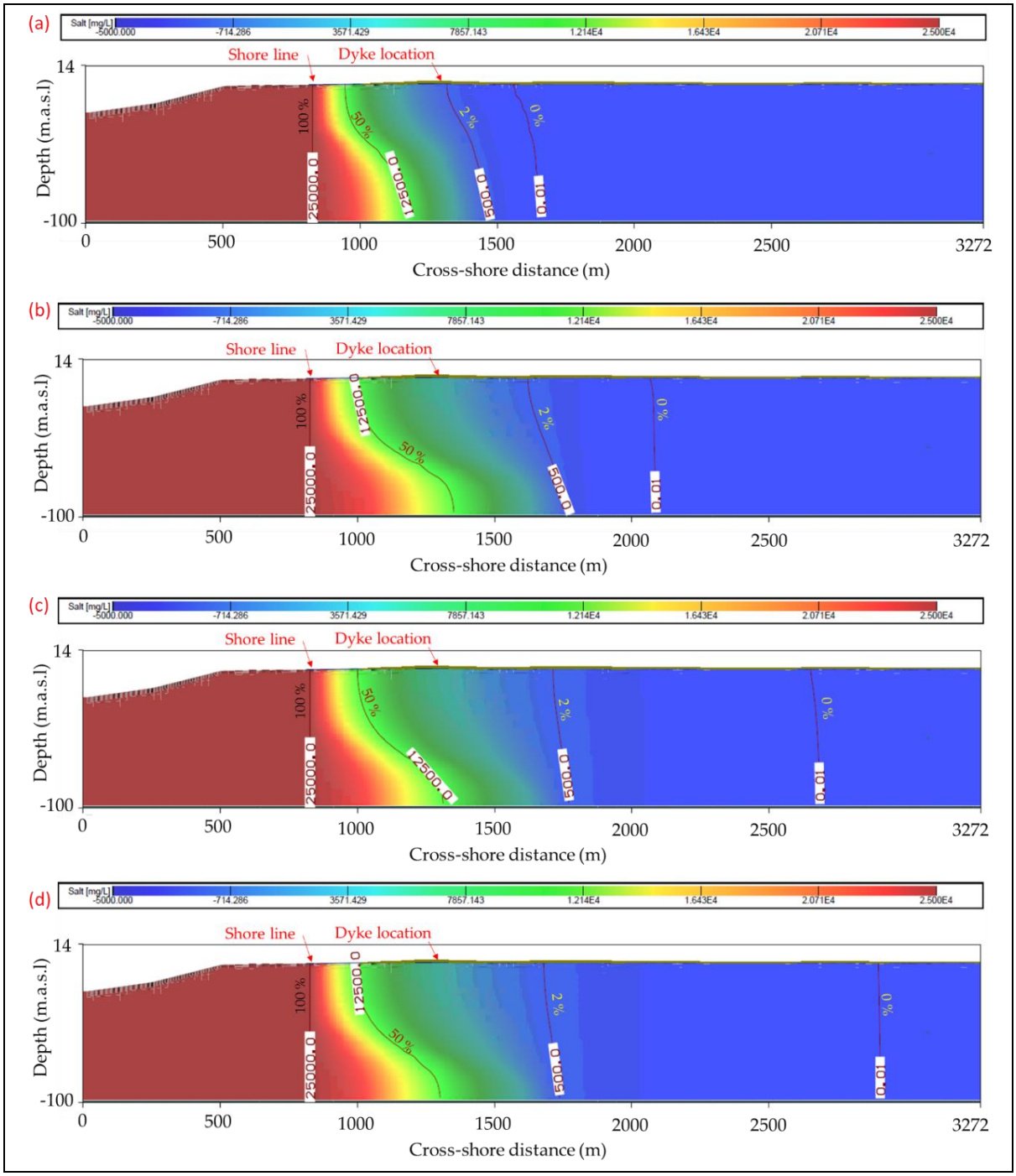

Fig 7. 15: Salt distribution in Bremerhaven aquifer due to the lateral intrusion after (a) 3 months, (b) 1 year, (c) 3 years and (d) 10 years. Salt-freshwater interface represented by 50% isoconcentration and the isoconcentration line of 500 mg/l (2%) are stationary in panels b, c and d (500 mg/l = max. salt concentration for drinkable water according to WHO).

It is also important to clarify that the equilibrium condition of the isoconcentration contours achieved here is a function of the model inputs. This means that any increase in the sea level will definitely result in further salt water intrusion landward. The same could be achieved by decreasing the effective recharge value less than 300 mm/year, which might decrease the GWT. Therefore, the sea level rise and the recharge value and/or the level of the GWT are the triggering factors, which determine

the equilibrium condition in the aquifer. These factors could be indeed affected by climate change (Parry et al. 2007; Stocker et al. 2014; Vousdoukas et al. 2017). Nevertheless, they are assumed stationary in this study.

7.4.4 Modelling storm and post-storm conditions

The main goal of analysing the pre-storm situation is to determine the elapsed time to achieve a steady state for the flow in addition to the equilibrium state for the mass transport. Such warming up phase was necessarily required to eliminate the effect of the assumed initial conditions and to achieve a real state in the aquifer before further analysis of the storm and post-storm conditions. It is found that the flow reaches the steady state after 1095 days (3 years) while the salt-freshwater interface induced by the lateral intrusion of seawater become stationary after 290 days (< 1 year). Therefore, it might be implied that the effect of the initial conditions on both flow and mass transport is totally eliminated after three years. Considering this result, a subsequent model for the storm and post-storm conditions can be run, so that the flood-induced head can be assigned to the model at any time after the three years of the warming up phase. In fact, in the analysis of the storm and post-storm conditions, the effect of the flood-induced inundation should be considered, in addition to the boundary conditions used in the pre-storm conditions. However, the latter effect should be applied after reaching the steady state in the aquifer (i.e. at any time after 3 years for model warming up). In the current situation, the inundation load is applied 5 years (1825 days) after the simulation start, i.e. 2 years after reaching the steady state.

The inundation effect can be assigned to the model of the storm and post-storm conditions through the Modflow River Package (RIV), see Section 7.1. The latter package enables a virtual definition of an external and uniform water head above the ground surface for a certain time. As a result, the interaction between the surface head and subsurface flow in the aquifer is possible through the conductance value calculated by the RIV package, which represents a proxy coefficient measure for calculating river-aquifer interaction (Korkmaz et al. 2016; Pérez-Paricio et al. 2010). The conductance value for the River boundary condition (C_r) in each grid cell is automatically calculated from the length of the river reach through a cell (= Δx = 24.6 m) (see Section 7.4.2 for the model meshing), the width of the river in the cell (= Δy = 1.0 m), the vertical distance (M) between riverbed (ground level) and the GWT, and a representative value for hydraulic conductivity of the soil beneath the river bed (Kr) using the following formula:

$$C_r = \frac{K_r \,.\Delta x \,.\Delta y}{M} \tag{7. 2}$$

Eq. 7.2 calculates uniform conductance rate C_r $[m^2/day]$ at any specific point under a constant head. Nevertheless, the conductance rate could vary spatially because of the spatial variation of M, K_r or Δx. Since the hydraulic conductivity Kr decreases significantly with the volumetric water content (see e.g. Nimmo 2009), Kr is assumed based on the soil type by 5 x 10^{-6} m/s for the vadose zone extending from the land surface to the GWT. Based on Eq 7.2, it is found that the inland volume of 2196 m^3 will be conducted to the aquifer within 4 days. In fact, the reliability of the latter conducting time is not of high importance since this time is very short relative to the natural remediation interval (see section 7.4.4.2). Therefore, conducting the flood volume to the aquifer in 4 days will not differ so much than conducting the same volume in 1.0 hour or even in two months. This is because the movement of water in the aquifer is very slow, which means that the conductance time is not of high importance to the salt transport in the aquifer. What is really important is the conductance volume (2196 m^3) which should equal to the inland water volume in order to ensure that the same overtopping volume is conducted to the aquifer.

Using the RIV package of Modflow, the inundation volume is transferred to the aquifer along the 5 km behind the dyke. It is assumed that the flood event will take place five years (1825 days) after the start of the simulation in order to totally ensure that the model reaches the steady state before activating the conduction through the RIV package. In order to cover the time needed for the natural remediation of the aquifer after such inundation event, the model is run to simulate a period of 50 years (18000 days). The first five years are prior to the inundation, followed by 4 days for the inundation, whilst the

remaining time (45 years minus 4 days) is used to specify the interval required for the natural remediation. The effect of such inundation event on the flow and mass (salt) transport in the aquifer are discussed in the following subsections.

7.4.4.1 Effect of salt water inundation on water flow in Bremerhaven aquifer

The model is run for 50 years (see Fig 7.16). The first five years are considered as a warming up time. As a result, the model reaches the steady state after 1095 days (3 years) as previously discussed in Section 7.4.3. The flow remains in the steady state till the application of the inundation effect at t = 1825 days (5 yr). During the steady state (t = 1095 - 1825 days), the net flow (inflow discharge minus outflow discharge) remains constant at 0.26 m^3/day (see Fig 7.16 Detail A). The constant uniform value for the net flow during the latter interval means that the change in storage is constant along the whole interval (inflow rate = outflow rate +/- change in storage). The conduction from the surface water at t = 1825 days due to flooding results in negative net flow values during and after the four days of inundation. Such a negative net flow remains indeed until t = 2000 days (i.e. for 171 days after the end of the inundation).

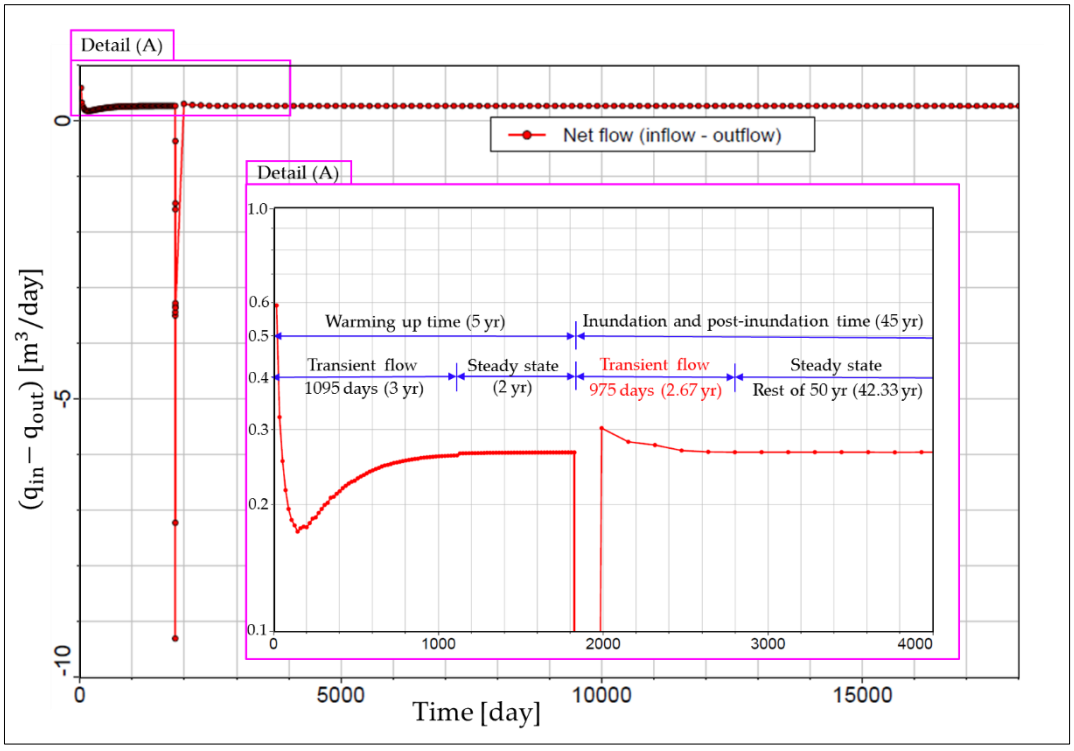

Fig 7. 16: Net flow rates from/to the aquifer under the considered boundary conditions: the system reaches a steady state after 1095 days (3 yr) and remains steady until the inundation event at t = 1825 days. Inundation disturbs the system, inducing transient flow for 975 days till flow returns to pre-flood conditions.

The negative net flow means that there is a defection in the storage budget in the aquifer (outflow is more than the inflow). By other words, the aquifer tends to release more water from the storage to substitute the sudden increase of the water head due to flooding. As a result, outflow through the seaside boundary during the latter interval (from t = 1825 to 2000 days) increases more during this interval than before the flooding, thus allowing more water to leave the aquifer and substitute local increase of head beneath the flood zone. In the same time, inflow through the landward boundary decreases for the same reason. In fact, the local increase of the water head beneath the inundated zone (see Fig 7.17 b and c) causes the inflow discharge from the landward boundary to decrease, while the outflow through the seaward increases. At t = 2000 days, the inflow to the aquifer increases, mainly because of the decrease of the local water table beneath the flooded zone. The latter results in a net flow equal 0.3 m^3/day (see Detail A in Fig 7.16), which decreases to 0.26 m^3/day within 800 days (i.e. from t = 2000 to 2800 days). Therefore, the surface conduction of the flood water to the aquifer disturbs the

flow in the aquifer for 975 days (from t = 1825 to 2800 days) until the flow reaches the steady state again at t = 2800 days and remain steady until the end of the simulation.

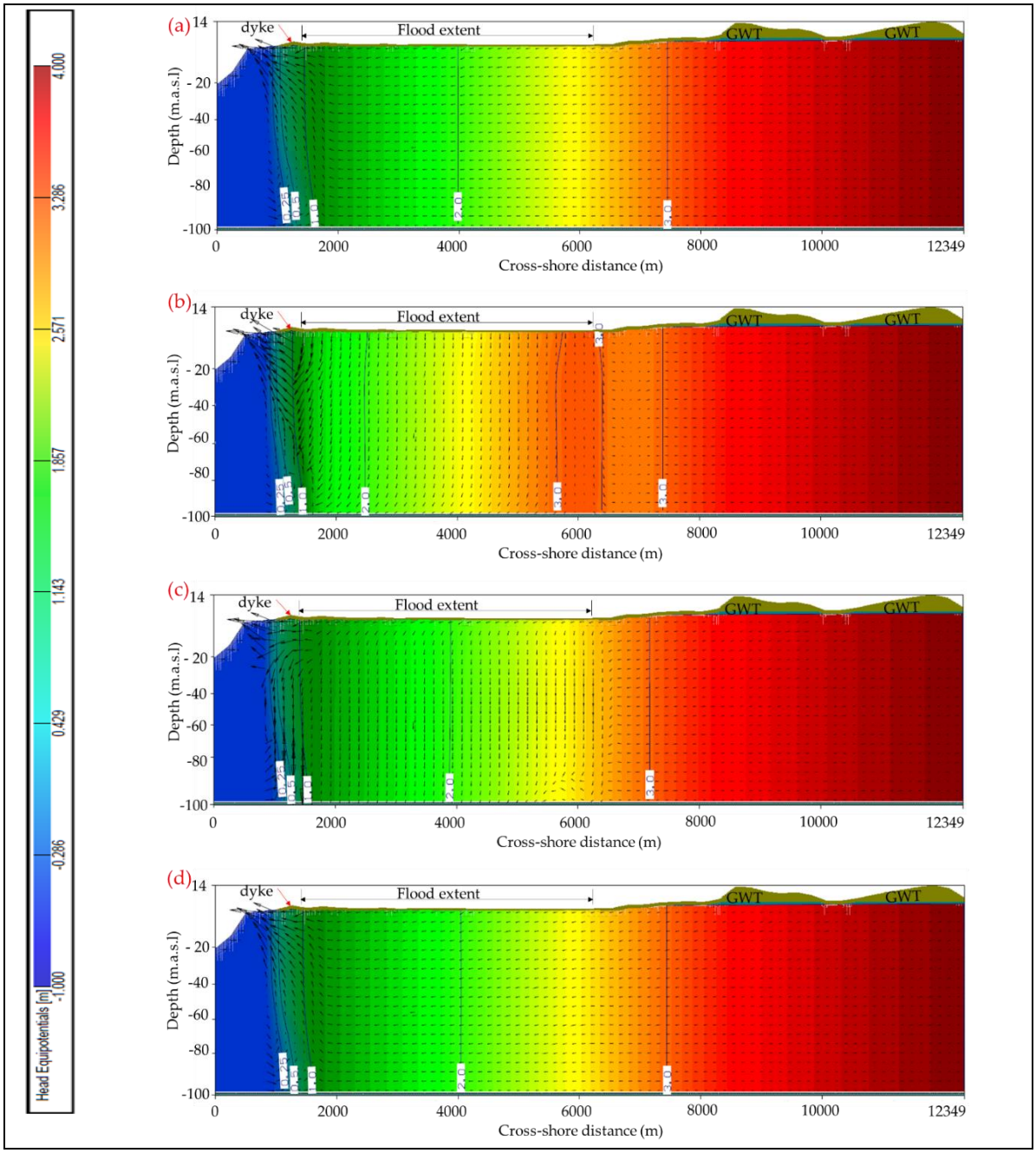

Fig 7. 17: Head distribution (equipotential heads above m.a.s.l) in Bremerhaven aquifer at (a) t = 1825 days (directly before the inundation), (b) t = 1827 days (during the inundation), where flow is directed downward beneath the inundated zone, (c) t = 2152 days (after the inundation interval by ~ 1 yr) and (d) t = 3000 days (after 3.2 yrs.). Inundation event starts at t = 1825 and ends at t = 1829. Constant heads of 4.0 m and 0.0 m at the landward and seaward boundaries, respectively, results in seaward directed flow. Arrows represent the flow directions. Equipotential head contours are stationary in panels a and d, meaning that flow reached again a steady state.

Fig 7.17 shows that the inundation event results in a local increase of the GWT beneath the inundated area. In fact, the flow in the aquifer is steady before the start of the inundation (at t = 1825 days) as shown in panel (a) of Fig 7.17. The latter panel is indeed identical to that at t = 1095 days, which is shown in Fig 7.13.d (comparison by considering locations of equipotential head contours); i.e. the

flow in the aquifer between t = 1095 days and t = 1825 days is in steady state. With the conductance from the surface water along the flood extent (x = 1400 - 6400 m) during the inundation (e.g. at t = 1827 days) as shown in panel (b) of Fig 7.17, the GWT increases locally beneath this extent (x = 1400 - 6400 m). The latter increase is quite clear from the shift of the equipotential head contours toward the sea boundary in panel (b) than in panel (a) of Fig 7.17. Such local increase in the GWT results (i) in downward directed flow velocities as shown in Fig 7.17 b and (ii) in a decrease of the inflow discharge from the landward boundary besides an increase of the outflow discharge at the seaside boundary, resulting in negative net flow discharges from t = 1825 to 2000 days as shown in Fig 7.16. With time marching, the flood-induced disturbance in the aquifer flow decreases until reaching again the pre-flooding steady state at t = 2800 days. The latter is clear from panel c of Fig 7.17 (at t = 2152 days), where the equipotential head contours shift landward again. The latter shift continues until reaching again the stationary condition starting from t = 2800 days till the end of the simulation at t =18000 days. The evidence for that is provided by the identical water heads at t = 3000 days in panel d and at t = 1825 days (for pre-flooding) in penal (a) of Fig 7.17.

Finally, it is worth to note that the conduction of 2196 m^3 of saltwater along the flood extent of 5000 m, in an interval of four days, results in a flow defection in Bremerhaven aquifer for 975 days (2.67 yrs.). This interval is relatively shorter than the interval needed for the natural remediation of the aquifer after such a saltwater intrusion event as discussed in the following section.

7.4.4.2 Effect of salt water inundation on fresh water in Bremerhaven aquifer

Being denser and miscible with freshwater in the aquifer, salt water at the ground surface along the flood extent infiltrates downward as shown in panels b & c of Fig 7.17. Infiltrating salt water blends with freshwater in the aquifer, which increases the groundwater salinity. Therefore, a defection of the salt mass budget of Bremerhaven aquifer is expected after such coastal flooding. In fact, the defection can be explained using the three curves in Fig 7.18, namely: the accumulative source in mass curve (red curve), the accumulative sink out mass curve (green curve) and the curve of total mass remaining in the aquifer (blue curve). The latter curve represents indeed the mismatch between the two former curves and therefore its values can be read separately from the vertical axis on the right (Fig 7.18).

The vertical leakage of saltwater within the conductance interval (t = 1825 – 1829 days) increases the accumulative source mass in the aquifer by 54.9 tonnes (See Detail (b) in Fig 7.18). Such increase of the source in mass cannot sink out immediately from the aquifer. The latter fact can indeed be interpreted through the accumulative sink out mass curve (green curve), which still shows the same gradual increase (without any defection) during the conductance interval despite the increase of the accumulative source in mass by 54.9 tonnes during the same interval. This means that the increase of the source in mass during the conductance interval is totally stored in the aquifer as represented by the blue curve. This stored mass sinks out the aquifer gradually until the aquifer is totally remediated after 44.3 years. The natural remediation interval is, therefore, the time needed after a coastal flood event in order to totally drain the contaminant (salt) from an aquifer and to reach again the pre-flooding situation. In this case, the Bremerhaven aquifer will be remediated totally and reach again the pre-flooding condition after 44.3 years. The latter means that freshwater zones in the aquifer, which are affected by the vertical leakage of salt water, will return to its initial state (0 mg/l of salt concentration) after this very long time. This recovery is due to the natural remediation of the aquifer owing to the seaward directed flow in addition to the recharged part of rain precipitations on the ground surface. In fact, seaward directed freshwater flow dilutes the infiltrating salt water and moves it seaward gradually until the aquifer is totally remediated. Indeed, latter processes are extremely slow and hence very long intervals are needed for total aquifer recovery. Nevertheless, shorter intervals can be accepted if higher concentration values are accepted. For instance, the pre-flood freshwater zones can achieve a salt concentration of 500 mg/l after 25 years (see panel (g) of Fig 7.19). The latter concentration is accepted as the maximum allowable salt concentration in drinkable water by the World Health Organisation (WHO) and the European water framework directive. The zones of higher/lower concentration can be determined by investigating the salt distribution in the aquifer at different times as shown in Fig 7.19.

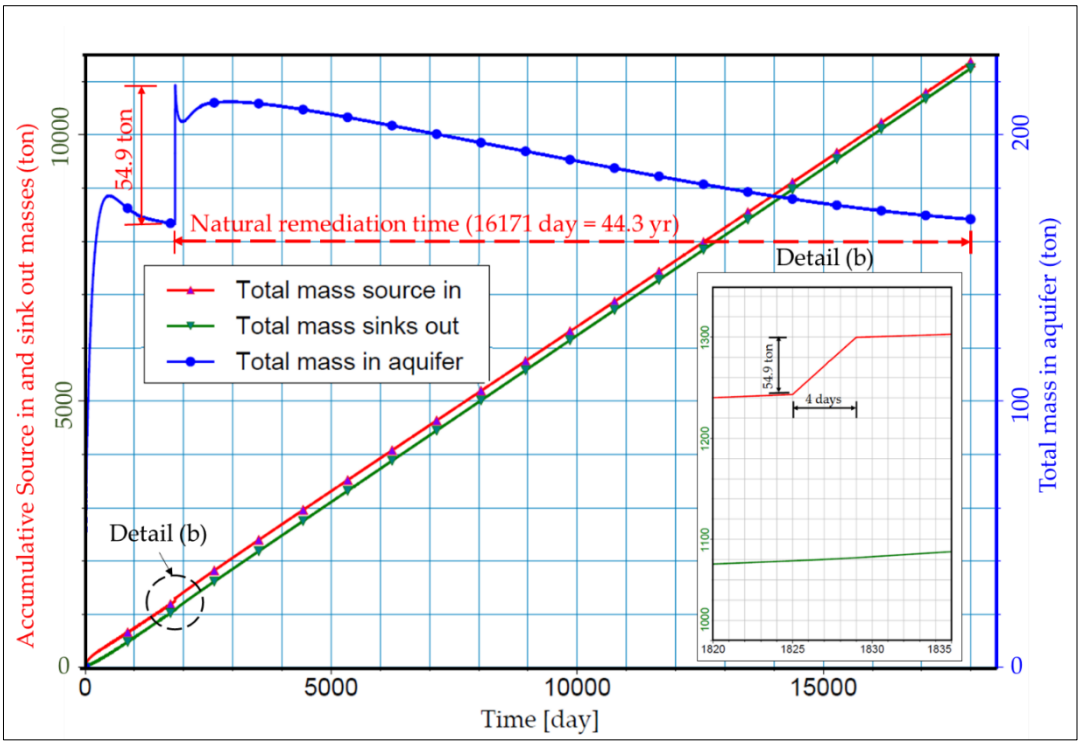

Fig 7. 18: Accumulative salt masses along the fifty years of simulation: red curve represents salt entering the aquifer as a source in, green curve represents salt leaving the aquifer as sink out and blue curve represents accumulative salt mass remaining in the aquifer. Detail (b) shows the increase of the source in starting from t = 1825 to t = 1829 days because of saltwater inundation, which results in an increase of the total mass in the aquifer by 54.9 tons during the inundation interval (4 days). The aquifer is remediated naturally after 44.3 years.

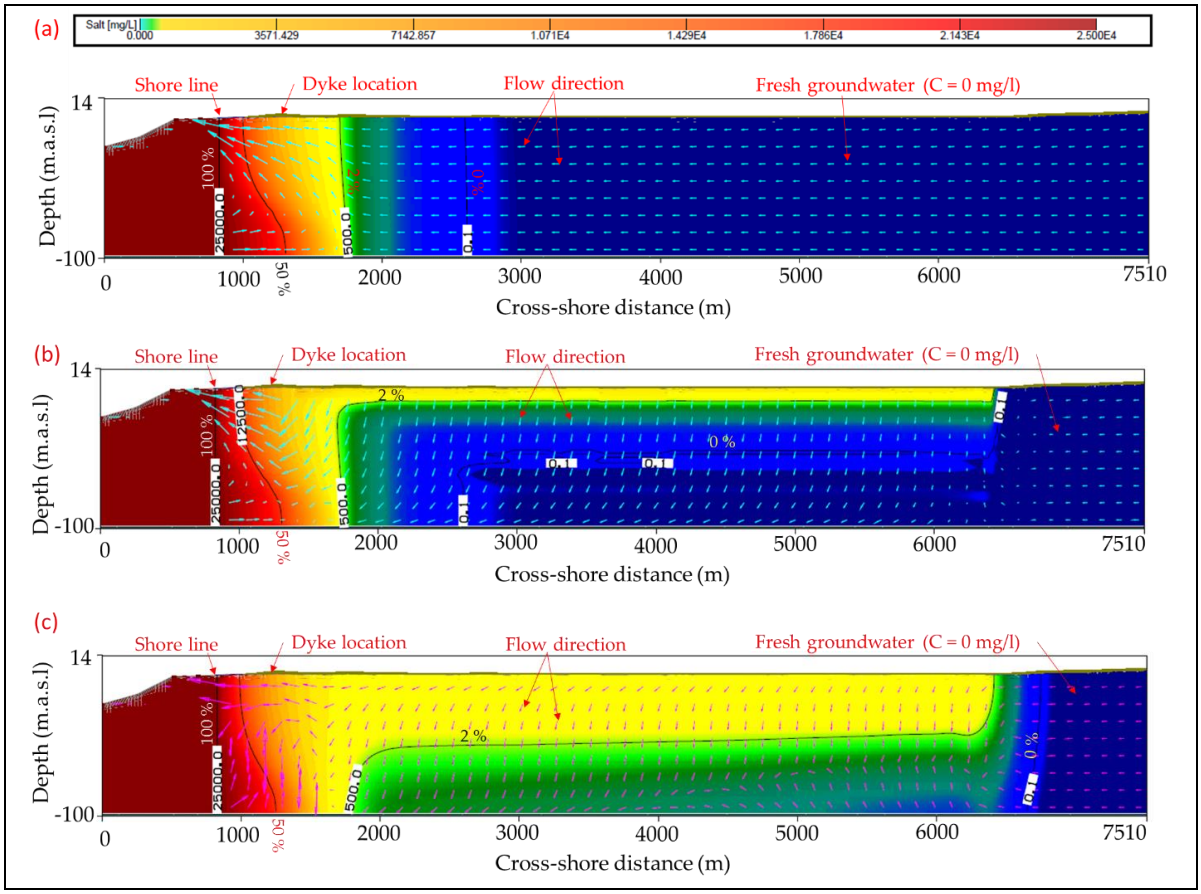

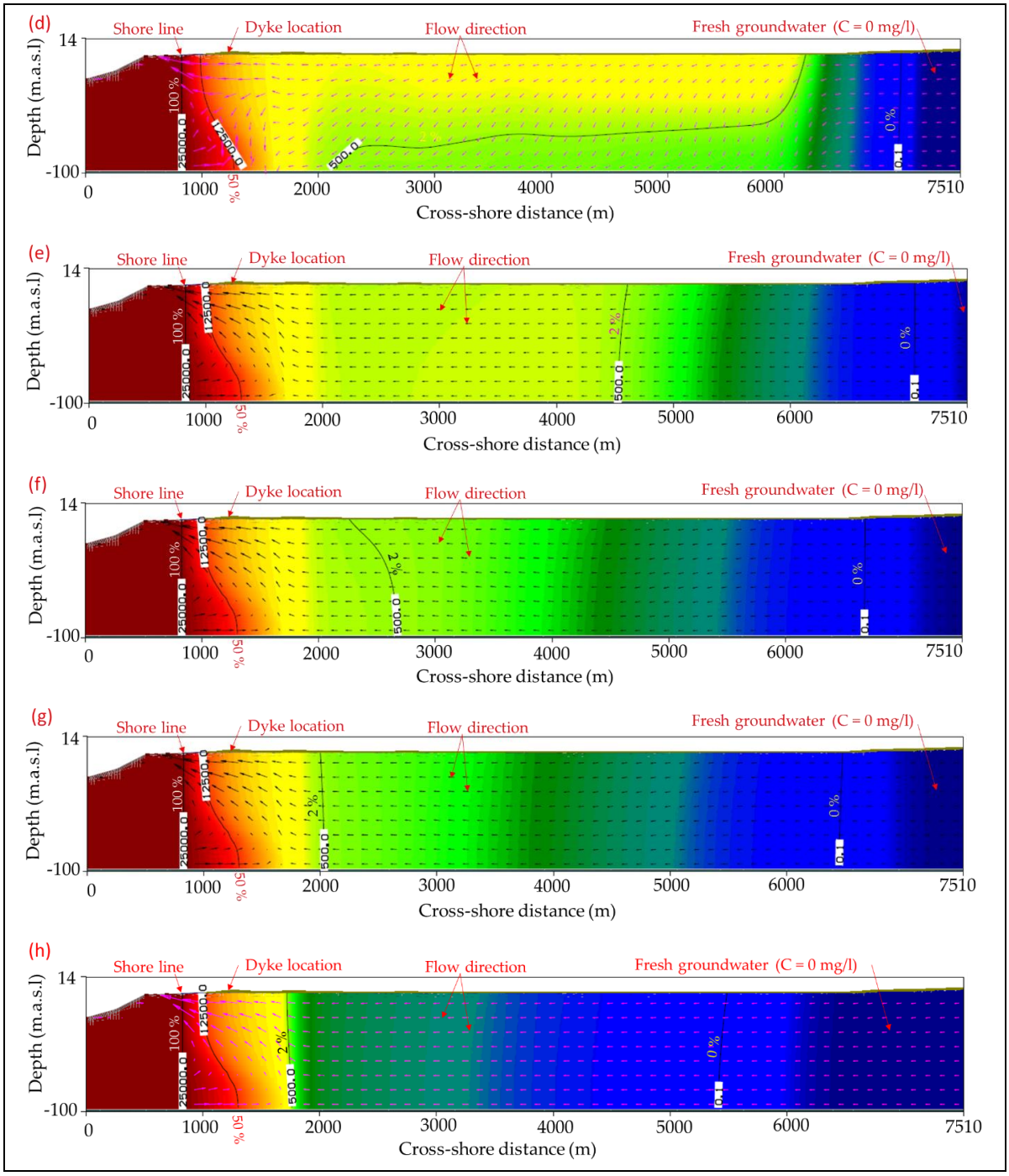

Fig 7.19: Evolution of salt distribution in Bremerhaven aquifer: (a) directly before inundation where the lateral intrusion only exists and (b - h) after the flood event where both lateral and vertical intrusions exist. Contamination extent is shown after 1 day (b), after 3 months (c), after 1 year (d), after 10 years (e), after 20 years (f), after 25 years (g) and after 45 years (h). Arrows represent the flow directions. Intruding salt water from the land surface moves almost vertically until it contaminates the whole aquifer depth (b-d) then it moves horizontally seaward (e - h) until reaching again the pre-flooding situation. Salt-freshwater interface, represented by the 50% iso-concentration contour, and the iso-concentration contour of 500 mg/l (2%) reach again the pre-flood situation (a) after 44.3 years (500 mg/l = max. salt concentration for drinkable water according to WHO).

Before the flood event, there is only lateral saltwater intrusion (panel (a) of Fig 7.19). After seawater overtopping, the salt water infiltrates into the aquifer along the 5-Km flood extent. The contaminant (salt) spreads vertically during the inundation interval as shown in panel (b) of Fig 7.19 since the infiltrating salt water is heavier in weight than the prevailing freshwater in the aquifer. Even after 3

months (panel (c)) and one year (panel (d)), the salt diffusion is still in the vertical direction. Therefore, saltwater moves vertically beneath the flood extent until it mixes with the fresh water along the aquifer depth. Such a vertical salt infiltration deviates toward the sea under the effect of seaward directed freshwater flow. In fact, freshwater moving seaward triggers the dilation process in the aquifer as shown in panels (e) – (h). This dilation process results in a process of natural remediation of the aquifer until the aquifer is almost remediated totally after 44.3 years as shown in panel (h) of Fig 7.19. By comparing the iso-concentration contours of 50 % and 2% in panels (a) and (h), one may notice that these contours are almost in the same position, which means that the aquifer is almost remediated after this relatively long interval.

The contamination of the same aquifer near Bremerhaven has also been studied by Yang et al., (2013) using the surface-subsurface model HydroGeoSphere. Yang's outcomes are shown in Fig 6.6 (see chapter 6). They reported that salt concentrations higher than 500 mg/l can still be found close to the aquifer bottom even after 20 years, which is consistent with the outcomes of this study in Fig 7.19 after 20 years (see panel (e)). The difference between both outcomes is the shape of saltwater spread. In Yang et al., (2013), plume fingers developed in the aquifer, while the analysis in this study show a uniform spread. The latter behaviour arose from applying a uniform hydraulic head as discussed in the modelling assumptions in Section 7.4.1. The former behaviour may be explained by the use of a surface-subsurface model in Yang et al. (2013) which enables earlier and longer infiltration time from the depressions, resulting in plume fingers (Yu et al. 2016b). Unlike this study, which specify the time interval for the total remediation by 44.3 years, Yang et al. (2013) did not specify this time interval because they were interested only in determining the remediation interval until reaching the limit 500 mg/l (the maximum salt concentration for drinkable water according to WHO).

It is finally important to stress the role of the purposed modelling assumptions on the results. By considering the study outcomes of Yang et al. (2013) as benchmarking for the current study, one may notice that the time needed to achieve the 500 mg/l salt concentration is 25 years which is only 5 years more than the time estimated by Yang et al. (2013) to achieve same concentration though the inland discharge was double. This means that longer time to reach the latter concentration was expected. In fact, part of differences may be returned to the many purposed modelling assumptions in this study which might affect the remediation time. Another part might be returned to the nonlinearity of the solute transport process, i.e. it is not necessarily accomplished that doubling the inland discharge will require doubling the remediation time even under same stationary hydrogeological conditions. However, further study to address the latter justification might be needed in future studies.

7.5 Subsurface drainage effect on coastal aquifers resilience against coastal floods

The analysis of storm-driven SWI at Bremerhaven showed that about 45 years are needed for a coastal aquifer to remediate after an inundation event of 2196 m^3 of saltwater over 2.8 hour (the overtopping interval). In fact, this reflects the significant threat of coastal floods to coastal aquifers. A flood over few hours can contaminate aquifers for decades, which limits the use of aquifers and increases the water treatment costs. Moreover, it hinders the dependence on coastal aquifers in possible sustainable development planning for coastal zones. Therefore, the search for an efficient mitigation measure that can make coastal aquifers more resilient during and after coastal floods is a curial issue, so that long intervals for natural remediation can be shortened. For the latter purpose, subsurface drainage network might be the right choice in flood prone coastal zones, especially agricultural areas, because saltwater infiltrating during and after a flood event can be partially absorbed and evacuated through drains before it contaminates the whole aquifer as shown in Fig 7.19 (see section 7.4).

A subsurface drainage system (Fig 7.20) is a man-made system that can induce excess water and dissolved salts to flow through the soil to pipes, from where it can be evacuated. Drainage, in general, is important in agricultural areas for improving the agricultural yield (Blann et al. 2009). For the latter purpose, surface and subsurface drainage systems can indeed be used. Nevertheless, surface drainage is not favoured in coastal zones since any kind of open channels might facilitate the enlargement of the contamination extent in the case of coastal flooding. Open channels in coastal areas might indeed act

as preferential pathways for landwards movement of salt water (Yang et al. 2015a). Therefore, subsurface drainage in coastal areas might function for the following two purposes: (i) improving the agricultural yield and (ii) absorbing the infiltrating salt water that intrudes vertically from the land surface to the fresh water aquifers during a coastal flood event.

Subsurface drainage is used where the soil is permeable enough to allow economical spacing of the drains and performant enough to justify the investment. Moreover, it should provide almost trouble-free service for many years. A subsurface drainage system consists of a surface or subsurface outlet and subsurface main and lateral drains. Water is carried into the outlet by the main drains, which receive water from the lateral drains (also known as inceptors or water collators). Because subsurface drainage is used primarily to lower the water table or to remove excess water that is percolating through the soil over a general area, the drains are placed in a pattern determined by the characteristics of the area (Kalita et al. 2007). In homogeneous soils, parallel patterns are used to lower the water table at the same rate on both sides of each drain. In heterogeneous soils, however, random patterns might be more appropriate. The spacing and depth of drains influence the groundwater level between drains. The required drain spacings and depths depend on soil permeability and on the amount and frequency of rainfall as well as on land topography. According to Drablos and Moe (1984), drain spacings in highly permeable soils should be 60 to 90 m and 30 to 60 m in moderately permeable soils. Where soil permeability is moderate, spacing should be 25 to 30 m. In soils with a low permeability or moderate permeability, drain spacing should be respectively spaced 10 to 22 m or 18 to 25 m.

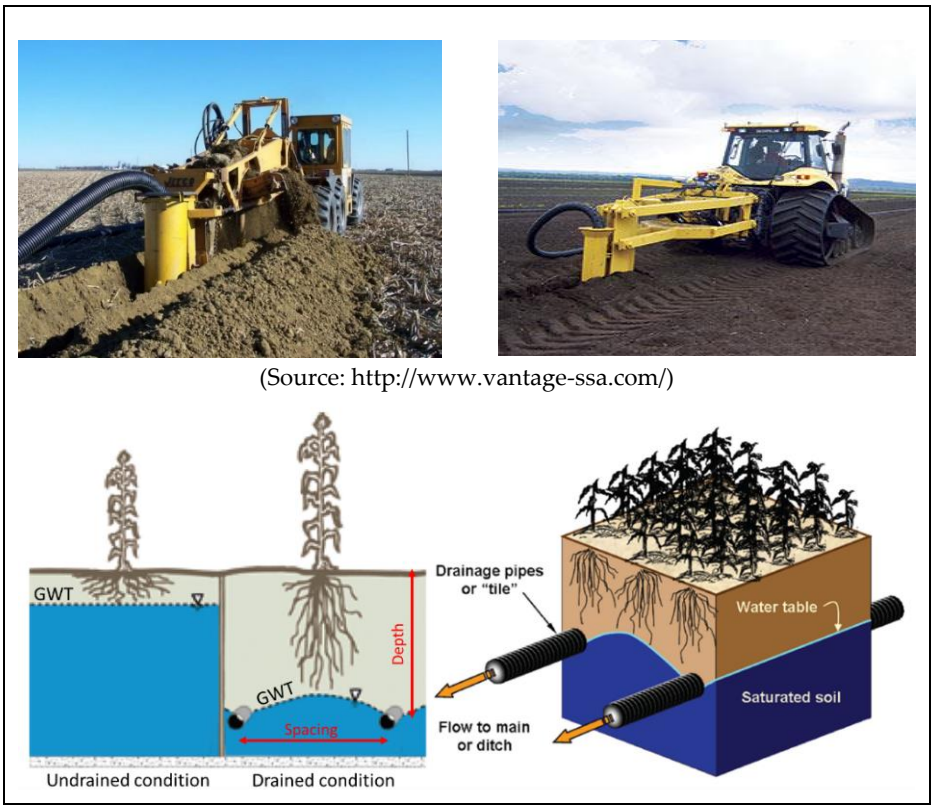

Fig 7. 20: Subsurface drainage: upper panels show the installation process and lower panels show the role of subsurface drains in lowering the GWT based on the spacing and depths of inceptor drains, after Blann et al. (2009).

Regarding the drains depth, subsurface drains are often installed based on the desired water table, so the depth ranges between 1 to 1.5 m beneath the pre-installation water table for highly to moderately permeable soils. The latter depth decreases to 0.3 m in the case of lowly permeable soils because the rate of lateral water movement does not increase in this case with depth. The range of slopes on which drains can be placed depends to some degree upon the topography of the land. The slope should be

steep enough to prevent silting but flat enough to prevent flow from exceeding the allowable velocity and from subjecting the drain to excessive pressure.

The inflow rate to the drains depends on the soil texture and permeability as well as on the surcharge rate to ground level and head distribution around the drain. Indeed, there is no general formulation for calculating subsurface drain conductance (C_d). This is due to lack of the detailed information required for the calculation. Such information may include the detailed head distribution around the drain, the aquifer hydraulic conductivity near the drain, the distribution of fill material, the number and size of the drain pipe openings, the amount of clogging materials and the hydraulic conductivity of clogging materials. Nevertheless, the available drainage manuals (e.g. Drablos and Moe (1984)) provide tentative values for subsurface drain conductance based on soil permeability. For instance, drain conductance in sandy soils ranges from 0.56 to 2 $m^3/day/m$, while the range of 1.2 - 8 $m^3/day/m$ is common for coarse sand and gravel soils. Silty soil conductance ranges between 0.32 – 0.8 $m^3/day/m$, while the range of 0.16 – 0.8 $m^3/day/m$ is common for clayey soils.

Based on these common values for drain spacing, depth and conductance, the effect of subsurface drainage on the saltwater intrusion at Bremerhaven aquifer can be studied in the following subsections

7.5.1 Model set up and parametrization for the aquifer with subsurface drainage in Visual Modflow

The conceptual model of the aquifer at the study site near Bremerhaven after considering the installation of subsurface water collectors can be drawn as shown in Fig 7.21.

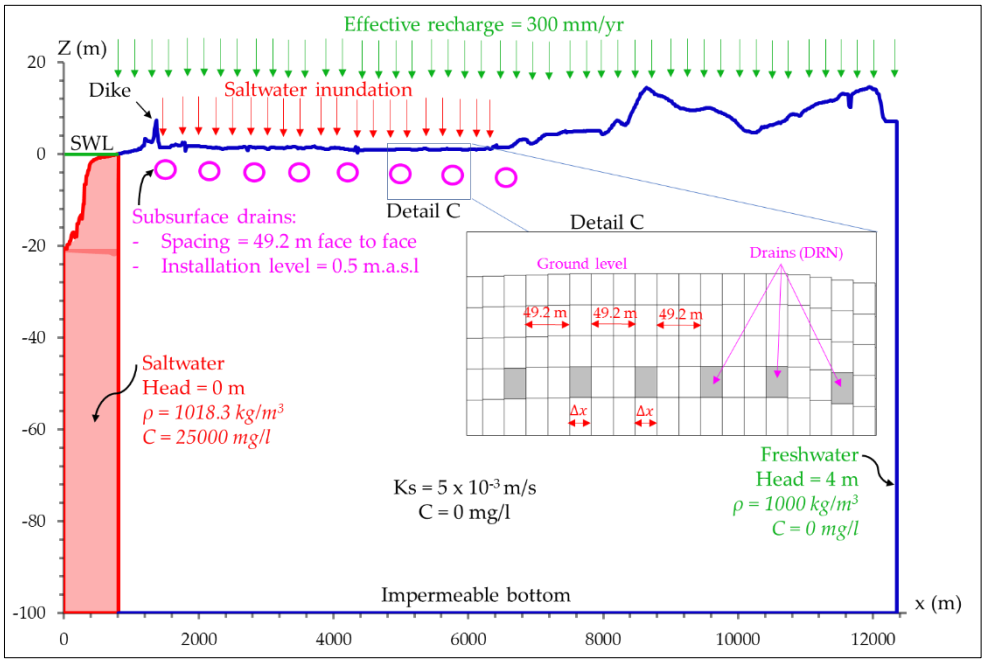

Fig 7. 21: Conceptual model for the aquifer near Bremerhaven with subsurface drainage of salt water infiltrating under storm-driven inundation: Red colours indicates seawater inflow with saline concentration (C) with the same value as in sea water while green colours indicate freshwater inflow. Purple colour indicates the subsurface drains, which are simulated in Visual Modflow as rectangle cells as shown in Detail C.

The conceptual model is the same as that in Fig 7.21. All boundary conditions are the same, but subsurface drains are added beneath the ground surface directly exposed to vertical saltwater intrusion from coastal flooding. Because the soil in Bremerhaven can be considered as homogeneous, parallel pattern consisting of parallel lateral drains are used. In order to avoid further lateral intrusion when using subsurface drainage, the balance between freshwater in the aquifer and salt water in the sea should be considered. This means that deepening the drains levels than necessary might allow further lateral intrusion. Therefore, the drains are set at level 0.50 m.a.s.l., which is at least 0.5 m lower than the ground level at the lowest point in the hinterland. The soil in Bremerhaven is highly permeable (Ks =

0.005 m/s), hence the spacing between the collectors is set at 73.8 m (centre to centre). Circular collectors as shown in Fig 7.21 cannot be defined in Visual Modflow because of being a finite difference based model utilising rectangular meshes. Therefore, cells containing subsurface drains are defined as drainage cells using the Modflow drainage package DRN (see section 7.1). Since the conceptual model is discretized uniformly in the cross-shore direction with $\Delta x = 24.6\ m$ (see Fig 7.11), the face to face distance between drainage cells is 49.2 m as referred to in Detail C in Fig 7.21.

Drain conductance is indeed the most important and the highly uncertain parameter when analysing the subsurface drainage effect. It is usually adjusted during model calibrations based on surcharge rate to the ground surface and head difference between drains and GWT. Based on the latter factors and the aforementioned tentative values for the subsurface drain conductance, the conductance value for each drain is assumed along the simulation time (50 years) as in Fig 7.22 and Table 7.4.

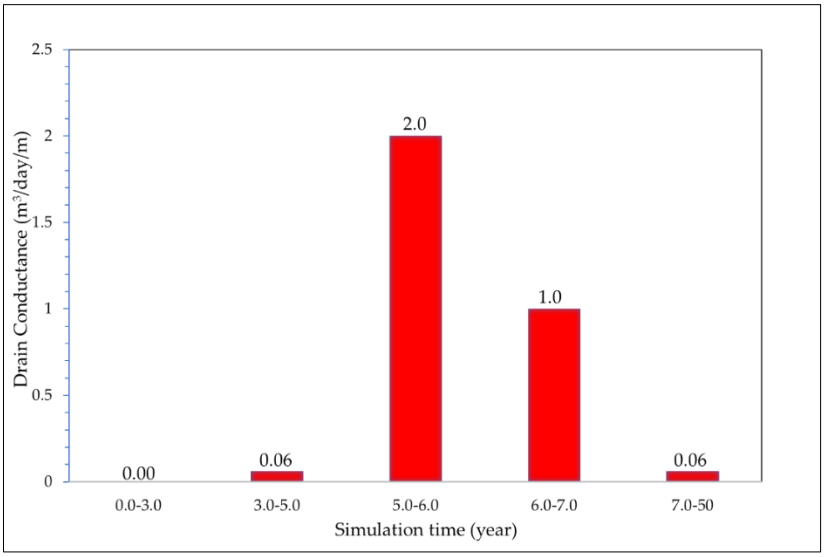

Fig 7. 22: Assumed values for subsurface drain conductance in Bremerhaven aquifer along the 50 years of simulation.

Table 7. 4: Reasoning behind assumed values for subsurface drain conductance in Bremerhaven aquifer along the 50 years of simulation.

Interval (year)	Conductance (C_d) (m^3/day/m)	Notes
0.0 - 3.0	0	The first 3 years is an interval of warming up for the model to reach the steady state. Therefore, C_d is set at 0.0 in order to reach the desired state within the 3 years.
3.0 - 5.0	0.06	Here it is assumed that drains collect the recharged rain only (300 mm/yr). Therefore, C_d is calculated based on the effect recharge and the area served by each drain
5.0 - 6.0	2	During and after coastal flooding, the highest C_d value can be used since the water surcharge increases the drainage.
6.0 - 7.0	1	The high C_d value in the previous year was able to reduce a bit the increased water level owing to coastal flooding. Therefore, lower conductance value is expected.
7.0 – 50.0	0.06	Starting from 2 years after the flood onward, it is reasonable to assume again that drains collect the recharged water from rains only.

Based on the parameterized values for drains spacing, depths and conductance, the effects of the considered subsurface drainage on both water flow and mass transport in Bremerhaven aquifer are respectively discussed in the following two sections.

7.5.2 Subsurface drainage effect on water flow in Bremerhaven aquifer

Drainage is an important factor in the aquifer budget since it is a sink out facility. This is the reason why it is sidestepped during the first 3 years of warming up by setting C_d = 0 as in Table 7.4 to allow the model to reach the steady state as aforementioned in section 7.4.3. After the first 3 years, the drains start to absorb water from the aquifer, as shown in Fig 7.23, based on the assigned value for drain

conductance (C_d). During the interval of the inundation-induced infiltration (4 days), the drainage rate reaches its maximum value, which is an evidence that drainage depends on both the drain conductance and the surcharge rate on the ground surface. Therefore, it was wise to change the drain conductance value with the surface load. Though the conductance value is constant during the first year after the flood (C_d = 2.0), the drainage rate decreases because of the drainage-induced lowering of the GWT during this year. The sudden drop in the conductance value from 2.0 to 1.0 at the start of the second year after the flood results in a sudden decrease in drainage rate, which become uniform during this year because of the constant conductance value. A similar behaviour takes place with the decrease of the conductance value at the end of the latter year. During the last 43 years, the drainage rate is constant because of the constant conductance and the steady state in the aquifer.

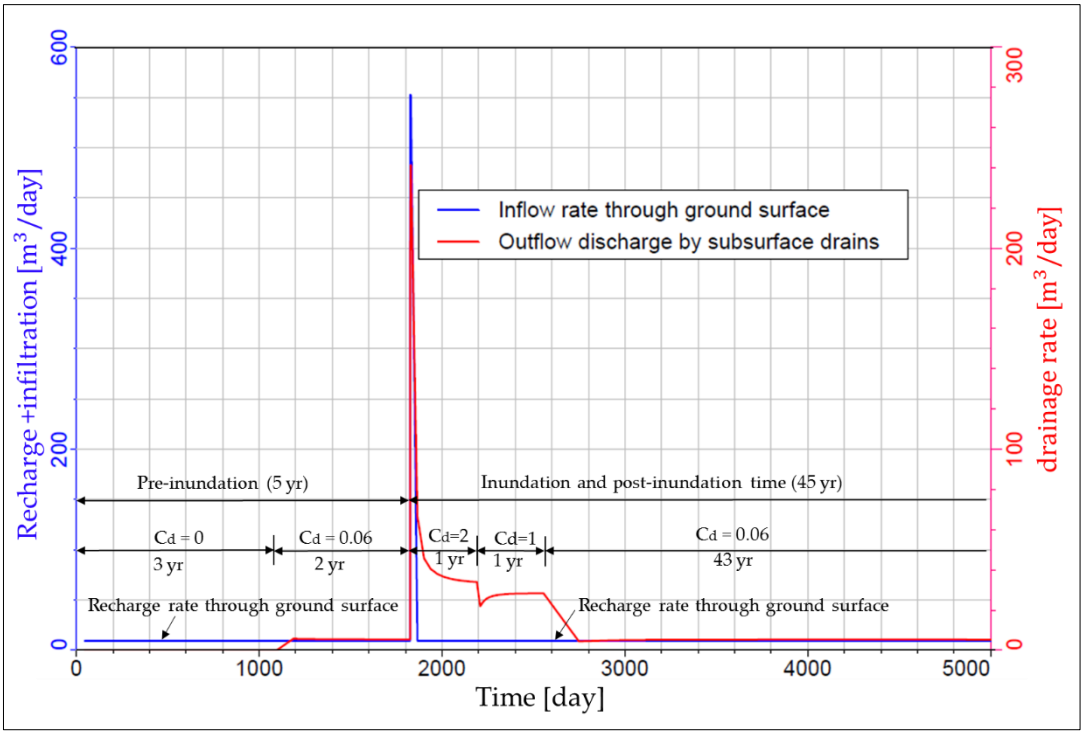

Fig 7. 23: Total inflow rate through the ground surface [left axis] vs drainage rate through the subsurface drains [right axis], Cd represents the conductance value for each individual drain [m³/day/m].

In fact, the drained water through the subsurface drains would sink part of the infiltrated salt water out the aquifer so that the time needed for the natural remediation would accordingly decrease. This aspect is examined in the next section.

7.5.3 Subsurface drainage effect on saltwater intrusion to the aquifer near Bremerhaven

Subsurface drainage is selected as a mitigation measure tool for the storm-driven saltwater intrusion, but does it really solve the problem? In order to answer this question, the accumulative source in and sink out masses should be compared side by side with the salt mass remaining in the aquifer as in Fig 7.24. The accumulative input mass (red curve) increases by 54.9 tons owing to the inundation. Such increase of the input leads to a sudden-like increase of the salt mass remaining in the aquifer (blue curve). After flooding, where higher conductance values of drains are assumed, the accumulative output mass decreases as shown in Detail (E) in the same figure because the GWT sinks owing to drainage. The decrease of the accumulative output mass increases indeed the mass remaining in the aquifer even more than the case without drainage as shown in Fig 7.25, which compares the salt masses remaining in the same aquifer under the same conditions with and without using the drainage system. Drainage, in fact, facilitate collecting the infiltrating salt water, but at the same time, it decreases the level of the GWT leading to more lateral intrusion from the seaside because of the balance defect between fresh water head in the aquifer and seawater head in the sea (see Fig 2.24).

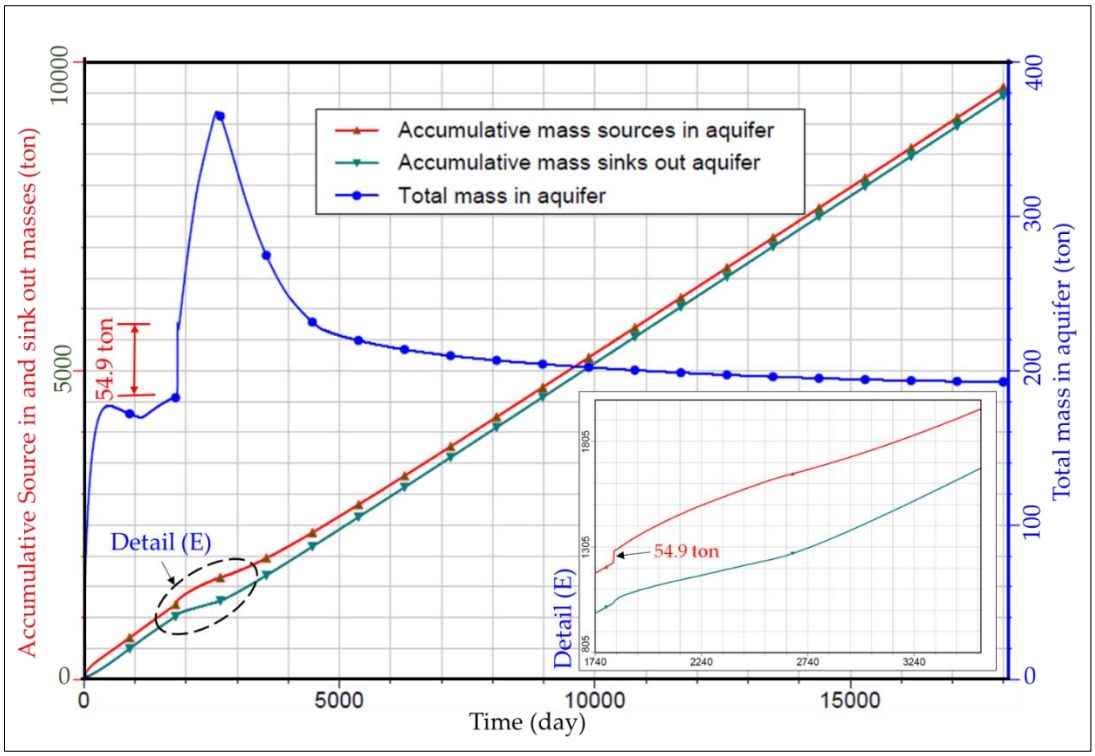

Fig 7. 24: Accumulative salt masses over the fifty years of simulation with subsurface drains: red curve represents salt entering the aquifer as a source in, green curve represents salt leaving the aquifer as a sink out and blue curve represents the accumulative salt mass remaining in the aquifer (blue = red – green). Detail (E) shows that the mismatch between the source in and sink out masses increases with higher drain conductance values, leading to more salt remaining in the aquifer.

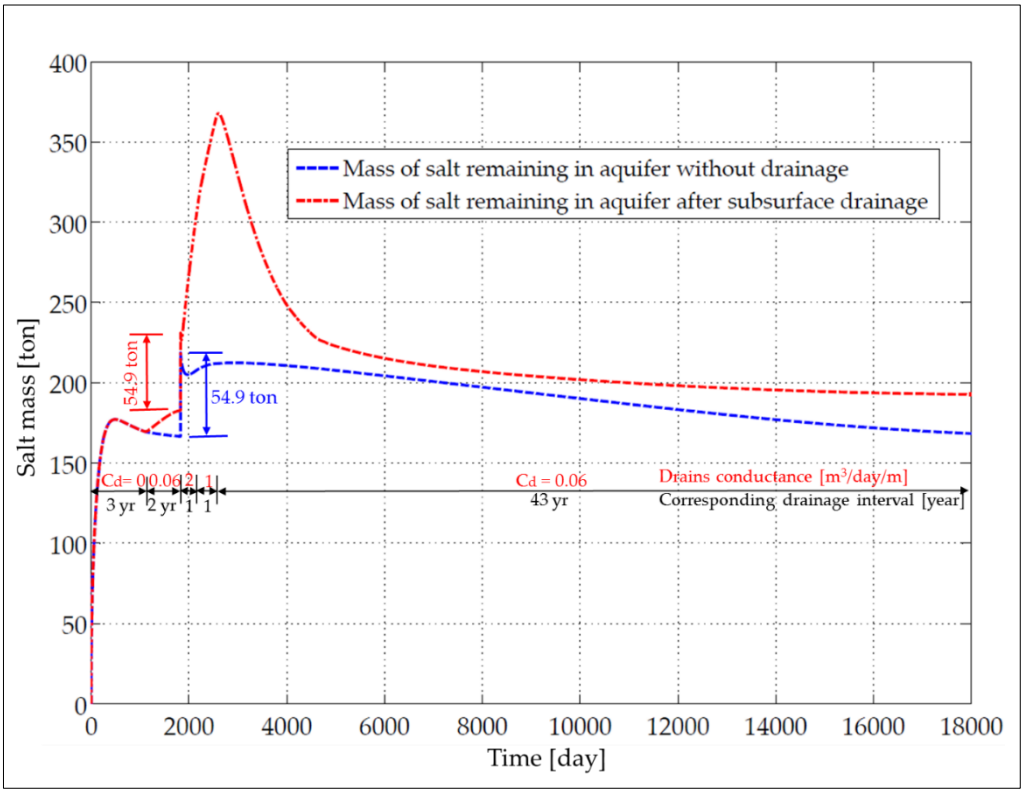

Fig 7. 25: Comparison between salt masses remaining in the aquifer after and before the inundation with and without subsurface drains. In the case of drainage, more salt intrudes to the aquifer, especially during higher conductance intervals.

As shown in Fig 7.25, the mass remaining in the aquifer during the warming up phase (the first 3 years) is the same with and without drainage because the drains conductance is set at zero. During the following two years, which are also before applying the flood effect, the salt mass remaining in the aquifer increases with the drainage than without it. The latter is because the drainage reduces the GWT, leading to a lateral shift in the salt-freshwater interface landward. During and after the flood by one year, the conductance value is the highest, but the mass of salt in the aquifer is increasing dramatically than without drainage. This increase extends to the second year of flooding until it reaches its peak with the reduction of the conductance value from 1 to 0.06 m^3/day/m. With the latter reduction, the mass in the aquifer decreases gradually. Nevertheless, the remaining salt mass in the aquifer in the case of using subsurface drainage keep on higher than without drainage even after the 45 years after the flood event.

The previous explanations can be clearer by visualising the salt distribution in the aquifer at different times as in Fig 7.26.

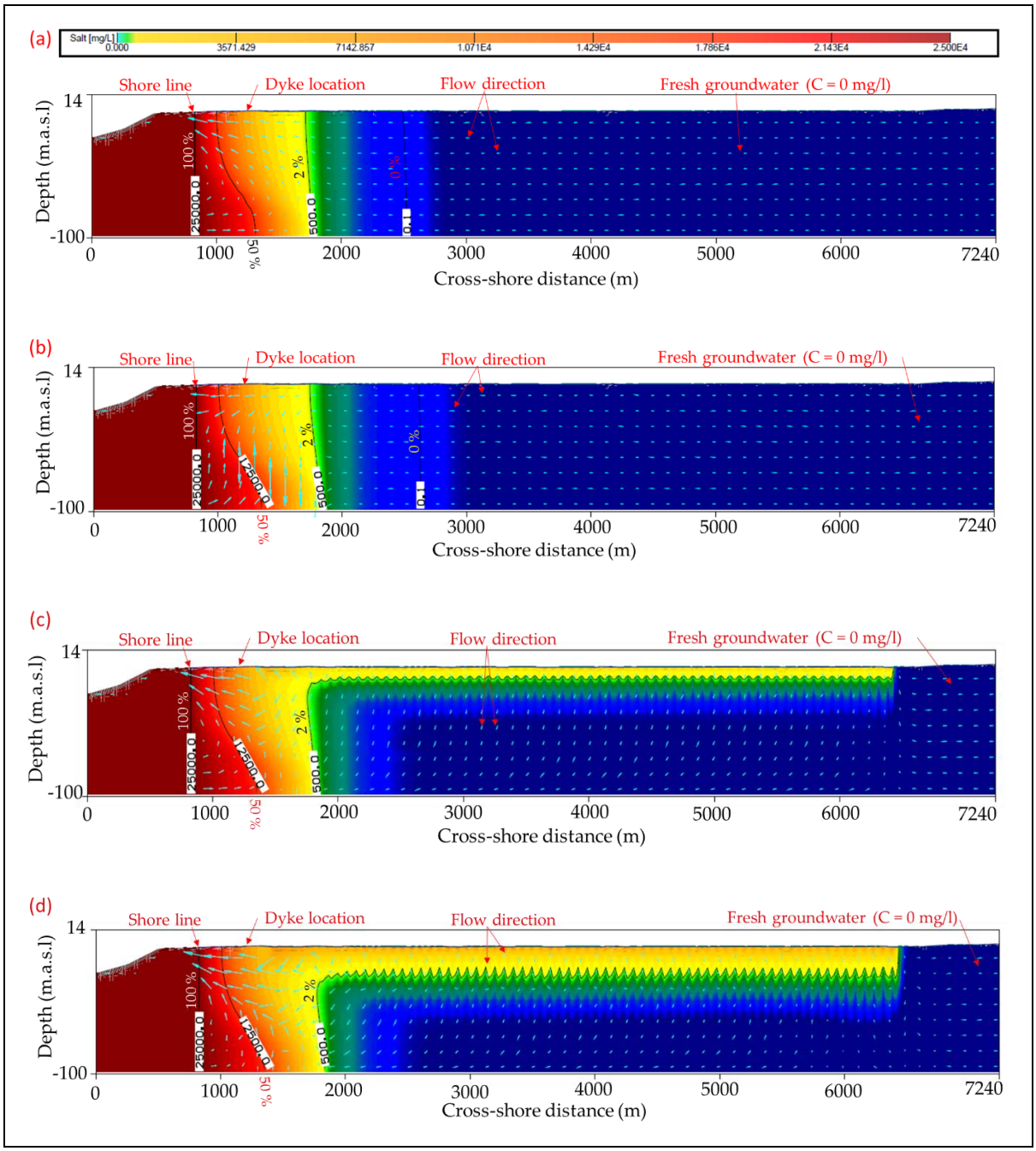

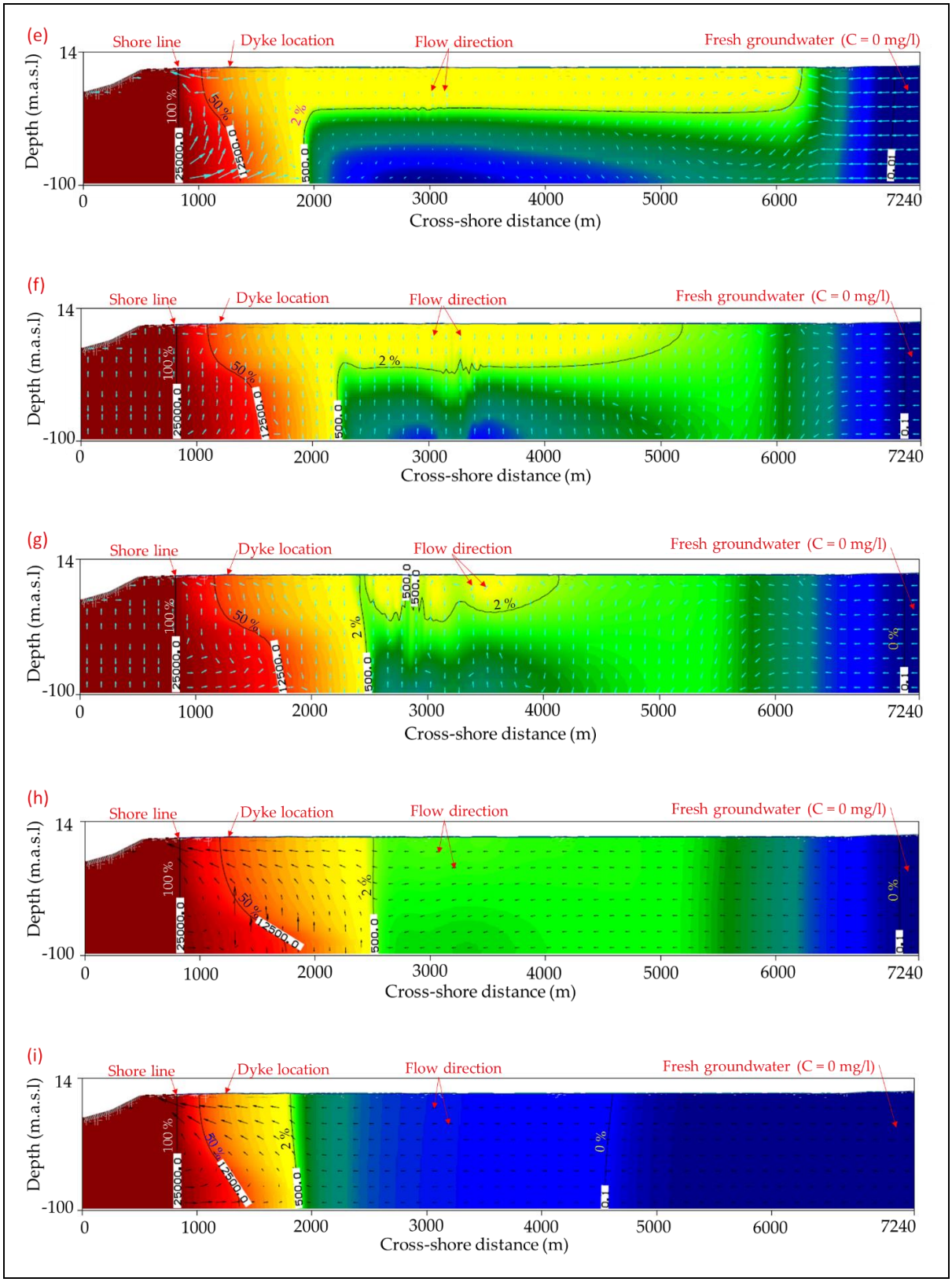

Fig 7. 26: Evolution of salt distribution in the aquifer with subsurface drains near Bremerhaven: (a) 2 years before inundation when lateral intrusion only exists without drainage, (b) directly before inundation with unnoticed shift of the 50% contour landward than in (a) because of drainage, and (c - i) after the flood event where both lateral and vertical intrusions exist. Contamination extent is shown after 1 day (c), after 4 days (d), after 3 months (e), after 1 year (f), after 2 years (g), after 3 years (h) and after 45 years (i). Arrows represent the flow directions. Salt-freshwater interface, represented by the 50% iso-concentration

contour, and the iso-concentration contour of 500 mg/l (2%) are shown on each panel. The 2% contour forms a zigzag-like during the conduction interval from the land surface (c - d) because part of the infiltrating water escapes downward in between drains. The interface shifts landward with higher conductance values. Nevertheless, salt dispersion to the deep aquifer is controlled by drainage and acceptable concentrations are achieved after 3 years (panel h). By reducing drain conductance, the interface shifts back seaward as in panel (i).

As shown in Fig 7.26 (panels c and d), the subsurface drains collect part of the infiltrating salt water, especially during intervals of higher drain conductance. Nevertheless, the rest is escaping downward among the drains, leading to the zigzag shape of the concentrations among drains. Panels (e - g) show that drainage has proved its efficiency in confining the high salt concentration near to the ground surface. In fact, drainage was capable of controlling the unwanted deeper infiltration of the high salt concentrations in the aquifer. Highly concentrated salt water is collected from the shallow zones within the three years after flooding as shown in panels (g) and (h). Therefore, shorter remediation intervals (< 3 years) can indeed be achieved using closer drains as the wider drains spacing allows more escaping of the saltwater to the deeper freshwater in the aquifer. However, the efficient role of the drainage in shortening the remediation time of the vertical intrusion is often at the expense of more lateral intrusion because of the drainage-induced lowering of the GWT during higher conductance intervals.

7.6 Summary and discussion of the results

In this chapter, the modelling scenario SC3 (see section 6.4) is applied to a pilot site near Bremerhaven, Germany to simulate the successive processes of coastal barrier overtopping, induced inundation and subsequent saltwater intrusion (SWI). The XBeach model is applied to simulate the first two processes whilst the SEAWAT model built in Visual Modflow is used to analyse the inundation-induced saltwater intrusion to the groundwater aquifers. Visual Modflow is selected because of its powerful capability in visualising the modelling outcomes in both maps and graphs forms. In addition, it includes river (RIV) and drain (DRN) packages that can respectively calculate the conductance of surface water to the groundwater and the drainage from an aquifer. As a result, SEAWAT is applied to a 2D cross-sectional profile that extends 12.3 km in the cross-shore direction to simulate a combination of lateral and vertical salt water intrusions. The lateral intrusion arises from the hydraulic continuity of seawater and freshwater in coastal aquifers. Therefore, it depends on the sea level, the groundwater table (GWT) and water density in each domain. In fact, further lateral intrusion is expected in the case of a sea level rise, a decrease of the GWT and/or change of the mismatch between seawater and freshwater densities. On the other hand, the vertical intrusion arises from coastal floods, which might be induced by direct inundation, overtopping of coastal barriers, or flooding subsequent to breaching of coastal barriers (see Fig 2.23).

A storm-induced barrier overtopping/breaching results in a relatively wide flood extent depending on the inland discharge and on the topography of the hinterland. Propagating salt water in the hinterland infiltrates to freshwater aquifers, resulting in their contamination. The remediation of an aquifer after such coastal floods is possible owing to the continuous dilation of the saltwater in the aquifer by both the recharged part of precipitation and the seaward directed flow. However, such remediation process is so long and may take decades to reach again the pre-flooding conditions. For the study area near Bremerhaven, which was also considered by Yang et al. (2013), the XBeach model is used to calculate, in combination, the overtopping rates over the dyke and the induced flood extent and water depths. The outcomes of this step exhibited more overtopping discharge and hence a wider flood extent than that were predicted in the study of Yang et al. (2013). The outcomes of XBeach are manually transferred to the Modflow model which simulates the subsequent SWI. Inundation-induced SWI takes around 45 years after the inundation to remediate the aquifer and reach again the pre-flooding conditions. Nevertheless, 25 years might be sufficient to achieve the maximum allowable concentration for drinkable water (500 mg/l). The latter interval is only 5 years more than the interval calculated by Yang et al. (2013) to achieve the same concentration in the aquifer. In order to shorten

such long remediation intervals, subsurface drainage is suggested as a structural mitigation measure. Drainage manuals (e.g. Blann et al. (2009), Drablos and Moe (1984)) are used to specify the spacing between the drains, the installation depth and expected drain conductance.

The use of the subsurface drainage system as a structural mitigation measure shortens the long intervals needed for the natural remediation but at the expense of landward shifting of the salt-freshwater interface (i.e. further lateral intrusion). Such a lateral intrusion arises from the fact that subsurface drains reduce the GWT or at least absorb a large part of the recharge from precipitation, which represents a continuous feeder for fresh water in the aquifer. Therefore, subsurface drainage is a good choice since it reduces the contamination extent in a relatively shorter time and hence it widens the usable part of the aquifer. The side effect of this choice is the possibility of further lateral intrusion (around 500 m in the study case near Bremerhaven), which might be acceptable in order to benefit from drainage, for instance by increasing the agricultural yield as well as by shortening the long remediation intervals after a coastal flood event.

Despite these encouraging results on the efficiency of subsurface drainage as a structural SDSWI mitigation measure, further research is still needed to better evaluate drains conductance in the light of experimental work by considering various recharge rates and different soil types. Moreover, drainage effect needs to be studied using a surface-subsurface model (e.g. HydroGeoSphere), so that the flow through the vadose zone can be better represented in the simulation. In fact, the simple representation of the flow through the vadose zone using the conductance concept might affect the simulation outcomes.

Despite the encouraging results applying modelling scenario SC3 to simulate the vertical SWI in the aquifer near Bremerhaven, the modelling approach suffers the following limitations:

(i) Many modelling assumptions need to be introduced as discussed in section 7.4.1, which may affect the reliability of the modelling outcomes.

(ii) A “manual” transfer from one model to another could not be avoided, which may also affect the accuracy of the modelling outcomes, i.e. assuming an equivalent uniform water head as indicated in Fig 7.9 results in uniform salt migration downward rather than forming salt plumes as in Yang et al. (2013).

Therefore, the best approach to simulate an SDSWI induced by barrier breaching is to simulate the involved processes in a single model. With some further developments to account for advection-dispersion of contaminants in porous media, XBeach model might be an eligible model for this purpose. Nevertheless, bearing in mind the current non-existence of such modelling capability, the application of XBeach to simulate barrier breaching and subsequent inundation besides using, for instance, HydroGeoSphere to simulate the surface-subsurface interaction and the accompanied contamination transport might represent an optimal modelling option. In this way, flood propagation in the hinterland will be calculated first by XBeach simulating breaching and subsequent inundation and second by feeding the inland hydrograph calculated by XBeach to the surface-subsurface model as explained in Elsayed and Oumeraci (2016b). This might help to confine the modelling inaccuracies.

The outlook for future research based on the outcomes of this chapter might be outlined as follows:

(i) Drain conductance represents the main uncertain parameter, which needs to be investigated in the light of experimental work by considering a wide range of recharge rates and different soil types.

(ii) The effect of soil heterogeneity on spacing and conductance of subsurface drains need to be investigated.

(iii) The drainage effect needs to be studied using a surface-subsurface model (e.g. HydroGeoSphere) so that the flow through the vadose zone can be better simulated.

8 Summary, concluding remarks and outlook

This study aimed at developing an overall methodology to reliably assess the possible implications of extreme storm surges on the safety of coastal barriers, the induced inundation as well as the subsequent saltwater contamination of coastal aquifers. During moderate sea conditions (Fig 8.1.a) wave attack is limited to the nearshore area and may cause shore erosion. At the same conditions, fresh groundwater is in equilibrium with the laterally intruding sea waters as long as the mean sea level (MSL) and the hydrogeological conditions at the sea/land boundary are stationary. The regional freshwater flow toward the sea controls the interface between salt water and fresh water in the aquifers. However, during extreme storm surges (Fig 8.1.b), higher water level may temporally lead to onshore inundation. In fact, the shortwaves riding on the temporally rising sea level may directly impact on the barrier, possibly causing wave overtopping or overflow through combined surge and waves. As a result, barriers may breach inducing coastal inundation and subsequent vertical salt water intrusion behind the breached barrier as shown in Fig 8.1.b. This study used a modified XBeach code with SEAWAT as a modelling methodology to simulate barrier breaching as well as subsequent inundation and saltwater intrusion.

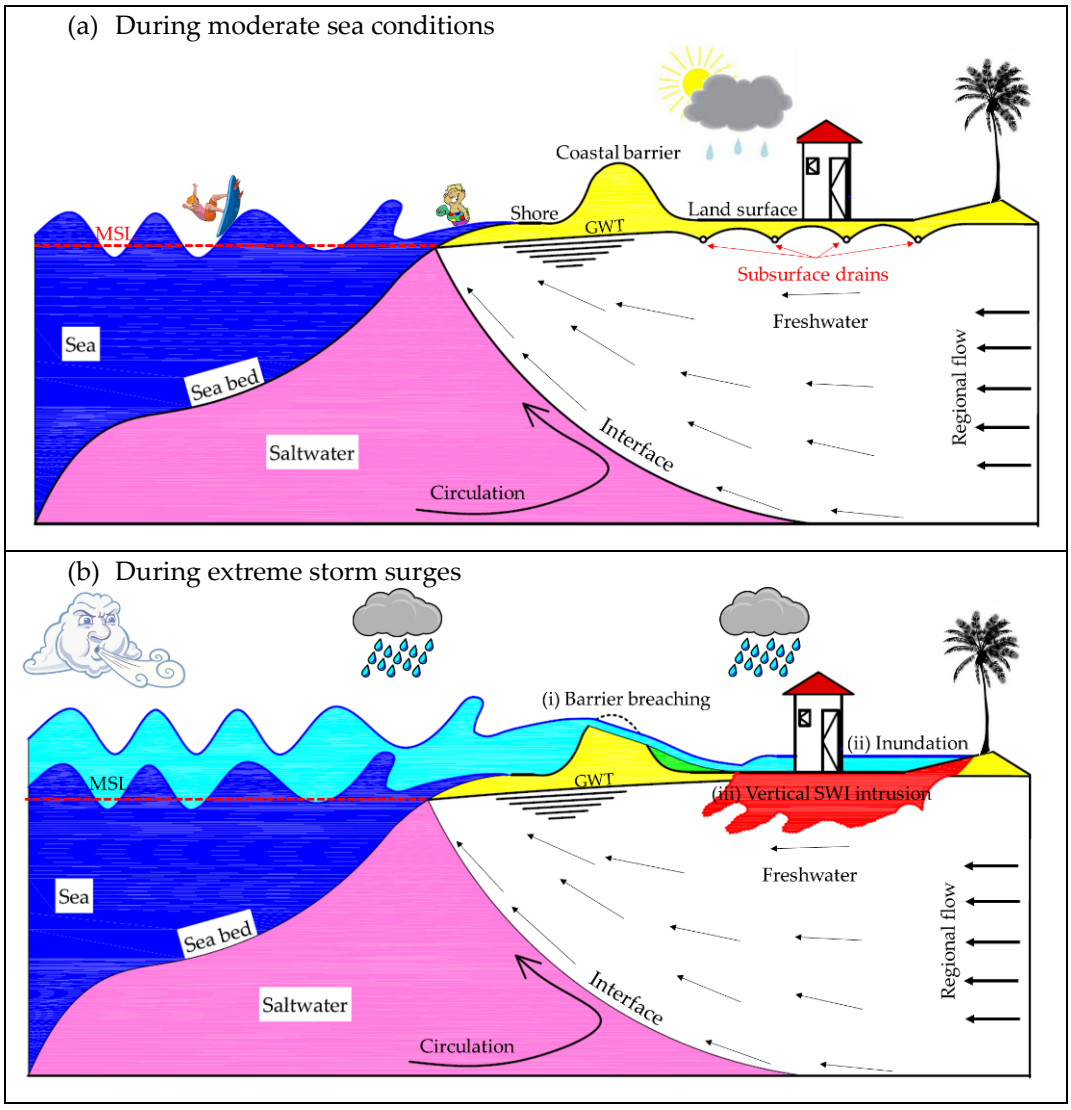

Fig 8. 1: Sea/land boundary (a) during moderate sea conditions, wave attack and induced coastal erosion are limited to nearshore and beach erosion. Moreover, freshwater and saltwater are in equilibrium determined by the interface; (b) during extreme storm surges, the coastal barrier is directly attacked by shortwaves riding on the surge thus possibly causing barrier breaching, coastal inundation and subsequent vertical salt water intrusion.

In this concluding chapter, the new contributions by this study are briefly outlined and the key results are summarised. Finally, the implications of these results for the engineering practice and for further research are drawn.

8.1 Novel contributions of the PhD study

Overall, this dissertation represents the first systematic research study that addresses the safety of natural coastal sandy barriers under extreme storm surge conditions together with the consequences of possible barrier breaching and overwash on subsequent flooding and saltwater intrusion into fresh groundwater. Moreover, it is the first study that introduces an overall physically based methodology to simulate breaching of coastal barriers, induced inundation and subsequent saltwater intrusion, including the simulation of each of the three aforementioned successive processes and their interactions. By this way, this study overcomes most of the modelling weaknesses from previous studies (see Remark 6.2 in section 6.3). Furthermore, it is the foremost study that attempts to mitigate storm-driven salt water intrusion through the use and modelling of subsurface drainage network (see Fig 8.1.a), making it quite relevant for the coastal engineering community, for flood risk managers, for groundwater suppliers as well as for sustainable development planners.

On the specific level, the contribution may be summarised as follows:

1. *Improvement of the XBeach model to properly predict the sediment stirring and transport:*
   a. Development of a prediction formula called *facua-asabeta* relationship (Eq. 4.13) for the calibration factor *facua* for the time-averaged flow depending on the wave skewness and asymmetry. This formula predicts the calibration factor *facua* based on the beach slope steepness.
   b. Introduction of a new approach to account for the grain-stabilization effect on sediment transport. It shows that the common Shields criterion (Shields 1936) for onset of sediment motion is no longer valid as long as the bed soil is interlocked and/or compacted. Thus, the approach suggests amplifying the value of the critical Shields parameter until fitting the in-situ degree of interlocking/compaction.
2. *Extension of the applicability of XBeach to coastal flood modelling in combination with breaching modelling.* This contribution facilitates the modelling of breaching-induced coastal floods because of the possibility to model barrier breaching and induced inundation in a single XBeach model, thus overcomes the weaknesses of the separate modelling as identified in chapter 5
3. *Introduction and simulation of a mitigating measure for vertical saltwater intrusion*: The applied subsurface drainage network was tentatively shown to substantially shorten the long remediation intervals of aquifers after a coastal flood.

In addition to the previous contributions, this thesis includes the following important contributions:

1. *Reproduction of the GWK-tests with XBeach:* this contribution helped in evaluating the performance of XBeach and in suggesting further model improvements (see chapter 3).
2. *Introducing a real study case to apply the suggested modelling methodology.*

Through these contributions, this study has arrived at many important conclusions, which are summarised in the following section.

8.2 Summary of main results and conclusions

Overall, this study provides an improved understanding of the breaching process and the subsequent inundation and saltwater intrusion. More specifically, the main results and conclusions may be outlined as follows:

Modelling of coastal erosion and breaching

Breaching of coastal barriers is not necessarily induced by wave overtopping or overflow through depression on the barrier crest. Breaching, in addition, might be initiated from the seaward side of the barrier due to wave impact, run up and run down. As a result, initiating scour from the seaward side

might be followed by offshore sediment transport accompanied with seaward avalanching and more lowering of the barrier crest. Thus, with successive crest lowering because of the seaward erosion, waves may overtop and then overflow the lowered crest, causing landward erosion and more crest lowering until inducing full breaching.

Avalanching of the breach wedges represents one of the main issues that trigger a breach growth. Slope avalanching is a highly uncertain process as it depends on soil properties and the saturation degree. Therefore, soil investigations are crucial for future breaching studies. Moreover, such investigations are highly important to account for the grain-stabilization effect on sediment stirring as well as on the spatial variability of the soil strength, which is also crucial in order to properly predict likely locations of possible breaches.

This study has shown that using artificial limiters to hinder over-predicted erosion under high flow velocity regimes is an unsuitable approach as such limiters cannot be applied to all case studies. Moreover, they cannot be physically explained. On the same way, the dilatancy theory of Van Rhee (2007, 2010) cannot also be generalised as a theory for hindering overestimated erosion rates during high flow velocity regimes. Nevertheless, the grain-stabilization approach proposed in this study is able to explain why erosion rates might differ from one case study to another or from site to another based on the grain interlocking state. Highly interlocked sediments are expected to experience less erosion whilst loose soils are expected to undergo more erosion.

The role of the longshore variability of the hydraulic load and the subsequent wave focusing on coastal barrier erosion, avalanching and breaching is also highlighted. Thus, breaching of coastal barriers is not only a function of the longshore variability of the shore topography but alongshore variability of the hydraulic load may also play an important role in determining the location of the breach initiation. Therefore, breaches are not necessarily initiated at the lowest crest level. This study, in addition, has highlighted the role of soil strength and grain-stabilization in breach initiation and development. As a result, breaches are more likely in less interlocked portions alongshore coastal barriers. Overall, the study clearly showed that breaching initiation is a function of the longshore variability of barrier topography, hydraulic loading and soil strength, thus making the prediction of a breach location a very complicated issue.

Skewed and asymmetric waves play also an important role in coastal erosion as they can stir more sediment onshore. Thus, ignoring or not properly implementing the waveform effect on sediment transport might result in a substantial overestimation of coastal erosion. To overcome this overestimation, this study related the wave nonlinearity effect to the beach slope steepness so that operating the new formula "*facua-asabeta*" would provide a better representation of the wave nonlinearity effect on sediment transport and coastal erosion.

Combined modelling of barrier breaching and induced inundation

Determining the inland discharge during a storm surge event over a barrier or through a breach represents one of the challenges in the coastal engineering field because of the high uncertainty of the sea state. Overtopping guidelines (e.g. EurOtop) facilitate the prediction of inland discharges induced by overtopping. Nevertheless, these empirical models cannot calculate inland discharges through breaches because they are only based on comparing water and ground elevations. For the latter purpose, numerical models are often used. This study introduced an approach (see Fig 5.12) to calculate inland discharges through breach induced inlet(s) using XBeach. Moreover, it successively extended the scope of XBeach to model not only the breaching but also the subsequent inundation in a single model. The comparison between separate and combined approaches showed that the former might provide inaccurate estimation of inundation extents, water depths and inland flow kinematics. Such incorrect estimation arises from omitting the velocity transfer (momentum conservation) between the breaching and the inundation simulations while considering only the flow (mass) transfer in the form of the inland discharge (inland hydrograph). Moreover, separate modelling cannot account for the dynamic nature of the breaching process.

Besides considering both the mass and momentum conservations between the breaching and the subsequent flood propagations, combined modelling of both processes by XBeach provide reliable

estimation of the inland discharge and the subsequent flood propagation. The CFD module of XBeach includes a solver for the full terms of the nonlinear shallow water equations (NLSWEs). Therefore, it provides more reliable inland discharges than other diffusive wave approximation codes (e.g. the CFD module of HydroGeoSphere), which generally omit the inertial terms of the NLSWEs. The inertial terms are responsible for accounting for the high flow velocities over barriers (during overtopping) or through breaches. Thus, inland discharges calculated by diffusive wave approximation are often less than those calculated using the full NLSWEs (as in XBeach).

Saltwater intrusion and efficiency of subsurface drainage

Breaching of coastal barriers, induced inundation and subsequent saltwater intrusion in coastal aquifers are naturally successive processes. However, the associated time scales differ significantly. The time scale of both breaching and induced inundation extents from hours to days, while that of saltwater intrusion extents for years and decades. For instance, an overflow event for 2.8 h near Bremerhaven may contaminate the freshwater aquifers for four decades until they are remediated naturally under the effect of both precipitation and seaward directed flow. The extent of the subsurface contamination is a function of the surface flood extent. Thus, retreated flood extent due to topography aspects may confine the contamination extent at the subsurface.

In order to shorten long remediation intervals after a storm-driven salt water intrusion event (SDSWI), this study applied a subsurface drainage system so that vertically intruding salt water may be absorbed before contaminating the deeper aquifers. This suggestion significantly shortens the natural remediation interval and limits the vertical extent of the contamination. Moreover, the installation of such subsurface drainage system might improve the agricultural yield because of lowering the groundwater table as shown in Fig 8.1.a. Nevertheless, lowering the groundwater table and shortening the remediation interval are often accompanied by an increased lateral intrusion because of the defection in the hydrostatic equilibrium between the mean sea level and the groundwater table.

8.3 Recommendations for practical applications

This research study provided several contributions to the current knowledge on the breaching of coastal barriers and the subsequent inundation and saltwater contamination of coastal aquifers. Based on the outcomes of this study, the following aspects are recommended for the practical applications:

(i) Soil investigations should be considered as an important part of future breaching studies.
(ii) Coastal inundation might cause long-term contamination of coastal aquifers. Therefore, it is recommended to include the costs of such contamination to future flood risk assessments. Indeed, such an intangible damage might hinder the development of coastal areas of rarely available water resources.
(iii) Having highly compacted/consolidated coastal defences that can cope with extreme overtopping without breaching is a crucial issue, especially in highly vulnerable coastal zones.
(iv) For the residual inland discharge due to overtopping, it is recommended to install a suitable subsurface drainage system.
(v) Open channels (e.g. surface drains or channels) should be avoided in coastal vulnerable zones as they might facilitate the enlargement of the contamination extent through acting as preferential pathways for landwards movement of salt water.
(vi) Open wells should be avoided in coastal vulnerable zones as they represent a direct contamination pathway to groundwater.

8.4 Limitations of the results and implications for future research

Based on the limitations of the modelling results identified in this study, specific and general recommendations for future research can be suggested in order to improve the reliability of modelling both breaching and salt water intrusion.

Specific recommendations to improve coastal erosion modelling by XBeach

In chapter 2, several XBeach limitations are reported. Two limitations are only addressed in this study. The other model limitations represent candidate topics for further XBeach improvement in order to account for (i) vegetation effect on sediment transport, (ii) cohesive sediment transport and (iii) spatial and along depth variability of soil strength. Including such effects to XBeach will open the way toward using XBeach with several environments and diverse soil properties so that its applicability might be extended to simulate deltaic beaches of muddy soils, composite barriers of different materials and vegetated barriers.

At the level of this study, an amplification factor (*facpi*) was used to account for the grain-stabilization effect. The selection of the proper amplification factor is made tentatively to fit the excessive in-situ critical shear stress for inception of motion. Nevertheless, a physically based estimation of this amplification factor is still necessary. In other words, omitted effects in Shields criterion (e.g. grain-stabilization) need to be accounted for in order to get reliable erosion rates.

A spatially varying grain-stabilization could also be implemented to XBeach in future studies for barrier breaching by defining spatially varying *facpi* that can be assigned to the model as a matrix containing different *facpi* for each cell of the computational grid. In this way, the spatially varying soil resistance could be considered to improve the prediction capability of breach location and dimensions. As a result, the interaction between soil resistance, longshore variability of hydraulic loads and longshore variability of barrier topography can be considered in future XBeach simulations.

Specific recommendations to improve the modelling of the subsurface drainage

The applied subsurface drainage was based on guiding values for the conductance of the drains. For more reliable drainage simulations, drain conductance needs to be investigated in the light of experimental work by considering a wide range of recharge rates and different soil types. Moreover, the effect of soil heterogeneity on spacing and conductance of subsurface drains need to be investigated. Furthermore, the drainage effect needs to be studied using a surface-subsurface model (e.g. HydroGeoSphere) so that the flow through the vadose zone can be better simulated.

General recommendations for combined modelling of breaching, inundation and saltwater intrusion

This study discussed the feasibility of XBeach for simulating salt water intrusion beside modelling both breaching/overtopping and subsequent inundation. It is found that the groundwater module of XBeach still need further development (Fig 8.2) to account for density dependent mass transport so that it can simulate breaching, inundation and saltwater intrusion.

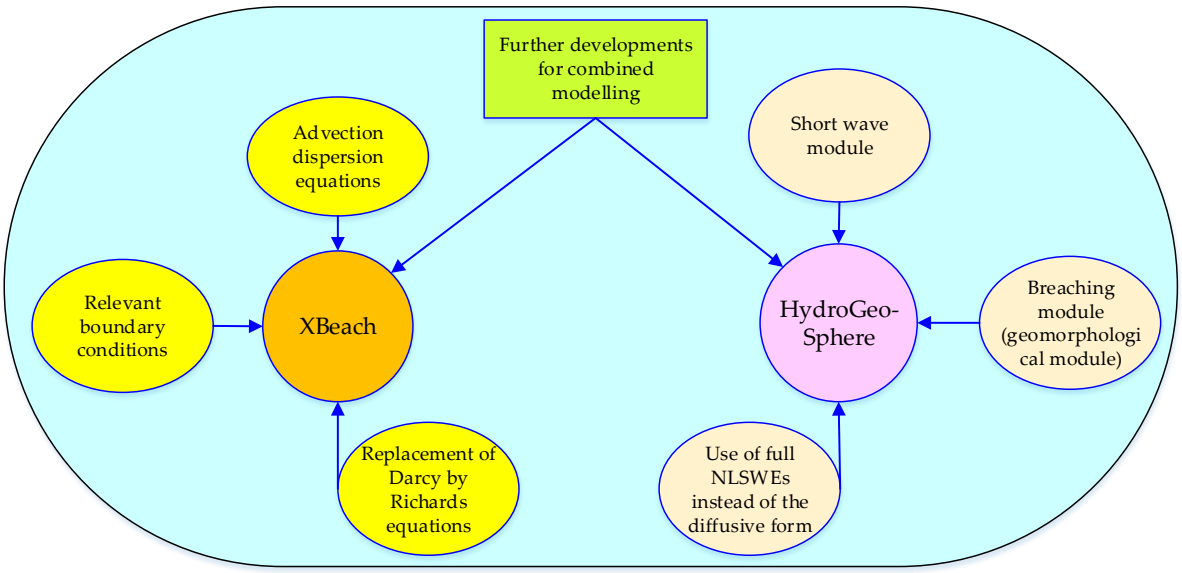

Fig 8. 2: Recommended improvements/extensions for both XBeach and HydroGeoSphere to successively simulate breaching/overtopping of coastal barrier, induced inundation and subsequent saltwater intrusion.

To provide more reliable simulations, Darcy equation for saturated flow need to be replaced by Richards equation for the variably saturated flow so that the flow above and beneath the phreatic line can be simulated. For the latter purpose, XBeach might need definitions of new boundary condition packages, so that recharge and seaward directed flow can be assigned. By these three improvements, XBeach might be able to simulate breaching, inundation and intrusion successively in a single model.

On the other side, a proper geo-morphodynamic module as shown in Fig 8.2 is necessary in the surface module of HydroGeoSphere in order to simulate breaching of coastal barriers. Moreover, the diffusive wave approximation needs to be replaced by a full NLSWEs so that the inertial terms can be considered in order to achieve reliable inland discharges by HydroGeoSphere. The model should also include a short-wave module to account for the short-wave action and the associated processes such breaking, run up, etc.

Despite the need for many improvement and extensions, XBeach and HydroGeoSphere still remain as the most eligible models for future improvement in order to successively simulate breaching-induced floods and subsequent saltwater intrusion.

Bibliography

Abd-Elhamid, H. (2010). *A simulation-optimization model to study the control of seawater intrusion in coastal aquifers*. PhD thesis, College of Engineering, Mathematics and Physical Sciences, the University of Exeter, Devon, United Kingdom.

Abderrezzak, K. E. K., Paquier, A., and Mignot, E. (2009). "Modelling flash flood propagation in urban areas using a two-dimensional numerical model." *Natural Hazards*, 50(3), 433–460.

Abdullah, A. D. (2017). "Modelling Approaches to Understand Salinity Variations in a Highly Dynamic Tidal River: The Case of the Shatt al-Arab River." PhD dissertation, Delft University of Technology and the UNESCO-IHE (Institute for Water Education), Delft, The Netherlands.

Abreu, T., Silva, P., Sancho, F., and Temperville, A. (2010). "Analytical approximate wave form for asymmetric waves." *Coastal Engineering*, 57(7), 656–667.

Al-Riffai, M. (2014). *Experimental Study of Breach Mechanics in Overtopped Noncohesive Earthen Embankments*. PhD dissertation, Ottawa-Carleton Institute of Civil Engineering, University of Ottawa, Canda.

Ambrosio, B., and Siegle, E. (2014). "Wave Energy Levels At Inlet Channel Margins: the Effects of the Ebb Tidal Delta Morphology." *Proceedings of the 17th Physics of Estuaries and Coastal Seas (PECS) conference*, Porto de Galinhas, Pernambuco, Brazil, 19–24.

Anderson, M. P., Woessner, W. W., and Hunt, R. J. (2015). *Applied groundwater modelling : simulation of flow and advective transport*. Elsevier, London, UK.

Anderson, W. P. J. (2002). "Aquifer salinization from storm overwash." *Journal of Coastal Research*, 18(3), 413–420.

Andrews, D., and McIntyre, M. (1978). "An exact theory of nonlinear waves on a Lagrangian-mean flow." *Journal of Fluid Mechanics*, 89(4), 609–646.

Bagnold, R. A. (1956). "The Flow of Cohesionless Grains in Fluids." *Philosophical Transactions of the Royal Society of London A: Mathematical, Physical and Engineering Sciences*, 249(964).

Bailey, R. T., and Jenson, J. W. (2014). "Effects of Marine Overwash for Atoll Aquifers: Environmental and Human Factors." *Groundwater*, Blackwell Publishing Ltd, 52(5), 694–704.

Bakker, W. T., Van der Graaff, J., Kraak, A., Smit, M. J., Snip, D. W., Steetzel, H. J., and Visser, P. J. (1996). *Het Zwin, successen en lessen: Bresgroeiexperimenten 6 en 7 oktober 1994" Het totale experiment geslaagd."* Delft - The Netherlands.

Barbu, I. A., and Ballestero, T. P. (2015). "Unsaturated Flow Functions for Filter Media Used in Low-Impact Development—Stormwater Management Systems." *Journal of Irrigation and Drainage Engineering*, American Society of Civil Engineers, 141(1), 4014041.

Barlow, P. M., and Reichard, E. G. (2010). "Saltwater intrusion in coastal regions of North America." *Hydrogeology Journal*, 18(1), 247–260.

Barnard, P. L., van Ormondt, M., Erikson, L. H., Eshleman, J., Hapke, C., Ruggiero, P., Adams, P. N., and Foxgrover, A. C. (2014). "Development of the Coastal Storm Modeling System (CoSMoS) for predicting the impact of storms on high-energy, active-margin coasts." *Natural Hazards*, Springer Netherlands, 74(2), 1095–1125.

Bates, P. D., Dawson, R. J., Hall, J. W., Horritt, M. S., Nicholls, R. J., Wicks, J., and Hassan., M. A. A. M. (2005). "Simplified two-dimensional numerical modelling of coastal flooding and example applications." *Coastal Engineering*, 52(9), 793–810.

Bear, J., and Cheng, A. (2010). *Modeling groundwater flow and contaminant transport*. Springer Science+Business Media.

Beevers, L., Popescu, I., Pan, Q., and Pender, D. (2016). "Applicability of a coastal morphodynamic model for fluvial environments." *Environmental Modelling & Software*, 80, 83–99.

Bendoni, M. (2015). *Salt marsh edge erosion due to wind-induced waves*. PhD Dissertation, Technische Universität Braunschweig & University of Florence, Braunschweig, Germany.

Bendoni, M., Elsayed, S. M., Mojabi, S., Schürenkamp, D., and Oumeraci, H. (2016). "Küstenmorphologische Modellierung am LWI–Ein Überblick." *11. FZK-Kolloquium*, Forschungszentrum Küste: FZK, Hannover, DE, 34.

Berard, N. A., Mulligan, R. P., da Silva, A. M. F., and Dibajnia, M. (2017). "Evaluation of XBeach performance for the erosion of a laboratory sand dune." *Coastal Engineering*, 125, 70–80.

Bertin, X., Li, K., Roland, A., Zhang, Y. J., Breilh, J. F., and Chaumillon, E. (2014). "A modeling-based analysis of the flooding associated with Xynthia, central Bay of Biscay." *Coastal Engineering*, Elsevier B.V., 94, 80–89.

Van Biersel, T. P., Carlson, D. A., and Milner, L. R. (2007). "Impact of hurricanes storm surges on the groundwater resources." *Environmental Geology*, Springer-Verlag, 53(4), 813–826.

Bisschop, F., Miedema, S. A., Visser, P. J., Keetels, G. H., and van Rhee, C. (2016). "Experiments on the Pickup Flux of Sand at High Flow Velocities." *Journal of Hydraulic Engineering*, 142(7), 4016013.

Bisschop, F., Visser, P., Van Rhee, C., and Verhagen, H. J. (2010). "Erosion due to high flow velocities: a description of relevant processes." *Proceedings of 32nd International Conference on Coastal Engineering ICCE*, 10.

Blann, K. L., Anderson, J. L., Sands, G. R., and Vondracek, B. (2009). "Effects of Agricultural Drainage on Aquatic Ecosystems: A Review." *Critical Reviews in Environmental Science and Technology*, Taylor & Francis Group, 39(11), 909–1001.

Bogaard, T., De Kleermaeker, S., Jaeger, W. S., and van Dongeren, A. (2016). "Development of Generic Tools for Coastal Early Warning and Decision Support." *FLOODrisk 2016: 3rd European Conference on Flood Risk Management*, M. Lang, F. Klijn, and P. Samuels, eds., EDP Sciences, Lyon, France, 4.

Booij, N., Holthuijsen, L. H., and Ris, R. C. (1997). "The 'Swan' Wave Model for Shallow Water." *Coastal Engineering 1996*, American Society of Civil Engineers, New York, NY, 668–676.

Bosboom, J., and Stive, M. J. (2015). *Coastal Dynamics I: Lectures Notes CIE4305*. Delft.

Botros, F. E., Onsoy, Y. S., Ginn, T. R., and Harter, T. (2012). "Richards Equation–Based Modeling to Estimate Flow and Nitrate Transport in a Deep Alluvial Vadose Zone." *Vadose Zone Journal*, The Soil Science Society of America, Inc., 11(4).

Brinkkemper, J. (2013). *Modelling the cross-shore evolution of asymmetry and skewness of surface gravity waves propagating over a natural intertidal sandbar*. M.Sc. thesis, Department of Physical Geography, Faculty of Geosciences Utrecht University, Utrecht, The Netherlands, Utrecht, The Netherlands.

Brunner, G. W. (2016). *HEC-RAS River Analysis System. Hydraulic Reference Manual. Version 5.0*. United States Army Corps of Engineers (USACE), Davis, CA, USA.

Brunner, P., and Simmons, C. T. (2012). "HydroGeoSphere: A Fully Integrated, Physically Based Hydrological Model." *Ground Water*, Blackwell Publishing Ltd, 50(2), 170–176.

Bruun, P. (1962). "Sea level rise as a cause of shore erosion." *American Society of Civil Engineers, Journal of Waterways Harbours Division*, 88, 117–130.

Buckley, M., Lowe, R., and Hansen, J. (2014). "Evaluation of nearshore wave models in steep reef environments." *Ocean Dynamics*, 64(6), 847–862.

Bugajny, N., Furmanczyk, K., Dudzinska-Nowak, J., and Paplinska-Swerpel, B. (2013). "Modelling morphological changes of beach and dune induced by storm on the Southern Baltic coast using XBeach (case study: Dziwnow Spit)." *Journal of Coastal Research*, 1(65), 672–677.

Callaghan, D. P., Nielsen, P., Short, A., and Ranasinghe, R. (2008). "Statistical simulation of wave climate and extreme beach erosion." *Coastal Engineering*, 55(5), 375–390.

Camenen, B., and Larson, M. (2007). "A Unified Sediment Transport Formulation for Coastal Inlet Application." Report no " ERDC/CHL CR-07-1", U.S. Army Corps of Engineers, Washington, DC

Carrion Aretxabala, B. (2015). *Morphological impact of the Sinterklaas storm at Het Zwin: Numerical modelling with XBeach*. M.Sc. dissertation, Delft University of Technology, Delft, the Netherlands, Delft - The Netherlands.

Cha, M. (2012). *Mineral dissolution in sediments*. PhD Thesis, Georgia Institute of Technology, Atlanta, Georgia, USA, Atlanta, Georgia, USA.

Chang, S. W., and Clement, T. P. (2013). "Laboratory and numerical investigation of transport processes occurring above and within a saltwater wedge." *Journal of Contaminant Hydrology*, 147, 14–24.

Chaumillon, E., Bertin, X., Fortunato, A. B., Bajo, M., Schneider, J.-L., Dezileau, L., Walsh, J. P., Michelot, A., Chauveau, E., Créach, A., Hénaff, A., Sauzeau, T., Waeles, B., Gervais, B., Jan, G., Baumann, J., Breilh, J.-F., and Pedreros, R. (2017). "Storm-induced marine flooding: Lessons from a multidisciplinary approach." *Earth-Science Reviews*, 165, 151–184.

Cheng, A., and Ouazar, D. (2016). *Coastal aquifer management-monitoring, modelling, and case studies*. CRC Press\Lewis Publishers, Oxford, Mississippi, USA.

Cheung, K. F., Phadke, A. C., Wei, Y., Rojas, R., Douyere, Y. J.-M., Martino, C. D., Houston, S. H., Liu, P. L.-F., Lynett, P. J., Dodd, N., Liao, S., and Nakazaki, E. (2003). "Modeling of storm-induced coastal flooding for emergency management." *Ocean Engineering*, 30(11), 1353–1386.

Chini, N., Stansby, P. K., Rogers, B. D., Vacondio, R., and Mignosa, P. (2012). "State-of-the-art coastal inundation models applied to the 2007 Norfolk storm." *Comprehensive Flood Risk Management: Research for Policy and Practice. proceedings of the 2nd European Conference on Flood Risk Management FLOODrisk2012.*, F. Klijn and T. Schweckendiek, eds., CRC Press, Rotterdam, The Netherlands, 8.

Christensen, B. B., Drønen, N., Klagenberg, P., Jensen, J., Deigaard, R., and Sørensen, P. (2013). "Multiscale Modelling of Coastal Flooding." *7th international conference for Coastal Dynamics*, W. Jörg-Olaf, ed., Springer, Arcachon Convention Centre, France, 339–350.

Chui, T. F. M., and Terry, J. P. (2012). "Modeling Fresh Water Lens Damage and Recovery on Atolls After Storm-Wave Washover." *Ground Water*, Blackwell Publishing Ltd, 50(3), 412–420.

Church, J. A. (2013). "Sea level change." *Climate Change 2013: The physical science basis: Working Group I contribution to the Fifth assessment report of the Intergovernmental Panel on Climate Change*, T. F. Stocker, D. Qin, G.-K. Plattner, M. Tignor, S. K. Allen, J. Boschung, A. Nauels, Y. Xia, V. Bex, and P. M. Midgley, eds., Cambridge University Press, Cambridge, UK, New York, NY, USA, 1137–1216.

Collier, N., Radwan, H., Dalcin, L., and Calo, V. M. (2011). "Diffusive Wave Approximation to the Shallow Water Equations: Computational Approach." *Procedia Computer Science*, 4, 1828–1833.

D'Eliso, C. (2007). *Breaching of sea dykes initiated by wave overtopping; A tiered and modular modelling approach*. PhD dissertation, TU Braunschweig and University of Florence, Braunschweig, Germany.

Daly, C., Roelvink, D., van Dongeren, A., van Thiel de Vries, J., and McCall, R. (2012). "Validation of an advective-deterministic approach to short wave breaking in a surf-beat model." *Coastal Engineering*, 60, 69–83.

Darcy, H. (1856). *Les fontaines publiques de la ville de Dijon: exposition et application.* Technical report, Dalmont, Paris.

Deltares. (2015a). *XBeach Manual*. Deltares- Delft University of Technology, Delft - The Netherlands.

Deltares. (2015b). *XBeach skillbed report (revision 4672)*. Deltares- Delft University of Technology.

Ding, F., Yamashita, T., Lee, H.-S., and Pan, J. (2014). "A Modelling Study of Seawater Intrusion in the Liao Dong Bay Coastal Plain, China." *Journal of Marine Science and Technology*, 22(2), 103–115.

Dingman, S. L. (2015). *Physical hydrology*. Waveland Press, Inc., Eastham, Massachusetts, USA.

Van Dongeren, A. R., Roelvink, D., McCall, R. T., Nederhoff, K., and Van Rooijen, A. A. (2017). "Modeling the Morphological Impacts of Coastal Storms." *Coastal Storms: Processes and Impacts*, P. Ciavola and G. Coco, eds., Wiley-Blackwell, 195–213.

Van Dongeren, A., Bolle, A., Vousdoukas, M. I., Plomaritis, T., Eftimova, P., Williams, J., Armaroli, C., Idier, D., Van Geer, P., Van Thiel de Vries, J., Haerens, P., Taborda, R., Benavente, J., Trifonova, E., Ciavola, P., Balouin, Y., and Roelvink, D. (2009). "MICORE: dune erosion and overwash model validation with data from nine European field sites." *Proceedings of Coastal Dynamics 2009: Impacts of Human Activities on Dynamic Coastal Processes*, M. Mizuguchi and S. Sato, eds., Tokyo, Japan, 1–15.

Donnelly, C. (2007). "Morphologic change by overwash: establishing and evaluating predictors." *Journal of Coastal Research*, (SI 50), 520–526.

Donnelly, C., Kraus, N. C., and Larson, M. (2004). "Coastal Overwash: Part 1, Overview of Processes."

Donnelly, C., Kraus, N., and Larson, M. (2006). "State of knowledge on measurement and modelling of coastal overwash." *Journal of Coastal Research*, 22(4), 965–991.

Donnelly, C., Wamsley, T. V., Kraus, N. C., Larson, M., and Hanson, H. (2007). "Morphologic classification of coastal overwash." *Coastal Engineering 2006*, World Scientific Publishing Company, 2805–2817.

Drablos, C., and Moe, R. (1984). *Illinois drainage guide*. *Illinois. University. Cooperative Extension*.

Van Drie, R., Simon, M., and Schymitzek, I. (2008). "HAZARD :- Is there a better definition? & Impact of Not accounting for buildings!" *Proceedings of the Second Emerging Technologies Conference*, I. Olney, G. Lefoe, J. Mantei, and J. Herrington, eds., University of Wollongong, Wollongong, New South Wales, Australia.

Elder, J. W. (1967). "Transient convection in a porous medium." *Journal of Fluid Mechanics*, Cambridge University Press, 27(3), 609.

Elsayed, S. M. (2013). *Comparative study of different scenarios for the morphological evolution in a river stream*. M.Sc. dissertation, Politecnico di Milano, Milan, Italy.
Available at: http://hdl.handle.net/10589/82763

Elsayed, S. M., and Oumeraci, H. (2014). *Breaching of Coastal Barriers under Extreme Storm Surges and Implications for Groundwater Contamination: State of the Art Report*. Internal Report no 1071, Leichtweiß-Institut für Wasserbau, TU Braunschweig, Braunschweig, Germany.
Available at:
https://www.researchgate.net/publication/304539691_State_of_the_Art_on_Breaching_of_Coastal_Barriers_under_Extreme_Storm_Surges_and_Implications_for_Groundwater_Contamination

Elsayed, S. M., and Oumeraci, H. (2015a). *Breaching of Coastal Barriers under Extreme Storm Surges and Implications for Groundwater Contamination: Assessment of the XBeach Model Performance under Storm Surges using GWK-Data*. Internal Report no 1072, Leichtweiß-Institut for Hydraulic Engineering and Water Resources, TU Braunschweig, Braunschweig, Germany.
Available at:
https://www.researchgate.net/publication/316351876_Assessment_of_the_XBeach_Model_Performance_under_Storm_Surges_using_GWK-Data

Elsayed, S. M., and Oumeraci, H. (2015b). *Breaching of Coastal Barriers under Extreme Storm Surges and Implications*

for Groundwater Contamination: Improvement and Extension of the XBeach Model to Account for New Physical Processes. Internal Report no 1073, Leichtweiß-Institut for Hydraulic Engineering and Water Resources, TU Braunschweig, Braunschweig, Germany.
Available at:
https://www.researchgate.net/publication/315819318_Improvement_and_Extension_of_the_XBeach_Model_to_Account_f.

Elsayed, S. M., and Oumeraci, H. (2016a). *Breaching of Coastal Barriers under Extreme Storm Surges and Implications for Groundwater Contamination: Application of XBeach in Coastal Flood Propagation*. Internal Report no 1074, Leichtweiß-Institut for Hydraulic Engineering and Water Resources, TU Braunschweig.
Available at:
https://www.researchgate.net/publication/315739116_Application_of_XBeach_in_Coastal_Flood_Propagation.

Elsayed, S. M., and Oumeraci, H. (2016b). "Combined Modelling of Coastal Barrier Breaching and Induced Flood Propagation Using XBeach." *Hydrology*, Multidisciplinary Digital Publishing Institute (MDPI), 3(4), 34.

Elsayed, S. M., and Oumeraci, H. (2017a). "Effect of beach slope and grain-stabilization on coastal sediment transport: An attempt to overcome the erosion overestimation by XBeach." *Coastal Engineering*, 121, 179–196.

Elsayed, S. M., and Oumeraci, H. (2017b). *Breaching of Coastal Barriers under Extreme Storm Surges and Implications for Groundwater Contamination: Implications of coastal floods for groundwater contamination.* Internal Report no 1075, Leichtweiß-Institut for Hydraulic Engineering and Water Resources, TU Braunschweig, Germany.
available at:
https://www.researchgate.net/publication/316459814_Implications_of_coastal_floods_for_groundwater_contamination.

Essaid, H. I. (1990). *The computer model SHARP, quasi-three-dimensional, numerical finite-difference model to simulate freshwater and saltwater flow separated by a sharp interface in layered coastal aquifer systems*. U.S. Geological Survey Water-Resources Investigations Report 90-4130, 181 p.

Evangelista, S., Giovinco, G., and Kocaman, S. (2017). "A multi-parameter calibration method for the numerical simulation of morphodynamic problems." *Journal of Hydrology and Hydromechanics*, 65(2), 175–182.

Evangelista, S., Greco, M., Iervolino, M., Leopardi, A., and Vacca, A. (2015). "A new algorithm for bank-failure mechanisms in 2D morphodynamic models with unstructured grids." *International Journal of Sediment Research*, 30(4), 382–391.

Fakhruddin, S. (2016). *Flood impact on agriculture risk management*. PhD dissertation, Politecnico di Milano, Milan, Italy.

Fan, X., Tang, C. X., van Westen, C. J., and Alkema, D. (2012). "Simulating dam-breach flood scenarios of the Tangjiashan landslide dam induced by the Wenchuan Earthquake." *Natural Hazards and Earth System Science*, Copernicus GmbH, 12(10), 3031–3044.

Faneca Sànchez, M., Bashar, K., Janssen, G., Vogels, M., Snel, J., Zhou, Y., Stuurman, R. J., and Oude Essink, G. (2015). *SWIBANGLA: Managing salt water intrusion impacts in coastal groundwater systems of Bangladesh*. Deltares, Utrecht, The Netherlands.

Fausey, N. R., Brown, L. C., Belcher, H. W., and Kanwar, R. S. (1995). "Drainage and Water Quality in Great Lakes and Cornbelt States." *Journal of Irrigation and Drainage Engineering*, American Society of Civil Engineers, 121(4), 283–288.

Feddersen, F., and Veron, F. (2005). "Wind Effects on Shoaling Wave Shape." *Journal of Physical Oceanography*, 35(7), 1223–1228.

Felisa, G., Ciriello, V., and Di Federico, V. (2013). "Saltwater Intrusion in Coastal Aquifers: A Primary Case Study along the Adriatic Coast Investigated within a Probabilistic Framework." *Water*, 5(4), 1830–1847.

Frank, P.-J. R. (2016). *Hydraulics of spatial dyke breaches*. PhD dissertation, the Laboratory of Hydraulics, Hydrology, and Glaciology (VAW), Swiss Federal Institute of Technology (ETH) Zurich., Zurich, Switzerland.

Fuhrman, D. R., Fredsøe, J., and Sumer, B. M. (2009). "Bed slope effects on turbulent wave boundary layers: 2. Comparison with skewness, asymmetry, and other effects." *Journal of Geophysical Research*, 114(C3), C03025.

Furman, A. (2008). "Modeling Coupled Surface–Subsurface Flow Processes: A Review." *Vadose Zone Journal*, Soil Science Society, 7(2), 741–756.

Gaaloul, N., Pliakas, F., Kallioras, A., Schuth, C., and P. Marinos. (2012). "Simulation of seawater intrusion in coastal aquifers: Forty five-years exploitation in an eastern coast aquifer in NE Tunisia." *The Open Hydrology Journal*, 6, 31–44.

Galappatti, G., and Vreugdenhil, C. (1985). "A depth-integrated model for suspended sediment transport." *Journal of Hydraulic Research*, 23(4), 359–377.

Gallien, T. (2016). "Validated coastal flood modelling at Imperial Beach, California: Comparing total water level, empirical and numerical overtopping methodologies." *Coastal Engineering*, 111, 95–104.

Gallien, T., and Guza, R. (2015). "Modelling and Observations of Wave Overtopping Flooding on a Southern California Beach." *E-proceedings of the 36th IAHR World Congress*, Tailor & Francis Groop, The Hague, the Netherlands, 2.

Gallien, T., Sanders, B., and Flick, R. (2014). "Urban coastal flood prediction: Integrating wave overtopping, flood defences and drainage." *Coastal Engineering*, 91, 18–28.

Van Geer, P. F. C., Van Thiel de Vries, J. S. M., Boers, M., Den Bieman, J. P., and McCall, R. T. (2014). "Modelling scour in front of dune revetments in a surf-beat model." *Proceedings of 34th Conference on Coastal Engineering (ICCE 2014)*, P. Lynett, ed., the Coastal Engineering Research Council, Seoul, Korea, 9.

van Gent, M. R. A., van Thiel de Vries, J. S. M., Coeveld, E. M., de Vroeg, J. H., and van de Graaff, J. (2008). "Large-scale dune erosion tests to study the influence of wave periods." *Coastal Engineering*, 55(12), 1041–1051.

Giambastiani, B. M. S., Colombani, N., Greggio, N., and Mastrocicco, M. A. M. (2017). "Coastal aquifer response to extreme storm events in Emilia-Romagna, Italy." *Hydrological Processes*.

Giardino, A., Briére, C., Deserti, M., and Malmonado, V. (2011). "Operational Modelling Applications for Coastal Engineering: new Developments." *Proceedings of the Tenth International Conference on the Mediterranean Coastal Environment (MEDCOAST 2011)*, E. Özhan, ed., Rhodes, Greece, 12.

Gopinath, S., Srinivasamoorthy, K., Saravanan, K., Suma, C. S., Prakash, R., Senthilnathan, D., Chandrasekaran, N., Srinivas, Y., and Sarma, V. S. (2016). "Modeling saline water intrusion in Nagapattinam coastal aquifers, Tamilnadu, India." *Modeling Earth Systems and Environment*, Springer International Publishing, 2(1), 10.

Grismer, M. (1990). "Leaching fraction, soil salinity, and drainage efficiency." *California Agriculture*, 44(6), 24–26.

Guedes Soares, C., Cherneva, Z., and Antão, E. M. (2004). "Steepness and asymmetry of the largest waves in storm sea states." *Ocean Engineering*, 31(8–9), 1147–1167.

Harley, M. D., Valentini, A., Armaroli, C., Perini, L., Calabrese, L., and Ciavola, P. (2016). "Can an early-warning system help minimize the impacts of coastal storms? A case study of the 2012 Halloween storm, northern Italy." *Natural Hazards and Earth System Sciences*, Copernicus GmbH, 16(1), 209–222.

Hartanto, I. M., Beevers, L., Popescu, I., and Wright, N. G. (2011). "Application of a coastal modelling code in fluvial environments." *Environmental Modelling & Software*, Elsevier Ltd, 26(12), 1685–1695.

Harter, C., and Figlus, J. (2017). "Numerical modelling of the morphodynamic response of a low-lying barrier island beach and foredune system inundated during Hurricane Ike using XBeach and CSHORE." *Coastal Engineering*, 120, 64–74.

He, Z., Hu, P., Zhao, L., Wu, G., and Pähtz, T. (2015). "Modeling of Breaching Due to Overtopping Flow and Waves Based on Coupled Flow and Sediment Transport." *Water*, Multidisciplinary Digital Publishing Institute, 7(8), 4283–4304.

Henry, H. (1964). *Effects of dispersion on salt encroachment in coastal aquifers: U.S. Geological Survey Water-Supply Paper, 1613-C*.

Herzberg, A. (1901). "Die Wasserversorgung einiger Nordseebader." *Wasserversorgung*, 44, 842–844.

Hinkel, J., Lincke, D., Vafeidis, A. T., Perrette, M., Nicholls, R. J., Tol, R. S. J., Marzeion, B., Fettweis, X., Ionescu, C., and Levermann, A. (2014). "Coastal flood damage and adaptation costs under 21st century sea-level rise." *Proceedings of the National Academy of Sciences of the United States of America*, (Hans Joachim Schellnhuber, ed.), National Academy of Sciences, 111(9), 3292–3297.

Holding, S., and Allen, D. M. (2015). "Wave overwash impact on small islands: Generalised observations of freshwater lens response and recovery for multiple hydrogeological settings." *Journal of Hydrology*, 529, 1324–1335.

Holthuijsen, L. H., Booij, N., and Herbers, T. H. C. (1989). "A prediction model for stationary, short-crested waves in shallow water with ambient currents." *Coastal Engineering*, 13(1), 23–54.

Hsu, T., and Hanes, D. (2004). "Effects of wave shape on sheet flow sediment transport." *Journal of Geophysical Research: Oceans*, 109(C05025).

Hughes, S. A. (2008). "Estimation of Overtopping Flow Velocities on Earthen Levees Due to Irregular Waves." Army Engineer Research and Development Center, Environmental Laboratory, Vicksburg, MS.

Illangasekare, T., Tyler, S. W., Clement, T. P., Villholth, K. G., Perera, A. P. G. R. L., Obeysekera, J., Gunatilaka, A., Panabokke, C. R., Hyndman, D. W., Cunningham, K. J., Kaluarachchi, J. J., Yeh, W. W. G., Van Genuchten, M. T., and Jensen, K. (2006). "Impacts of the 2004 tsunami on groundwater resources in Sri Lanka." *Water Resources Research*, 42(5), 1–9.

Izaguirre, C., Losada, I. J., Espejo, A., Diez-Sierra, J., and Díaz-Simal, P. (2017). "Coastal flooding risk associated to tropical cyclones in a changing climate. Application to Port of Spain (Trinidad and Tobago)." *Natural Hazards*

and Earth System Sciences Discussions, Copernicus GmbH, 1–24.

Johnson, B., Kobayashi, N., and Gravens, M. (2012). "Cross-shore numerical model CSHORE for waves, currents, sediment transport and beach profile evolution." Coastal and Hydraulics Laboratory U.S. Army Engineer Research and Development Center, Vicksburg, MS.

Kaika, M. (2003). "The Water Framework Directive: A New Directive for a Changing Social, Political and Economic European Framework." *European Planning Studies*, Taylor & Francis Group, 11(3), 299–316.

Kalaoun, O., Al Bitar, A., Gastellu-Etchegorry, J.-P., and Jazar, M. (2016). "Impact of Demographic Growth on Seawater Intrusion: Case of the Tripoli Aquifer, Lebanon." *Water*, Multidisciplinary Digital Publishing Institute, 8(3), 18.

Kalita, P., Cooke, R., Anderson, S., and Hirschi, M. (2007). "Subsurface drainage and water quality: The Illinois experience." *Transactions of the ASABE*, 50(5), 1651–1656.

Ketabchi, H., Mahmoodzadeh, D., Ataie-Ashtiani, B., and Simmons, C. T. (2016). "Sea-level rise impacts on seawater intrusion in coastal aquifers: Review and integration." *Journal of Hydrology*, 535, 235–255.

Kobayashi, N., Agarwal, A., and Johnson, B. D. (2007). "Longshore Current and Sediment Transport on Beaches." *Journal of Waterway, Port, Coastal, and Ocean Engineering*, 133(4), 296–304.

Kolditz, O., Bauer, S., Bilke, L., Böttcher, N., Delfs, J. O., Fischer, T., Görke, U. J., Kalbacher, T., Kosakowski, G., McDermott, C. I., Park, C. H., Radu, F., Rink, K., Shao, H. B., Shao, H. B., Sun, F., Sun, Y. Y., Singh, A. K., Taron, J., Walther, M., Wang, W., Watanabe, N., Wu, Y., Xie, M., Xu, W., and Zehner, B. (2012). "OpenGeoSys: an open-source initiative for numerical simulation of thermo-hydro-mechanical/chemical (THM/C) processes in porous media." *Environmental Earth Sciences*, Springer-Verlag, 67(2), 589–599.

Komar, P., and Miller, M. (1975). "On the comparison between the threshold of sediment motion under waves and unidirectional currents with a discussion of the practical evaluation of the threshold." *Journal of Sedimentary Research*, 45(1), 362–367.

Kooi, H., Groen, J., and Leijnse, A. (2000). "Modes of seawater intrusion during transgressions." *Water Resources Research*, 36(12), 3581–3589.

Korkmaz, S., Pekkan, E., and Güney, Y. (2016). "Transient Analysis with *MODFLOW* for Developing Water-Diversion Function." *Journal of Hydrologic Engineering*, 21(6), 5016009.

Kourakos, G., and Mantoglou, A. (2015). "An efficient simulation-optimization coupling for management of coastal aquifers." *Hydrogeology Journal*, 23(6), 1167–1179.

Kraus, N. C., and Wamsley, T. V. (2003). "Coastal Barrier Breaching. Part 1. Overview of Breaching Processes." *Engineer Research and Development Centre Vicksburg Ms Coastal and Hydraulics Lab*.

Kresic, N. (2006). *Hydrogeology and groundwater modelling*.

Kumar, C. (2006). "Groundwater flow models: an overview." *Groundwater modelling and management*, N. C. Ghosh and K. D. Sharma, eds., Capital Publishing Company, New Delhi, 153–178.

Kumar, C. (2016). "Sea water intrusion in coastal aquifers." *EPRA International Journal of Research and Development*, 1(3), 27–31.

Lamb, M. P., Dietrich, W. E., and Venditti, J. G. (2008). "Is the critical Shields stress for incipient sediment motion dependent on channel-bed slope?" *Journal of Geophysical Research: Earth Surface*, 113(F2), 20.

Larroudé, P., Daou, M., Cartier, A., and Hequette, A. (2015). "Sediment Transport Formulae for Coastal Morphodynamic Simulation: Calculated Sediment Flux Against In Situ Data." Springer Netherlands, 191–206.

Larson, M., Kraus, N. C., and Byrnes, M. R. (1989). *SBEACH: numerical model for simulating storm-induced beach change. Report 1. Empirical foundation and model development*. Vicksburg, MS.

Levanon, E., Shalev, E., Yechieli, Y., and Gvirtzman, H. (2016). "Fluctuations of fresh-saline water interface and of water table induced by sea tides in unconfined aquifers." *Advances in Water Resources*, 96, 34–42.

Li, L., Barry, A. D., Jeng, S. D., and Prommer, H. (2004). "Tidal Dynamics of Groundwater Flow and Contaminant Transport in Coastal Aquifers." *Coastal aquifer management: monitoring, modelling and case studies*, A. Cheng and D. Ouazar, eds., CRC Press\Lewis Publishers, London, 226.

Lilai, X., Yuanrong, H., Wei, H., and shenghui, C. (2016). "A multi-dimensional integrated approach to assess flood risks on a coastal city, induced by sea-level rise and storm tides." *Environmental Research Letters*, IOP Publishing, 11(1), 14001.

Lin, B., Wicks, J. M., Falconer, R., and Adams, K. (2006). "Integrating 1D and 2D hydrodynamic models for flood simulation." *Proceedings of the Institution of Civil Engineers ICE - Water Management*, 159, 19–25.

Longuet-Higgins, M. S., and Stewart, R. W. (1962). "Radiation stress and mass transport in gravity waves, with application to 'surf beats.'" *Journal of Fluid Mechanics*, 13(4), 481–504.

Lonquet-Higgins, M., and Stewart, R. (1964). "Radiation Stress in water waves: a physical discussion with

application." *Deep-Sea Research*, 11(529–562).

Masselink, G., and van Heteren, S. (2014). "Response of wave-dominated and mixed-energy barriers to storms." *Marine Geology*, 352, 321–347.

Maxwell, R. M., Putti, M., Meyerhoff, S., Delfs, J.-O., Ferguson, I. M., Ivanov, V., Kim, J., Kolditz, O., Kollet, S. J., Kumar, M., Lopez, S., Niu, J., Paniconi, C., Park, Y.-J., Phanikumar, M. S., Shen, C., Sudicky, E. A., and Sulis, M. (2014). "Surface-subsurface model intercomparison: A first set of benchmark results to diagnose integrated hydrology and feedbacks." *Water Resources Research*, 50(2), 1531–1549.

McCabe, M. V., Stansby, P. K., and Apsley, D. D. (2013). "Random wave runup and overtopping a steep sea wall: Shallow-water and Boussinesq modelling with generalised breaking and wall impact algorithms validated against laboratory and field measurements." *Coastal Engineering*, 74, 33–49.

McCall, R. (2008). *The longshore dimension in dune overwash modelling: development, verification and validation of XBeach*. M.Sc. dissertation, Delft University of Technology, Delft, the Netherlands, Delft - The Netherlands.

McCall, R. (2015). "Process-based modelling of storm impacts on gravel coasts." PhD dissertation, Plymouth University, Plymouth, England.

McCall, R. T., Masselink, G., Poate, T. G., Roelvink, J. A., Almeida, L. P., Davidson, M., and Russell, P. E. (2014). "Modelling storm hydrodynamics on gravel beaches with XBeach-G." *Coastal Engineering*, 91, 231–250.

McCall, R. T., Masselink, G., Roelvink, D., Russell, P., Davidson, M., and Poate, T. (2012). "Modelling overwash and infiltration on gravel barriers." *Coastal Engineering Proceedings*, Santander, Spain, 34.

McCall, R. T., Van Thiel de Vries, J. S. M., Plant, N. G., Van Dongeren, A., Roelvink, J. A., Thompson, D. M., and Reniers, A. J. H. M. (2010). "Two-dimensional time dependent hurricane overwash and erosion modelling at Santa Rosa Island." *Coastal Engineering*, 57(7), 668–683.

Van der Meer, J. W., Allsop, N. W. H., Bruce, T., De Rouck, J., Kortenhaus, A., Pullen, T., Schüttrumpf, H., Troch, P., and Zanuttigh, B. (2016). *EurOtop II 2016: Manual on wave overtopping of sea defences and related structures An overtopping manual largely based on European research, but for worldwide application*.

Meilianda, E., Alfian, D., and Huhn, K. (2011). "Sediment grain-size distribution analysis at the shallow sandy shelf of the North Sea using multivariate geostatistics." *Procedia Environmental Sciences*, 7, 317–322.

Meyer-Peter, E., and Müller, R. (1948). "Formulas for bed-load transport." *Proceedings of the 2nd Meeting of the International Association for Hydraulic Structures Research.*, 39–64.

Mishra, S., and Dwibedy, S. (2015). "Geohydrology of South Mahanadi Delta and Chilika Lake, Odisha." *International Journal*, 3(11), 430–445.

Möller, I., Kudella, M., Rupprecht, F., Spencer, T., Paul, M., van Wesenbeeck, B. K., Wolters, G., Jensen, K., Bouma, T. J., Miranda-Lange, M., and Schimmels, S. (2014). "Wave attenuation over coastal salt marshes under storm surge conditions." *Nature Geoscience*, Nature Research, 7(10), 727–731.

Mora, M. F. (2015). *On cross-shore beach profile morphodynamics*. *Materia (s)*, PhD dissertation, Universitat Politècnica de Catalunya, Catalonia, Spain, Catalonia, Spain.

Morris, M., Kortenhaus, A., Visser, P., D'Eliso, C., Geisenhainer, P., Mohamed, H., Stanczak, G., Wahl, T., and Zhu, Y. (2009). *Modelling breach initiation and growth*.

Morris, M. W. (2011). *Breaching of earth embankments and dams*. PhD dissertation, Open University, UK, United Kingdom.

Mullan, B., Salinger, J., Thompson, C., Ramsay, D., and Wild, M. (2005). *Chatham Islands Climate Change*. Wellington, New Zealand.

Muller, H., Rooijen, A. van, Idier, D., Pedreros, R., and Rohmer, J. (2016). "Assessing Storm Impact on a French Coastal Dune System Using Morphodynamic Modeling." *Journal of Coastal Research*, The Coastal Education and Research Foundation.

Narayan, K. A., Schleeberger, C., and Bristow, K. L. (2007). "Modelling seawater intrusion in the Burdekin Delta Irrigation Area, North Queensland, Australia." *Agricultural Water Management*, 89(3), 217–228.

Nederhoff, C. (2014). *Modelling the effects of hard structures on dune erosion and overwash*. M.Sc. dissertation, Delft University of Technology, Delft, the Netherlands, Delft - The Netherlands.

Nederhoff, C. M., Lodder, Q. J., Boers, M., den Bieman, J. P., and Miller, J. K. (2015). "Modeling the effects of hard structures on dune erosion and overwash: a case study of the impact of Hurricane Sandy on the New Jersey coast." *Coastal Sediments 2015: The Proceedings of the Coastal Sediments*, P. Wang, J. Rosati, and J. Cheng, eds., world scientific publishing, San Diego, California, USA, 17.

Neumann, B., Vafeidis, A. T., Zimmermann, J., Nicholls, R. J., Schmidt, J., and Doorn, E. van. (2015). "Future Coastal Population Growth and Exposure to Sea-Level Rise and Coastal Flooding - A Global Assessment." *PLOS ONE*, (L. Kumar, ed.), Socioeconomic Data and Applications Centre (SEDAC), Columbia University, 10(3), e0118571.

Nickling, W. G., and Ecclestone, M. (1981). "The effects of soluble salts on the threshold shear velocity of fine sand." *Sedimentology*, 28(4), 505–510.

Nimmo, J. R. (2009). "Vadose Water." *Encyclopedia of inland waters*, G. E. Likens, ed., Elsevier, Oxford, Mississippi, USA, 766–777.

NOAA. (2008). "Introduction to Storm Surge." available at: http://www.nws.noaa.gov/om/hurricane/resources/surge_intro.pdf.

Nofal, E., Fekry, A., and El-Didy, S. (2014). "Adaptation to the Impact of Sea Level Rise in the Nile Delta Coastal zone, Egypt." *Journal of American Science*, 10(9), 1–7.

Nowell, A. R., Jumars, P. A., and Eckman, J. E. (1981). "Effects of biological activity on the entrainment of marine sediments." *Marine Geology (Sedimentary dynamics of continental shelves)*, 42(1–4), 133–153.

Olbert, A. I., Comer, J., Nash, S., and Hartnett, M. (2017). "High-resolution multi-scale modelling of coastal flooding due to tides, storm surges and rivers inflows. A Cork City example." *Coastal Engineering*, 121, 278–296.

Othman, I. K., Baldock, T. E., and Callaghan, D. P. (2014). "Measurement and modelling of the influence of grain size and pressure gradient on swash uprush sediment transport." *Coastal Engineering*, 83, 1–14.

Oude Essink, G. H. . (2001). "Improving fresh groundwater supply—problems and solutions." *Ocean & Coastal Management*, 44(5), 429–449.

Oumeraci, H. (2017). "Wellentransformation." Braunschweig, Germany.

Oumeraci, H., Kortenhaus, A., Strusińska-Correia, A., Hinze, K., and Brühl, M. (2014). *Wellenüberlauf des Deckwerks und Erosion der Dünen an der Westseite der Nordseeinsel Wangerooge*. : Technische Universität Braunschweig, Leichtweiß-Institut für Wasserbau, Abteilung Hydromechanik und Küsteningenieurwesen.

Oumeraci, H., Kortenhaus, H., Burzel, A., Naulin, M., Dassanayake, D. R., Jensen, J., Wahl, T., Mudersbach, C., Gonnert, G., Gerkensmeier, B., Frohle, P., and Ujeyl, G. (2015). "XtremRisK—Integrated flood risk analysis for extreme storm surges at open coasts and in estuaries: Methodology, key results and lessons learned." *Coastal Engineering Journal*, 57(1), 1–23.

Oz, I., Shalev, E., Yechieli, Y., Gavrieli, I., and Gvirtzman, H. (2014). "Flow dynamics and salt transport in a coastal aquifer driven by a stratified salt water body: Lab experiment and numerical modelling." *Journal of Hydrology*, 511, 665–674.

Özer, I. E., van Damme, M., Schweckendiek, T., and Jonkman, S. N. (2016). "On the importance of analysing flood defense failures." *FLOODrisk 2016 - 3rd European Conference on Flood Risk Management (Section: Performance and behaviour of flood defences)*, M. Lang, F. Klijn, and P. Samuels, eds., EDP Sciences, E3S Web of Conferences 7, 03013, Lyon, France, 9.

Palmsten, M. L., and Splinter, K. D. (2016). "Observations and simulations of wave runup during a laboratory dune erosion experiment." *Coastal Engineering*, 115, 58–66.

Parry, M., Canziani, O., Palutikof, J., van der Linden, P., and Hanson, C. (2007). *IPCC, 2007: Climate change 2007-impacts, adaptation and vulnerability: Working group II contribution to the fourth assessment report of the Intergovernmental Panel on Climate Change*. Cambridge University Press, Cambridge, UK.

Pender, D., and Karunarathna, H. (2013). "A statistical-process based approach for modelling beach profile variability." *Coastal Engineering*, 81, 19–29.

Pender, D., Patidar, S., and Haynes, H. (2015). "Incorporating River Bed Level Changes Into Flood Risk Modelling." *E-proceedings of the 36th IAHR World Congress*, The Hague, the Netherlands, 1–9.

Pérez-Paricio, A., Hunink, J. E., Kupper, E., Quintana, J. R., and Raso, J. (2010). "Estimation of the river conductance coefficient using streambed slope for modelling of regional river-aquifer interaction." *18th International Conference on Water Resources*, J. Carrera, ed., International Center for Numerical Methods in Engineering, Barcelona, Spain, 9.

Phillips, B., Brown, J., Bidlot, J.-R., and Plater, A. (2017). "Role of Beach Morphology in Wave Overtopping Hazard Assessment." *Journal of Marine Science and Engineering*, Multidisciplinary Digital Publishing Institute, 5(1), 18.

Popescu, I., Jonoski, A., Van Andel, S. J., Onyari, E., and Moya Quiroga, V. G. (2010). "Integrated modelling for flood risk mitigation in Romania: case study of the Timis–Bega river basin." *International Journal of River Basin Management*, Taylor & Francis , 8(3–4), 269–280.

Post, V. E. A. a, Groen, J., Kooi, H., Person, M., Ge, S., and Edmunds, W. M. (2013). "Offshore fresh groundwater reserves as a global phenomenon." *Nature*, Nature Research, 504(7478), 71–78.

Prancevic, J., and Lamb, M. (2015). "Unraveling bed slope from relative roughness in initial sediment motion." *Journal of Geophysical Research: Earth Surface*, 120(3), 474–489.

Pullen, T., Allsop, N. W. H., Bruce, T., Kortenhaus, A., Schüttrumpf, H., and Van der Meer, J. W. (2007). *EurOtop Wave Overtopping of Sea Defences and Related Structures: Assessment Manual*. Die Küste.

Radice, A., and Elsayed, S. M. (2014). "Hydro-morphologic modelling for different calamitous scenarios in a mountain stream." *River Flow 2014 7th International Conference on Fluvial Hydraulics*, CRC Press 2014 (Taylor & Francis Group), Lausanne, GB, 1603–1610.

Ranasinghe, R. (2016). "Assessing climate change impacts on open sandy coasts: A review." *Earth-Science Reviews*.

Reid, I., and Frostick, L. E. (1984). "Particle Interaction and Its Effect on the Thresholds of Initial and Final Bedload Motion in Coarse Alluvial Channels." *Sedimentology of Gravels and Conglomerates*, CSPG Special Publications, Memoir 10, 61–68.

Reniers, A. J. H. M., Roelvink, J. A., and Thornton, E. B. (2004). "Morphodynamic modelling of an embayed beach under wave group forcing." *Journal of Geophysical Research*, 109(C1), 22.

Van Rhee, C. (2007). "Erosion of granular sediments at high flow velocity." *Hydrotransport 17. In The 17th International Conference on the Hydraulic Transport of Solids*, Cape Town, South Africa.

Van Rhee, C. (2010). "Sediment entrainment at high flow velocity." *Journal of hydraulic engineering*, 136(9), 572–582.

Richards, L. A. (1931). "Capillary conduction of liquids through porous mediums." *Physics*, American Institute of Physics, 1(5), 318.

Richardson, J. F., and Zaki, W. N. (1997). "Sedimentation and fluidisation: Part I." *Chemical Engineering Research and Design*, Elsevier, 75, S82–S100.

van Rijn, L. C. (1984). "Sediment Transport, Part III: Bed forms and Alluvial Roughness." *Journal of Hydraulic Engineering*, 110(12), 1733–1754.

Van Rijn, L. C., Walstra, D. J. R., Grasmeijer, B., Sutherland, J., Pan, S., and Sierra, J. P. (2003). "The predictability of cross-shore bed evolution of sandy beaches at the time scale of storms and seasons using process-based profile models." *Coastal Engineering*, 47(3), 295–327.

Van Rijn, L. (2007a). "Unified view of sediment transport by currents and waves. I: Initiation of motion, bed roughness, and bed-load transport." *Journal of Hydraulic Engineering*, 133(6), 649–667.

Van Rijn, L. (2007b). "Unified view of sediment transport by currents and waves. II: Suspended transport." *Journal of Hydraulic Engineering*, 133(6), 668–689.

Van Rijn, L. (2007c). "Unified view of sediment transport by currents and waves. III: Graded beds." *Journal of Hydraulic Engineering*, 133(7), 761–775.

Van Rijn, L. (2007d). "Unified view of sediment transport by currents and waves. IV: Application of morphodynamic model." *Journal of Hydraulic Engineering*, 133(7), 776–793.

Robinson, C., Xin, P., Li, L., and Barry, D. A. (2014). "Groundwater flow and salt transport in a subterranean estuary driven by intensified wave conditions." *Water Resources Research*, 50(1), 165–181.

Roelvink, D., van Dongeren, A., McCall, R., Hoonhout, B., Rooijen, A. van, Geer, P. van, de Vet, L., Nederhoff, K., and Quataert, E. (2015). *XBeach Technical Reference (Kingsday Release): Model description and reference guide to functionalities*. Deltares, UNESCO-IHE Institute of Water Education and Delft University of Technology, Delft - the Netherlands.

Roelvink, D., McCall, R., Mehvar, S., Nederhoff, K., and Dastgheib, A. (2017a). "Improving predictions of swash dynamics in XBeach: The role of groupiness and incident-band runup." *Coastal Engineering*.

Roelvink, D., McCall, R., Mehvar, S., Nederhoff, K., and Dastgheib, A. (2017b). "Improving predictions of swash dynamics in XBeach: The role of groupiness and incident-band runup." *Coastal Engineering*.

Roelvink, D., and Reniers, A. (2012). *A guide to modelling coastal morphology*. World Scientific.

Roelvink, D., Reniers, A., van Dongeren, A., van Thiel de Vries, J., McCall, R., and Lescinski, J. (2009). "Modelling storm impacts on beaches, dunes and barrier islands." *Coastal Engineering*, Elsevier B.V., 56(11–12), 1133–1152.

Roelvink, D., Reniers, A. J. H. M., Van Dongeren, A., Van Thiel de Vries, J., Lescinski, J., and McCall, R. (2010). *XBeach model description and manual. Unesco-IHE Institute for Water Education, Deltares and Delft University of Technology*, Delft - The Netherlands.

Roger, S., Dewals, B. J., Erpicum, S., Schwanenberg, D., Archambeau, P., Köngeter, J., Pirotton, M., and Schüttrumpf, H. (2010). "Hybrid modelling of dike-break induced flows." *River flow 2010 : proceedings of the International Conference on Fluvial Hydraulics*, A. Dittrich, K. Koll, J. Aberle, and P. Geisenhainer, eds., Karlsruhe : Bundesanstalt für Wasserbau, Braunschweig, Germany, 523–531.

Roland, A., Zhang, Y. J., Wang, H. V., Meng, Y., Teng, Y.-C., Maderich, V., Brovchenko, I., Dutour-Sikiric, M., and Zanke, U. (2012). "A fully coupled 3D wave-current interaction model on unstructured grids." *Journal of Geophysical Research*, 117, C00J33.

Van Rooijen, A. A., Lowe, R. J., Ghisalberti, M., Hansen, J., Mccall, R. T., and Dongeren, A. R. Van. (2016a). "Physical and Numerical Modelling of Wave Transformation through a Coastal Canopy." *20th Australasian Fluid Mechanics Conference*, Perth, Australia, 1–4.

Van Rooijen, A. A., McCall, R. T., van Thiel de Vries, J. S. M., van Dongeren, A. R., Reniers, A. J. H. M., and Roelvink, J. A. (2016b). "Modeling the effect of wave-vegetation interaction on wave setup." *Journal of Geophysical Research: Oceans*, 121(6), 4341–4359.

Van Rooijen, A. A., Van Thiel de Vries, J. S. M., McCall, R. T., Van Dongeren, A. R., Roelvink, J. A., and Reniers, A. J. H. M. (2015). "Modeling of wave attenuation by vegetation with XBeach." *E-proceedings of the 36th IAHR World Congress*, The Hague, the Netherlands, 7.

Ruessink, B., Ramaekers, G., and Rijn, L. Van. (2012). "On the parameterization of the free-stream nonlinear wave orbital motion in nearshore morphodynamic models." *Coastal Engineering*, 65, 56–63.

Saint-Venant, A. (1871). "Theorie du mouvement non permanent des eaux, avec application aux crues des rivieres et a l'introduction de marees dans leurs lits." *Comptes rendus des seances de l'Academie des Sciences*, 36, 174–154.

Sallenger, A. H. J. (2000). "Storm impact scale for barrier islands." *Journal of Coastal Research*, 16(3), 890–895.

de Santiago, I., Morichon, D., Abadie, S., Reniers, A. J. H. M., and Liria, P. (2017). "A comparative study of models to predict storm impact on beaches." *Natural Hazards*, Springer Netherlands, 1–23.

Scheidegger, A. E. (1960). *The Physics of Flow Through Porous Media. : Soil Science*. Canada : University of Toronto Pr., Toronto.

Schiereck, G. (2005). *Introduction to bed, bank and shore protection*. Taylor & Francis e-Library, London, UK.

Shibayama, T., and Horikawa, K. (1982). "Sediment Transport and Beach Transformation." *Coastal Engineering 1982*, American Society of Civil Engineers, New York, NY, 1439–1458.

Shields, A. (1936). *Anwendung der Aehnlichkeitsmechanik und der Turbulenzforschung auf die Geschiebebewegung [Application of similarity principles and turbulence research to bed-load movement]*. Mitteilungen der Preußischen Versuchsanstalt für Wasserbau, Berlin.

Siebert, S., Burke, J., Faures, J. M., Frenken, K., Hoogeveen, J., Döll, P., and Portmann, F. T. (2010). "Groundwater use for irrigation – a global inventory." *Hydrology and Earth System Sciences*, Copernicus GmbH, 14(10), 1863–1880.

Sills, G. L., Vroman, N. D., Wahl, R. E., and Schwanz, N. T. (2008). "Overview of New Orleans Levee Failures: Lessons Learned and Their Impact on National Levee Design and Assessment." *Journal of Geotechnical and Geoenvironmental Engineering*, 134(5), 556–565.

Šimůnek, J., van Genuchten, M. T., and Šejna, M. (2016). "Recent Developments and Applications of the HYDRUS Computer Software Packages." *Vadose Zone Journal*, The Soil Science Society of America, Inc., 15(7), 0.

Smallegan, S. M., Irish, J. L., Van Dongeren, A. R., and Den Bieman, J. P. (2016). "Morphological response of a sandy barrier island with a buried seawall during Hurricane Sandy." *Coastal Engineering*, 110, 102–110.

Smit, P. B., Stelling, G. S., Roelvink, J. D., van Thiel de Vries, J., McCall, R. T., Van Dongeren, A. R., Zwinkels, C., and Jacobs, R. (2010). *XBeach: Non-hydrostatic model (Validation, verification and model description)*. *Deltares*, Delft, the Netherlands.

Smith, K. (2013). *Environmental hazards : assessing risk and reducing disaster*. Routledge Taylor & Francis Group.

Smith, R. A. E., Bates, P. D., and Hayes, C. (2011). "Evaluation of a coastal flood inundation model using hard and soft data." *Environmental Modelling & Software*.

Sorensen, R. M. (2006). *Basic coastal engineering*. Springer US.

Soulsby, R. (1997). *Dynamics of marine sands: a manual for practical applications*. Thomas Telford Publications, London.

Splinter, K., and Palmsten, M. (2012). "Modeling dune response to an East Coast Low." *Marine Geology*, 329, 46–57.

Stanczak, G. (2008). *Breaching of sea dykes initiated from the seaside by breaking wave impacts*. PhD dissertation, Leichtweiß-Institute for Hydraulic Engineering and Water Resources, Technische Universität Braunschweig, Braunschweig, Germany.

Steetzel, H. J. (1993). "Cross-Shore Transport during Storm Surges." *Coastal Engineering 1990*, PhD Thesis, Delft University of Technology, Delft, The Netherlands.

Steffler, P., and Blackburn, J. (2002). "Two-dimensional depth averaged model of river hydrodynamics and fish habitat." *Introduction to Depth Averaged Modeling and User's Manual*, University of Alberta.

Steyer, G. D., Perez, B. C., Piazza, S. C., and Suir, G. (2007). "Potential Consequences of Saltwater Intrusion Associated with Hurricanes Katrina and Rita." *Science and the storms: The USGS Response to the Hurricanes of 2005*, G. S. Farris, G. J. Smith, C. R. Crane, M. P., Demas, L. L. Robbins, and D. L. Lavoie, eds., US Geological Survey, 137–146.

Stocker, T., Qin, D., Plattner, G., Tignor, M., and Allen, S. (2014). *Climate Change 2013: The Physical Science Basis - Working Group I Contribution to the Fifth Assessment Report of the Intergovernmental Panel on Climate Change (Summary for Policymakers)*.

Suh, S.-W., Kim, M.-J., and Kim, H.-J. (2017). "Prediction of Sand Beach Variations by Coupling of Hydrodynamic

and Morphological Models during Extreme Storms." *Journal of Coastal Research*, Coastal Education and Research Foundation, 79, 284–288.

Sultan, N. (1992). *Irregular Wave-Induced Velocities in Shallow Water*. Texas.

Surinaidu, L., Nandan, M., Prathapar, S., Gurunadha Rao, V., and Rajamohan, N. (2016). "Groundwater Evaporation Ponds: A Viable Option for the Management of Shallow Saline Waterlogged Areas." *Hydrology*, Multidisciplinary Digital Publishing Institute, 3(3), 30.

Sutherland, J., Peet, A. H., and Soulsby, R. L. (2004). "Evaluating the performance of morphological models." *Coastal Engineering*, 51(8), 917–939.

Swartenbroekx, C., Soares-Frazão, S., Staquet, R., and Zech, Y. (2010). "Two-dimensional operator for bank failures induced by water-level rise in dam-break flows." *Journal of Hydraulic Research*, Taylor & Francis, 48(3), 302–314.

Szymkiewicz, R. (1996). "Numerical stability of implicit four-point scheme applied to inverse linear flow routing." *Journal of Hydrology*, 176(1–4), 13–23.

Tadesse, Y., and Fröhle, P. (2014). "An Integrated Approach To Simulate Flooding Due To River Dike Breach." *International Conference on Hydroinformatics*.

Tayel, M. (2015). *Combined Neural Network and CFD Modelling of Extreme Storm Surges*. PhD dissertation, Leichtweiß-Institute for Hydraulic Engineering and Water Resources, Technische Universität Braunschweig, Braunschweig, Germany.

Tayel, M., and Oumeraci, H. (2015). "A Hybrid Approach Using Hydrodynamic Modeling and Artificial Neural Networks for Extreme Storm Surge Prediction." *Coastal Engineering Journal*, World Scientific Publishing Company and Japan Society of Civil Engineers, 57(1), 1540004.

Tek, M. R. (1957). "Development of a Generalized Darcy Equation." *Journal of Petroleum Technology*, Society of Petroleum Engineers, 9(6), 45–47.

Terlouw, A. (2013). *Predicting morphological storm impact on coastal dunes at Ameland: Simulating storm response on coastal dunes at barrier islands, in the presence of gentle slope*. M.Sc. dissertation, Delft University of Technology, Delft, the Netherlands, Delft - The Netherlands.

Terry, J. P., and Falkland, A. C. (2010). "Responses of atoll freshwater lenses to storm-surge overwash in the Northern Cook Islands." *Hydrogeology Journal*, Springer-Verlag, 18(3), 749–759.

Therrien, R., McLaren, R. G., Sudicky, E. A., and Panday, S. M. (2010). *HydroGeoSphere: a three-dimensional numerical model describing fully-integrated subsurface and surface flow and solute transport*. ON.

Therrien, R., and Sudicky, E. A. (1996). "Three-dimensional analysis of variably-saturated flow and solute transport in discretely-fractured porous media." *Journal of Contaminant Hydrology*, Elsevier, 23(1), 1–44.

Van Thiel de Vries, J. (2009). *Dune erosion during storm surges*. PhD dissertation, Delft University of Technology, Delft.

Van Thiel de Vries, J., van Dongeren, A., McCall, R., and Reniers., A. (2011). "The effect of the longshore dimension on dune erosion." *32nd International Conference on Coastal Engineering, ICCE*, 13.

Tian, Y., Zheng, Y., and Zheng, C. (2016). "Development of a visualization tool for integrated surface water–groundwater modelling." *Computers & Geosciences*, 86, 1–14.

Trefry, M. G., and Muffels, C. (2007). "FEFLOW: A Finite-Element Ground Water Flow and Transport Modeling Tool." *Ground Water*, Blackwell Publishing Inc, 45(5), 525–528.

Tsoukala, V. K., Chondros, M., Kapelonis, Z. G., Martzikos, N., Lykou, A., Belibassakis, K., and Makropoulos, C. (2016). "An integrated wave modelling framework for extreme and rare events for climate change in coastal areas – the case of Rethymno, Crete." *Oceanologia*, 58(2), 71–89.

Tuan, T. Q. (2007). *Seasonal breaching of coastal barriers*. PhD dissertation, Delft University of Technology, Delft, the Netherlands.

Tuan, T., and Verhagen, H. (2008). "Breach initiation by the response of coastal barriers during storm surges." *Seventh International Conference on Coastal and Port Engineering in Developing Countries*, Dubai, U.A.E, 10.

Ujeyl, G., and Rose, J. (2015). "Estimating Direct and Indirect Damages from Storm Surges: The Case of Hamburg–Wilhelmsburg." *Coastal Engineering Journal*, World Scientific Publishing Company and Japan Society of Civil Engineers, 57(1), 1540006.

Vellinga, P. (1982). "Beach and dune erosion during storm surges." *Coastal Engineering*, 6(4), 361–387.

De Vet, P. (2014). *Modelling sediment transport and morphology during overwash and breaching events*. M.Sc. dissertation, Delft University of Technology, Delft, the Netherlands.

De Vet, P., McCall, R., Den Bieman, J. P., Stive, M. J., and Van Ormondt, M. (2015). "Modelling dune erosion, overwash and breaching at Fire Island (NY) during Hurricane Sandy." *Coastal Sediments 2015: The Proceedings of the Coastal Sediments 2015*, World Scientific Publishing Company, San Diego, USA, 10.

Vetsch, D., Müller, R., Rousselot, P., Volz, C., Vonwiller, L., Farshi, D., Veprek, R., and Fäh, R. (2015). *BASEMENT - Basic Simulation Environment for Computation of Environmental Flow and Natural Hazard Simulation: Basement Reference Manual*. Laboratory of Hydraulics, Hydrology and Glaciology (VAW) of the Swiss Federal Institute of Technology (ETH), Zürich, Switzerland.

Villholth, K., and Neupane, B. (2011). "Tsunamis as long-term hazards to coastal groundwater resources and associated water supplies." *Tsunami - A Growing Disaster*, M. Mokhtari, ed., InTech, 87–104.

Violette, S., Boulicot, G., and Gorelick, S. M. (2009). "Tsunami-induced groundwater salinization in southeastern India." *Comptes Rendus Geoscience*, 341(4), 339–346.

Visser, P. J. (1998). *Breach growth in sand-dikes*. PhD dissertation, Delft University of Technology, Delft - The Netherlands.

Visser, P. J. (1999). "Breach Erosion in Sand-Dikes." *Coastal Engineering 1998*, American Society of Civil Engineers, Reston, VA, 3516–3528.

Vithanage, M., Engesgaard, P., Jensen, K. H., Illangasekare, T. H., and Obeysekera, J. (2012). "Laboratory investigations of the effects of geologic heterogeneity on groundwater salinization and flush-out times from a tsunami-like event." *Journal of Contaminant Hydrology*, 136, 10–24.

Vousdoukas, M., Ferreira, Ó., Almeida, L., and Pacheco, A. (2012). "Toward reliable storm-hazard forecasts: XBeach calibration and its potential application in an operational early-warning system." *Ocean Dynamics*, 62(7), 1001–1015.

Vousdoukas, M. I., Mentaschi, L., Voukouvalas, E., Verlaan, M., and Feyen, L. (2017). "Extreme sea levels on the rise along Europe's coasts." *Earth's Future*, 5, 20.

Vousdoukas, M. I., Voukouvalas, E., Mentaschi, L., Dottori, F., Giardino, A., Bouziotas, D., Bianchi, A., Salamon, P., and Feyen, L. (2016). "Developments in large-scale coastal flood hazard mapping." *Natural Hazards and Earth System Sciences*, Copernicus GmbH, 16(8), 1841–1853.

Vreugdenhil, C. (2013). *Numerical methods for shallow-water flow: volume 13*. Springer Science & Business Media.

Wadey, M. P. M., Nicholls, R. R. J., and Hutton, C. (2012). "Coastal flooding in the Solent: an integrated analysis of defences and inundation." *Water*, Multidisciplinary Digital Publishing Institute (MDPI), 4(2), 430–459.

Wainwright, D. J., and Baldock, T. E. (2015). "Measurement and modelling of an artificial coastal lagoon breach." *Coastal Engineering*, 101, 1–16.

Walstra, D. J. R. J. R., Roelvink, J. A. A., and Groeneweg, J. (2000). "Calculation of wave-driven currents in a 3D mean flow model." *Proceedings of the 27th International Conference on Coastal Engineering ICCE*, B. L. Edge, ed., ASCE, Sydney, Australia, 1050–1063.

Walstra, D. J. R., Van Rijn, L. C., Van Ormondt, M., Brière, C., and Talmon, A. M. (2007). "The effects of bed slope and wave skewness on sediment transport and morphology." *Proceedings of the Sixth International Symposium on Coastal Engineering and Science of Coastal Sediment Process: coastal sediment'07*, N. C. Kraus and J. D. Rosati, eds., American Society of Civil Engineers, New Orleans, Louisiana, United States, 137–150.

Walther, M., Bilke, L., Delfs, J.-O., Graf, T., Grundmann, J., Kolditz, O., and Liedl, R. (2014). "Assessing the salt water remediation potential of a three-dimensional, heterogeneous, coastal aquifer system." *Environmental Earth Sciences*, Springer Berlin Heidelberg, 72(10), 3827–3837.

Waterloo Hydrogeologic. (2015). *Visual MODFLOW 2011.1 User's Manual: For Professional Applications in Three-Dimensional Groundwater Flow and Contaminant Transport Modeling*. Waterloo Hydrogeologic Ink., Waterloo, ON, Canada.

Weaver, R. J., and Slinn, D. N. (2005). "Effect of wave forcing on storm surge." *Coastal Engineering 2004*, World Scientific Publishing Company, 1532–1538.

Weiyan, T. (1992). *Shallow water hydrodynamics: Mathematical theory and numerical solution for a two-dimensional system of shallow-water equations*. (Y. Cunli. and T. Xinhua, eds.), Water &. Power Press and Elsevier Science Publishers, Beijing, China.

Werner, A. D., Bakker, M., Post, V. E. A., Vandenbohede, A., Lu, C., Ataie-Ashtiani, B., Simmons, C. T., and Barry, D. A. (2013). "Seawater intrusion processes, investigation and management: Recent advances and future challenges." *Advances in Water Resources*, 51, 3–26.

Werner, A. D., Jakovovic, D., and Simmons, C. T. (2009). "Experimental observations of salt water up-coning." *Journal of Hydrology*, 373(1–2), 230–241.

WHO. (2011). *Guidelines for Drinking-water Quality*. *WHO chronicle*.

Williams, V. J. V. (2010). "Identifying the Economic Effects of Salt Water Intrusion after Hurricane Katrina." *Journal of Sustainable Development*, 3(1), 29–37.

Wilson, A. A. M., Moore, W. W. S., Joye, S. S. B., Anderson, J. L., and Schutte, C. A. (2011). "Storm-driven groundwater flow in a salt marsh." *Water Resources Research*, 47(2), 1–11.

de Winter, R. C., and Ruessink, B. G. (2017). "Sensitivity analysis of climate change impacts on dune erosion: case study for the Dutch Holland coast." *Climatic Change*, Springer Netherlands, 141(4), 685–701.

Winterwerp, J., and Kesteren, W. Van. (2004). *Introduction to the physics of cohesive sediment dynamics in the marine environment*.

Worni, R., Huggel, C., Clague, J. J., Schaub, Y., and Stoffel, M. (2014). "Coupling glacial lake impact, dam breach, and flood processes: A modelling perspective." *Geomorphology*, 224, 161–176.

Wu, W., Mustafa, S., Altinakar, S. F., Bradford, Q. J., Chen, S., Jennifer, G., Duan, D., and Michael, G. (2011). "Earthen Embankment Breaching." *Journal of Hydraulic Engineering*, 137(12), 1549–1564.

Yang, J., Graf, T., Herold, M., and Ptak, T. (2013). "Modelling the effects of tides and storm surges on coastal aquifers using a coupled surface–subsurface approach." *Journal of Contaminant Hydrology*, 149, 61–75.

Yang, J., Graf, T., and Ptak, T. (2015a). "Impact of climate change on freshwater resources in a heterogeneous coastal aquifer of Bremerhaven, Germany: A three-dimensional modelling study." *Journal of Contaminant Hydrology*, 177, 107–121.

Yang, J., Graf, T., and Ptak, T. (2015b). "Sea level rise and storm surge effects in a coastal heterogeneous aquifer: a 2D modelling study in northern Germany." *Grundwasser*, Springer Berlin Heidelberg, 20(1), 39–51.

Yu, X., Duffy, C. J., Rousseau, A. N., Bhatt, G., Pardo Álvarez, Á., and Charron, D. (2016a). "Open science in practice: Learning integrated modelling of coupled surface-subsurface flow processes from scratch." *Earth and Space Science*, 3(5), 190–206.

Yu, X., Yang, J., Graf, T., Koneshloo, M., O'Neal, M. A., and Michael, H. A. (2016b). "Impact of topography on groundwater salinization due to ocean surge inundation." *Water Resources Research*, 52(8), 5794–5812.

Zhong, Q., Chen, S., and Deng, Z. (2017). "Numerical model for homogeneous cohesive dam breaching due to overtopping failure." *Journal of Mountain Science*, Science Press, 14(3), 571–580.

Zhou, M., Roelvink, D., Zou, Z., and van Wijhe, H. J. (2014). "Effects of Passing Ship With a Drift Angle on a Moored Ship." *Volume 8B: Ocean Engineering*, ASME, 7.

Zhu, Y. (2006). "Breach growth in clay-dikes." PhD dissertation, Delft University of Technology.

Zijlema, M., Stelling, G., and Smit, P. (2011). "SWASH: An operational public domain code for simulating wave fields and rapidly varied flows in coastal waters." *Coastal Engineering*, 58(10), 992–1012.

Coastal floods induced by a coastal barrier breaching under extreme storm surges represent a significant humanitarian, socioeconomic and ecological hazard. Moreover, it is a multi-scale problem governed by complex interactions between a variety of hydrodynamic and sediment-related processes at different spatiotemporal scales. With global warming and expected climate change, many coastal systems may experience accelerated coastal erosion, coastal barrier breaching, coastal flooding and subsequent seawater intrusion into fresh groundwater. However, the current models of breaching-induced coastal floods and subsequent saltwater intrusion are mainly based on modelling each of these processes separately, which often leads to unreliable simulations because the mutual interactions among these naturally successive processes are ignored. Therefore, to consider such interactions, this study explored the possibility to simulate breaching, flooding and saltwater intrusion in a single model system in order to reliably draw the implications of coastal floods for groundwater contamination. For this purpose, the XBeach model is selected as the most suitable breaching model that can properly calculate inland discharges through breaching induced inlets. Second, the study attempts to couple XBeach with suitable inundation and saltwater intrusion models in order to simulate successively the breaching-induced inundation and the subsequent saltwater intrusion.

In fact, this dissertation represents the first systematic research study that addresses the safety of natural coastal sandy barriers under extreme storm surge conditions together with the consequences of possible barrier breaching and overwash on subsequent flooding and saltwater intrusion into fresh groundwater. Moreover, it is the first study that introduces an overall physically based methodology to simulate breaching of coastal barriers, induced inundation and subsequent saltwater intrusion, including the simulation of each of the three successive processes and their interactions. By this way, this study overcomes most of the modelling weaknesses from previous studies. Furthermore, it is the foremost study that attempts to mitigate storm-driven saltwater intrusion through the use and modelling of subsurface drainage network. Thus, this study is quite relevant for the coastal engineering community, for flood risk managers, for groundwater suppliers as well as for sustainable development planners.

On the specific level, this study introduces two novel improvements of the XBeach model in order to properly predict the sediment stirring and transport: (i) development of a prediction formula for the calibration of the time-averaged flow depending on the wave skewness and asymmetry, and (ii) introduction of a new approach to account for the grain-stabilisation effect on sediment transport. Moreover, this study successfully examined the applicability extension of XBeach to coastal flood modelling in combination with breaching modelling. This contribution facilitates the modelling of breaching-induced coastal floods because of the possibility to model barrier breaching and induced inundation in a single XBeach model, thus overcomes the weaknesses of the separate modelling. Furthermore, this is the first study that introduces and simulate a mitigating measure for vertical saltwater intrusion induced by coastal floods through the use of subsurface drainage network. The applied subsurface drainage network was tentatively shown to substantially shorten the long remediation intervals of aquifers after a coastal flood.

To highlight the value of the study outcomes, the modelling system applying the improved XBeach to simulate both inland discharges and induced hinterland inundation in addition to Visual Modflow/SEAWAT to simulate the subsequent saltwater intrusion is used to draw the implications of possible coastal flood near Bremerhaven, northern Germany. The outcome of this case study showed that a flood event for 2.8 hours might contaminate the aquifers near Bremerhaven so that they might remain contaminated for around 45 years, i.e. until they get remediated naturally. The application of the subsurface drainage system shortens the latter interval to three years and prevents the contamination of the deeper aquifers.


State of the Art Report
Breaching of Coastal Barriers under Extreme Storm Surges and Implications for Groundwater Contamination
Internal Report No. 1071
Saber M. Elsayed, M.Sc. (Ph.D. Student)
Adviser: Prof. Dr. Hocine Oumeraci
Braunschweig March 2017

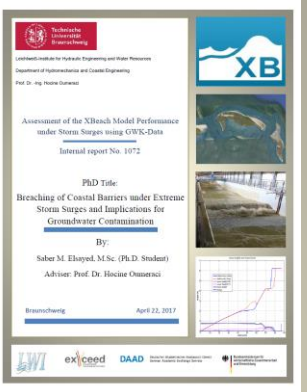
Assessment of the XBeach Model Performance under Storm Surges using GWK-Data
Internal report No. 1072
PhD Title:
Breaching of Coastal Barriers under Extreme Storm Surges and Implications for Groundwater Contamination
By:
Saber M. Elsayed, M.Sc. (Ph.D. Student)
Adviser: Prof. Dr. Hocine Oumeraci
Braunschweig April 22, 2017


Improvement and Extension of the XBeach Model to Account for New Physical Processes
Internal Report No 1073
PhD Title:
Breaching of Coastal Barriers under Extreme Storm Surges and Implications for Groundwater Contamination
By:
Saber M. Elsayed, M.Sc. (Ph.D. Student)
Adviser: Prof. Dr. Hocine Oumeraci
Braunschweig April 7, 2017

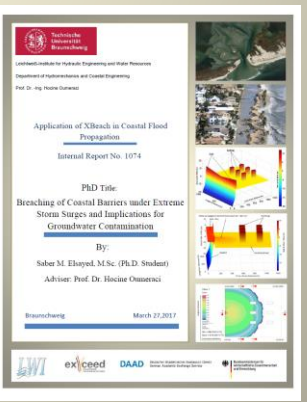
Application of XBeach in Coastal Flood Propagation
Internal Report No. 1074
PhD Title:
Breaching of Coastal Barriers under Extreme Storm Surges and Implications for Groundwater Contamination
By:
Saber M. Elsayed, M.Sc. (Ph.D. Student)
Adviser: Prof. Dr. Hocine Oumeraci
Braunschweig March 27,2017

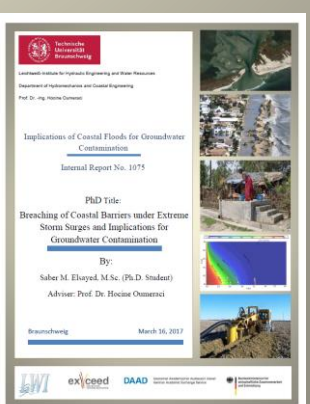
Implications of Coastal Floods for Groundwater Contamination
Internal Report No. 1075
PhD Title:
Breaching of Coastal Barriers under Extreme Storm Surges and Implications for Groundwater Contamination
By:
Saber M. Elsayed, M.Sc. (Ph.D. Student)
Adviser: Prof. Dr. Hocine Oumeraci
Braunschweig March 16, 2017


hydrology
Article
Combined Modelling of Coastal Barrier Breaching and Induced Flood Propagation Using XBeach
Saber M. Elsayed * and Hocine Oumeraci


Coastal Engineering
Effect of beach slope and grain-stabilization on coastal sediment transport: An attempt to overcome the erosion overestimation by XBeach
Saber M. Elsayed*, Hocine Oumeraci